

INTERNATIONAL COURT OF JUSTICE

DISPUTE OVER THE STATUS AND USE OF THE
WATERS OF THE SILALA

(CHILE v. BOLIVIA)

REPLY OF THE
REPUBLIC OF CHILE

ANNEXES XI - XIV TO THE EXPERT REPORTS

VOLUME 3 OF 3

15 FEBRUARY 2019

**LIST OF ANNEXES TO THE
EXPERT REPORTS**

VOLUME 3

ANNEXES XI - XIV

ANNEX N°	TITLE	PAGE N°
Annex XI	Herrera, C. and Aravena, R., 2019. <i>Chemical and Isotopic Characterization of Surface Water and Groundwater of the Silala River Transboundary Basin, Second Region, Chile</i>	1
Annex XII	Herrera, C. and Aravena, R., 2019. <i>Chemical Characterization of Surface Water and Groundwater of the Quebrada Negra, Second Region, Chile</i>	69
Annex XIII	Muñoz, J.F. and Suárez, F., 2019. <i>Quebrada Negra Wetland Study</i>	83
Annex XIV	SERNAGEOMIN (National Geology and Mining Service), 2019. <i>Geology of the Silala River: An Updated Interpretation</i>	187
Data CD	CD-ROM containing supporting data to Annexes XI – XIV	273
Appendix C to Annex XIV	Blanco, N. and Polanco, E., 2018. <i>Geology of the Silala River Basin, Northern Chile</i>	273

Annex XI

Herrera, C. and Aravena, R., 2019. *Chemical and Isotopic Characterization of Surface Water and Groundwater of the Silala River Transboundary Basin, Second Region, Chile*

**CHEMICAL AND ISOTOPIC CHARACTERIZATION OF SURFACE
WATER AND GROUNDWATER OF THE SILALA RIVER
TRANSBOUNDARY BASIN, SECOND REGION, CHILE**

Christian Herrera (PhD)

Associate Professor, Universidad Católica del Norte

Ramón Aravena (PhD)

Emeritus and Adjunct Professor, University of Waterloo

January 2019

GLOSSARY

Alkalinity: The name given to the quantitative capacity of an aqueous solution to neutralize an acid.

Anion: An ionic species, with a net negative charge.

Aquifer: A permeable region of rock or soil capable of storing, transmitting and yielding exploitable quantities of water.

Cation: An ionic species with a net positive charge.

Deuterium excess: The concept of deuterium excess (d) is defined as $d = \delta^2\text{H} - 8\delta^{18}\text{O}$. The deuterium excess can be used to identify vapor source regions for air masses producing precipitation that contribute to groundwater recharge.

Global meteoric line: An equation defined by the geochemist Harmon Craig that states the average relationship between hydrogen and oxygen isotope ratios in natural terrestrial waters, expressed as a worldwide average: $\delta^2\text{H} = 8\delta^{18}\text{O} + 10\text{‰}$.

Headwater: A tributary stream of a river, close to or forming part of its source.

Hydrochemical: Dealing with the chemical characteristics of bodies of water.

Ion: An atom or molecule with a net electrical charge due to the gain or loss of one or more electrons.

Ion chromatography: A chromatography process that separates ions and polar molecules based on their affinity to an ion exchanger.

Isotope: One or two or more species of the same chemical element, having the same numbers of protons in the nucleus but differing from one another by having a different numbers of neutrons. The isotopes of an element have slightly different physical properties, owing to their mass differences, by which they can be separated.

Isotopic characterization: The identification of isotopic signature, the distribution of certain stable isotopes and radioactive isotopes within chemical compounds.

Meteoric water line: A linear equation that defines the average relationship between hydrogen and oxygen isotope ratios in rain waters in a defined area.

Mineralization: Process by which groundwater through interaction with minerals in the aquifer incorporated chemical elements in the water.

Percent Modern Carbon (pMC): Unit to report radiocarbon dates. The reference is the radiocarbon content of the atmospheric CO₂ before 1950 defined as 100 percent modern carbon.

Perched aquifer: Groundwater body, generally of moderate dimensions, supported by a relatively impermeable stratum and which is located between a deeper water table and the ground surface.

Plasma emission spectrometry: An analytical technique used for the detection of trace elements. It is a type of emission spectroscopy that uses the inductively coupled plasma to produce excited atoms and ions that emit electromagnetic radiation at wavelengths characteristic of a particular element.

Radioactive isotope: A radioactive form of an element, consisting of atoms with unstable nuclei, which undergo radioactive decay to stable forms, emitting characteristic alpha, beta, or gamma radiation. These may occur naturally, as in the cases of tritium and radiocarbon, or may be created artificially.

Recharge: Groundwater recharge (or deep drainage or deep percolation) is a hydrologic process whereby water that has infiltrated the surface moves downward from the unsaturated zone to groundwater. Recharge is the primary method through which water enters an aquifer. Its source can be precipitation or surface water.

Redox process: A chemical reaction in which the oxidation states of atoms are changed. Any such reaction involves both a reduction process and a complementary oxidation process, two key concepts involved with electron transfer processes.

Salinity: The concentration of dissolved salts in water.

Silicate: A compound whose crystal structure contains SiO_4^{2-} , either isolated or joined through one or more of the oxygen atoms, to form groups, chains, sheets, or three dimensional structures with metallic elements.

Silicate minerals: Silicate minerals are rock-forming minerals made up of silicate groups. They are the largest and most important class of rock-forming minerals and make up approximately 90 percent of the Earth's crust.

Stable isotope: One that does not transmute into another element with emission of corpuscular or electromagnetic radiations.

Tritium: A radioactive isotope of hydrogen. The nucleus of tritium contains one proton and two neutrons. Naturally occurring tritium is rare on Earth, where trace amounts are formed by the interaction of the atmosphere with cosmic rays.

Volumetric method: A quantitative chemical analysis that involves the measurement of volume of a solution of known concentration that is used to determine the concentration of the analyte.

Weathering: The destructive process by which earth materials on exposure to atmospheric agents (water, wind, temperature, etc.) at or near the Earth's surface are changed in color, texture, composition, firmness or form, with little or no transport of the loosened or altered material.

TABLE OF CONTENTS

1. INTRODUCTION	1
1.1 Presentation.....	1
1.2 Location of the investigated area	1
1.3 Objective of the report	2
1.4 Methodology.....	3
1.5 Hydrogeochemical and isotopic data collected in the Bolivian sector (DHI, 2018) .	7
1.6 Structure of the report	8
2. RESULTS AND DISCUSSION.....	8
2.1 Geochemistry data	8
2.2 Environmental isotope data.....	16
2.2.1 $\delta^{18}\text{O}$ and $\delta^2\text{H}$ data	17
2.2.2 Tritium data	22
2.2.3 Carbon-14 and Carbon-13 data	24
3. CONCLUSIONS	30
4. REFERENCES	33
APPENDIX A	35
APPENDIX B.....	37
APPENDIX C.....	41
APPENDIX D	43
APPENDIX E.....	55
APPENDIX F.....	58
APPENDIX G	60

1. INTRODUCTION

1.1 Presentation

The National Director of the Dirección Nacional de Fronteras y Límites del Estado (DIFROL) of the Ministry of Foreign Affairs of Chile, Mrs. Ximena Fuentes, requested a study on the hydrochemical and isotopic characterization of the transboundary basin of the Silala River in the northern region of Chile as part of a study aimed at deepening the hydrogeological knowledge of this basin. This report updates a 2017 report of Herrera and Aravena (Chile's Memorial (CM), Vol. 4, Annex III) and includes hydrogeochemical and isotopic data collected in the Bolivian sector of the Silala River presented in DHI (2018) as part of the Bolivian Counter-Memorial (BCM).

The study of the chemical and isotopic evolution of surface and groundwater in the Silala River basin can contribute to the understanding of the complex interactions between the river and the groundwater and mechanisms of local and regional recharge to the river flow. In this context, the hydrogeochemical study of groundwater has been an important approach to understand the flow of groundwater and to validate or discard hypotheses about the conceptual understanding of the hydrogeology. This report was elaborated under the supervision and instruction of Professors Howard Wheeler and Denis Peach.

1.2 Location of the investigated area

The headwaters of the Silala River are located above 4300 m.a.s.l. in Bolivian territory where the perennial river flow originates from two wetland areas, the Cajones ravine and the Orientales area, which are fed by groundwater from many springs. The recharge area for these springs has been estimated to be much larger than the topographic catchment and is included in Figure 1. After the river enters a ravine it crosses into Chilean territory. In Chile, the basin is located between S -21.98° and S -22.06° latitude and W -68.08° and W -68.02° longitude, in the second region of Chile. The Silala River has carved a ravine at the border between Chile and Bolivia, into the existing bedrock, that in some places is more than 10 m deep (Latorre and Frugone, 2017). Part of the flow of the river is abstracted at a small impoundment just south west of the international border in Chilean territory. A major ephemeral tributary, called the Quebrada Negra (Figure 1), reaches the Silala River from the southeast, some 1700 m downstream from the border. The upper course of the Silala River in Chile in this report refers to the area between the international border and the junction with the Quebrada Negra, whereas the lower course term refers to the area between the Quebrada Negra

and the CODELCO intake (Figure 1), which is a surface water abstraction intake structure located downstream in the Silala River.

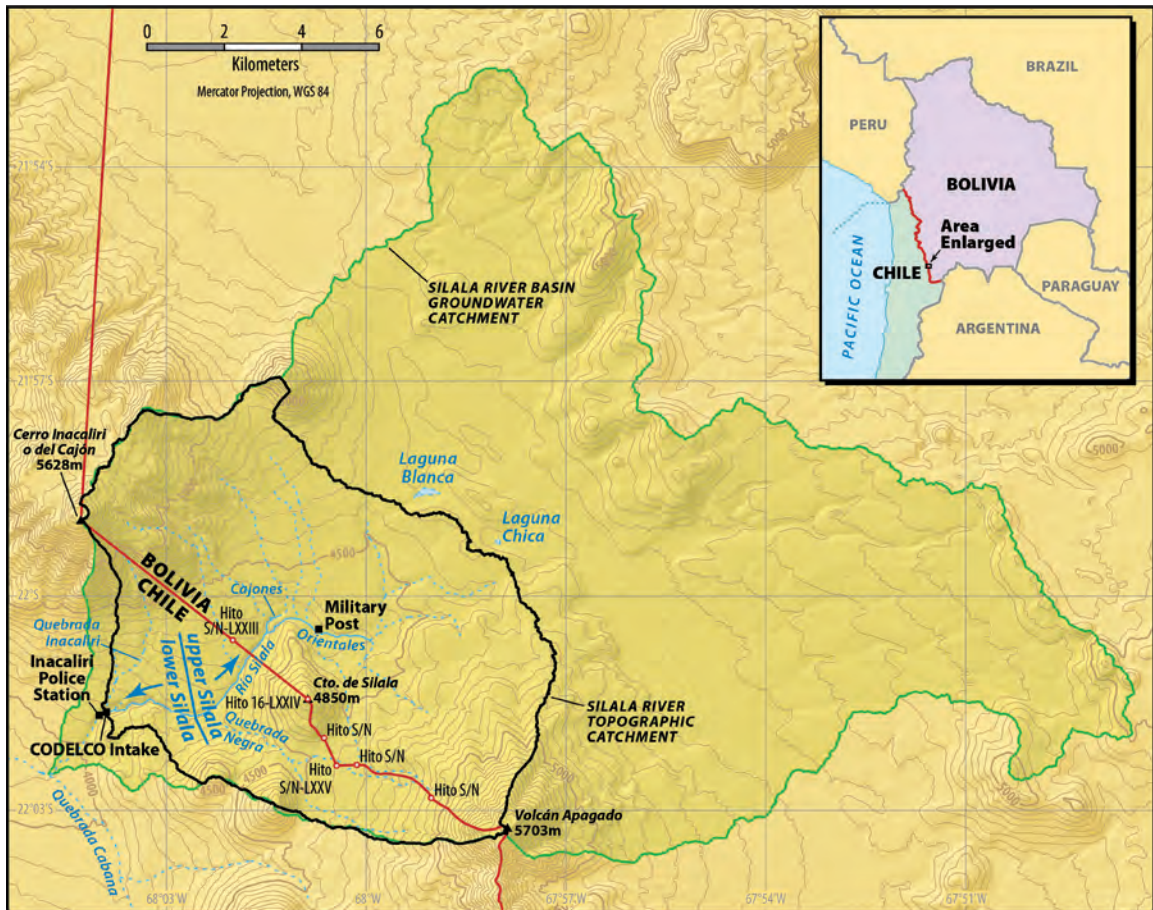


Figure 1. Location map of the study area. It depicts key features of the area, for example the CODELCO intake and the upper and lower part of the Silala River in Chile, as defined in this report.

1.3 Objective of the report

The main objective of this study is to characterize the chemistry and isotopic composition of the surface and groundwater of the Silala River basin. Chemical and isotopic tracers can potentially provide information to evaluate the mechanisms of river-groundwater interaction and the origins of waters in the Silala River basin. This report also includes hydrogeochemical and isotopic data collected in the Bolivian sector of the Silala River basin presented in DHI (2018) as part of the BCM. This information will be used to complement the analysis of the data collected in the study carried out in the Chilean part of the Silala River basin.

1.4 Methodology

Four periods of field work were conducted in Chile during the study. The first was carried out on 28 August 2016 by a multidisciplinary team. The main activities performed during this field trip focused on evaluating the hydrogeological context of the study area, and an evaluation of spring systems. The second and third field campaigns were carried out between 19 and 21 December 2016 and during the period 31 January 2017 to 3 February 2017, respectively, and focused on water sample collection. These campaigns were carried out in the rainy season. The fourth campaign was carried out from 11 to 15 October 2017 corresponding to the dry season. During the second field campaign, samples from springs, river and groundwater were collected for chemical and isotopic analysis, the groundwater being sampled from boreholes drilled as part of the hydrogeological investigation in the study area (Arcadis, 2017). A sampling location map is presented in Figure 2. During the third campaign, samples of river water and a larger number of springs were collected for chemical and isotope analysis. A sampling location map for the third campaign is presented in Figure 3. During the third campaign a survey of all the springs found on the northern flank of the ravine in the upper course of the river in Chile was performed and in situ parameters including pH, electrical conductivity and temperature were also measured. A location map showing the spring sites is presented in Figure 4. During the fourth campaign, samples from river, springs and groundwater from wells were collected for chemical and isotopic analysis. The sampling locations are presented in Figure 5. The sampling protocol including materials used is described in Appendix A; pictures of some of the sampling locations are presented in Appendix B; and the analytical methods are detailed in Appendix C. Note that samples are identified by sample location XXX-YYY-ZZ followed by a sample date descriptor (-16, -17 and O17 for December 2016, January-February 2017, and October 2017, respectively).

The chemical analysis included major cations and anions. The anions were determined by ion chromatography (chloride, sulfate, nitrate) (Cl^- , SO_4^{2-} , NO_3^-) and volumetric titration (bicarbonate) (HCO_3^-), and cations (sodium, potassium, calcium, magnesium) (Na^+ , K^+ , Ca^{2+} , Mg^{2+}) by plasma emission spectrometry (ICP-OES). The chemical analyses were performed at the ALS Laboratory in Chile and the results are presented in Tables 1 and 2 of this report.

The isotope analysis included oxygen-18 (^{18}O) and deuterium (^2H), tritium (^3H) in water samples and carbon 13 (^{13}C) and carbon 14 (^{14}C) in dissolved inorganic carbon. The isotope analyses were carried out at IT2 Isotope Tracer Technologies Inc. in Canada as presented in Appendix D, and the isotope data are reported in Tables 3 to 8 of this report.

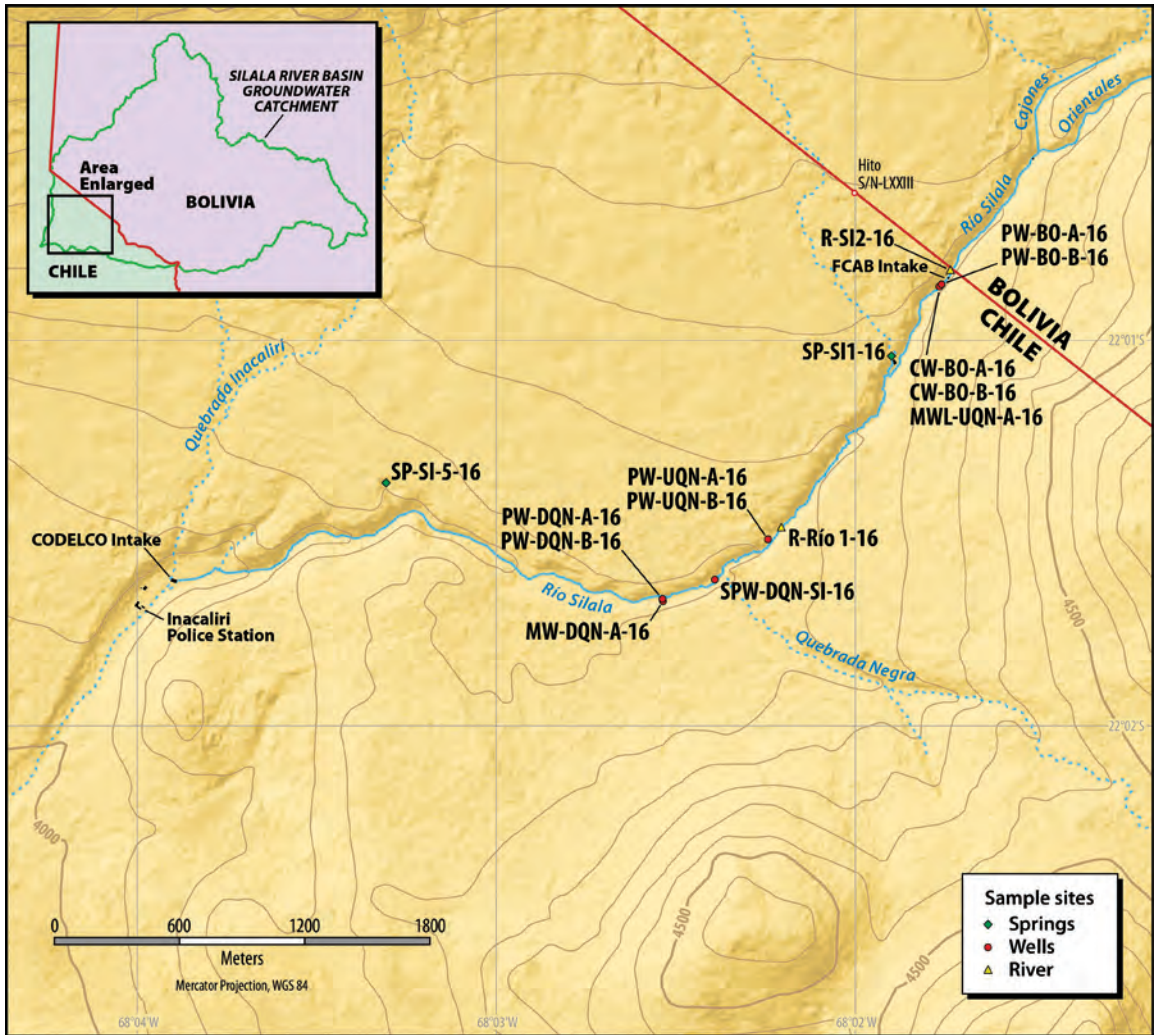


Figure 2. Sampling location map, second campaign, December 2016.

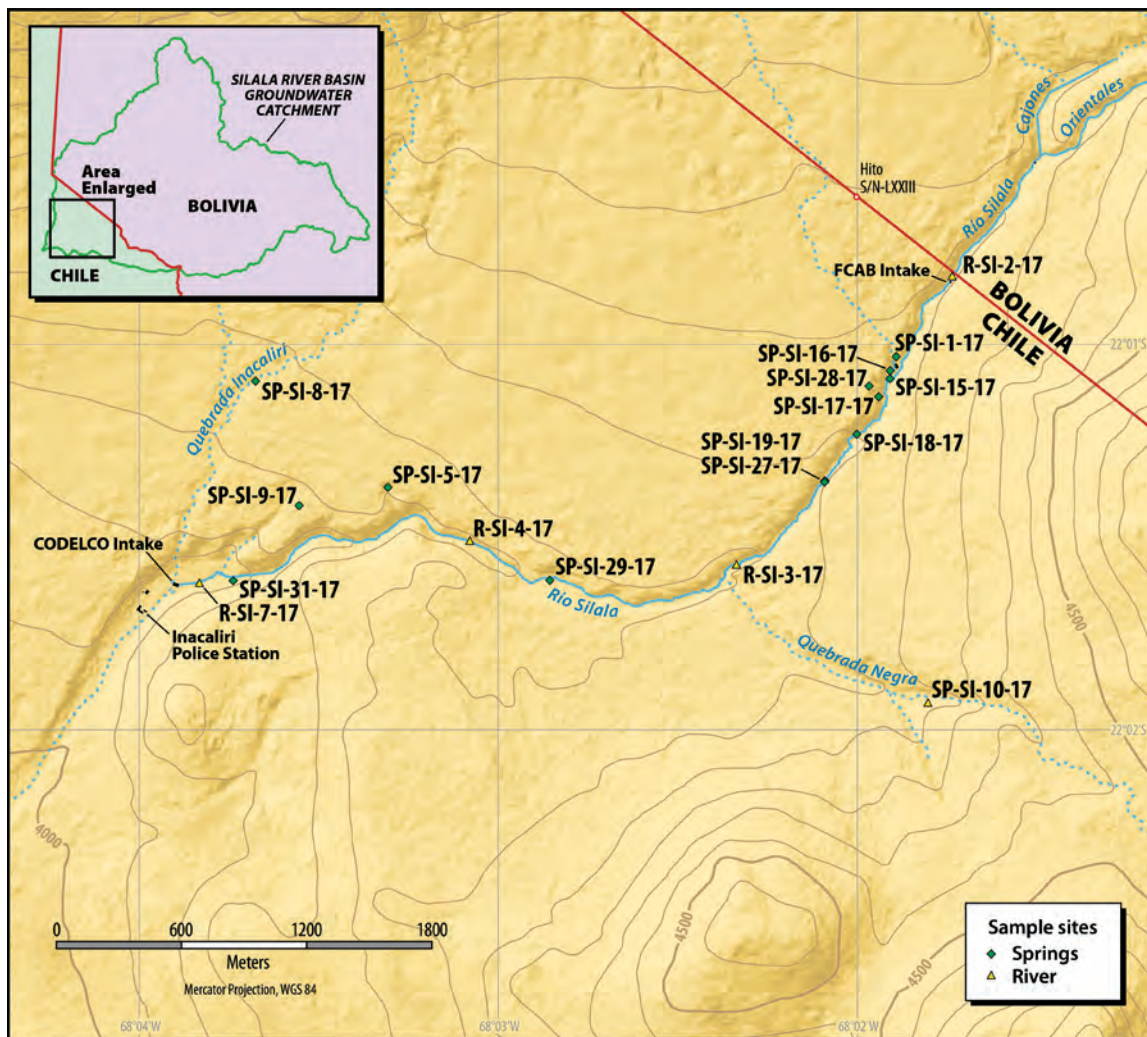


Figure 3. Sampling location map, third campaign, January-February 2017.

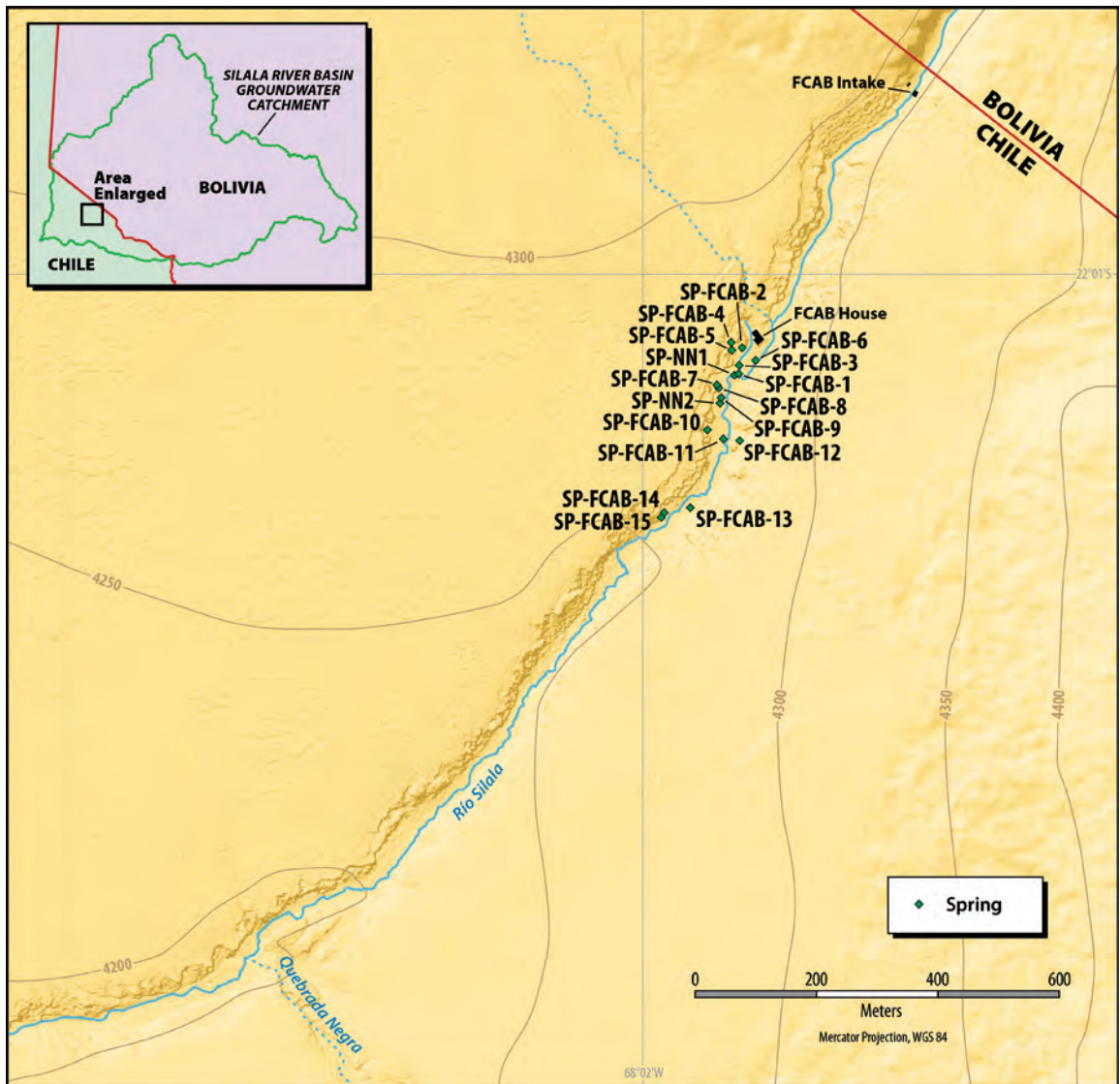


Figure 4. Location map of the spring survey in the upper course of the river in Chile.

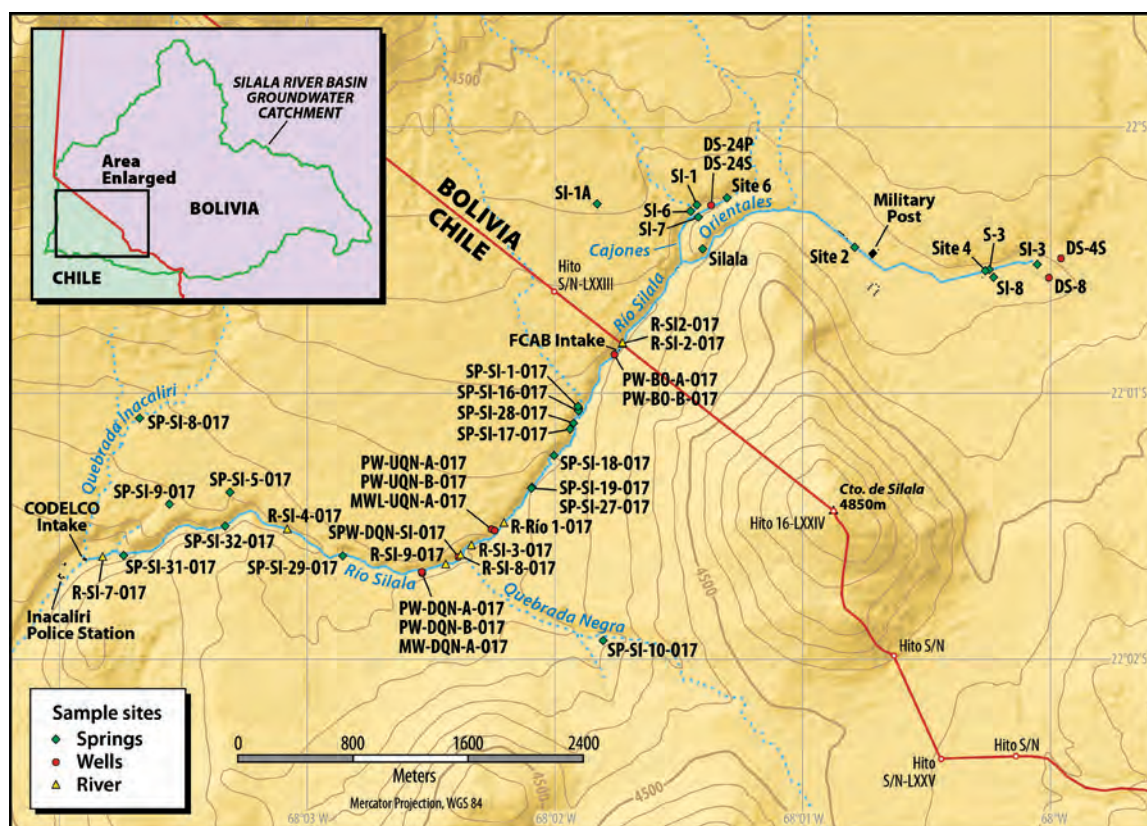


Figure 5. Sampling location map, fourth campaign, October 2017. This map also shows the location of the samples collected in the Bolivian sector (DHI, 2018).

1.5 Hydrogeochemical and isotopic data collected in the Bolivian sector (DHI, 2018)

Hydrogeochemical and isotopic data collected in the Bolivian sector of the Silala River basin and reported in DHI (2018) (BCM, Vol. 4, pp. 89-94), are used in this report as part of the evaluation of the data collected in the Chilean sector.

The information provided in the Bolivian studies corresponds to:

- 14 chemical analyses of water samples from the Silala River basin in Bolivia, which included springs and groundwater (piezometers). No data were reported for the Silala River. The data were collected during different sampling campaigns carried out for different studies between the years 2000-2001 and 2016-2017 (BCM, Vol. 4, pp. 539-542).
- 3 tritium and ^{14}C analyses of springs obtained in 2004 (BCM, Vol. 4, p. 92) (see Appendix G of this report).

Only samples that have less than 10% ionic balance error in the chemical analyses were used to construct the Stiff diagrams. These included samples from the Cajones ravine (referred to in DHI (2018) as the North Wetland or Bofedal) and the Orientales area (referred to in DHI (2018) as the South Wetland or Bofedal).

1.6 Structure of the report

Chapter 2 provides a description and discussion of the river, spring and groundwater hydrochemistry from the three sampling campaigns in Chile. The discussions focus on salinity patterns and the chemical composition of the different water types analyzed in the study. It also contains a brief discussion of the Bolivian data. Subsequently the stable isotopic composition of these waters is presented for each campaign. Here the discussion focuses on the differences between the isotopic signatures of the river, springs and groundwater in wells and their possible relationship to local and regional recharge. The tritium and Carbon 14 data are also presented and discussed in Chapter 2, within the context of the conceptual model of river-groundwater interaction in the Silala River basin system. Chapter 3 details the conclusions drawn from the study where all the data and information are integrated and a conceptual model for the river-groundwater interaction is proposed. Details of the sampling methods are reported in Appendix A, whereas photographs recording some sampling activities are part of Appendix B. Detailed information about analytical methods is described in Appendix C and finally the official isotope data reported by the laboratory are presented in Appendix D. Appendix E contains the Piper and Stiff diagrams for the rainy season. Appendix F presents the chemical data from Bolivian lake, spring and well samples contained in DHI (2018) and cited in this report, and Appendix G reproduces the Tritium and Carbon 14 data presented by DHI (2018), also cited in this report.

2. RESULTS AND DISCUSSION

2.1 Geochemistry data

The chemical data collected in the upper course of the Silala River basin in the territory of Bolivia will be used to complement the chemical data collected in the Chilean sector. These Bolivian waters included one group of springs and groundwater from wells collected in the North Bofedal in Bolivia (Cajones ravine). The springs, which are close to the border with Chile, are located in the foothills of the Cerro Inacaliri. The second group corresponds to water samples from springs and piezometers located east of the

first group of springs, in the South Bofedal in Bolivia (Orientales), where the springs are characterized by more diffuse discharges.

In order to facilitate the discussion of the data, the study area in Chile was divided into the upper and lower course of the river, which correspond to the zones above and below the Quebrada Negra (Figure 1).

The first results of the chemical characterization of the surface and groundwater of the Silala River area in Chile were presented in Herrera and Aravena (2017). All samples were obtained in the months of December 2016 and January-February 2017 and correspond to the rainy season of the Altiplano. Table 1 presents all the chemical analyses of river samples, springs and boreholes obtained in the rainy season. Table 2 shows the more recent analytical results from the Silala River, springs and boreholes in Chile that were sampled in the dry season (October 2017).

The water in the study area is characterized by low salinity. No appreciable differences in conductivity values were observed during the rainy and dry season (Tables 1 and 2). The conductivity values for the Silala River range between 150 and 330 $\mu\text{S}/\text{cm}$ in the rainy season and 178 and 264 $\mu\text{S}/\text{cm}$ in the dry season. The springs are characterized by conductivity values ranging between 84 and 290 $\mu\text{S}/\text{cm}$ in the rainy season and between 69 and 379 $\mu\text{S}/\text{cm}$ in the dry season. The higher conductivity values of 290 and 379 $\mu\text{S}/\text{cm}$ in the spring waters are observed in the Quebrada Negra spring SP-SI-10.

The waters of springs located in the upper part of the Silala River course in Chile with EC values ranging between 149 and 220 $\mu\text{S}/\text{cm}$ tend to have a relatively higher mineralization, compared to the springs located in the northern part of the lower course of the Silala River in Chile, which are characterized by EC values between 69 and 160 $\mu\text{S}/\text{cm}$. Furthermore, the springs in the upper part of the Silala River course in Chile tend to have conductivity values in the range of the Silala River. These patterns were observed in both the dry season (base flow condition) and rainy season campaigns (Tables 1 and 2).

The groundwater collected in the wells tends to have higher salinity than the Silala River and the springs. The conductivity values range between 309 and 440 $\mu\text{S}/\text{cm}$ and 226 and 342 $\mu\text{S}/\text{cm}$, in the rainy and dry season respectively (Tables 1 and 2).

Sample ID	Coordinates		Date	Sampling depth (m.b.s.)	Water type	T°C	pH lab	EC field (µS/cm)	Alkalinity (mg/l of CaCO ₃)	Cl mg/L	SO ₄ mg/L	HCO ₃ mg/L	Ca mg/L	Mg mg/L	K mg/L	Si mg/L	Na mg/L	NO ₃ mg/L
	x	y																
R-SI-16	600242	7565357	20-12-2016		River	17.5	8.89	150	91	2.34	5.92	91.622	9.9	4.099	2.5	18.8	19.74	0.19
R-Rio 1-16	599410	7564117	21-12-2016		River	14.5	8.57	163	104	4.55	7.4	93.818	9.8	4.014	2.78	21.9	18.07	0.25
R-SI-2-17	600227	7565333	31-01-2017		River	17.1	9.03	100	66	2.36	6.27	95.6	8.37	3.633	2.01	22.1	17.44	0.22
R-SI-3-17	599184	7563959	01-02-2017		River	18.3	7.33	220	22	2.31	6.48	91.6	9.29	3.664	2.44	19.8	16.56	0.23
R-SI-4-17	597908	7564081	01-02-2017		River	20.8	7.04	330	96	1.99	7.89	133	16.04	7.164	3.74	25.9	18.39	0.24
R-SI-7-17	596611	7563887	01-02-2017		River	18.4	9.02	215	119	1.92	9.33	115	14.42	6.407	3.55	25.3	17.16	0.19
SP-SI-16	599943	7564936	20-12-2016		Spring	15.2	8.07	160	77	2.13	6.11	92.72	10.34	4.293	2.96	22	16.75	0.33
SP-SI-1-17	599956	7564952	31-01-2017		Spring	15.2	7.92	160	63	2.12	6.64	100	9.96	4.106	2.71	21.7	15.97	0.35
SP-SI-5-16	597518	7564344	21-12-2016		Spring	20.3	8.06	177	25	1.28	8.26	30.378	3.93	0.646	2.91	21.4	10.37	0.27
SP-SI-5-17	597517	7564342	01-02-2017		Spring	20.2	8.05	160	48	1.24	8.19	34	3.79	0.563	2.57	21.9	9.41	0.29
SP-SI-8-17	596886	7564854	01-02-2017		Spring	19.2	7.61	88	25	1.18	11.5	31	3.95	0.489	2.25	20.4	10.66	0.24
SP-SI-9-17	597091	7564257	01-02-2017		Spring	18.5	7.5	90.7	64	1.09	9.72	32	4.24	0.525	2.58	21.1	9.77	0.21
SP-SI-10-17	600098	7563292	01-02-2017		Spring	13.6	7.05	290	74	2.16	14.88	99	14.63	6.294	6.68	30.6	11.86	0.22
SP-SI-15-17	599926	7564847	31-01-2017		Spring	15.6	8.11	131	43	2.09	6.24	76	8.45	3.09	2.36	19.7	14.88	0.35
SP-SI-16-17	599927	7564885	31-01-2017		Spring	15.5	8.18	84	48	2.09	5.94	73	7.06	2.55	2.04	23	13.52	0.36
SP-SI-17-17	599871	7564761	31-01-2017		Spring	15.1	7.25	170	28	2.06	5.81	68	6.54	2.119	2.12	18.6	13.66	0.34
SP-SI-18-17	599765	7564582	31-01-2017		Spring	15.6	7.13	220	19	2.06	6.08	62	6.12	2.175	1.96	22.9	12.91	0.34
SP-SI-19-17	599609	7564354	31-01-2017		Spring	16.1	7	190	28	2.04	5.94	66	6.6	2.463	2.06	19.6	13.35	0.34
SP-SI-27-17	599611	7564360	31-01-2017		Spring	16.6	6.87	220	83	2.03	6.52	74	7.66	3.107	2.18	23.8	14.02	0.33
SP-SI-28-17	599825	7564812	31-01-2017		Spring	11.5	7.13	230	17	2.13	7.1	87	9.6	3.908	2.63	22	15.45	0.34
SP-SI-29-17	598290	7563892	01-02-2017		Spring	21.5	7.22	220	44	2.01	6.28	78	8.59	2.762	2.81	19.6	14.81	0.31
SP-SI-31-17	596773	7563900	02-02-2017		Spring	19.1	7	210	75	2.32	6.55	82	8.73	2.907	3.71	26.6	16.17	0.44
SPW-DQN-SI-16	599090	7563871	21-12-2016		Well	20.7	7.6	309	150	1.86	9.8	170.31	21.89	10.3	5.07	30.7	21.09	0.32
PW-BO-A-16	600185	7565278	21-12-2016	50	Well	18.9	8.15	430	586	9.8	5.86	206.91	24.99	13.9	5.11	29.3	26.7	0.35
PW-BO-B-16	600185	7565278	21-12-2016	75	Well	17.7	7.94	430	152	5.36	11.03	201.18	24.9	12.7	4.99	28	24.79	0.3
CW-BO-A-16	600175	7565267	21-12-2016	55	Well	16.9	8.48	-	148	7.29	13.69	181.78	21.57	11.89	4.9	29.6	26.12	0.58
CW-BO-B-16	600175	7565267	21-12-2016	110	Well	16.0	8.56	440	147	6.48	17.13	179.22	22.09	11.66	4.81	29.1	26.51	0.56
PW-UQN-A-16	599346	7564063	21-12-2016	40	Well	19.4	7.94	390	147	2.19	10.35	183.85	23.11	10.47	5.61	32.8	21.97	0.28
PW-UQN-B-16	599346	7564063	22-12-2016	75	Well	20.1	7.29	390	168	4.65	11.33	187.51	22.99	10.44	5.55	32.2	21.73	0.31
MWL-UQN-A-16	600175	7565267	22-12-2016	50	Well	20.3	7.28	390	110	5.35	11.57	181.78	22.69	10.02	5.39	32.1	21.31	0.31
PW-DQN-A-16	598839	7563780	22-12-2016	45	Well	17.40	7.40	370	3.5	17.75	128.34	16.32	7.567	4.16	25.8	4.23	20.5	0.29
PW-DQN-B-16	598839	7563780	22-12-2016	35	Well	17.70	7.65	320	102	3.39	19	129.93	16.45	7.302	4.23	27.2	20.5	0.29
MW-DQN-A-16	598841	7563769	22-12-2016	35	Well	19.5	7.52	360	137	2.58	11.73	167.14	20.93	9.243	5.22	28.5	22.06	0.29

Table 1. Location, field parameters and chemical data for the rainy season campaign.

Sample ID	Coordinates		Date	Sampling depth (m.b.s.)	Water type	T °C	pH lab	EC lab (µS/cm)	Alkalinity (mg/l of CaCO3)	Cl	SO ₄	HCO ₃	Ca	Mg	K	Si	Na	NO ₃
	x	y																
R-SI-2-O17	600242	7565357	13-10-2017	-	River	15.8	8.86	178	105	2.25	4.42	85.5	10.16	5.031	2.206	21.01	19.82	0.25
R-Río 1-O17	599411	7564113	12-10-2017	-	River	13.1	8.4	178	169	2.05	5.14	82.3	10.80	5.110	3.074	23.31	19.43	0.26
R-SI-8-O17	599109	7563893	13-10-2017	-	River	14.9	8.49	178	2.03	2.03	4.41	81.2	10.26	4.992	2.667	22.37	19.30	0.23
R-SI-9-O17	599005	7563829	13-10-2017	-	River	17.8	8.02	264	1.87	1.87	7.56	128.3	18.78	9.081	3.917	29.41	20.81	0.30
SPW-DQN-SI-O17	599093	7563881	11-10-2017	63	Well	21.4	7.71	292	158	1.72	8.27	157.1	24.63	11.890	5.729	34.09	22.71	0.33
PW-BO-A-O17	600185	7565278	12-10-2017	45	Well	17	7.71	342	168	1.86	7.84	174.2	25.77	13.092	5.372	31.44	24.36	0.32
PW-BO-B-O17	600185	7565278	12-10-2017	70	Well	17.2	7.75	344	168	1.81	7.10	174.2	25.89	13.231	5.385	31.92	24.55	0.35
PW-UQN-A-O17	599346	7564063	12-10-2017	40	Well	19	7.74	335	121	1.75	8.44	150.7	24.57	11.431	5.824	35.28	22.57	0.33
PW-UQN-B-O17	599346	7564063	12-10-2017	70	Well	19.4	7.7	324	169	1.76	8.73	162.5	25.26	11.768	6.282	35.66	23.45	0.33
MWL-UQN-A-O17	599325	7564072	13-10-2017	40	Well	19.1	7.65	312	174	1.74	8.88	156.1	24.74	11.379	4.752	35.40	22.63	0.33
PW-DQN-A-O17	598839	7563780	13-10-2017	40	Well	17.2	7.68	226	1.97	1.97	7.30	100.5	15.02	7.432	4.048	28.48	19.68	0.32
PW-DQN-B-O17	598839	7563780	13-10-2017	30	Well	17.1	7.71	225	1.93	1.93	7.34	94.1	15.12	7.544	4.217	28.61	20.08	0.31
MW-DQN-A-O17	598841	7563769	11-10-2017	39	Well	18.7	7.8	277	133	1.79	8.30	133.6	21.23	9.973	5.103	31.97	20.73	0.32
R-SI-2-O17	600244	7565351	12-10-2017	-	River	15.8	8.86	178	105	2.25	4.42	85.5	10.16	5.031	2.206	21.01	19.82	0.25
R-SI-3-O17	599184	7563959	12-10-2017	-	River	12.3	8.26	169	72	2.09	5.64	80.2	10.65	5.025	2.634	22.62	18.96	0.26
R-SI-4-O17	597906	7564078	13-10-2017	-	River	18.6	8.79	247	1.95	1.95	7.08	113.3	17.84	8.528	4.342	29.06	20.51	0.23
R-SI-7-O17	596623	7563895	13-10-2017	-	River	17.2	8.96	253	1.74	1.74	6.90	103.7	15.87	7.507	4.259	28.22	19.59	0.14
SP-SI-1-O17	599930	7564920	12-10-2017	-	Spring	15.1	7.97	149	115	2.09	4.90	80.2	10.94	5.109	2.817	23.62	16.84	0.35
SP-SI-5-O17	597510	7564339	11-10-2017	-	Spring	19.8	8.51	69.6	25	1.20	5.74	28.9	4.25	2.361	2.698	22.13	9.96	0.29
SP-SI-8-O17	596886	7564858	11-10-2017	-	Spring	18.3	7.84	97.5	32	1.07	8.44	26.7	4.32	1.417	1.745	22.45	11.45	0.28
SP-SI-9-O17	597089	7564260	12-10-2017	-	Spring	13.9	7.5	89.2	89	1.07	6.96	29.3	4.77	2.283	2.212	22.05	10.32	0.28
SP-SI-10-O17	600095	7563296	13-10-2017	-	Spring	13.7	8.29	379	87	1.92	13.63	90.9	16.31	7.570	7.883	34.36	13.05	0.21
SP-SI-16-O17	599934	7564889	12-10-2017	-	Spring	14.4	8.13	142.4	87	1.93	5.00	73.8	9.84	4.601	2.116	22.95	16.78	0.35
SP-SI-17-O17	599874	7564763	13-10-2017	-	Spring	15.7	8.3	132	82	2.00	4.21	55.6	7.15	3.158	2.334	20.52	15.57	0.36
SP-SI-18-O17	599762	7564581	13-10-2017	-	Spring	14.6	8.13	140	82	1.90	4.73	57.7	7.42	3.479	2.517	21.58	15.57	0.34
SP-SI-19-O17	599603	7564355	12-10-2017	-	Spring	15.3	8.24	138	82	1.90	4.81	57.7	7.52	3.496	2.222	21.44	15.83	0.39
SP-SI-27-O17	599608	7564362	12-10-2017	-	Spring	15	8.7	148	105	1.94	4.87	64.1	8.60	4.030	2.556	22.53	15.60	0.33
SP-SI-28-O17	599899	7564804	13-10-2017	-	Spring	14.8	8.27	138	192	1.92	4.79	56.7	7.33	3.145	2.440	20.82	15.50	0.32
SP-SI-29-O17	598290	7563894	13-10-2017	-	Spring	18	8.24	175	2.76	2.76	5.60	72.7	9.66	3.853	4.455	22.78	16.98	0.31
SP-SI-31-O17	596769	7563906	13-10-2017	-	Spring	18.5	8.01	123	123	1.87	5.71	74.8	9.74	3.958	2.106	29.42	17.77	0.30
SP-SI-32-O17	597475	7564106	13-10-2017	-	Spring	18	8.95	244	1.85	1.85	7.42	106.9	14.24	6.948	3.712	24.34	17.60	0.24

Table 2. Location, field parameters and chemical data for the dry season campaign.

Piper diagrams were used to summarize the main contrasts in chemical composition between the different types of water in the Chilean part of the catchment. These diagrams are similar for the rainy and dry season, so the Piper diagram for the dry season is used for the data discussion (Figure 6). The Piper diagram for the rainy season is presented in Appendix E. The Piper diagram shows that all the waters have a very similar anionic composition excepting the waters of the springs located in the lower course of the Silala River in Chile (SP-SI-5, SP-SI-8 and SP-SI-9). The main anion is bicarbonate with slightly more sulfate in the springs of this lower part of the Silala River. The cationic compositions of the analyses plot more or less along a line with the spring waters located in the northern part of the Chilean lower river course, plotting towards the high sodium end of the line compared to the borehole waters and the Quebrada Negra spring water, which have a higher calcium content.

The waters in the Silala River basin in Chile are all either Sodium (Na) Bicarbonate or Calcium (Ca) Bicarbonate water type. The spatial variation of the waters' chemical composition can be better visualized using Stiff diagrams. The Stiff diagram consists of a polygonal shape of three parallel horizontal axes extending on either side of a vertical zero axis. Cations are plotted in milliequivalents on the left side of the zero axes, one to each horizontal axis, and anions are plotted on the right side. The Stiff diagrams do not show significant differences between the chemical composition of the waters sampled in the dry season and those sampled in the rainy season. The Stiff diagrams for the rainy season are presented in Appendix E and the Stiff diagrams for the dry season presented in Figure 7 are used for the discussion of the chemical data.

The Silala River and all but one of the springs in Chile are Na-Bicarbonate type water with relatively high content of Ca, and in general no significant differences are observed between the springs located in the upper or lower part of the river course in Chile. The exception is the Quebrada Negra spring SP-SI-10-O17, which besides Na and Ca, is also characterized by a relatively high proportion of Magnesium (Mg). The groundwaters of wells sampled in Chile, which are Ca-Bicarbonate type water, tend to have a different chemical composition to the river and spring waters. The high Na and Ca content is probably related to weathering of silicate minerals, which is supported by the high silica content of these waters, which ranges between 18 and 37 mg/L (Tables 1 and 2).

The chemical data have shown that the spring system located near the river in the upper part of the river course in Chile does not have the chemical fingerprint associated with groundwater discharge of the deep, perhaps regional, aquifer system. This pattern suggests that the springs are part of a subsurface flow system associated with a perched aquifer, which drains into the river. The chemical data do not preclude the possible

influence of local recharge for the spring system and the river. The chemistry of the river and springs along the river are clearly related.

A difference in chemical composition is observed in the Silala River in Chile and the groundwater along the river course. This difference is observed below the junction between the Quebrada Negra and the Silala River. The Stiff diagrams show an appreciable difference between the Silala River water R-SI-9-O17 below the junction with the River water above the junction represented by R-SI-3-O17. This pattern is also observed between the groundwater below the junction at PW-DQN-A-O17 and PW-DQN-B-O17 and the groundwater above the junction represented by well SPW-DQN-SI-O17. The waters below the junction tend to have more Mg in comparison to Ca and Na than the water upstream of this junction. This change in chemical composition could be associated with input of water from the Quebrada Negra for which the spring water is characterized by higher Mg content compared to Ca and Na than the rest of the waters found in the Silala River basin in Chile (Figure 7).

A clear difference is observed in the bicarbonate content. In its upper part in Chile, the Silala River is characterized by a range of values between 80 and 128 mg/L, the springs vary between 57 and 100 mg/L and the groundwaters show much higher bicarbonate values between 157 and 206 mg/L. The higher values of bicarbonate are due to dissolution of carbonates and possible influence of some input of CO₂ of volcanic origin that has dissolved in the deep groundwater flow system.

Figure 8 presents the Stiff diagrams of the waters of springs, wells and the Silala River sampled in both Chile (rainy season) and Bolivia. The waters of the springs located in the northern part of the Silala River in Bolivia (Cajones ravine) are characterized by low salinity ranging between 113 and 129 $\mu\text{S}/\text{cm}$ (Appendix F), which is similar to the springs located in the northern part of the Silala River in Chile (Tables 1 and 2). These samples correspond to points SP-SI-8-17, SP-SI-18-17 and SP-SI-19-17 in Chile and to samples SI-1A, SI-7, SI-6 and SI-1 in Bolivia. The groundwater in the Cajones ravine is also characterized by low salinity similar to the spring waters (Appendix F). The groundwater was collected from shallow piezometers, DS-24S (2-4 m) and DS-24P (7.2-8.2 m).

All these samples tend to be Na-Ca bicarbonate type as shown in the Stiff diagrams.

Much more saline spring waters, ranging between 254 and 394 $\mu\text{S}/\text{cm}$, are observed in the easternmost part of the Silala River basin, in the Orientales wetland in Bolivia (samples SI-3 and SI-8, see Appendix F). The groundwater in the Orientales wetland has also relatively high salinity, similar to the springs. The groundwater in the Orientales wetland was collected from shallow piezometers, DS-4S (5-10 m), DS-8 (8.7-14.8 m). These spring waters in the Orientales ravine have much higher salinity

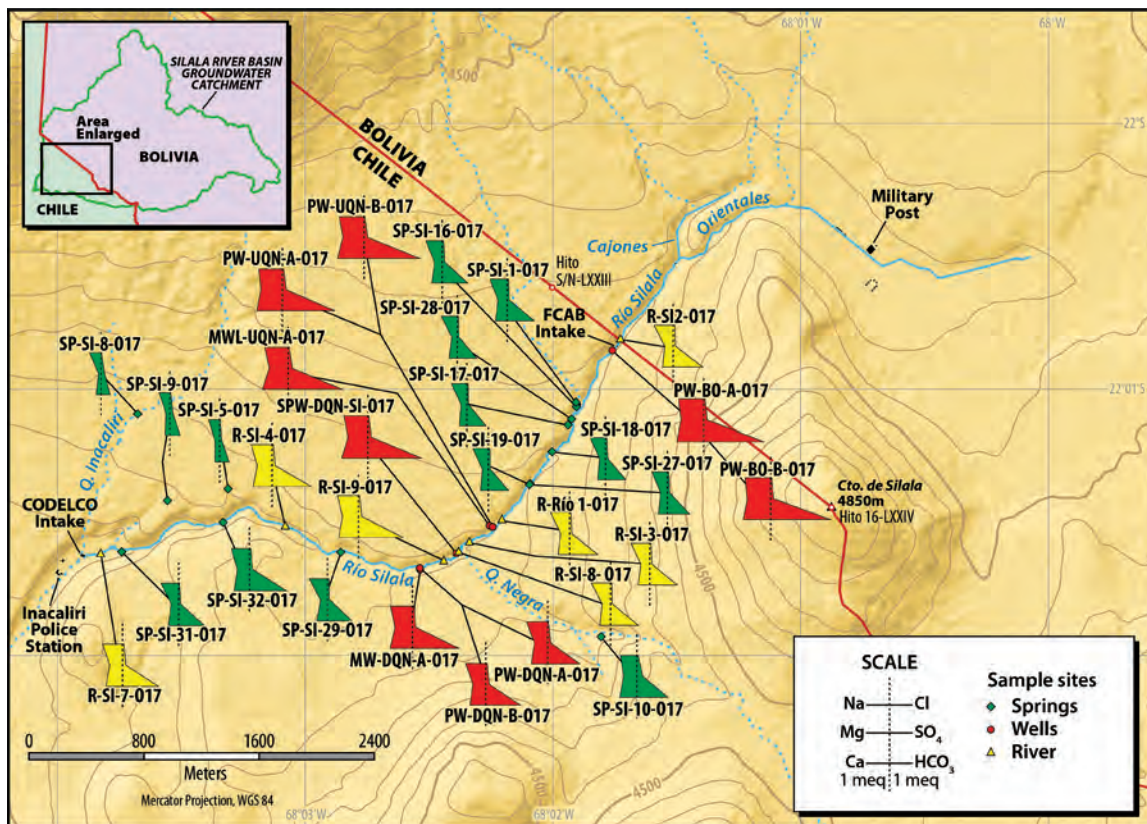


Figure 7. Modified Stiff diagrams of the waters from Silala River area in Chile in the dry season.

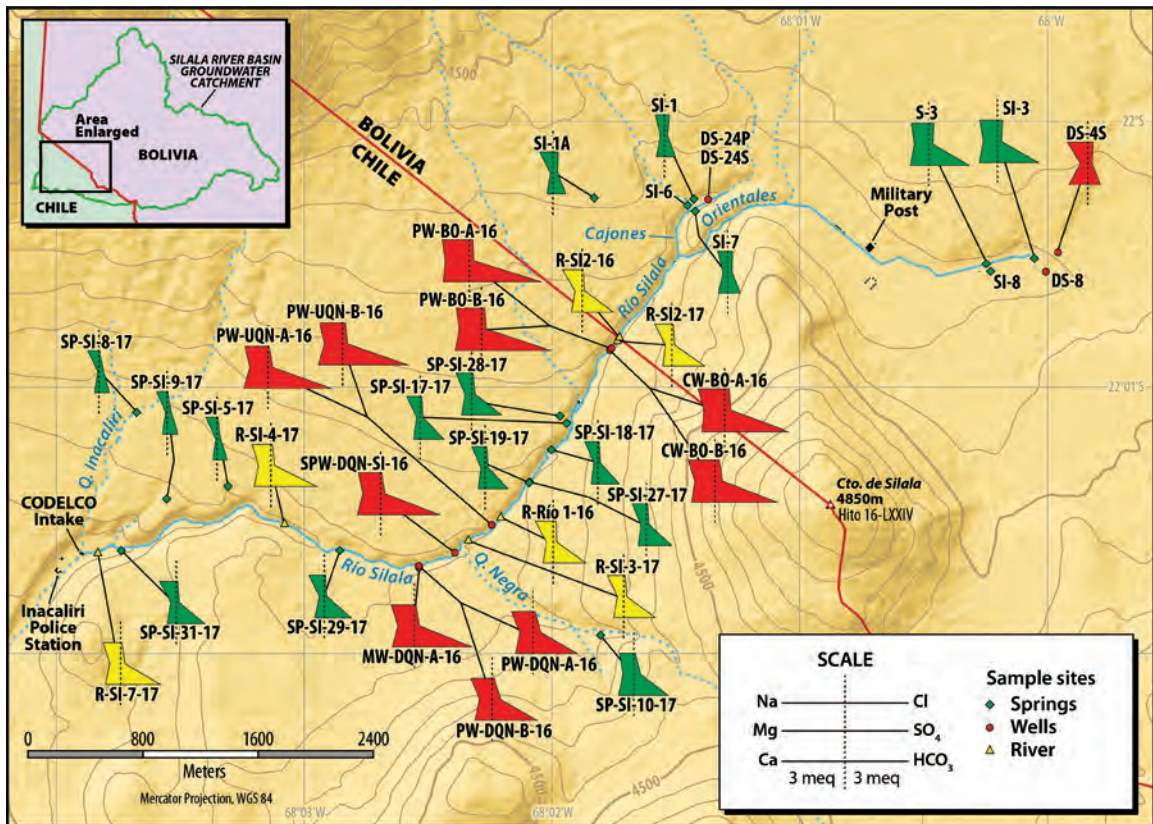


Figure 8. Modified Stiff diagrams of the waters from Silala River area in Chile (rainy season) and Bolivia.

2.2 Environmental isotope data

This section focuses on the evaluation of environmental isotope data collected from springs, river and wells in the study area. The stable isotopes used in this research were ^{18}O , ^2H and ^{13}C , while the radioactive isotopes were tritium (^3H) and carbon 14 (^{14}C). Isotopic sampling was carried out in both the dry season and the rainy season. The ^{18}O and ^2H provide information about the origin of groundwater, and therefore are used for evaluation of recharge areas, and ^3H and ^{14}C provide information about groundwater residence time. Carbon 13 (^{13}C) provides information about geochemical reactions that can affect the dissolved inorganic carbon (DIC) through the groundwater flow system (Clark and Fritz, 1997). These tracers have been extensively used in groundwater studies in Northern Chile (Magaritz et al., 1989; Aravena and Suzuki, 1990; Herrera et al., 2006; Uribe et al., 2015).

2.2.1 $\delta^{18}\text{O}$ and $\delta^2\text{H}$ data

The isotope data for the river, springs and groundwater from wells collected during the rainy season and dry season campaigns in Chile are reported in Tables 3 and 4, respectively. One key aspect that needs to be defined to allow the interpretation of the isotope data, using the typical diagram of $\delta^2\text{H}$ vs $\delta^{18}\text{O}$, is the local meteoric water line, which reflects the isotopic composition of the precipitation in the study area. A description of the preparation of the local meteoric water line is described below.

The isotopic characterization of precipitation has been made using data from the city of La Paz for the period 1995-2009 (International Atomic Energy Agency (IAEA)) and from precipitation data corresponding to different locations in northern Chile. Most of the northern Chile data were obtained from Aravena et al. (1999), which relate to locations higher than 4000 m.a.s.l. Precipitation data from the city of La Paz have been used because of the continuous monitoring of the precipitation isotopic composition (IAEA/World Meteorological Organization (WMO)) and the large amount of information available for the different months of the year. All samples show a good correlation between $\delta^{18}\text{O}$ and $\delta^2\text{H}$ at all sampling points, regardless of the proximity to the study area. Having discarded the rain samples that were suspected of being affected by evaporation, a local meteoric line has been calculated by linear interpolation using least squares which has the following expression: $\delta^2\text{H} = 7.9\delta^{18}\text{O} + 14$. A special characteristic of the precipitation in Northern Chile is the existence of an isotopic gradient with altitude where the high-altitude rainfall tends to be isotopically more depleted than rainfall at lower altitude (Fritz et al., 1981; Chaffaut, 1998; Aravena et al., 1999; Uribe et al., 2015). This explains the rationale behind the use of environmental isotopes in water resource studies in the Northern Chile, Bolivian and Peruvian Altiplano regions.

Figure 9 and Figure 10 show these data compared with the global meteoric water line ($\delta^2\text{H} = 8\delta^{18}\text{O} + 10$) and the local meteoric water line ($\delta^2\text{H} = 7.9\delta^{18}\text{O} + 14$). A clear pattern is observed in these data. The springs located in the upper course of the river in Chile have a different isotope fingerprint to the springs located in the northern part of the lower course of the river (Figure 9 and Figure 10). The lower course springs plot near the local meteoric water line with higher deuterium excess values (around 15‰) while the upper springs in Chile are located below the local meteoric water line. Based on the isotope data, the springs in the northern part of the lower course of the river in Chile should represent local recharge. Furthermore, the data showed that some springs located in the southern part of the lower river course in Chile showed a similar isotopic fingerprint to the upper river course springs. This pattern suggests that these springs are part of the same hydrogeological system that generates the springs in the upper course of the river in Chile and/or part of a subsurface flow system fed by groundwater

discharge associated with the Quebrada Negra valley, represented by the spring SP-SI-10-17, which has an isotopic composition in the range of the upper river course springs.

Concerning the river waters, they have a similar isotopic fingerprint to the upper springs in Chile and the lower springs located in the southern part of the river (Tables 4 and 5), therefore they plot in the same group. This is observed in the data collected in both the rainy and dry season. The isotope data indicate that both types of water have a similar origin. The isotopic data for the groundwater in both seasons also plotted as part of the river and upper springs group, which suggests that all these waters are associated with recharge areas at similar altitudes. However, the deep groundwater in the dry season tends to separate from the group with isotope values slightly more depleted than the river and the springs. This can imply that the regional aquifer is recharged at higher altitude than the river and springs in Chile. The isotope composition of these waters is all plotted below the local meteoric water line, which is a typical feature for groundwater and springs in Northern Chile (Fritz et al., 1981; Magaritz et al., 1989; Uribe et al., 2015). This pattern has been associated with evaporation during the waters' residence time in the unsaturated zone (Magaritz et al., 1989). Therefore, assuming a slope of 3 for the evaporation line in soil (Clark and Fritz, 1997) and extrapolating the data using this slope, the evaporation line would intersect the local meteoric water line around $-14,5\text{‰}$ of $\delta^{18}\text{O}$, which is within the range of isotope values measured for precipitation above 3500 m.a.s.l (Aravena et al., 1999; Uribe et al., 2015).

The isotope data indicate that the river, the upper springs in Chile and the groundwater are part of a regional flow system mainly recharged in the high Andes of Bolivia, which is supported by the location of the river headwaters. However, some springs identified in the Chilean side of the Silala River basin may correspond to more local flow systems.

Based on the isotope and chemical data, it is clear that the river and upper spring waters in Chile could be closely related. It seems likely that the origins are from recharge to a perched series of aquifers overlying the Silala Ignimbrite and possibly the Cabana Ignimbrite and the widespread andesitic lava flow (SERNAGEOMIN, 2017) that forms the eastern edge of the Orientales wetland. The water stored in these subsurface perched units moves through alluvial deposits (Arcadis, 2017; SERNAGEOMIN, 2017) or horizontal fractures in the near surface levels of the ignimbrites. The water level data obtained in the new wells drilled in the deeper aquifer, as part of the hydrogeological investigation (Arcadis, 2017), which showed the water level in the Ignimbrite aquifer is lower than the river water level, tend to support this hypothesis.

Sample ID	Water type	$\delta^{18}\text{O}$ VSMOW (‰)	$\delta^2\text{H}$ VSMOW (‰)
R-SI-02-16	River	-11.47	-91.7
R-Rfo 1-16	River	-11.50	-91.3
R-SI-2-17	River	-11.61	-92.5
R-SI-3-17	River	-11.64	-91.8
SP-SI-01-16	Spring	-11.67	-91.6
SP-SI-21-16	Spring	-10.92	-82.1
SP-SI-5-16	Spring	-11.54	-82.7
SP-SI-1-17	Spring	-11.84	-92.6
SP-SI-5-17	Spring	-11.72	-82.9
SP-SI-8-17	Spring	-12.04	-83.7
SP-SI-9-17	Spring	-12.01	-84.0
SP-SI-10-17	Spring	-11.72	-89.4
SP-SI-15-17	Spring	-11.83	-92.4
SP-SI-16-17	Spring	-11.82	-92.3
SP-SI-17-17	Spring	-11.77	-91.9
SP-SI-18-17	Spring	-11.77	-91.8
SP-SI-19-17	Spring	-11.79	-91.5
SP-SI-27-17	Spring	-11.80	-91.8
SP-SI-28-17	Spring	-11.78	-92.3
SP-SI-29-17	Spring	-11.73	-91.4
SP-SI-31-17	Spring	-11.72	-90.2
SPW-DQN-SI-16	Well	-11.95	-93.2
PW-BO-A-16	Well	-11.97	-93.9
PW-BO-B-16	Well	-11.91	-92.2
CW-BO-A-16	Well	-11.89	-93.5
CW-BO-B-16	Well	-11.87	-93.5
PW-UQN-A-16	Well	-11.95	-92.9
PW-UQN-B-16	Well	-11.97	-93.2
MWL-UQN-A-16	Well	-11.9	-92.6
PW-DQN-A-16	Well	-11.73	-91.7
PW-DQN-B-16	Well	-11.77	-92.0
MWL-DQN-A-16	Well	-11.85	-92.5

Table 3. Stable isotope results of the rainy season samples.

Sample ID	Water type	$\delta^{18}\text{O}$ VSMOW (‰)	$\delta^2\text{H}$ VSMOW (‰)
R-SI-2-O17	River	-12.15	-93.6
R-RIO-1-O17	River	-12.09	-92.9
R-SI-3-O17	River	-12.09	-92.8
R-SI-8-O17	River	-12.05	-92.9
R-SI-9-O17	River	-12.32	-93.1
R-SI-4-O17	River	-12.26	-93.1
R-SI-7-O17	River	-11.98	-90.0
SP-SI-10-O17	Spring	-12.21	-90.8
SP-SI-28-O17	Spring	-12.20	-92.8
SP-SI-16-O17	Spring	-12.22	-93.0
SP-SI-17-O17	Spring	-12.20	-92.4
SP-SI-18-O17	Spring	-12.18	-92.8
SP-SI-19-O17	Spring	-12.10	-91.4
SP-SI-27-O17	Spring	-12.23	-92.7
SP-SI-1-O17	Spring	-12.25	-93.1
SP-SI-32-O17	Spring	-12.19	-92.4
SP-SI-5-O17	Spring	-12.03	-84.3
SP-SI-8-O17	Spring	-12.41	-84.0
SP-SI-9-O17	Spring	-12.40	-84.1
SP-SI-31-O17	Spring	-12.13	-91.8
SP-SI-29-O17	Spring	-12.08	-92.0
SPW-DQN-SI-O17	Well	-12.54	-94.6
PW-BO-B-O17	Well	-12.53	-95.1
MWL-UQN-A-O17	Well	-12.48	-94.6
PW-UQN-A-O17	Well	-12.51	-94.6
PW-UQN-B-O17	Well	-12.55	-94.9
MW-DQN-A-O17	Well	-12.44	-93.9
PW-DQN-A-O17	Well	-12.30	-93.2
PW-DQN-B-O17	Well	-12.30	-93.3
PW-BO-A-O17	Well	-12.52	-95.0

Table 4. Stable isotope results of the dry season samples.

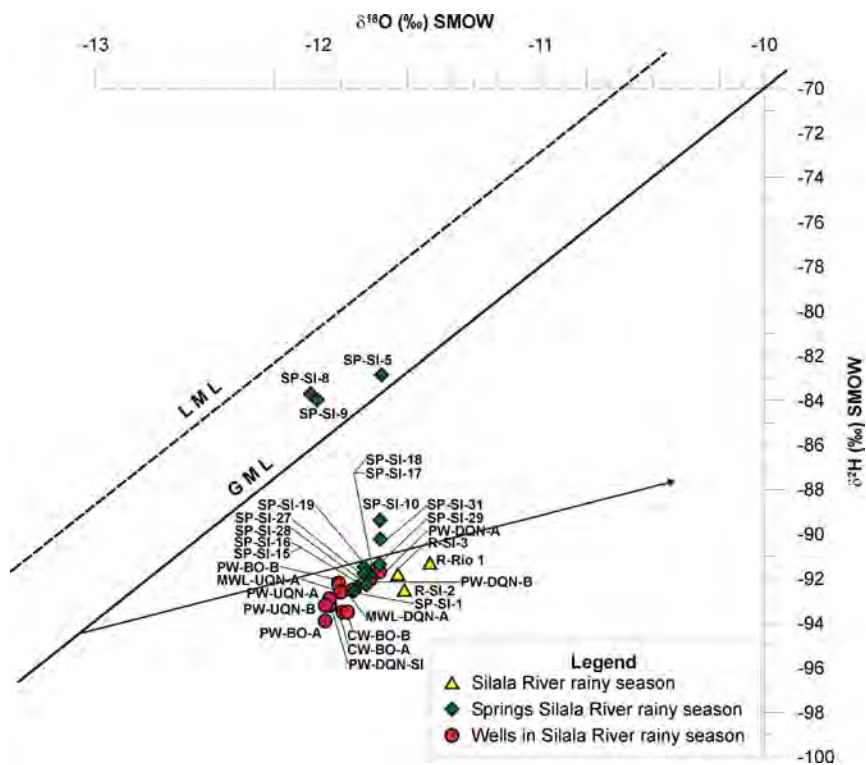


Figure 9. Plot of $\delta^{18}\text{O}$ and $\delta^2\text{H}$ for river, spring water and wells water in the rainy season.

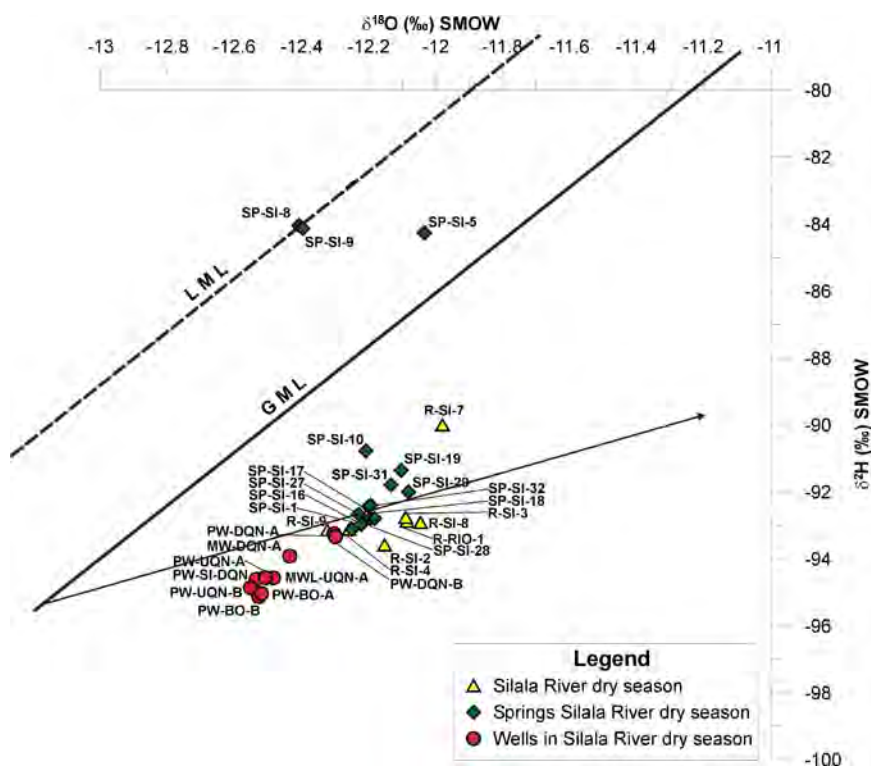


Figure 10. Plot of $\delta^{18}\text{O}$ and $\delta^2\text{H}$ for river, spring water and wells water in the dry season.

2.2.2 Tritium data

The interpretation of tritium data in groundwater requires a reconstruction of the tritium content of the precipitation during the last seven decades. One of the difficulties in reconstructing the tritium input function in the study area is the lack of continuous monitoring of tritium activity in rainwater from 1954 to the present. In South America, there is no observation station with a continuous series of data. The most complete data are from Porto Alegre and Rio de Janeiro, which are part of the IAEA monitoring network. There are four observation stations at a latitude relatively close to the Silala area. These are Cuzco (3246 m.a.s.l.) in Peru, La Paz (4071 m.a.s.l.) in Bolivia, and Los Molinos (1300 m.a.s.l.) and Salta (1187 m.a.s.l.) in Argentina (Herrera et al., 2006) (Figure 11). To reproduce the tritium input function, it is necessary to know its concentrations in rainwater since 1953, when thermonuclear tests were initiated in the atmosphere. The period between 1954 and 1968 of the series was completed with tritium data from Porto Alegre and Rio de Janeiro, Brazil. The tritium input function for the southern Hemisphere is presented in Figure 11. Based on this figure the tritium data for recent precipitation in the study area should be between 3 and 5 TU.

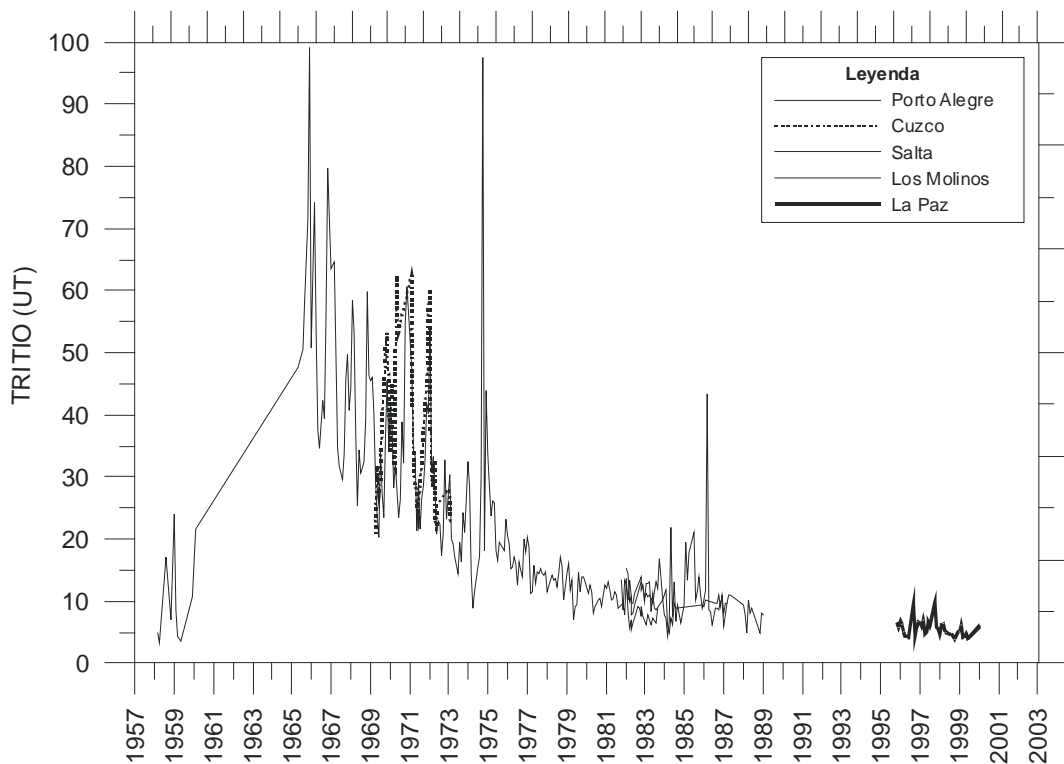


Figure 11. Concentrations of monthly rainwater tritium measured at IAEA stations in the Southern Hemisphere in South America (Herrera et al., 2006).

The tritium data for both rainy and dry seasons are presented in Tables 5 and 6. These data showed that the springs, river water and well waters in Chile basically do not contain tritium, indicating that these waters were recharged before the 1960s. This conclusion is supported by tritium data collected in three springs in Bolivia, which showed nil values of tritium in the Silala River basin in the Bolivian territory (Appendix G).

Sample ID	Collection Date	TU	Water type	$\pm 1\sigma$
PW-BO-B-16	21-12-2016	<0.05	Well	0.23
PW-UQN-B-16	22-12-2016	0.07	Well	0.23
PW-DQN-B-16	22-12-2016	0.22	Well	0.23
R-SI-2-16	20-12-2016	0.16	River	0.23
SP-SI-21-16	21-12-2016	0.18	Spring	0.22
SP-SI-5-16	21-12-2016	< 0.05	Spring	0.19
SP-SI-8-17	01-02-2017	<0.05	Spring	0.2
SP-SI-15-17	31-01-2017	0.31	Spring	0.29
SP-SI-10-17	01-02-2017	<0.05	Spring	0.11
R-SI.7-17	01-02-2017	<0.05	River	0.31

Table 5. Tritium data obtained in rainy season.

Sample ID	Collection Date	TU	Water type	$\pm 1\sigma$
R-SI-2-O17	12-10-2017	< 0.8	River	0.7
R-SI-3-O17	12-10-2017	< 0.8	River	0.8
R-SI-7-O17	13-10-2017	< 0.8	River	0.8
R-SI-8-O17	13-10-2017	< 0.8	River	0.8
R-SI-9-O17	14-10-2017	< 0.8	River	0.8
SP-SI-8-O17	13-10-2017	< 0.8	Spring	0.8
SP-SI-10-O17	14-10-2017	< 0.8	Spring	0.7
SP-SI-18-O17	13-10-2017	< 0.8	Spring	0.7
SP-SI-31-O17	13-10-2017	< 0.8	Spring	0.8
SP-SI-32-O17	14-10-2017	< 0.8	Spring	0.6
SPW-DQN-SI-O17	11-10-2017	< 0.8	Well	0.7

Table 6. Tritium data obtained in dry season.

2.2.3 Carbon-14 and Carbon-13 data

By convention, the radiocarbon dating technique assumes that the ^{14}C content of the atmospheric carbon dioxide (CO_2) was 100 percent modern carbon (pMC) at and before 1950 (before atmospheric nuclear testing) and was constant in the past. For example, if a sample of wood has a ^{14}C content of 50 pMC, which corresponds to half of the initial ^{14}C of the atmospheric CO_2 , then based on the known ^{14}C half-life of 5730 years, it can be estimated that the wood sample has a radiocarbon age of 5730 years before 1950. In the case of groundwater, the ^{14}C gets into the groundwater during dissolution of soil CO_2 during recharge events. The CO_2 from the soil has a ^{14}C content of 100 pMC but during groundwater flow in the aquifer, the ^{14}C content can be affected by the input of old carbon, for example from dissolution of carbonate, from old organic carbon involved in redox processes such as sulfate reduction, or input of volcanic CO_2 in volcanic areas (Clark and Fritz, 1997).

The ^{13}C data provide information about processes and input of old carbon to the dissolved inorganic carbon along the groundwater flow system. $\delta^{13}\text{C}$ values for CO_2 soil in the recharge areas of arid environments can be around -18‰ (Fritz et al., 1981).

In the Chilean part of the Silala basin, the $\delta^{13}\text{C}$ values for groundwater during the rainy season range between -7.3 and -8.0‰, the river waters vary between -8.0 and -9.1‰ and the springs range between -5.8 and -7‰. During the dry season, the groundwater is characterized by $\delta^{13}\text{C}$ values between -6.8 and -7.4‰ and the river showed values between -5.9 and -7.9‰ and the springs range between -5.9 and -9.3‰.

The $\delta^{13}\text{C}$ enrichment pattern observed in the dissolved inorganic carbon compared to the expected $\delta^{13}\text{C}$ value of -18‰ for CO_2 in the recharge area should be associated with dissolution of carbonate minerals during groundwater flow in the aquifer. The other process that could control the ^{13}C content in surface water is isotopic exchange between dissolved CO_2 and atmospheric CO_2 . However, because of the relatively high slope of the Silala River implying fast flow, this process should not be significant. Carbonate minerals tend to have $\delta^{13}\text{C}$ values close to 0‰ (Clark and Fritz, 1997). This also should be reflected in the ^{14}C content, which will be influenced by the input of old carbon from dissolution of carbonate minerals and radioactive decay during groundwater flow in the aquifer. The other factor that could affect the ^{14}C in the study area is some contributions from volcanic CO_2 , which has been documented previously in the Loa River basin (Aravena and Suzuki, 1990). This potential contribution will decrease the ^{14}C of the dissolved inorganic carbon in the groundwater since volcanic CO_2 is devoid of ^{14}C . Typically $\delta^{13}\text{C}$ values for volcanic CO_2 range between -3 and -7‰ (Gerlach and Thomas, 1986; Chivas et al., 1987).

Because of these complications, for this study, the ^{14}C data will not be used to estimate water residence time and it will only be used as a tracer to evaluate the river-groundwater interactions and river-springs interactions. The ^{14}C data from the Silala River area in rainy and dry seasons are reported in Tables 7 and 8, respectively.

The ^{14}C content of the river at the sampling site in Chile near the border (R-SI-2-16, Figure 12) in the rainy season has a ^{14}C value of 26.66 pMC. Downstream, the ^{14}C content of the Silala River before reaching the Quebrada Negra increases to 45.97 pMC (R-SI-3-17, Figure 12). A similar pattern is observed during the dry season. The sampling site in Chile near the border (R-SI-2-O17) showed a value of 31.25 pMC, increasing to a value of 39.15 pMC (R-SI-3-O17) before the junction with the Quebrada Negra (Figure 13). The increase in ^{14}C as the water flows from the upper course to the middle course of the Silala River in Chile is attributed to an increase of the lateral shallow groundwater contributions that have been recharged in the same area of the Silala River. Further down-gradient near the junction with the Quebrada Negra, the ^{14}C content of the river was found to be 39.55 pMC at R-SI-8-O17 and 18.1 pMC at R-SI-09-O17 (Figure 13). Further downstream the river shows an increase to a value of 32.53 pMC in the sampling point (R-SI-7-O17, Figure 13). The large decrease of ^{14}C content in the river after the junction is caused by a contribution from groundwater discharge from the artesian well SPW-DQN-SI-O17, which is characterized by a ^{14}C content of 8.36 pMC (Figure 13). The increase of ^{14}C content in the last part of the river course downstream is due to lateral contribution from the northern and southern part of the basin. There is no information on C-14 values from river samples in the Bolivian study.

The ^{14}C content of the springs located in the upper part of the river course in Chile have values of 32.41 pMC (SP-SI-15-17, Figure 12) and 39.75 pMC (SP-SI-18-O17, Figure 13) during the rainy and dry season, respectively. These values are within the range of ^{14}C content of the river during the rainy and dry season in this part of the basin. A range of values between 23.96 and 34.49 pMC is observed in the springs (SP-SI-29-O17, SP-SI-32-O17 and SP-SI-31-O17, Figure 13) located in the southern lower course of the river in Chile. Much higher ^{14}C values are observed in the springs located in the northern lower part of the river course (SP-SI-5 and SP-SI-8) in the rainy and dry season with respect to the waters of the springs located close to the main course of the Silala River (Table 7 and Table 8). These springs showed values between 67.44 and 78.39 pMC during the rainy and dry seasons (Figure 12 and Figure 13). A high ^{14}C value of 86.29 pMC was also reported in a spring located in the northern part in the Bolivian sector associated with discharge in the foothills of the Cerro Inacaliri (Appendix G). Lower ^{14}C values of 25.67 and 30.67 pMC similar to the springs in the Chilean sector are observed in the springs located in the Orientales wetland in Bolivia (Figure 13). These springs have higher salinity than the northern (Cajones) wetland

springs, but similar to the groundwater from boreholes in Chile. This suggests that the springs are associated with groundwater discharge of a regional groundwater flow system. The spring located in the Quebrada Negra (SP-SI-10), which may represent discharge of a regional flow system, perhaps recharged at higher altitude in Bolivia, has a ^{14}C value of 30.06 pMC and 27.57 pMC during the rainy and dry seasons, respectively (Table 7 and Table 8).

The deep groundwater in Chile is characterized by much lower ^{14}C values than the springs and the Silala River and showed values of 9.93 (PW-BO-B-16) and 14.54 pMC (PW-UQN-B-16) in the rainy season, and 8.36 (SPW-DQN-SI-O17), 9.15 (PW-BO-B-O17), 9.96 (PW-UQN-B-O17), 21.82 (PW-DQN-A-O17) and 22.06 (PW-DQN-B-O17) pMC in the dry season (Figure 12 and Figure 13). The lowest ^{14}C value of 8.36 pMC in the groundwater is observed in the artesian well SPW-DQN-SI-O17, which is flowing under confined conditions.

The ^{14}C data show an increase in ^{14}C content along the groundwater flow system comparing data above and below the junction with the Quebrada Negra. The groundwater increases from 14.54 pMC (PW-UQN-B-16, Figure 12) above the junction to values of 22 pMC below the junction (PW-DQN-A-O17 and PW-DQN-B-O17, Figure 13). This pattern could be associated with a contribution from the Quebrada Negra water, which is characterized by a ^{14}C content of around 29 pMC. Re-interpretation of drill cuttings in borehole MW-DQN (only 15 metres from PW-DQN) has shown that the borehole penetrates only 3 metres of Fluvial deposits and below this 8 metres of Silala ignimbrite before entering Pliocene lavas (SERNAGEOMIN, 2017). Downstream of this point the Silala River flows over bedrock (Silala Ignimbrite) and no fluvial deposits are present. These geological changes may allow that groundwater flow originating from the Quebrada Negra is forced to enter the river along this reach.

The higher salinity and lower ^{14}C of the sampled groundwater compared to the river and springs water indicates that the groundwater is part of a regional groundwater flow system, which is not connected to the river and spring system in Chile. This tends to support the hydrogeological conceptual model developed by Arcadis (2017), which postulated the existence of a confined aquifer in the Silala River area in Chile.

Based on the ^{14}C data, as part of the conclusions in the DHI (2018) report, it is suggested a ***“relatively old age in the southern wetland (up to ~ 11,000 years old) and a significant younger age for the northern wetlands (up to ~ 1,000 years)”*** (BCM, Vol. 4, p. 103). These estimates are not correct since they do not take into account the dilution effect due to dissolution of carbonates along the groundwater flow system and the potential input of volcanic CO_2 , as was explained above.

ID sample	Water Type	$\delta^{13}\text{C}$ (PDB)	^{14}C	
		DIC	pMC	$\pm 1\sigma$
R-SI-2-16	River	-8	26.66	0.13
SP-SI-5-16	Spring	-7	76.86	0.35
PW-BO-B-16	Well	-7.3	9.93	0.08
PW-UQN-B-16	Well	-8	14.54	0.09
R-SI-3-17	River	-9.1	45.97	0.27
SP-SI-8-17	Spring	-6.8	78.39	0.24
SP-SI-15-17	Spring	-5.8	32.41	0.15
SP-SI-10-17	Spring	-6.7	30.06	0.15

Table 7. ^{14}C data for river, springs and wells obtained during the rainy season.

ID sample	Water Type	$\delta^{13}\text{C}$ (PDB)	^{14}C	
		DIC	pMC	$\pm 1\sigma$
R-SI-2-O17	River	-7.3	31.25	0.20
R-SI-3-O17	River	-7.9	39.15	0.31
R-SI-7-O17	River	-5.9	32.53	0.38
R-SI-8-O17	River	-7.9	39.55	0.21
R-SI-9-O17	River	-7.0	18.08	0.20
SP-SI-5-O17	Spring	-6.8	70.66	0.41
SP-SI-8-O17	Spring	-9.3	67.44	0.31
SP-SI-10-O17	Spring	-7.9	27.57	0.18
SP-SI-18-O17	Spring	-6.8	39.75	0.44
SP-SI-29-O17	Spring	-8.7	34.49	0.49
SP-SI-31-O17	Spring	-7.7	29.75	0.34
SP-SI-32-O17	Spring	-5.9	23.96	0.20
SPW-DQN-SI-O17	Well	-6.8	8.36	0.11
PW-DQN-A-O17	Well	-7.4	21.82	0.14
PW-DQN-B-O17	Well	-7.4	22.06	0.15
PW-BO-B-O17	Well	-6.4	9.15	0.11
PW-UQN-B-O17	Well	-7.3	9.96	0.18

Table 8. ^{14}C data for river, springs and wells obtained during the dry season.

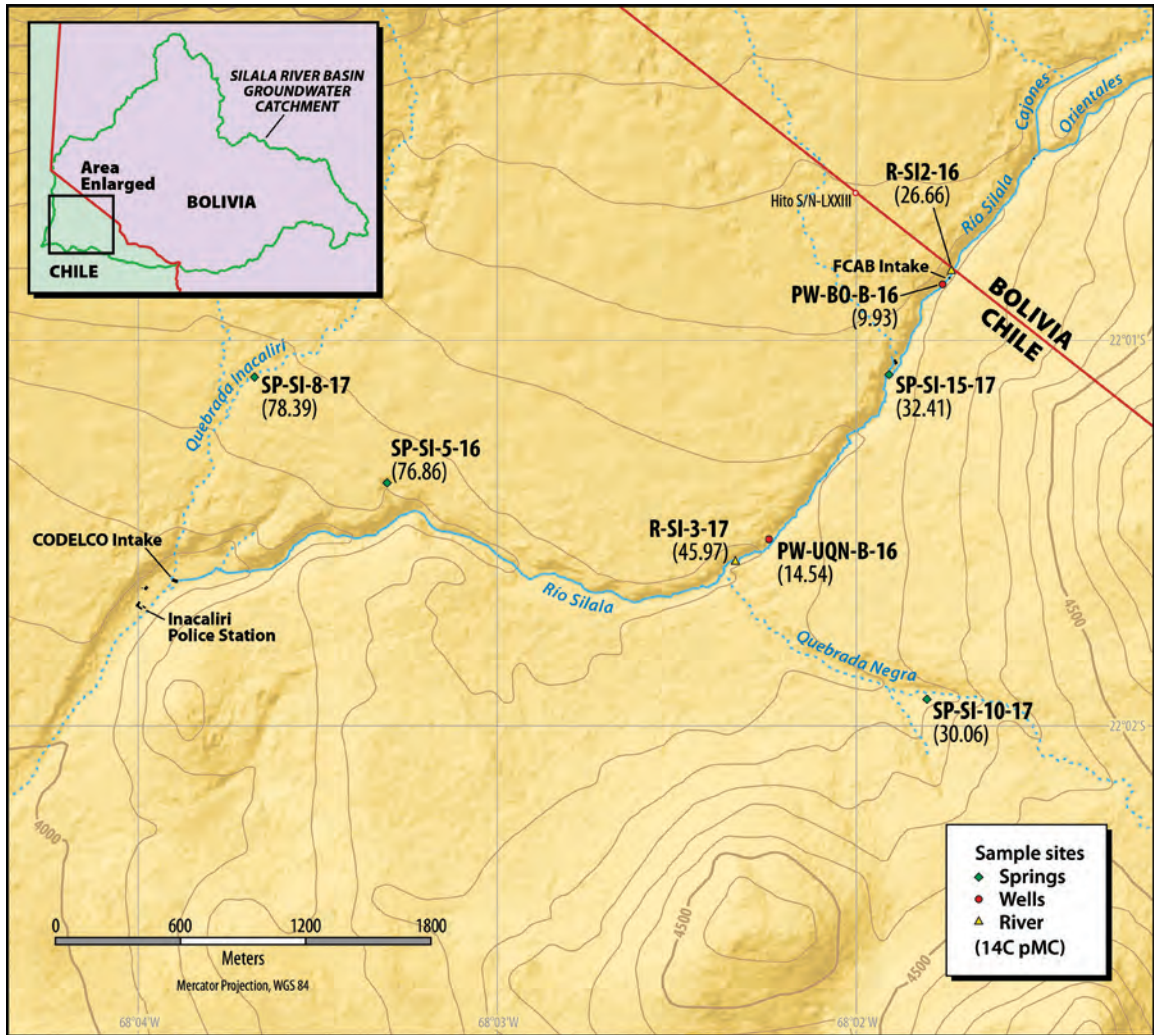


Figure 12. Distribution of ^{14}C sampling points in the Silala River basin in Chile (for the rainy season). This figure is complemented by Table 7, which contains the sample point values.

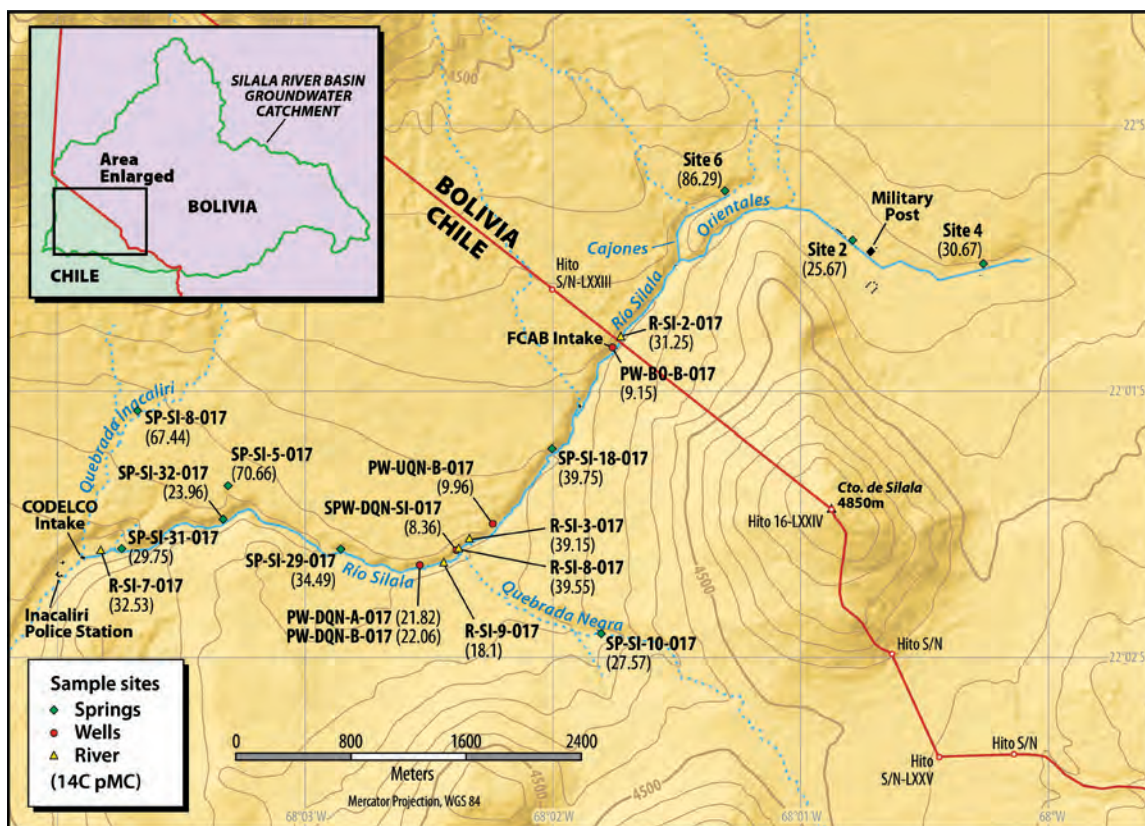


Figure 13. Distribution of ^{14}C sampling points in the Silala River basin in Chile (for the dry season) and Bolivia (Appendix G). This figure is complemented by Table 8, which contains the sample point values for Chilean analyses.

3. CONCLUSIONS

The water of the Silala River is primarily related to spring discharge located in Bolivian territory. The waters enter Chilean territory through the course of the Silala River and through underground flows.

The chemical data show that the river, springs and groundwater of wells are characterized by low salinity. The springs in the upper part of the river course in Chile tend to be more saline than the springs located in the northern side of the lower river course in Chile. The river has similar salinity to the upper springs in Chile, and the groundwater from all wells has a higher salinity than the river and springs. In general, the water is Na-bicarbonate type with differing degrees of Ca content. The groundwater of wells is Ca-Na-bicarbonate type. The high silicate content of these waters indicates that the main source of the chemical composition of the water is weathering of silicate minerals. The chemical data suggest that the springs in the upper part of the river course in Chile are not a reflection of groundwater discharge from the deeper aquifer, indicating that the springs probably emerge from a subsurface flow associated with a perched aquifer.

Springs and groundwater (collected from shallow piezometers) in the Cajones wetland area in the Bolivian sector are characterized by salinity values and a chemical composition similar to the waters of springs located in the northern part of the Silala River in Chile (SP-SI-8, SP-SI-9 and SP-SI-5). Both spring systems seem to be associated to local recharge occurring in the Cerro Inacaliri. Higher salinity than the Cajones waters are observed in springs and groundwater in the Orientales wetland area, which are likely to be associated with discharge from a regional aquifer system. Their salinity and chemical composition are characteristic of the groundwater in the Chilean sector.

The isotopic composition of $\delta^{18}\text{O}$ and $\delta^2\text{H}$ show that the springs located in the northern part of the lower river course in Chile have a different isotopic fingerprint to the springs located in the upper course of the river in Chile, which indicates a different origin. The river water has a similar isotopic pattern to the upper springs in Chile indicating they are likely to have a similar origin. Furthermore, the isotope data show the springs located in the lower southern part of the river in Chile might be similar in origin to the Chilean springs located in the upper river course. This could mean that they are part of the same hydrogeological system and/or part of the subsurface flow system fed by a regional groundwater flow system also associated with the spring discharge in the upper Quebrada Negra. No $\delta^{18}\text{O}$ and $\delta^2\text{H}$ data were reported for the waters in the Bolivian sector, which could be used for comparison with the results obtained in Chile.

The sampled groundwaters in wells tend to have a similar or slightly more depleted isotope composition than the upper springs and the river in Chile. This is interpreted as indicating that these waters were recharged from precipitation falling at a similar altitude and/or from a relatively higher altitude. Based on the chemical and isotope data, visual observation in the field and water level data in the wells compared to the river, this information tends to confirm the hypothesis that the upper springs in Chile are discharging features of a perched aquifer and that the deep water characterized in the wells in Chile would correspond to a confined or semi confined aquifer in the volcanic deposits of regional extent.

The tritium data in upper and lower springs, groundwater and river water show that the tritium concentration is practically nil indicating these waters are not likely to be very recent.

Concerning the ^{14}C data, a wide range in values is observed. The springs representing the lower northern course of the Silala River in Chile, which based on the stable isotope data appear to represent local recharge, showed the highest ^{14}C values ranging between 67.44 and 78.39 pMC. A similar ^{14}C pattern is observed in springs discharging at the foothill of the Cerro Inacaliri in the Cajones area located in the northern part in the Bolivian sector. Both springs systems seem to be associated with recharge in the Cerro Inacaliri area.

The river values in Chile increase from 26.66 and 31.25 pMC in the first sampling location near the border to values of 45.97 and 39.15 pMC before the junction with the Quebrada Negra during the rainy and dry seasons, respectively, indicating some contribution of recent shallow groundwater into the river, related to precipitation events during the rainy season. The river also receives a contribution from groundwater discharge from an artesian well and lateral contributions from downstream northern and southern areas in the lower part of the river course.

The Carbon-14 data of 32.4 and 39.7 pMC obtained for the upper springs in Chile, which is within the range of ^{14}C values of the river, support the conceptual model postulated above based on the isotope, chemical and hydrogeological data. This model includes an interaction between a perched aquifer, probably in alluvial deposits on the flanks of the high mountains, and the river as result of a complex system of fractures present in the near surface levels of Silala Ignimbrite. These waters are likely to be part of a flow system recharged in the high Andes of Bolivia and the flanks of the Volcán Apagado and Cerro Inacaliri in Chile.

In Chile, much lower ^{14}C content is observed in the deep groundwater than the river and springs water. This groundwater is characterized by values of 8.4 and 14.54 pMC in water collected in the wells located in the upper course of the Silala River in Chile. The

^{14}C content in the groundwater increases to values around 22 pMC in the lower course of the Silala River, which could be related to a contribution of water from the Quebrada Negra basin, which is characterized by ^{14}C values around 29 pMC. Low ^{14}C values in the range of values of the groundwater in the Chilean sector are observed in the springs and groundwater in the Orientales area in the Bolivian sector, associated with a regional groundwater flow system.

The lower ^{14}C content of the deep groundwater, beside longer residence time, could reflect input of old carbon from dissolution of carbonates and possible influence of volcanic CO_2 and the latter could partly explain the higher concentration of bicarbonates of the groundwater compared to river and springs waters.

Summarizing, the similarity between the chemical and isotopic composition of the waters of the Silala River and the waters of the Chilean springs indicates that there is a close relationship between the shallow aquifer and the Silala River, so it is likely that a significant contribution to the flow in the river comes from the shallow perched aquifer. The waters of the shallow aquifer would circulate through the alluvial deposits and the Silala Ignimbrite (Arcadis, 2017). However, the waters of the deep aquifer show chemical and isotopic differences to the waters of the shallow aquifer and the Silala River, and contribute to the flow from the Orientales springs. It seems likely that these waters are mixtures of deep groundwater and shallow perched groundwater. Differences in chemical and isotopic composition in the deep confined aquifer system, found in boreholes in Chile indicate that there is no current hydraulic connection between these two systems in Chile. This agrees with the observations made by Arcadis (2017) that assign a confined character to the waters of the deep aquifer.

4. REFERENCES

- Aravena, R. and Suzuki, O., 1990. Isotopic evolution of rivers in Northern Chile. *Water Resources Research*, 26 (12), 2887-2895.
- Aravena, R., Suzuki, O., Peña, H., Pollastri, A., Fuenzalida, H. and Grilli, A., 1999. Isotopic composition and origin of the precipitation in Northern Chile. *Applied Geochemistry*, 14 (4), 411-422.
- Arcadis, 2017. *Detailed Hydrogeological Study of the Silala River. (Chile's Memorial, Vol. 4, Annex II).*
- Chaffaut, I., 1998. *Precipitations d'Altitude, Eau Souterraines et Changements Climatiques de L'Altiplano Nord-Chile.* Universite de Paris Sud U.F.R. Scientifique D'Orsay. Paris, France.
- Chivas, A.R., Barnes, I., Evans, W.C., Lupton, J.E. and Stone, J.O., 1987. Liquid carbon dioxide of magmatic origin and its role in volcanic eruptions. *Nature*, 326, 587-589.
- Clark, I.D. and Fritz, P., 1997. *Environmental Isotopes in Hydrogeology.* Lewis Publishers, Boca Raton, Florida, pp. 342.
- Custodio, E. and Llamas, M.R., 1983. *Hidrología subterránea.* Omega. Barcelona.
- Danish Hydraulic Institute (DHI), 2018. *Study of the flows in the Silala Wetlands and Springs System (Bolivia's Counter-Memorial, Volume 4, Annex 17).*
- Fritz, P., Suzuki, O., Silva, C. and Salati, E., 1981. Isotope hydrology of groundwaters in the Pampa del Tamarugal, Chile. *Journal of Hydrology*, 53, 161-184.
- Gerlach, T.M. and Thomas, D.M., 1986. Carbon and sulphur isotopic composition of Kilauea parental magma. *Nature*, 319, 480-483.
- Herrera, C. and Aravena, R., 2017. *Chemical and Isotopic Characterization of Surface Water and Groundwater of the Silala River Transboundary Basin, Second Region, Chile. (Chile's Memorial, Vol. 4, Annex III).*
- Herrera, C., Pueyo, J., Sáez, A. and Valero-Garcés, B., 2006. Relación de aguas superficiales y subterráneas en el área del lago Chungará y lagunas de Cotacotani, norte de Chile: Un estudio isotópico. *Revista Geológica de Chile*, 33 (2), 299-325.
- IAEA/WMO, 2015. Global Network of Isotopes in Precipitation (GNIP). Available at: <https://www.iaea.org/services/networks/gnip>.
- Latorre, C. and Frugone, M., 2017. *Holocene Sedimentary History of the Río Silala (Antofagasta Region, Chile). (Chile's Memorial, Vol. 5, Annex IV).*

Magaritz, M., Aravena, R., Pena, H., Suzuki, O. and Grilli, A., 1989. Water chemistry and isotope study of streams and springs in northern Chile. *Journal of Hydrology*, 108, 323-341.

SERNAGEOMIN (National Geology and Mining Service), 2017. *Geology of the Silala River Basin. (Chile's Memorial, Vol. 5, Annex VIII).*

Uribe, J., Muñoz, J.F., Gironás, J., Oyarzún, R., Aguirre, E. and Aravena, R., 2015. Assessing groundwater recharge in an Andean closed basin using isotopic characterization and a rainfall-runoff model: Salar del Huasco basin, Chile. *Hydrogeology Journal*, 23, 1535-1551.

APPENDIX A

Materials used in the sampling events included:

- Notebook and pencil.
- Containers for sampling.
- Ice Packs.
- Transparent adhesive tape.
- Scissors or carton.
- Container or bottle for measurements of physical and chemical parameters in situ.
- Equipment for in situ measurements (pH meter, conductivity meter, thermometer).
- Replacement batteries.
- Measuring tape.
- Photographic camera.
- Bailer for manual sampling with rope (optional).
- Submersible pump, controller and generator in case the sampling is carried out through the well drain.
- Latex gloves.
- Distilled water for the washing of the multiparameter probes.

The containers used for each sampling point is listed below as a reference.

- 1 plastic container of 1000 mL without additives, labeled for analysis of General Parameters.
- 1 plastic container of 500 - 1000 mL with additive included (H_2SO_4) inside, labeled for nutrient analysis.
- 1 plastic container of 500 mL with additive included (NaOH) inside, labeled for cyanide analysis.
- 1 500 mL plastic container with additive included (HNO_3) inside, labeled for total metal analysis.
- 1 plastic container of 250 - 500 mL without additives, labeled for total suspended solids (SST) analysis.
- 1 plastic container of 250 mL without additives, labeled for analysis of dissolved metals.
- 1 plastic container with double lid of 100 - 250 mL, without additives, labeled for isotopic analysis of deuterium ($\delta^2\text{H}$) and oxygen ($\delta^{18}\text{O}$) of the water.

Each of these containers was labeled with the following information:

- Name of the sample.

- Date of sampling.
- Place of sampling (basin or place name or coordinates, etc.)
- Type of sample (groundwater, surface, residual, precipitation, etc.)

At each of the sampling points mentioned above, the following in situ parameters were measured:

- pH
- Conductivity
- Alkalinity
- Temperature

After sampling, the following information was entered on a spreadsheet:

- Sampling time
- Indicate the characteristics of the sample taken, whether it is filtered or not, and whether it contains preservatives or additives, and label with the type of additive.
- The label of each container is protected with thick transparent tape to prevent it from getting wet and deforming or erasing the labeled information.

The field pH measurement was performed using a Hanna portable pH/mV meter, model HI9124, which has a precision range of ± 0.01 pH unit. The same equipment was used to measure temperature, which has a precision range of ± 0.4 °C. The equipment was calibrated before obtaining the first sample of each day, using two buffers, 4 and 7. The field conductivity was measured using a Hanna multi-range portable conductivity meter with waterproof temperature compensation, model HI-9033. This equipment has a precision range of $\pm 1\%$. Finally, the alkalinity was measured with the "Digital Tester - Water Alkalinity Checker HI772", which performs the measurements using the colorimetric method. Since this alkalinity measurement methodology is not validated, the value obtained in the field will only be used as a reference for those obtained in the laboratory and by the modeling, considering the concentrations of HCO_3 . For water filtration, a 0.45 mm filter was used, along with a Geotech Geopump™ Series I and II peristaltic pump, which are designed for single or multiple stage pressure or liquid suction.

In the case of carbon 14 sampling, these steps were followed:

- The water was taken from the mouth of the well, spring, or river.
- Before collecting the sample, the water was allowed to flow for a sufficient time so that the collected water comes directly from the aquifer, spring, or river.
- The bottle was filled but leaving the neck of the bottle empty to allow the liquid to expand during transport. During this step the peristaltic pump with the filter was used.
- Adhesive tape was placed around the cap to prevent exchange or loss of CO_2 from the water.

APPENDIX B

Pictures of some of the sampling locations for the second field campaign:



Picture B1. Sampling of the spring SP-SI-5-17. The up gradient area was under vegetation, so the whole sample set was filtered using the peristaltic pump to avoid any type of contamination.



Picture B2. The Silala River sample point, just across the Chile-Bolivia boundary, in Chile.

Pictures of some of the sampling locations for the third field campaign:



Picture B3. R-SI-7-17 sampling point.



Picture B4. SP-SI-8-17 sampling point.



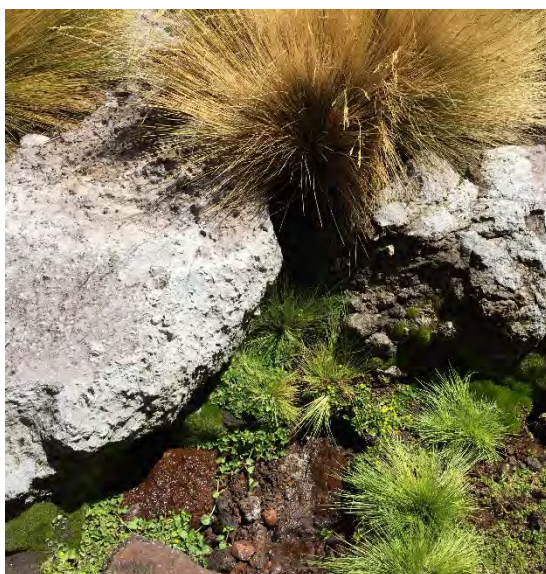
Picture B5. SP-SI-9-17 sampling point.



Picture B6. SP-SI-16-17 sampling point.



Picture B7. Spring SP-SI-2-17 sampling point.



Picture B8. Spring SP-SI-5-17 sampling point.

APPENDIX C

The anions were determined by ion chromatography (Cl⁻, SO₄²⁻, NO₃⁻) and volumetric method (HCO₃⁻), and cations by plasma emission spectrometry (ICP-OES). δ²H and δ¹⁸O were measured on a gas-source isotope ratio mass spectrometer (Finnigan Delta S). The hydrochemical data presented in stiff diagrams correspond to those with better analytical quality. To evaluate the quality of the chemical analyzes the ionic balance was carried out in all samples, where the sum of milliequivalents of anions must be practically equal to the amount of milliequivalents of cations. This condition is checked taking into account the ionic contributions of the majority elements calculating the balance error by the following formula (Custodio and Llamas, 1983):

$$\text{error (\%)} = 200 \times \frac{\sum \text{cations} - \sum \text{anions}}{\sum \text{cations} + \sum \text{anions}}$$

In general, samples with balance errors greater than those admitted are discarded for comparison with other samples and/or analysis dates. Negative balance errors indicate that the concentration of some of their anionic species have been overestimated, or that cationic species analyzes have underestimated some of these concentrations. Positive balance errors indicate otherwise. The errors allowed (in absolute value) are generally up to a maximum of 10%, although sometimes for very dilute waters, with electrical conductivities (EC) of less than 200 μS/cm, slightly higher errors can be accepted.

Water samples were analyzed for both oxygen and hydrogen isotopes in Isotope Tracer Technologies, on a Picarro CRDS (Model L1102-i). The Picarro CRDS isotopic water analyzers provides both δ¹⁸O and δ²H stable isotope ratios with high precision in one fast measurement. The instrument is equipped with a high precision autosampler, capable of making consistent small volume injections into the vaporizer. In addition, the instrument is configured with a unique vaporization module that converts the liquid water sample to the vapour phase in a flash process at 140°C. The vapour is then delivered into the CRDS cavity for analysis. This process avoids any possible fractionation effects that may occur with other liquid/vapour transitions, such as nebulizers. The Picarro analyzers are equipped with a thermally controlled optical cavity that ensures minimal drift, even in the harshest environments. In addition, an onboard wavelength monitor enables the absorption lines unique to H₂¹⁶O, H₂¹⁸O, and HD¹⁶O to be scanned repeatedly, quickly and precisely.

Three to four calibrated internal standards are included at the beginning and end of every run, as well as after every 10 samples. The employed internal standards have been calibrated to VSMOW, GISP, and SLAP. The results are evaluated and corrected against standards that bracket the samples, and then reported against the international

reference material. Precision is 1.0 per mil or better for $\delta^2\text{H}$ and 0.1 per mil or better for $\delta^{18}\text{O}$ based on repeated internal standards.

Tritium was measured by liquid scintillation spectrometry on samples that were first distilled to remove non-volatile solutes, and then enriched by electrolysis by a factor of about 9. Enriched samples were mixed 1:1 with Ultimagold Low Level Tritium (R) cocktail, and counted for 1500 minutes in a Quantulus 1220 Spectrometer in an underground counting laboratory at the Isotope Trace Technologies. The detection limit under these conditions is 0.6 TU. Standardization is relative to NIST SRM 4361C. Tritium is reported in Tritium Units. 1TU = 3.221 Picocuries/L per IAEA, 2000 Report. 1TU = 0.11919 Becquerels/L per IAEA, 2000 Report.

Due to the large amount of dissolved sulfate and the low dissolved inorganic carbon concentrations in water, the ^{14}C content was determined by accelerator mass spectrometry (AMS) in a United States laboratory. The CO_2 was prepared at the Isotope Tracer Technologies Laboratory and send to the AMS lab for analysis. AMS dating involves accelerating the ions to extraordinarily high kinetic energies followed by mass analysis. Samples are converted to graphite prior to AMS carbon dating. Although more expensive than radiometric dating, AMS dating has higher precision, and needs small sample sizes. The standard used was OX: 1.05×10^{-10} ; OX2: 1.35×10^{-10} ; C6: 1.5×10^{-10} ; and C7: 0.5×10^{-10} , and the typical standard deviation is 5 to 10% of Standard values. The ^{13}C DIC analyses were measured using a Finnigan Mat, DeltaPlus XL IRMS in the Isotope Tracer Technologies, with a standard IT2-27, IT2-34, NBS-18, NBS-19 and a typical standard deviation of 0.2 per mil.

REFERENCES

Custodio, E. and Llamas, M.R., 1983. *Hidrología subterránea*. Omega, Barcelona.

APPENDIX D



Isotope Analyses for:
Arcadis-Chile

**IT2 FILE #
170006**

2017-02-16

Approved by:

Orfan SStash

**Orfan Shouakar-Stash, PhD
Director**

Isotope Tracer Technologies Inc.
695 Rupert St. Unit B, Waterloo, ON, N2V 1Z5
Tel: 519-886-5555 | Fax: 519-886-5575
Email: orfan@it2isotopes.com
Website: www.it2isotopes.com



Client: Arcadis Chile
Address: Antonio Varas 621
 Providencia, Santiago
 8320000
Tel: 56 2 23816229
Attn.: Ximena Orrego
E-mail: ximena.orrego@arcadis.com
E-mail: alejandra.palacios@arcadis.com

File Number: **170006**

#	Sample ID	Collection		Sample #	E ³ H (ULL)	Repeat	± 1σ
		Date	Time				
1	SI1-B	2016-12-21	15:30	42768	X	< 0.05	0.23
2	SI2-I	2016-12-21	19:25	42769			
3	SI3	2016-12-22	17:50	42770			
4	Silala1-I	2016-12-22	18:15	42771			
5	SI2-II	2016-12-22	11:05	42772	X	0.07	0.23
6	Silala1A(Previously SI1A)	2016-12-22	19:20	42773			
7	SI4-A	2016-12-21	15:40	42774			
8	SI1A	2016-12-21	13:00	42775			
9	Silala1-II	2016-12-22	16:20	42776	X	0.22	0.23
10	SI4-B	2016-12-21	16:25	42777			
11	SI2B-I	2016-12-22	13:40	42778			
12	SI-02	2016-12-20	15:20	42779	X	0.16	0.23
13	SI-01	2016-12-20	16:00	42780			
14	Rio	2016-12-21	17:45	42781			
15	SI-11	2016-12-21	13:44	42782			
16	SI-21	2016-12-21	12:12	42783	X	0.18	0.22
17	SI-05	2016-12-21	15:15	42784	X	< 0.05	0.19

Tritium is reported in Tritium Units.

1TU = 3,221 Picocuries/L per IAEA, 2000 Report.

1TU = 0.11919 Becquerels/L per IAEA, 2000 Report.

Approved by:

Orfan S Stash

Orfan Shouakar-Stash, PhD
Director

Isotope Tracer Technologies Inc.
 695 Rupert St. Unit B, Waterloo, ON, N2V 1Z5

Tel: 519-886-5555 | Fax: 519-886-5575

Email: orfan@it2isotopes.com

Website: www.it2isotopes.com

3/3

2017-02-16



Client: Arcadis Chile
Address: Antonio Varas 621
 Providencia, Santiago
 8320000
Tel: 56 2 23816229
Attn.: Ximena Orrego
E-mail: ximena.orrego@arcadis.com
E-mail: alejandra.galacios@arcadis.com

File Number: **170006**

#	Sample ID	Collection		Sample #	$\delta^{13}\text{C}$ DIC	Result	Repeat	^{14}C DIC	Fraction of Modern	
		Date	Time						pmc	$\pm 1\sigma$
1	SI1-B	2016-12-21	15:30	42768	X	-7.3	-7.5	X	9.93	0.08
2	SI2-I	2016-12-21	19:25	42769						
3	SI3	2016-12-22	17:50	42770						
4	Silala1-I	2016-12-22	18:15	42771						
5	SI2-II	2016-12-22	11:05	42772	X	-8.0		X	14.54	0.09
6	Silala1A(Previously SI1A)	2016-12-22	19:20	42773						
7	SI4-A	2016-12-21	15:40	42774						
8	SI1A	2016-12-21	13:00	42775						
9	Silala1-II	2016-12-22	16:20	42776						
10	SI4-B	2016-12-21	16:25	42777						
11	SI2B-I	2016-12-22	13:40	42778						
12	SI-02	2016-12-20	15:20	42779	X	-8.0	-7.7	X	26.66	0.13
13	SI-01	2016-12-20	16:00	42780						
14	Rio	2016-12-21	17:45	42781						
15	SI-11	2016-12-21	13:44	42782						
16	SI-21	2016-12-21	12:12	42783						
17	SI-05	2016-12-21	15:15	42784	X	-7.0	-7.3	X	76.86	0.35

13C DIC Analyses

Instrument Used: Finnigan Mat, DeltaPlus XL IRMS, Germany.

Standard Used: IT2-27/ IT2-34/ NBS-18/NBS-19

Typical Standard deviation: $\pm 0.2\text{‰}$

14C DIC Analyses

Instrument Used: AMS (Accelerator Mass Spectrometry)

Standard Used:

OX1: 1.05×10^{-10}

OX2: 1.35×10^{-10}

C6: 1.5×10^{-10}

C7: 0.5×10^{-10}

Typical Standard deviation: 5 to 10% of Standard values listed above

Approved by:

Orfan S Stash

Orfan Shouakar-Stash, PhD

Director

Isotope Tracer Technologies Inc.

695 Rupert St. Unit B, Waterloo, ON, N2V 1Z5

Tel: 519-886-5555 | Fax: 519-886-5575

Email: orfan@it2isotopes.com

Website: www.it2isotopes.com

695 Rupert St. Unit B - Waterloo - Ontario - N2V 1Z5 - Tel. 519-886-5555 - Fax: 519-886-5575 - www.it2isotopes.com



Isotope Analyses for:
Arcadis Chile

**IT2 FILE #
170031**

2017-04-11

Approved by:

Orfan SStash

**Orfan Shouakar-Stash, PhD
Director**

Isotope Tracer Technologies Inc.
695 Rupert St. Unit B, Waterloo, ON, N2V 1Z5
Tel: 519-886-5555 | Fax: 519-886-5575
Email: orfan@it2isotopes.com
Website: www.it2isotopes.com



Client: Arcadis Chile
 Address: Antonio Varas 621
 Providencia, Santiago
 8320000
 Tel: 56 2 23816229
 Attn: Natalia Navarrete
 E-mail: natalia.navarrete@arcadis.com
 E-mail: ximena.orrego@arcadis.com

File Number: **170031**

#	Sample ID	Collection		Field Parameters			Sample #	$\delta^{18}\text{O}$	Aver	Stdv	$\delta^2\text{H}$	Aver	Stdv	
		Date	Time	Alkalinity (ppm)	pH	Temp. (°C)								Conductivity (mS/cm)
1	SP-SI-5-17	2017-02-01	14:00	48	8.05	20.2	160	43058	X	-11.72	0.03	X	-82.9	0.2
2	Blank Sample	/	/	/	/	/	/	43059	X	-10.92	0.02	X	-77.9	0.2
3	SP-SI-31-17	2017-02-02	12:00	75	7	19.1	210	43060	X	-11.72	0.02	X	-90.2	0.4
4	R-SI-3-17	2017-02-01	17:20	22	7.33	18.3	220	43061	X	-11.64	0.01	X	-91.8	0.1
5	R-SI-6-17	2017-02-01	13:40	90	7.58	21.3	220	43062	X			X		
6	R-SI-26-17	2017-02-01	12:19	119	9.02	18.4	213	43063	X			X		
7	SP-SI-16-17	2017-01-31	18:30	48	8.18	15.5	84	43064	X	-11.82	0.02	X	-92.3	0.1
8	SP-SI-8-17	2017-02-01	11:15	-	7.61	19.2	88	43065	X	-12.04	0.03	X	-83.7	0.4
9	SP-SI-15-17	2017-01-31	18:07	43	8.11	15.6	131	43066	X	-11.83	0.03	X	-92.4	0.3
10	SP-SI-9-17	2017-02-01	12:45	-	7.5	18.5	90.7	43067	X	-12.01	0.03	X	-84.0	0.3
11	SP-SI-1-17	2017-01-31	16:18	63	7.92	15.2	170	43068	X	-11.84	0.03	X	-92.6	0.3
12	R-SI-2-17	2017-01-31	15:24	66	9.03	17.1	100	43069	X	-11.61	0.03	X	-92.5	0.1
13	R-SI-4-17	2017-02-01	13:30	96	7.54	20.8	130	43070	X			X		
14	SP-SI-10-17	2017-02-01	11:00	74	7.05	13.6	290	43071	X	-11.72	0.03	X	-89.4	0.3
15	SP-SI-29-17	2017-02-01	15:30	44	7.22	21.5	220	43072	X	-11.73	0.03	X	-91.4	0.2
16	R-SI-7-17	2017-02-01	12:19	119	9.02	18.4	213	43073	X			X		
17	SP-SI-28-17	2017-01-31	18:10	17	7.13	11.5	230	43074	X	-11.78	0.02	X	-92.3	0.1
18	SP-SI-17-17	2017-01-31	17:55	28	7.25	15.1	170	43075	X	-11.77	0.02	X	-91.9	0.1
19	SP-SI-18-17	2017-01-31	17:10	19	7.13	15.6	220	43076	X	-11.77	0.02	X	-91.8	0.1
20	SP-SI-27-17	2017-01-31	15:30	83	6.87	16.6	220	43077	X	-11.80	0.02	X	-91.8	0.1
21	SP-SI-19-17	2017-01-31	15:50	28	7	16.1	190	43078	X	-11.79	0.02	X	-91.5	0.1

Do not run as per Ramon's instructions on Feb. 23, 2017

18O & 2H Analyses

Instrument Used: Cavity Ring Down Spectroscopy (CRDS)
 CRDS (Model L2130-i) (Picarro, California, USA).

Standard Used:
 IT2-12A / IT2-13A / IT2-00 Calibrated with IAEA Standards (V-SMOW, SLAP, and GISP)

Typical Standard deviation:

($^{18}\text{O} \pm 0.1\%$) ($^2\text{H} \pm 1\%$)

Approved by:

Orfan SStash

Orfan Shouakar-Stash, PhD
 Director
 Isotope Tracer Technologies Inc.
 695 Rupert St. Unit B, Waterloo, ON, N2V 1Z5
 Tel: 519-886-5555 | Fax: 519-886-5575
 Email: orfan@it2isotopes.com
 Website: www.it2isotopes.com



Client: Arcadis Chile
 Address: Antonio Varas 621
 Providencia, Santiago
 8320000
 Tel: 56 2 23816229
 Attn.: Natalia Navarrete
 Attn.: Ximena Orrego
 E-mail: natalia.navarrete@arcadis.com
 E-mail: ximena.orrego@arcadis.com

File Number: 170031

#	Sample ID	Collection		Field Parameters			Sample #	Ultra- ³ H	Repeat	± 1σ
		Date	Time	Alkalinity (ppm)	pH	Temp. (°C)				
1	SP-SI-5-17	2017-02-01	14:00	48	8.05	20.2	160			
2	Blank Sample	/	/	/	/	/	/			
3	SP-SI-31-17	2017-02-02	12:00	75	7	19.1	210			
4	R-SI-3-17	2017-02-01	17:20	22	7.33	18.3	220			
5	R-SI-6-17	2017-02-01	13:40	90	7.68	21.3	320			
6	R-SI-26-17	2017-02-01	17:10	115	5.02	18.4	215			
7	SP-SI-16-17	2017-01-31	18:30	48	8.18	15.5	84			
8	SP-SI-8-17	2017-02-01	11:15	-	7.61	19.2	88	X	< 0.05	0.20
9	SP-SI-15-17	2017-01-31	18:07	43	8.11	15.6	131	X	0.31	0.29
10	SP-SI-9-17	2017-02-01	12:45	-	7.5	18.5	90.7			
11	SP-SI-1-17	2017-01-31	16:18	63	7.92	15.2	170			
12	R-SI-2-17	2017-01-31	15:24	66	9.03	17.1	100			
13	R-SI-4-17	2017-02-01	13:30	96	7.04	20.8	310			
14	SP-SI-10-17	2017-02-01	11:00	74	7.05	13.6	290	X	< 0.05	0.11
15	SP-SI-29-17	2017-02-01	15:30	44	7.22	21.5	220			
16	R-SI-7-17	2017-02-01	17:10	119	9.02	18.4	215	X	< 0.05	0.31
17	SP-SI-28-17	2017-01-31	18:10	17	7.13	11.5	230			
18	SP-SI-17-17	2017-01-31	17:55	28	7.25	15.1	170			
19	SP-SI-18-17	2017-01-31	17:10	19	7.13	15.6	220			
20	SP-SI-27-17	2017-01-31	15:30	83	6.87	16.6	220			
21	SP-SI-19-17	2017-01-31	15:50	28	7	16.1	190			

Do not run as per Ramon's instructions on Feb. 23, 2017

3H ANALYSES

Tritium is reported in Tritium Units.

1TU = 3.221 Picocuries/L per IAEA, 2000 Report.

1TU = 0.11919 Becquerels/L per IAEA, 2000 Report.

Approved by:

Orfan S Stash

Orfan Shouakar-Stash, PhD
 Director
 Isotope Tracer Technologies Inc.
 695 Rupert St. Unit B, Waterloo, ON, N2V 1Z5
 Tel: 519-886-5555 | Fax: 519-886-5575
 Email: orfan@it2isotopes.com
 Website: www.it2isotopes.com

3/3

2017-04-11



Client: Arcadis Chile
 Address: Antonio Varas 621
 Providencia, Santiago
 8320000
 Tel: 56 2 23816229
 Attn: Natalia Navarrete
 Attn: Ximena Orrego
 E-mail: natalia.navarrete@arcadis.com
 E-mail: ximena.orrego@arcadis.com

File Number: 170031

#	Sample ID	Collection		Field Parameters			Sample #	$\delta^{13}\text{C}$ DIC	Result	Repeat	^{14}C DIC	Fraction of Modern	
		Date	Time	Alkalinity (ppm)	pH	Temp. (°C)						Conductivity (mS/cm)	pmc
1	SP-SI-5-17	2017-02-01	14:00	48	8.05	20.2	160	43058					
2	Blank Sample	/	/	/	/	/	/	43059					
3	SP-SI-31-17	2017-02-02	12:00	75	7	19.1	210	43060					
4	R-SI-3-17	2017-02-01	17:20	22	7.33	18.3	220	43061	X	-9.1	X	45.97	0.27
5	R-SI-6-17	2017-02-01	13:40	90	7.66	21.3	320	43062					
6	R-SI-26-17	2017-02-01	17:19	139	8.02	18.4	215	43063					
7	SP-SI-16-17	2017-01-31	18:30	48	8.18	15.5	84	43064					
8	SP-SI-8-17	2017-02-01	11:15	-	7.61	19.2	88	43065	X	-6.8	X	78.39	0.24
9	SP-SI-15-17	2017-01-31	18:07	43	8.11	15.6	131	43066	X	-5.8	X	32.41	0.15
10	SP-SI-9-17	2017-02-01	12:45	-	7.5	18.5	90.7	43067					
11	SP-SI-1-17	2017-01-31	16:18	63	7.92	15.2	170	43068					
12	R-SI-2-17	2017-01-31	15:24	66	9.03	17.1	100	43069					
13	R-SI-4-17	2017-02-01	13:30	96	7.54	20.8	330	43070					
14	SP-SI-10-17	2017-02-01	11:00	74	7.05	13.6	290	43071	X	-6.7	X	30.06	0.15
15	SP-SI-29-17	2017-02-01	15:30	44	7.22	21.5	220	43072					
16	R-SI-7-17	2017-02-01	17:19	139	8.02	18.4	215	43073	X		X		
17	SP-SI-28-17	2017-01-31	18:10	17	7.13	11.5	230	43074					
18	SP-SI-17-17	2017-01-31	17:55	28	7.25	15.1	170	43075					
19	SP-SI-18-17	2017-01-31	17:10	19	7.13	15.6	220	43076					
20	SP-SI-27-17	2017-01-31	15:30	83	6.87	16.6	220	43077					
21	SP-SI-19-17	2017-01-31	15:50	28	7	16.1	190	43078					

Do not run as per Ramon's instructions on Feb. 23, 2017.

Client asked to run ^{14}C analysis for this sample in email received Feb. 14Client asked to run ^{14}C analysis for this sample in email received Feb. 23 **^{13}C DIC Analyses****Instrument Used:**Finnigan MAT, Delta^{Plus} XL IRMS, Germany.**Standard Used:**IT²-27IT²-34

NBS-18

NBS-19

Typical Standard deviation: $\pm 0.2\text{‰}$ **^{14}C DIC Analyses****Instrument Used:**

AMS (Accelerator Mass Spectrometry)

Standard Used:OX1: $1.05 \times e^{-10}$ OX2: $1.35 \times e^{-10}$ C6: $1.5 \times e^{-10}$ C7: $0.5 \times e^{-10}$ **Typical Standard deviation:**

5 to 10% of Standard values listed above

Approved by:

Orfan Shouakar-Stash, PhD

Director

Isotope Tracer Technologies Inc.

695 Rupert St. Unit B, Waterloo, ON, N2V 1Z5

Tel: 519-886-5555 | Fax: 519-886-5575

Email: orfan@it2isotopes.comWebsite: www.it2isotopes.com695 Rupert St. Unit B - Waterloo - Ontario - N2V 1Z5 - Tel. 519-886-5555 - Fax: 519-886-5575 - www.it2isotopes.com



Isotope Analyses for:
Universidad Catolica
del Norte

IT2 FILE #
170286 & 170287

2019-01-08

Approved by:

Orfan SStash

Orfan Shouakar-Stash, PhD
Director

Isotope Tracer Technologies Inc.
695 Rupert St. Unit B, Waterloo, ON, N2V 1Z5

Tel: 519-886-5555 | Fax: 519-886-5575

Email: orfan@it2isotopes.com

Website: www.it2isotopes.com

2019-01-08



Client: Universidad Catolica del Norte
 Address: Angamos 0610
 Departamento de Ciencias Geologicas
 Antofagasta, Chile
 Tel: 55-2355908
 Attn: Christian Herrera Lameli
 E-mail: cherrera@ucn.cl

File Number	Sample ID	Collection		Sample #	¹⁴ C	Result				$\delta^{18}\text{O}$		Aver	Stdev	$\delta^3\text{H}$		Aver	Stdev
		Date	Time			DIC	14C yr BP	\pm	F14C	\pm	H ₂ O			VSMOW	H ₂ O		
170287	R-SI-2-017	12-10-2017	13:43	47576	X	9343	52	0.3125	0.002	X	-12.15	0.02	X	-93.6	0.2		
170287	R-RIO-1-017	12-10-2017	17:45	47586						X	-12.09	0.03	X	-92.9	0.3		
170287	R-SI-3-017	12-10-2017	18:30	47578	X	7533	45	0.3915	0.0022	X	-12.09	0.03	X	-92.8	0.3		
170286	R-SI-8-017	13-10-2017	15:30	47563	X	7452	42	0.3955	0.0021	X	-12.05	0.04	X	-92.9	0.2		
170287	R-SI-9-017	14-10-2017	12:00	47580	X	13736	87	0.18087	0.00197	X	-12.32	0.06	X	-93.1	0.5		
170286	R-SI-4-017	13-10-2017	14:00	47569						X	-12.26	0.04	X	-93.1	0.3		
170286	R-SI-7-017	13-10-2017	11:00	47558	X	9021	93	0.3253	0.0038	X	-11.96	0.01	X	-90.0	0.4		
170287	SP-SI-10-017	14-10-2017	11:25	47579	X	10350	54	0.2757	0.0018	X	-12.21	0.02	X	-90.8	0.1		
170287	SP-SI-28-017	13-10-2017	17:40	47588						X	-12.20	0.02	X	-92.8	0.1		
170287	SP-SI-16-017	12-10-2017	15:45	47584						X	-12.22	0.01	X	-93.0	0.3		
170286	SP-SI-17-017	13-10-2017	17:15	47572						X	-12.20	0.01	X	-92.4	0.3		
170286	SP-SI-18-017	13-10-2017	16:30	47564	X	7410	88	0.3975	0.0044	X	-12.18	0.01	X	-92.8	0.1		
170286	SP-SI-19-017	12-10-2017	11:50	47568						X	-12.10	0.01	X	-91.4	0.4		
170287	SP-SI-27-017	12-10-2017	12:05	47583						X	-12.23	0.03	X	-92.7	0.3		
170287	SP-SI-1-017	12-10-2017	15:10	47582						X	-12.25	0.03	X	-93.1	0.1		
170287	SP-SI-32-017	14-10-2017	14:00	47561	X	11477	67	0.2596	0.002	X	-12.19	0.05	X	-92.4	0.3		
170287	SP-SI-5-017	10-10-2017	/	47574	X	2790	46	0.7066	0.0041								
170287	SP-SI-6-017	11-10-2017	16:35	47573	X	3164	36	0.6744	0.0031								
170286	SP-SI-9-017	12-10-2017	10:30	47571						X	-12.40	0.02	X	-84.1	0.2		
170286	SP-SI-31-017	13-10-2017	11:30	47559	X	9738	92	0.2975	0.0034	X	-12.13	0.03	X	-91.8	0.3		
170286	SP-SI-29-017	13-10-2017	13:35	47560	X	8551	115	0.3449	0.0049	X	-12.08	0.02	X	-92.0	0.1		
170286	SPW-DQN-SI-017	11-10-2017	13:23	47565	X	19939	102	0.0836	0.0011	X	-12.54	0.04	X	-94.6	0.3		
170287	PW-BO-B-017	12-10-2017	12:45	47575	X	19210	100	0.0915	0.0011	X	-12.53	0.02	X	-95.1	0.1		
170287	MWL-UQN-A-017	13-10-2017	/	47589						X	-12.48	0.02	X	-94.6	0.1		
170287	PW-UQN-A-017	12-10-2017	18:00	47587						X	-12.51	0.04	X	-94.6	0.1		
170287	PW-UQN-B-017	12-10-2017	16:30	47577	X	18530	146	0.0996	0.0018	X	-12.55	0.03	X	-94.9	0.1		
170286	MW-DQN-A-017	11-10-2017	17:35	47570						X	-12.44	0.01	X	-93.9	0.1		
170286	PW-DQN-A-017	13-10-2017	14:56	47561	X	12230	53	0.2182	0.0014	X	-12.30	0.01	X	-93.2	0.3		
170286	PW-DQN-B-017	13-10-2017	15:50	47562	X	12141	56	0.2206	0.0015	X	-12.30	0.02	X	-93.5	0.0		
170287	PW-BO-A-017	12-10-2017	19:00	47585						X	-12.52	0.01	X	-95.0	0.1		

14C DIC Analyses**Instrument Used:**

AMS (Accelerator Mass Spectrometry)

Standard Used:OXI: 1.05 \pm 10OX2: 1.35 \pm 10C6: 1.5 \pm 10C7: 0.5 \pm 10**Typical Standard deviation:**

5 to 10% of Standard values listed above

18O & 2H (CRDS)**Instrument Used:** Cavity Ring Down Spectroscopy (CRDS)

CRDS (Model L2130-1) (Picarro, California, USA)

Standard Used:

IT2-12B / IT2-13A / IT2-00 Calibrated with IAEA Standards (V-SMOW, SLAP, and GISP)

Typical Standard deviation:(¹⁸O \pm 0.1‰) (²H \pm 1‰)

Approved by:

Orfan Shouakar-Stash, PhD

Director

 Isotope Tracer Technologies Inc.
 695 Rupert St. Unit B, Waterloo, ON, N2V 1Z5
 Tel: 519-886-5555 | Fax: 519-886-5575
Email: orfan@it2isotopes.comWebsite: www.it2isotopes.com



Isotope Analyses for:
Universidad Catolica
del Norte

IT2 FILE #
170286

2017-12-07

Approved by:

Orfan SStash

**Orfan Shouakar-Stash, PhD
Director**

Isotope Tracer Technologies Inc.
695 Rupert St. Unit B, Waterloo, ON, N2V 1Z5
Tel: 519-886-5555 | Fax: 519-886-5575
Email: orfan@it2isotopes.com
Website: www.it2isotopes.com



Cliente: Universidad Catolica del Norte
 Address: Angamos 0610
 Departamento de Ciencias Geologicas
 Antofagasta, Chile
 Tel: 55-2355968
 Attn.: Christian Herrera Lameli
 E-mail: cherrera@uocn.cl

File Number: 170286

#	Sample ID	Collection		Sample #	$\delta^{13}\text{C}$	Result	Repeat	^{14}C	Result			
		Date	Time						DIC	PDB	DIC	14C yr BP
1	R-SI-7-O17	13-10-2017	11:00	47558	X	-5.9	-6.1	X	9021	93	0.3253	0.0038
2	SP-SI-31-O17	13-10-2017	11:30	47559	X	-7.7		X	9738	92	0.2975	0.0034
3	SP-SI-29-O17	13-10-2017	13:35	47560	X	-8.7		X	8551	115	0.3449	0.0049
4	PW-DQN-A-O17	13-10-2017	14:56	47561	X	-7.4	-7.3	X	12230	53	0.2182	0.0014
5	PW-DQN-B-O17	13-10-2017	15:50	47562	X	-7.4		X	12141	56	0.2206	0.0015
6	R-SI-8-O17	13-10-2017	15:30	47563	X	-7.9		X	7452	42	0.3955	0.0021
7	SP-SI-18-O17	13-10-2017	16:30	47564	X	-6.8	-6.6	X	7410	88	0.3975	0.0044
8	SP-W-DQN-O17	11-10-2017	13:23	47565	X	-6.8		X	19939	102	0.0836	0.0011
9	SP-SI-8-O17	11-10-2017	16:35	47566								
10	SP-SI-5-O17	11-10-2017	18:30	47567								
11	SP-SI-19-O17	12-10-2017	11:50	47568								
12	R-SI-4-O17	13-10-2017	14:00	47569								
13	MW-DQN-A-O17	11-10-2017	17:35	47570								
14	SP-SI-9-O17	12-10-2017	10:30	47571								
15	SP-SI-17-O17	13-10-2017	17:15	47572								

13C DIC Analyses

Instrument Used:
 Finnigan MAT, Delta^{Plus} XL IRMS, Germany.
Standard Used:
 IR²-27
 IR²-34
 NBS-18
 NBS-19
Typical Standard deviation:
 $\pm 0.2\%$

14C DIC Analyses

Instrument Used:
 AMS (Accelerator Mass Spectrometry)
Standard Used:
 OX1: $1.05 \times e-10$
 OX2: $1.35 \times e-10$
 C6: $1.5 \times e-10$
 C7: $0.5 \times e-10$
Typical Standard deviation:
 5 to 10% of Standard values listed above

Approved by:

Orfan S Stash

Orfan Shouakar-Stash, PhD
 Director
 Isotope Tracer Technologies Inc.
 695 Rupert St. Unit B, Waterloo, ON, N2V 1Z5
 Tel: 519-886-5555 | Fax: 519-886-5575
 Email: orfan@it2isotopes.com
 Website: www.it2isotopes.com

695 Rupert St. Unit B - Waterloo - Ontario - N2V 1Z5 - Tel: 519-886-5555 - Fax: 519-886-5575 - www.it2isotopes.com



Client: Universidad Catolica del Norte
 Address: Angamos 0610
 Departamento de Ciencias Geologicas
 Antofagasta, Chile
 Tel: 55-2355968
 Attn.: Christian Herrera Lameli
 E-mail: cherrera@ucn.cl

File Number: 170286

#	Sample ID	Collection		Sample #	$\delta^{18}\text{O}$		$\delta^2\text{H}$		Aver	Stdv
		Date	Time		H_2O	VSMOW	H_2O	VSMOW		
1	R-SI-7-O17	13-10-2017	11:00	47558	X	-11.98	0.01	X	-90.0	0.4
2	SP-SI-31-O17	13-10-2017	11:30	47559	X	-12.13	0.03	X	-91.8	0.3
3	SP-SI-29-O17	13-10-2017	13:35	47560	X	-12.08	0.02	X	-92.0	0.1
4	PW-DQN-A-017	13-10-2017	14:56	47561	X	-12.30	0.01	X	-93.2	0.3
5	PW-DQN-B-017	13-10-2017	15:50	47562	X	-12.30	0.02	X	-93.3	0.0
6	R-SI-8-O17	13-10-2017	15:30	47563	X	-12.05	0.04	X	-92.9	0.2
7	SP-SI-18-O17	13-10-2017	16:30	47564	X	-12.18	0.01	X	-92.8	0.1
8	SP-W-DQN-O17	11-10-2017	13:23	47565	X	-12.54	0.04	X	-94.6	0.3
9	SP-SI-8-O17	11-10-2017	16:35	47566	X	-12.41	0.00	X	-84.0	0.2
10	SP-SI-5-O17	11-10-2017	18:30	47567	X	-12.03	0.03	X	-84.3	0.2
11	SP-SI-19-O17	12-10-2017	11:50	47568	X	-12.10	0.01	X	-91.4	0.4
12	R-SI-4-O17	13-10-2017	14:00	47569	X	-12.26	0.04	X	-93.1	0.3
13	MW-DQN-A-017	11-10-2017	17:35	47570	X	-12.44	0.01	X	-93.9	0.1
14	SP-SI-9-O17	12-10-2017	10:30	47571	X	-12.40	0.02	X	-84.1	0.2
15	SP-SI-17-O17	13-10-2017	17:15	47572	X	-12.20	0.01	X	-92.4	0.3

18O & 2H (CRDS)

Instrument Used: Cavity Ring Down Spectroscopy (CRDS)
 CRDS (Model L2130-i) (Picarro, California, USA).

Standard Used:

IT2-12B / IT2-13A / IT2-00 Calibrated with IAEA Standards (V-SMOW, SLAP, and GISP)

Typical Standard deviation:

($^{18}\text{O} \pm 0.1\%$) ($^2\text{H} \pm 1\%$)

Approved by:

Orfan S Stash

Orfan Shouakar-Stash, PhD
 Director
 Isotope Tracer Technologies Inc.
 695 Rupert St. Unit B, Waterloo, ON, N2V 1Z5
 Tel: 519-886-5555 | Fax: 519-886-5575
 Email: orfan@it2isotopes.com
 Website: www.it2isotopes.com

APPENDIX E

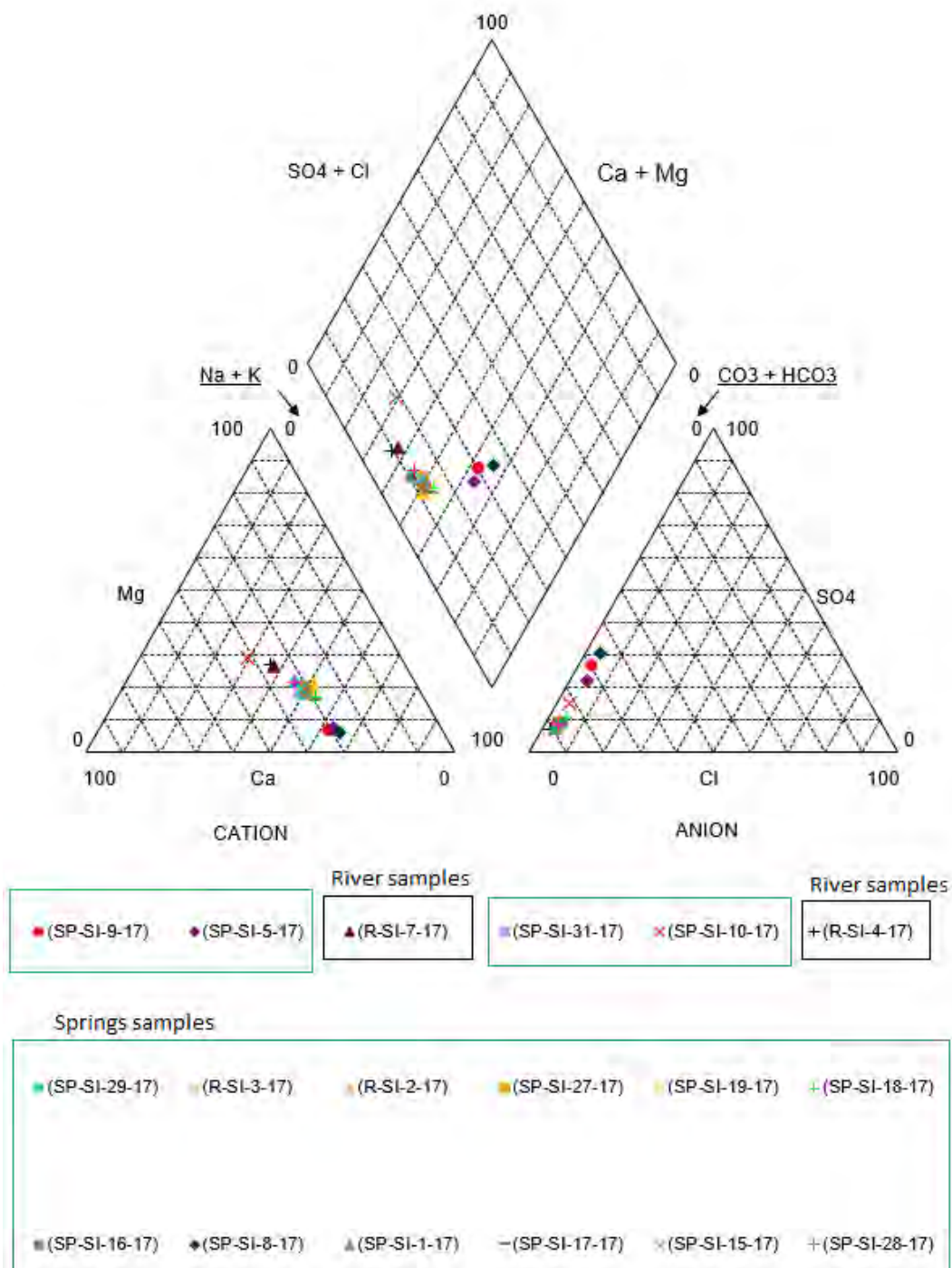


Figure E1. Piper diagrams for the rainy season.

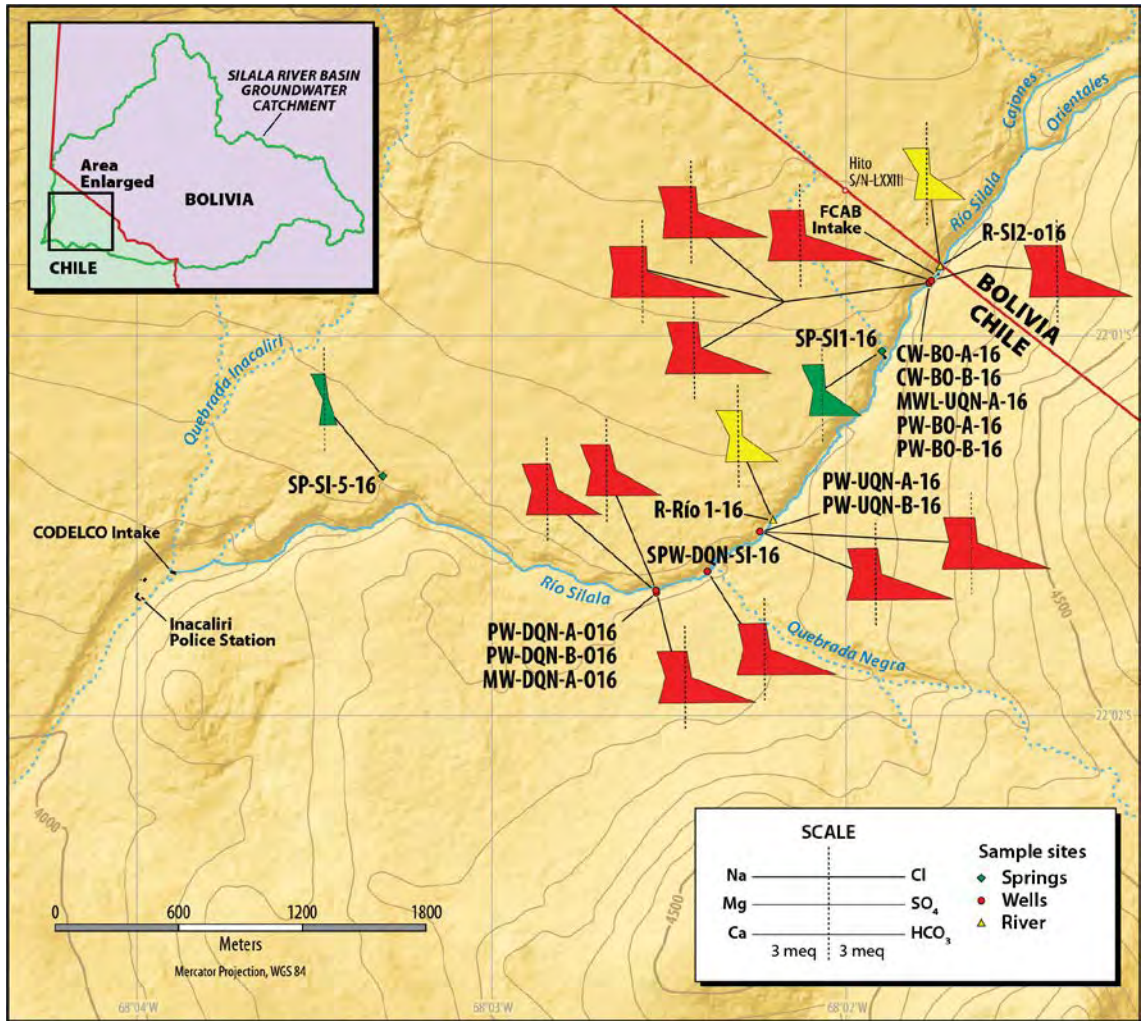


Figure E2. The Stiff diagrams of water samples collected during the second campaign in the Silala River basin (rainy season).

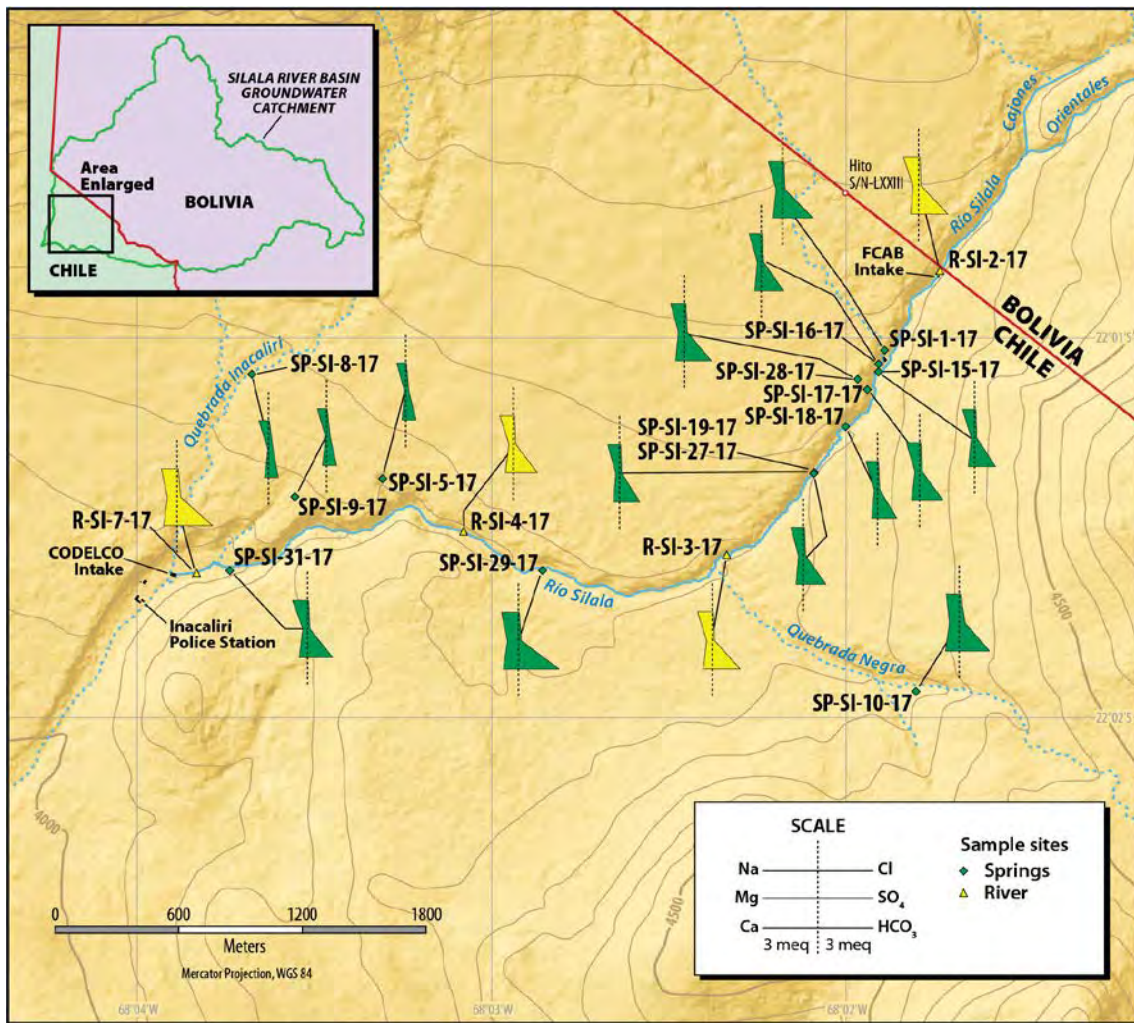


Figure E3. The Stiff diagrams of water samples collected during the third campaign in the Silala River basin (rainy season).

APPENDIX F

Date	Organization	Country	Sample name	Water type	T (°C)	pH lab	EC (µS/cm)	Cl (mg/l)	SO ₄ (mg/l)	Ca (mg/l)	Mg (mg/l)	NO ₃ (mg/l)	Si (mg/l)	Na (mg/l)	K (mg/l)	HCO ₃ (mg/l)	Error (%)
mar-00	Diremar	Bolivia	Laguna Khara	Lake	10	8.3	715	112.38	16.5	11.83	19.61	0.1	54	136	27	110.26	49.5
oct-16	VRHR- MMaya	Bolivia	SI-1	Spring	15	8.64	115.2	6.94	7.29	7.7	2.28	2.41	17.37	8.8	1.9	31.41	10.9
oct-16	VRHR- MMaya	Bolivia	SI-1R	Spring	15.9	8.58	112.9	6.75	7.43	7.2	2.31	2.39	16.52	8.6	1.8	29.78	10.8
oct-16	VRHR- MMaya	Bolivia	SI-2	Spring	15.6	8.04	244	7.98	9.81	18.47	6.79	2.67	21.31	17	2.8	115.24	-2.8
oct-16	VRHR- MMaya	Bolivia	SI-3	Spring	14.5	7.91	254	7.32	10.05	17.1	8.07	2.55	22.44	17	2.95	118.5	-2.7
oct-16	VRHR- MMaya	Bolivia	SI-4	Spring	15.5	8.8	229	7.6	7.33	16.67	6.49	2.75	20.19	17	2.7	109.81	-1.5
oct-16	VRHR- MMaya	Bolivia	SI-5	Spring	9.2	8.64	285	6.18	9.81	19.9	9.49	1.34	22.26	17	3.71	127.44	4.9
oct-16	VRHR- MMaya	Bolivia	SI-6	Spring	16.6	8.51	113.8	7.13	6.61	7.93	1.72	2.3	17.27	8.7	2	24.16	22.6
oct-16	VRHR- MMaya	Bolivia	SI-7	Spring	16.1	8.53	128.6	6.46	9.6	8.74	2.64	2.39	23.38	9.8	2.1	37.79	8.7
oct-16	VRHR- MMaya	Bolivia	SI-8	Spring	16.1	7.69	394	8.55	10.02	29.87	15.57	2.3	31.65	17	5.21	210.19	-7.4
oct-16	VRHR- MMaya	Bolivia	SI-9	Spring	15	8.57	123.5	6.84	7.74	9.73	3.14	2.39	17.46	9.6	2	47.72	3.3
oct-16	VRHR- MMaya	Bolivia	SI-10	Spring	14.2	8.23	96.4	6.08	7.12	6.87	1.95	1.85	23.01	7.5	2.6	36.24	-5.0
oct-16	VRHR- MMaya	Bolivia	SI-11	Spring	15.5	8.61	85.8	5.42	8.36	6.21	1.97	1.71	16.99	6.5	2.1	24.16	7.6
oct-16	VRHR- MMaya	Bolivia	SI-1	Spring	5.82	8.87	191.6	6.94	11.74	6.53	9.4	2.58	16.19	13.68	1.34	76.95	-0.6
oct-16	VRHR- MMaya	Bolivia	SI-1A	Spring	16.2	8.85	113.3	6.75	10.53	5.75	1.45	1.91	13.99	13.52	1.94	36.36	0.8
oct-16	VRHR- MMaya	Bolivia	SI-2A	Spring	15.6	8.48	237	7.98	10.77	14.33	6.19	2.05	17.69	21.08	2.93	115	-6.5
oct-16	VRHR- MMaya	Bolivia	SI-3A	Spring	15.5	8.45	253	7.32	13.43	15.63	7.06	2.13	18.13	23.18	3.13	125.15	-4.7
oct-16	VRHR- MMaya	Bolivia	SI-4A	Spring	15.7	8.57	228	7.6	11.62	10.18	5.59	2.3	17.78	22.07	2.83	101.47	-7.4
oct-16	VRHR- MMaya	Bolivia	SI-5A	Spring	16.7	9.62	294	6.18	3.53	15.95	8.8	0.04	18.66	24.07	4.63	120.08	19.3
oct-16	VRHR- MMaya	Bolivia	SI-6A	Spring	16.6	9.06	115.2	7.13	10.17	5.33	1.34	1.99	15.84	13.85	1.94	45.66	-14.8
oct-16	VRHR- MMaya	Bolivia	SI-7A	Spring	16.2	9.1	127.3	6.46	12.22	6.18	1.78	1.88	16.11	15.38	1.94	54.12	-14.2
oct-16	VRHR- MMaya	Bolivia	SI-8A	Spring	16.6	8.32	410	8.55	20.99	30.47	15.68	2.24	30.73	24.24	5.73	208.02	-2.6

Date	Organization	Country	Sample name	Water type	T (°C)	pH lab	EC (µS/cm)	Cl (mg/l)	SO ₄ (mg/l)	Ca (mg/l)	Mg (mg/l)	NO ₃ (mg/l)	Si (mg/l)	Na (mg/l)	K (mg/l)	HCO ₃ (mg/l)	Error (%)
oct-16	VRHR-MMaya	Bolivia	SI-9A	Spring	15,5	9,16	122,7	6,84	11,49	5,95	1,67	1,99	15,05	14,83	1,84	51,58	-15,0
oct-16	VRHR-MMaya	Bolivia	SI-10A	Spring	14,7	9,06	99,3	6,08	9,81	4,08	0,9	1,66	14,52	11,95	1,94	37,21	-17,7
oct-16	VRHR-MMaya	Bolivia	SI-11A	Spring	15,5	9,31	85,2	5,42	10,77	6,06	1,23	1,66	16,11	8,89	1,94	33,82	-13,1
jun-00	SERGEOMIN	Bolivia	Silala Boca toma (canal)	Spring	N/A	7,65	176	7,16	9,05	10,8	4,85	N/A	N/A	23	2,5	106	-6,0
jul-00	SERGEOMIN	Bolivia	Silala Sur Canal	Spring	N/A	7,7	112	7,16	7,82	6,6	1,09	N/A	N/A	20	1,9	68,93	-11,0
ago-00	SERGEOMIN	Bolivia	Silala Norte Canal Norte	Spring	N/A	7,9	207	8,95	9,47	12,8	6,43	N/A	N/A	25,8	2,9	131,76	-9,7
sept-00	SERGEOMIN	Bolivia	Silala Sur Pozo	Groundwater	N/A	7,7	124	7,16	11,11	6,6	1,82	N/A	N/A	20	1,9	69,93	-12,2
oct-00	SERGEOMIN	Bolivia	Silala Norte Pozo	Groundwater	N/A	8,35	95	7,16	4,12	6,4	1,7	N/A	N/A	15	2	50,02	5,0
nov-00	SERGEOMIN	Bolivia	Silala Norte Vertiente	Spring	N/A	7,4	96	7,1	9,05	5,4	2	N/A	N/A	18	2	56,12	-3,1
dic-00	SERGEOMIN	Bolivia	Silala Norte Vertiente	Spring	N/A	7,7	120	7,16	9,47	6,4	1,82	N/A	N/A	23	2	75,03	-6,8
ene-01	SERGEOMIN	Bolivia	Silala Sur Bofedal	Spring	N/A	7,5	340	7,16	13,99	25,4	13,71	N/A	N/A	30	5,1	218,99	-6,2
feb-01	SERGEOMIN	Bolivia	Silala Sur Pozo	Groundwater	N/A	7,55	237	7,52	11,94	11,4	4,12	N/A	N/A	29	3,1	150,06	-25,9
nov-17	SERGEOMIN	Bolivia	DS-24P 7.2-8.2 m*	Groundwater	13,9	8,94	104,7	4,6	13,47	8,65	1,13	1,71	17,5	9,26	1,36	91,622	-67,3
nov-17	SERGEOMIN	Bolivia	DS-4S 5-10 m*	Groundwater	12,9	8,81	249	7,54	10,36	17,85	4,26	3,29	0,93	20,87	2,05	93,818	8,8
nov-17	SERGEOMIN	Bolivia	DS-8 8.7-14.8 m*	Groundwater	12,7	8,8	293	11,41	12,74	20,09	9,93	4,89	22,73	25,78	2,35	92,72	31,6
nov-17	SERGEOMIN	Bolivia	DS-24S 2-4 m*	Groundwater	12,6	8,64	132,6	7,67	19,46	8,53	3,97	2,5	18,26	12,8	1,26	30,378	14,7

Table F1. Presentation of the chemical data from Bolivian lake, spring and well samples contained in DHI (2018) and cited in this report.

APPENDIX G

Table 14 Tritium and ^{14}C results (Sergeotecmin, 2005 (Bolivian) and Arcadis, 2017 (Chilean)).

Date	^3H (UT)	^{14}C (pMC)	Reported Apparent Age (years)
<i>Bolivian collected test results</i>			
Site 2: Southern Wetland Up-Gradient	0±0.13	25.67±0.26	10,950±80*
Site 4: Intermediate Site	0±0.13	30.67±0.27	9,490±70*
Site 6: Northern Wetland	0±0.14	86.29±0.83	1,180±80

Table G1. Tritium and ^{14}C data presented by DHI (2018) and cited in this report (BCM, Vol. 4, p. 92).

Annex XII

Herrera, C. and Aravena, R., 2019. *Chemical Characterization of Surface Water and Groundwater of the Quebrada Negra, Second Region, Chile*

**CHEMICAL CHARACTERIZATION OF SURFACE WATER AND
GROUNDWATER OF THE QUEBRADA NEGRA, SECOND REGION, CHILE**

Christian Herrera (PhD)

Associate Professor, Universidad Católica del Norte

Ramón Aravena (PhD)

Emeritus and Adjunct Professor, University of Waterloo

January 2019

GLOSSARY

Alkalinity: The name given to the quantitative capacity of an aqueous solution to neutralize an acid.

Anion: An ionic species, with a net negative charge.

Cation: An ionic species, with a net positive charge.

Headwater: A tributary stream of a river, close to or forming part of its source.

Hydrochemical: Dealing with the chemical characteristics of bodies of water.

Ion: An atom or molecule with a net electrical charge due to the gain or loss of one or more electrons.

Ion chromatography: A chromatography process that separates ions and polar molecules based on their affinity to an ion exchanger.

Plasma emission spectrometry: An analytical technique used for the detection of trace elements. It is a type of emission spectroscopy that uses the inductively coupled plasma to produce excited atoms and ions that emit electromagnetic radiation at wavelengths characteristic of a particular element.

Recharge: Groundwater recharge (or deep drainage or deep percolation) is a hydrologic process whereby water that has infiltrated the surface moves downward from the unsaturated zone to groundwater. Recharge is the primary method through which water enters an aquifer. Its source can be precipitation or surface water.

Salinity: The concentration of dissolved salts in water.

TABLE OF CONTENTS

1. INTRODUCTION	1
2. LOCATION OF THE INVESTIGATED AREA.....	1
3. OBJECTIVE OF THE REPORT	1
4. METHODOLOGY	2
5. GEOCHEMISTRY	4
6. CONCLUSIONS	7
7. REFERENCES	8

1. INTRODUCTION

The National Director of the Dirección Nacional de Fronteras y Límites del Estado (DIFROL) of the Ministry of Foreign Affairs, Mrs. Ximena Fuentes, requested a study concerning the hydrochemical characterization of the Quebrada Negra area located in the transboundary basin of the Silala River in the northern region of Chile, as part of a study aimed at deepening the hydrogeological knowledge of this basin.

The study of the chemical evolution of surface and groundwater in the Quebrada Negra area can contribute to the understanding of the complex interaction between the surface waters and the groundwater and mechanisms of local and regional recharge to the river flow. In this context, the hydrogeochemical study of groundwater has been an important approach to understand the flow of groundwater and to validate or discard hypotheses about the conceptual understanding of the hydrogeology. This report was elaborated under the supervision and instruction of Professors Howard Wheater and Denis Peach.

2. LOCATION OF THE INVESTIGATED AREA

The Quebrada Negra area is a major ephemeral tributary of the Silala River transboundary watershed in Chile (Figure 1 and Figure 2), which reaches the Silala River from the southeast, some 1700 metres downstream from the international border. The headwaters of the Silala River are located above 4300 m.a.s.l. in Bolivian territory where the perennial river flow originates from two wetland areas, the Cajones ravine and the Orientales area, which are fed by groundwater from many springs. After the river enters a ravine it crosses into Chilean territory.

3. OBJECTIVE OF THE REPORT

The main objective of this report is to characterize the chemical composition of the surface waters and groundwater of the Quebrada Negra area in the Silala River basin. This information will be used to complement the analysis of the data collected in the Quebrada Negra as part of the study, “*Chemical and isotopic characterization of surface water and groundwater of the Silala River transboundary basin, Second Region, Chile*” (Herrera and Aravena, 2019).

4. METHODOLOGY

For the hydrogeochemical characterization of the waters of the Quebrada Negra, 7 samples of surface water (surface runoff) and groundwater were collected in the study area during November 2018. Groundwater samples were obtained in shallow piezometers from 1 to 2.5 metres deep. The location of the sampling points can be found in Figures 1 and 2.

The chemical analysis included major cations and anions. The anions were determined by ion chromatography (chloride, sulfate, nitrate) (Cl^- , SO_4^{2-} , NO_3^-) and volumetric titration (bicarbonate) (HCO_3^-), and cations (sodium, potassium, calcium, magnesium) (Na^+ , K^+ , Ca^{2+} , Mg^{2+}) by plasma emission spectrometry (ICP-OES). The hydrochemical data presented in Stiff diagrams correspond to those with better analytical quality. To evaluate the quality of the chemical analyzes the ionic balance was carried out for all samples, where the sum of milliequivalents of anions must be practically equal to the amount of milliequivalents of cations. This condition is checked considering the ionic contributions of the majority elements calculating the balance error by the following formula (Custodio and Llamas, 1983):

$$\text{error (\%)} = 200 \times \frac{\sum \text{cations} - \sum \text{anions}}{\sum \text{cations} + \sum \text{anions}}$$

In general, samples with balance errors greater than those permitted are discarded for comparison with other samples and/or analysis dates. The errors allowed (in absolute value) are generally up to a maximum of 10%, although sometimes for very dilute waters, with electrical conductivities (EC) of less than 200 $\mu\text{S}/\text{cm}$, slightly higher errors can be accepted.

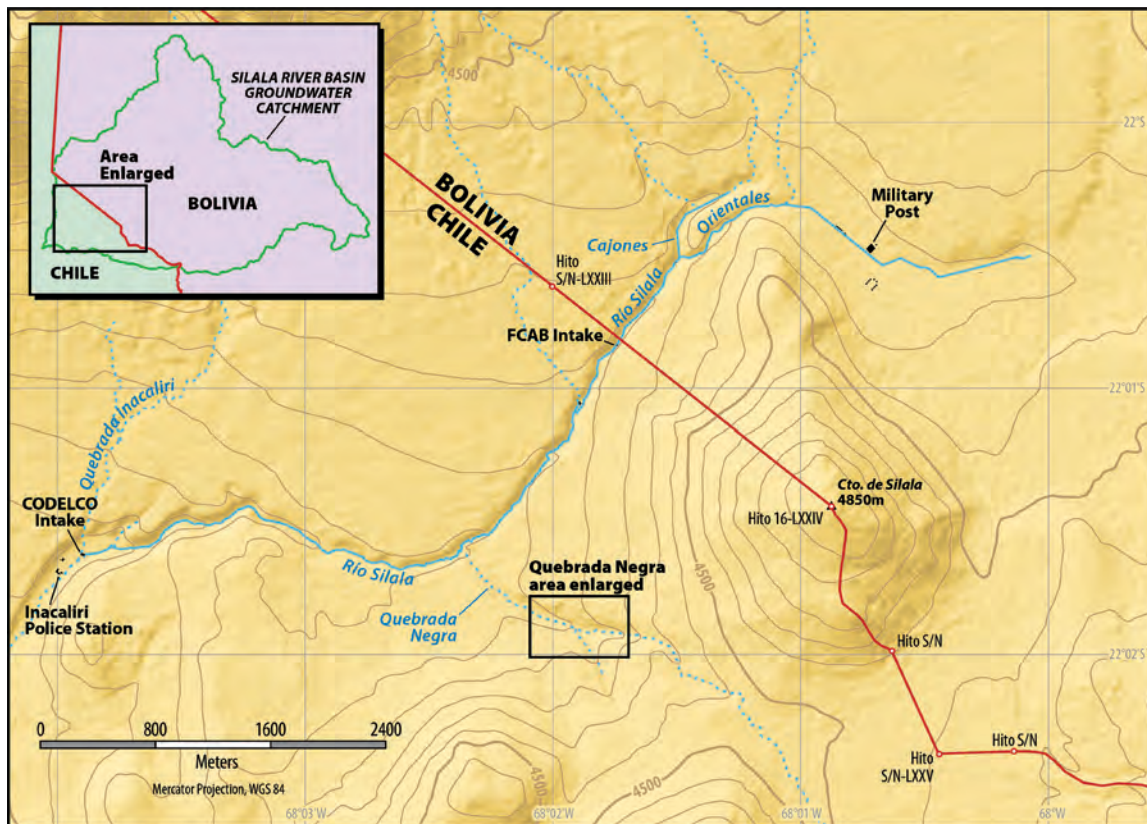


Figure 1. Location map of the study area in the Silala River transboundary watershed.

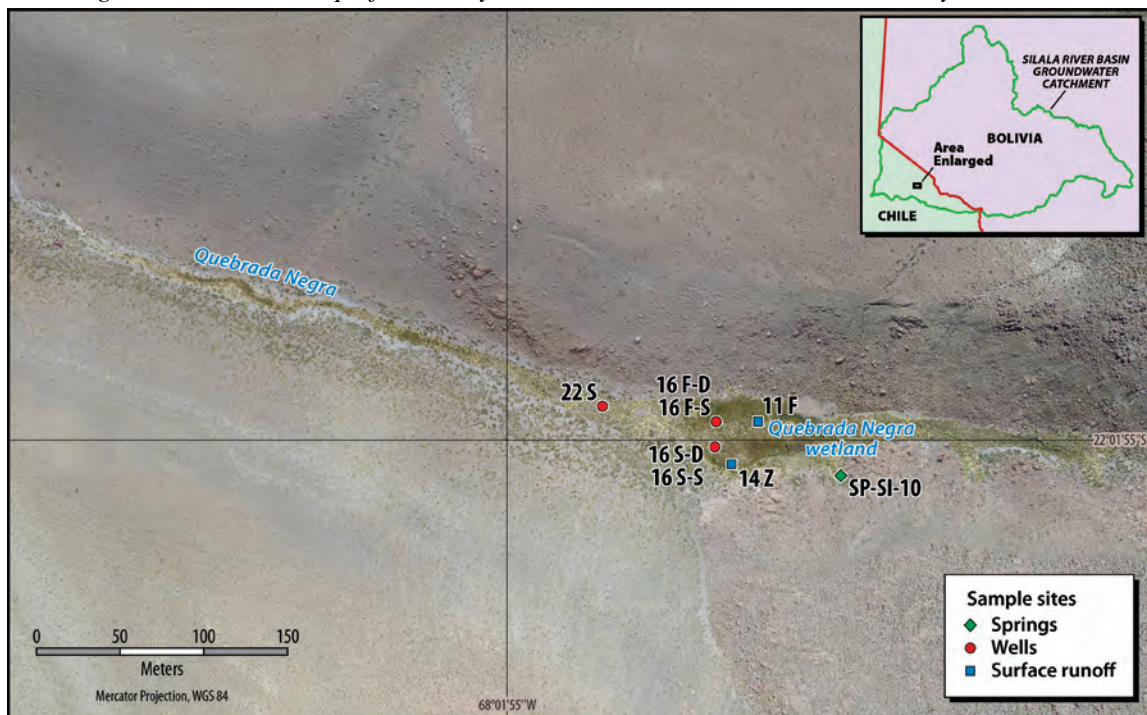


Figure 2. The Quebrada Negra area in the Silala River basin showing the sampling location of surface runoff, spring and groundwater.

5. GEOCHEMISTRY

The chemical data for groundwater and surface runoff are presented in Table 1. These data show a wide range in electrical conductivity (EC) values that vary between 249 and 450 $\mu\text{S}/\text{cm}$. The surface runoff samples with EC values of 249 and 262 $\mu\text{S}/\text{cm}$ show the lowest values, which are closer to the range of values for the Quebrada Negra spring SP-SI-10, ranging between 290 (rainy season) and 379 $\mu\text{S}/\text{cm}$ (dry season) (Herrera and Aravena, 2019). The waters of the deep piezometers tend to have the highest EC values. The value of 450 $\mu\text{S}/\text{cm}$ is very close to EC values of groundwater of wells in other regions of the Chilean and Bolivian sector of the Silala River topographic catchment (Herrera and Aravena, 2019).

The waters are mainly Ca-Na-Bicarbonate type (Figure 3), like the chemical composition, for the rainy season, of the spring sample SP-SI-10-17 analyzed in the previous study (Herrera and Aravena, 2019), however there is one groundwater and one surface runoff water sample that is Na-Ca-Bicarbonate. The chemical composition of the Quebrada Negra waters tends to be similar to the springs in the Orientales area in Bolivia and the groundwater in the Chilean sector (Figure 4).

One key difference between the Quebrada Negra spring and the other springs in the Silala River basin in the Chilean sector is its relative higher magnesium (Mg) content. Mg is the second most abundant cation in the more saline groundwater (16 F-D) in the Quebrada Negra (Table 1 and Figure 3). Based on a relative increase in the Mg content in the river down-gradient from the intersection of the Quebrada Negra with the Silala River, it was postulated that this pattern was related to the input of water from the Quebrada Negra (Herrera and Aravena, 2019). The additional chemical data collected in the Quebrada Negra supports this hypothesis.

One of the characteristics of the Quebrada Negra water in the present study is the bicarbonate content, which as mentioned above is much higher in two of the waters analyzed than that in the waters that have been analyzed in the other regions of the Chilean and Bolivian sector of the Silala River topographic basin. It was postulated (Herrera and Aravena, 2019) that part of the bicarbonate in the groundwater in the Silala River catchment could be associated to a contribution of volcanic CO_2 .

Sample ID	Date	Coordinates		Hour	Water Type	pH lab	Depth	T °C	EC Lab uS/cm	Alkalinity mg/L of CaCO ₃	Cl mg/L	SO ₄ mg/L	HCO ₃ mg/L	Ca mg/L	Mg mg/L	K mg/L	Si mg/L	Na mg/L	NO ₃ mg/L
		x	Y																
22 S	16-11-2018	599931.84	7563358.63	14:20	Piezometer	6.99	1.07	21.3	332	150	2.41	0.38	193.9	23.32	11.101	13.158	30.61	21.63	0.5
11 F	16-11-2018	600022.35	7563348.83	15:07	Surface runoff	6.71		19.3	262	120	1.46	10.45	145.1	19.27	8.404	7.599	31.4	17.88	< 0.5
14 Z	16-11-2018	600006.51	7563323.11	15:33	Surface runoff	7.21		20.4	249	144	2.1	14.9	123.1	19.32	7.966	7.76	37.27	15.79	< 0.5
16 S-D	16-11-2018	599998.85	7563333.92	16:47	Piezometer	6.7	2.31	10.9	450	226	1.44	2.74	285.3	38.3	14.895	16.06	16.25	19.89	< 0.5
16 S-S	16-11-2018	599998.85	7563333.92	16:40	Piezometer	6.53	0.81	10.8	290	147	1.01	5.34	173.1	21.7	9.669	9.889	30.42	17.13	< 0.5
16 F-D	16-11-2018	599999.69	7563348.95	17:11	Piezometer	6.61	2.03	7.3	378	217	0.92	28.86	302.4	56.37	17.356	13.226	35.1	16.63	< 0.5
16 F-S	16-11-2018	599999.69	7563348.95	17:41	Piezometer	6.83	0.85	11.6	343	218	0.74	0.5	215.8	29.89	11.883	12.44	40.29	17.98	< 0.5

Table 1. Location and chemical data of the water in the Quebrada Negra. The letter "D" indicates "deep" and "S" stands for "shallow" level, as defined by Muñoz and Suárez. (2019).

6. CONCLUSIONS

A wide range in salinity is observed in the Quebrada Negra waters. Some of these waters tend to be more saline than surface and groundwater analyzed in the Chilean and Bolivian sectors of the Silala River basin, whereas others are similar in salinity. This wide range in salinity observed in this small area is likely to reflect a complex interaction between deep and shallow groundwater flow systems, suggesting that the waters are varying mixtures of two different groundwater systems. The higher salinity and high bicarbonate of these waters is likely to be associated with discharge of a regional groundwater flow system, whereas the lower salinity, lower bicarbonate waters suggest a closer association with a local flow system. Hydraulic head measurements in some of the piezometers (Muñoz and Suárez, 2019) show an upward gradient indicating a potential for groundwater discharge from a deeper flow system. The existence of faults in this area could explain discharge of a more saline groundwater from a deeper regional groundwater flow system. The low salinity water represented by the spring sample SP-SI-10-17 (see Figure 4) and one of the surface runoff water samples in the Quebrada Negra could well correspond to the discharge of a shallow groundwater flow system.

The new chemical data in the Quebrada Negra agree with previous data from the spring SP-SI-10 which showed that this water has relatively more Mg than the springs and the Silala River in the Chilean sector of the catchment. This finding supports the hypothesis of a contribution of the Quebrada Negra to the Silala River based on relative changes in Mg in the river between up and down gradient of the intersection of the Silala River with the Quebrada Negra.

7. REFERENCES

Custodio, E. and Llamas, M.R., 1983. *Hidrología subterránea*. Omega. Barcelona.

Muñoz, J.F. and Suárez, F., 2019. *Quebrada Negra Wetland Study*. **(Chile's Reply, Vol. 3, Annex XIII)**.

Herrera, C. and Aravena, R., 2019. *Chemical and isotopic characterization of surface water and groundwater of the Silala River transboundary basin, Second Region, Chile*. **(Chile's Reply, Vol. 3, Annex XI)**.

Annex XIII

Muñoz, J.F. and Suárez, F., 2019. *Quebrada Negra Wetland Study*

QUEBRADA NEGRA WETLAND STUDY

José Francisco Muñoz (PhD)

Professor, Pontificia Universidad Católica de Chile

Francisco Suárez (PhD)

Associate Professor, Pontificia Universidad Católica de Chile

Assistants:

María José Fuenzalida, Civil Engineer

Magdalena Lagos, Civil Engineer, MSc

Magdalena Mendoza, Civil Engineer

Tomás Oportus, Civil Engineer

Andrés Pereira, Civil Engineer, MSc

Pedro Sanzana, Civil Engineer, MSc, PhD

Andrés Sarabia, Civil Engineer, MSc

Fernanda Stegmaier, Civil Engineer

January 2019

GLOSSARY

This glossary of hydrological terms is based on the following:

- http://www.wmo.int/pages/prog/hwrrp/publications/international_glossary/385_IGH_2012.pdf
- http://www.nws.noaa.gov/om/hod/SHManual/SHMan014_glossary.htm
- <http://www.geo.utexas.edu/faculty/jmsharp/sharp-glossary.pdf>

Conductivity: Hydraulic Conductivity is a property of a porous medium which, according to Darcy's law, relates the specific discharge to the hydraulic gradient.

Discharge: Volume of water flowing per unit time, for example through a river cross-section or from a spring or a well.

Evaporation: Process by which water changes from liquid to vapour.

Evapotranspiration: Combination of evaporation from free water surfaces and transpiration of water from plant surfaces to the atmosphere.

Gauge: (verb) To estimate an amount by using a measuring device.

Groundwater: Subsurface water occupying the saturated zone (i.e. where the pore spaces (or open fractures) of a porous medium are full of water).

Landsat: Group of satellites built and placed in orbit by the USA for high-resolution observation of the Earth's surface.

Net Radiation: Difference between incident and reflected radiation.

Normalized Difference Vegetation Index: Indicator that can be used to analyze remote sensing measurements and assess whether the target being observed contains live green vegetation or not.

Penman-Monteith Approach: Method for estimating evapotranspiration.

Psychrometric Constant: Constant that relates the partial pressure of water in air to the air temperature.

River Basin: Area having a common outlet for its surface runoff.

Spring: Place where groundwater emerges naturally from the rock or soil.

Soil Heat Flux Density: Heat flux entering the ground per unit area.

Wells: Any artificial excavation or borehole constructed with the aim of either exploring for or producing groundwater, or injection, monitoring or dewatering purposes.

Wetland: Areas under or contiguous to open water or with a shallow water table, including swamps, marshes, bogs, wet meadows, river overflows, mud flats, and natural ponds. Wetlands are typically characterized by water-loving vegetation (phreatophytes or, in areas with brackish water, halophytes).

TABLE OF CONTENTS

1. INTRODUCTION	1
1.1 Objective	1
1.2 Summary of the methodology	1
1.3 Structure of the report.....	2
2. SUMMARY AND CONCLUSIONS	2
3. STUDY AREA	4
4. METHODS	11
4.1 Quebrada Negra Wetland meteorological station	11
4.1.1 Anemometer.....	14
4.1.2 Net radiometer	14
4.1.3 Tipping bucket rain gauge	15
4.1.4 Ambient temperature and relative humidity probe	15
4.1.5 Soil sensors	16
4.2 Spatial and temporal distribution of vegetation cover.....	18
4.2.1 Spatial distribution of vegetation cover.....	18
4.2.2 Temporal evolution of vegetation cover.....	20
4.3 Evapotranspiration estimations	21
4.3.1 Potential evapotranspiration	21
4.3.2 Spatial distribution of estimated actual evapotranspiration.....	21
4.4 Soil characterization	23
4.4.1 Field campaign to determine peat depth, describe soil particle distribution and permeability.....	23
4.4.2 Field saturated hydraulic conductivity.....	35
4.4.3 Thermal properties.....	37
4.5 Groundwater level monitoring	37
4.5.1 Monitoring network.....	37
4.5.2 Ground water level measurements.....	44
5. RESULTS AND DISCUSSION	44

5.1	Quebrada Negra Wetland meteorological station	45
5.1.1	Air temperature	45
5.1.2	Precipitation	45
5.1.3	Relative Humidity	46
5.1.4	Wind speed and Wind direction	47
5.1.5	Net radiation	48
5.1.6	Soil heat flux	49
5.2	Spatial and temporal distribution of vegetation cover	49
5.2.1	Spatial distribution of vegetation cover	49
5.2.2	Temporal evolution of vegetation cover	55
5.3	Evapotranspiration estimates	61
5.3.1	Potential evapotranspiration	61
5.3.2	Spatial distribution of estimated actual evapotranspiration	61
5.4	Soil characterization	64
5.4.1	Peat depth determination	64
5.4.2	Soil particle distribution	64
5.4.3	Falling-head Permeability Test results	67
5.4.4	Field saturated hydraulic conductivity	68
5.4.5	Thermal properties	73
5.5	Groundwater level monitoring	73
5.5.1	Spatial interpolation	73
5.5.2	Groundwater profiles	77
5.5.3	Continuous monitoring records	80
5.5.4	Discussion	80
6.	CONCLUSIONS	82
7.	REFERENCES	85
	APPENDIX A	88
	APPENDIX B	91
	APPENDIX C	94
	APPENDIX D	95

1. INTRODUCTION

The National Director of the Dirección Nacional de Fronteras y Límites del Estado (DIFROL) of the Ministry of Foreign Affairs of Chile, Mrs. Ximena Fuentes, requested professors José Francisco Muñoz and Francisco Suárez to perform hydrological studies of the Quebrada Negra wetland, which is within the Silala River basin.

This final report describes the field work, data analysis and results obtained from a monitoring programme developed for the Quebrada Negra wetland, which is an undisturbed wetland located within the Silala topographic catchment in Chile, of comparable nature and areal extent to the Bolivian Cajones and Orientales wetlands. The characterization of this wetland will help to understand the hydrological and hydrogeological processes that are occurring in the various wetlands located in the headwaters of the basin. In addition, satellite products were used to compare vegetation activity and evaporation rates from the Quebrada Negra with the Cajones and Orientales wetlands. This study was led by Drs. José Francisco Muñoz and Francisco Suárez, under the supervision and instruction of Drs. Howard Wheeler and Denis Peach.

1.1 Objective

The objective of this work is to characterize the Quebrada Negra wetland by: (1) measuring meteorological variables, with the aim of determining potential evaporation; (2) characterizing the vegetation cover in the Quebrada Negra, Cajones and Orientales wetlands using satellite products; (3) estimating actual evapotranspiration in the Quebrada Negra, Cajones and Orientales wetlands using satellite products; (4) characterizing the main soil properties (soil particle distribution, hydraulic conductivity and thermal properties); and (5) measuring groundwater levels, to characterize the groundwater-surface water interactions. The collection of these data will thus help in understanding the hydrological functioning of the Quebrada Negra wetland and its water balance.

1.2 Summary of the methodology

The main activities of this work can be separated into five main groups: (1) activities related to the analysis of meteorological data to estimate potential evapotranspiration in the Quebrada Negra wetland; (2) activities related to the spatial and temporal characterization of the vegetation cover in the Quebrada Negra, Cajones and Orientales wetlands using satellite products; (3) activities related to the estimation of actual evapotranspiration in the Quebrada Negra, Cajones and Orientales wetlands using satellite products; (4) activities related to soil characterization; and (5) activities related to groundwater level monitoring.

Activities of the first group include: deployment of a meteorological station with soil sensors to measure necessary variables for energy balance and potential evapotranspiration estimation using the Penman-Monteith equation (Allen et al., 1998).

Activities of the second and third group consider the use of satellite images to estimate spatial and temporal distribution of vegetation cover in the Quebrada Negra, Cajones and Orientales wetlands, and to estimate actual evapotranspiration in those wetlands using a vegetation index (Groeneveld et al., 2007).

Activities of the fourth group include: a field campaign in which peat depth was determined and soil samples were collected to determine soil particle distribution and hydraulic conductivity with a falling head permeameter; execution of slug tests at selected monitoring points to determine the field hydraulic properties of the wetland deposits by using the Cooper et al. model (Cooper et al., 1967).

Activities of the fifth group consider the following: construction of a network of 82 monitoring points consisting of pairs of piezometers; field campaigns to measure the water levels at each well with a water level dipper; and continuous water level measurements at 5 monitoring points distributed inside the main wetland area, using pressure transducers.

1.3 Structure of the report

The structure of the remainder of this report is as follows: Chapter 2 provides a summary and the conclusions of the study; Chapter 3 describes the study area; Chapter 4 depicts the methods used in this study; Chapter 5 describes the main results; Chapter 6 presents the main conclusions; and Chapter 7 lists the references cited in this report.

2. SUMMARY AND CONCLUSIONS

In this study, during the transition from winter to spring (June to November 2018), the meteorological conditions, the vegetation cover and the groundwater levels of the Quebrada Negra wetland (Chile) were captured and analyzed. The vegetation cover of the Cajones and Orientales wetlands (Bolivia) was also analyzed. The results include a detailed meteorological description of the Quebrada Negra to estimate potential evapotranspiration; the spatial (July to November 2018) and temporal (January 1986 to April 2017) distribution of vegetation cover of the Quebrada Negra, Cajones and Orientales wetlands; and measurements of groundwater level in the Quebrada Negra wetland from August to October 2018.

To analyze the spatial distribution and the temporal evolution of the vegetation cover in the three wetlands mentioned above, Sentinel-2 and Landsat images were used. NDVI images were obtained for each of three wetlands. The high-resolution (10 m) Sentinel-2 data set was used to analyze the spatial distribution of the vegetation cover (July to November 2018), and the coarser resolution (30 m) LANDSAT product series was used to analyze its temporal evolution (January 1986 to April 2017).

Sentinel-2 NDVI data show, for each of the three wetlands, that the vegetation covers the whole of the available flat valley bottom area and extends up the adjacent hillslopes where slopes are less than approximately 15%. The maximum observed area of vegetation cover in Quebrada Negra was 4.12 ha in October 2018 and the mean area was 2.9 ha. Although the total area covered by vegetation changed, the extent of the vegetation cover in a studied lateral cross section did not vary. However, an increase in vegetation cover in the Quebrada Negra wetland during the studied period was observed in river cross sections located downstream and upstream of the studied cross section, where the width of vegetation cover increased in the north-south direction.

Monthly vegetation cover over the period 1986-2017 from LANDSAT data shows that vegetation cover peaks between April and May and there is strong variability for all the sites, especially in the Cajones wetland, during the December-May period. Vegetation coverage increased from July to December 2018 as seen from the Sentinel-2 images, which is consistent with the historical average variation curves (1986-2017) obtained by the LANDSAT images. Nevertheless, the values obtained from Sentinel and LANDSAT products are not directly comparable as the latter are less accurate. However, LANDSAT presents a longer period over which imagery is offered and therefore, allows for more years to be considered in the analysis.

Actual evapotranspiration was estimated using the Groeneveld et al. method (Groeneveld et al., 2007) at the annual time scale. This method was developed to estimate actual evaporation using remotely sensed NDVI data, for arid and semi-arid areas where evaporation is dominated by vegetation fed by shallow groundwater sources. The estimates of annual actual evapotranspiration showed that the highest annual value was observed in the Cajones wetland and the lowest in the Quebrada Negra wetland.

Two pits were excavated in the Quebrada Negra wetland, where a high content of organic material was found. For this reason, particle distribution tests could not be performed for all of the samples obtained. Saturated hydraulic conductivity of the peat present in the Quebrada Negra wetland was measured and estimated in the laboratory using a falling head permeameter and in the field with slug tests, with good agreement, showing relatively low permeabilities. Although measured hydraulic conductivities

show that the soil is semi-pervious to impervious, during the excavation of the pits, they needed to be constantly drained, because of water ingress.

The Quebrada Negra wetland exists because it is fed by groundwater. However, groundwater levels show a complex and spatially heterogeneous behavior. In much of the main wetland area, the vertical hydraulic gradient is mostly close to zero and dominated by downwelling gradients. Upwelling occurs at specific locations within the wetland, and there is evidence of spring emergence close to the base of the adjacent lateral hillslopes, at the upstream boundary of the wetland area, and there are upwelling gradients in the downslope ravine. Groundwater emerges within the main wetland, flows through distinct surface channels and re-infiltrates. The groundwater levels in the Quebrada Negra wetland show that there is an overall groundwater gradient parallel to the topographic gradient in the downhill direction towards the Silala ravine, i.e., the Quebrada Negra hydrogeological system feeds the Silala River system. This connection between the waters of the Quebrada Negra and the Silala hydrogeological systems is also supported by the geochemical analyses performed by Herrera and Aravena (Herrera and Aravena, 2019(a) and 2019(b)). They found high concentrations of Magnesium in the Quebrada Negra wetland as well as in the Silala River downstream of the junction of the two ravines. Therefore, there is a strong connection between these two hydrogeological systems.

3. STUDY AREA

The study area is the Silala River basin, a transboundary watershed shared by Bolivia (upstream) and Chile (downstream). The Silala River basin is located in the Andean Plateau of the Atacama Desert, approximately 300 km northeast of Antofagasta. The Silala River originates in Bolivian territory and flows towards the Antofagasta Region in Chilean territory (Figure 3-1). The Silala River is one of the main tributaries of the San Pedro de Inacaliri River, which in turn is a tributary of the Loa River. The Loa River is the longest Chilean river (440 km long) and the main watercourse in the Atacama Desert. It drains to the Pacific Ocean where its outlet is located at latitude 21°26' S.



Figure 3-1. The Loa River and its main tributaries. The Silala River topographic catchment (delineated in black) and groundwater catchment (delineated in green) are also shown.

The Quebrada Negra wetland is a densely vegetated area of approximately 30,000 m² (3 ha) on average (over the measurement period of June 2018 to November 2018), which has developed in the Quebrada Negra ravine, at ~4200 m.a.s.l. (Figure 3-2). Under the present climate, the Quebrada Negra ravine does not have a significant

perennial surface flow, but geochemical analysis suggests that there is a strong connection between its waters and the Silala River waters downstream of the junction with the Quebrada Negra ravine (Herrera and Aravena, 2019(b)). These authors show high concentrations of Magnesium in the Quebrada Negra wetland as well as in the Silala River downstream of the Quebrada Negra confluence. The Quebrada Negra wetland exhibits a green vegetation cover over almost the entire extent of the wetland, as shown in Figure 3-3 to Figure 3-6. Small surface flow networks are observed to occur extensively in the wetland (Figure 3-5), where spring flows emerge, flow overland in inter-connected natural networks of surface channels, and subsequently infiltrate. Some of the springs that feed the wetland emerge at the base of the rocky slopes that border the wetland, which is evidenced by vegetation growing at or towards the base of the hillslopes (Figures 3-3, 3-5 and 3-6) particularly on the southern side of the ravine. Downstream of the wetland, an ephemeral stream has been observed. The spatial extent of this streamflow changes with the season, but at least since October 2016 has never reached the Silala River.

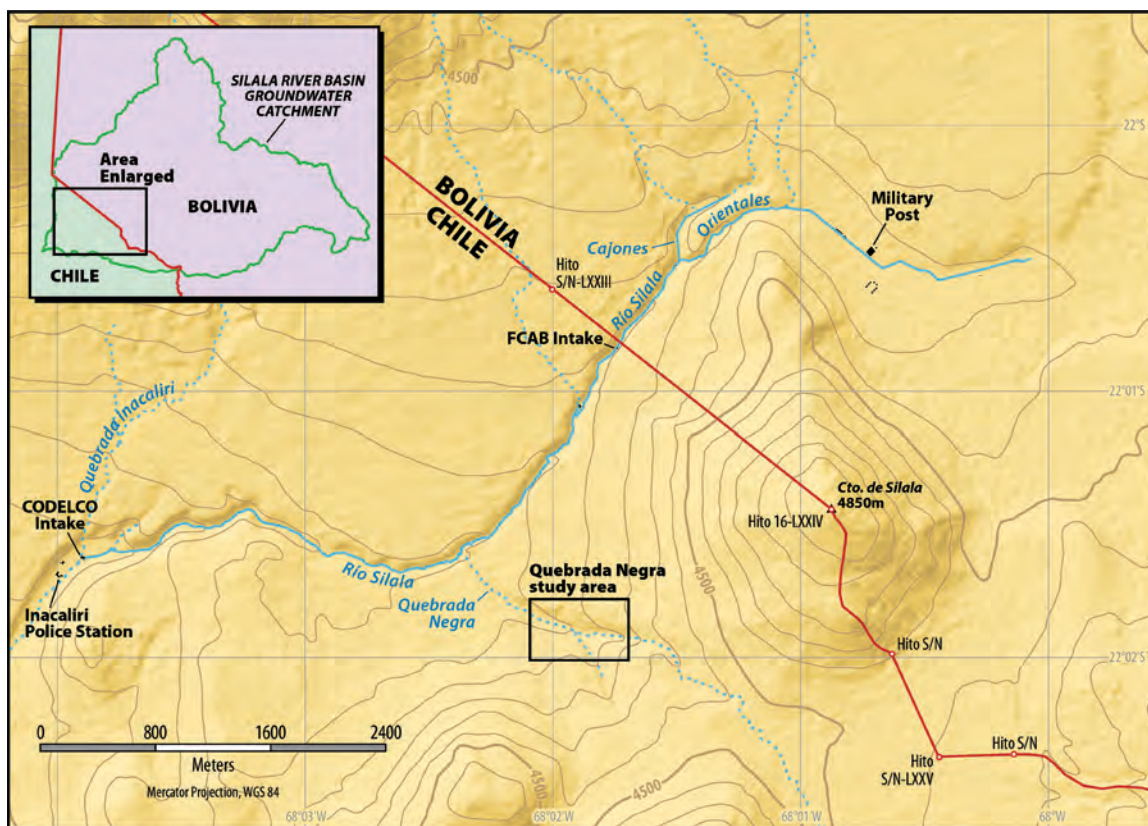


Figure 3-2. Location of the Quebrada Negra wetland.



Figure 3-3. Photograph of the Quebrada Negra wetland (taken from the northern slope).



Figure 3-4. Photograph of the Quebrada Negra wetland (taken from the southern slope).



Figure 3-5. Photograph taken at the Quebrada Negra wetland (looking upstream).



Figure 3-6. Photograph taken at the Quebrada Negra wetland (looking downstream).

An unmanned aerial vehicle (UAV) was used to take pictures from ~100 metres height to build a more detailed map of the study site and its surroundings, to determine the topography, and to be able to work using a GIS platform. Figure 3-7 to Figure 3-9 show some of the pictures taken and Figure 3-10 presents a three-dimensional surface model produced from the image analysis.



Figure 3-7. Photograph of Quebrada Negra wetland meteorological station (QWS) site with fence.

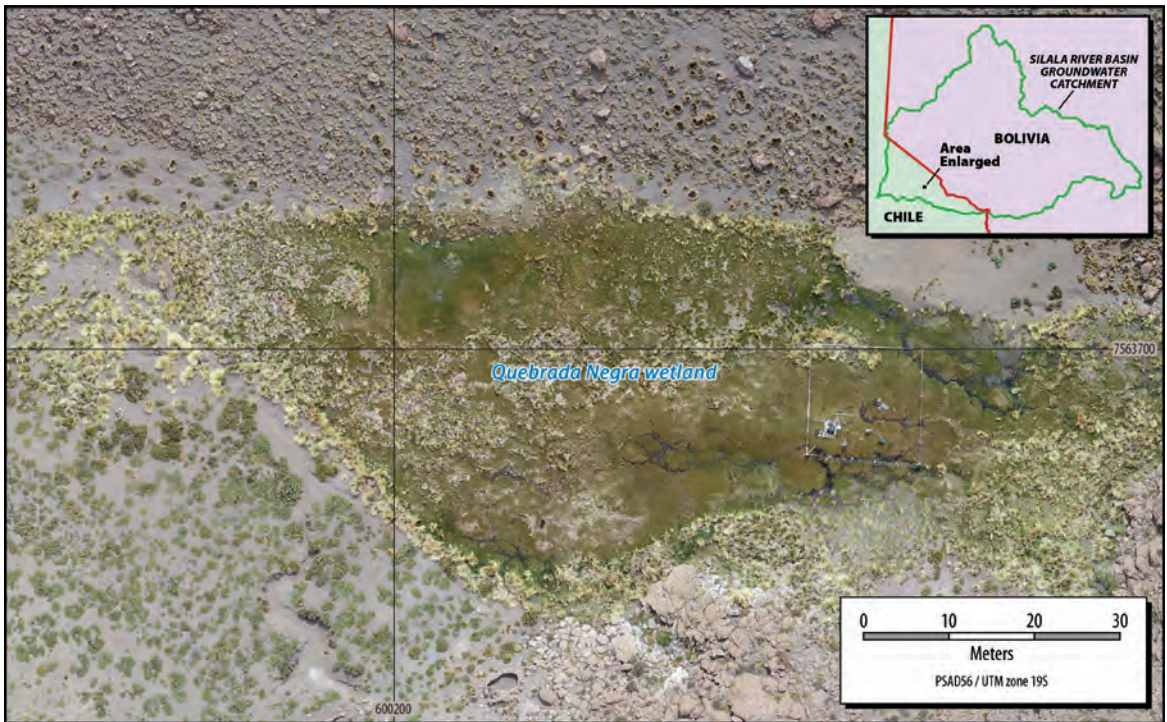


Figure 3-8. Photograph of the Quebrada Negra wetland (main wetland area).

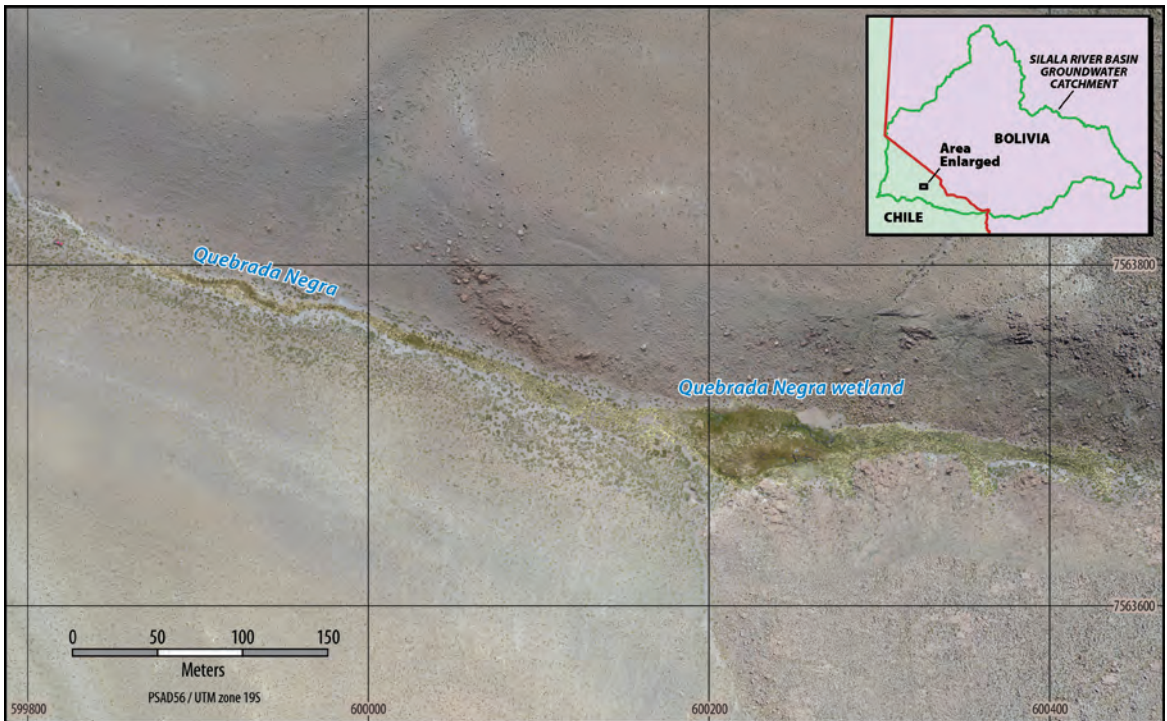


Figure 3-9. Photograph of the Quebrada Negra wetland and river bank.

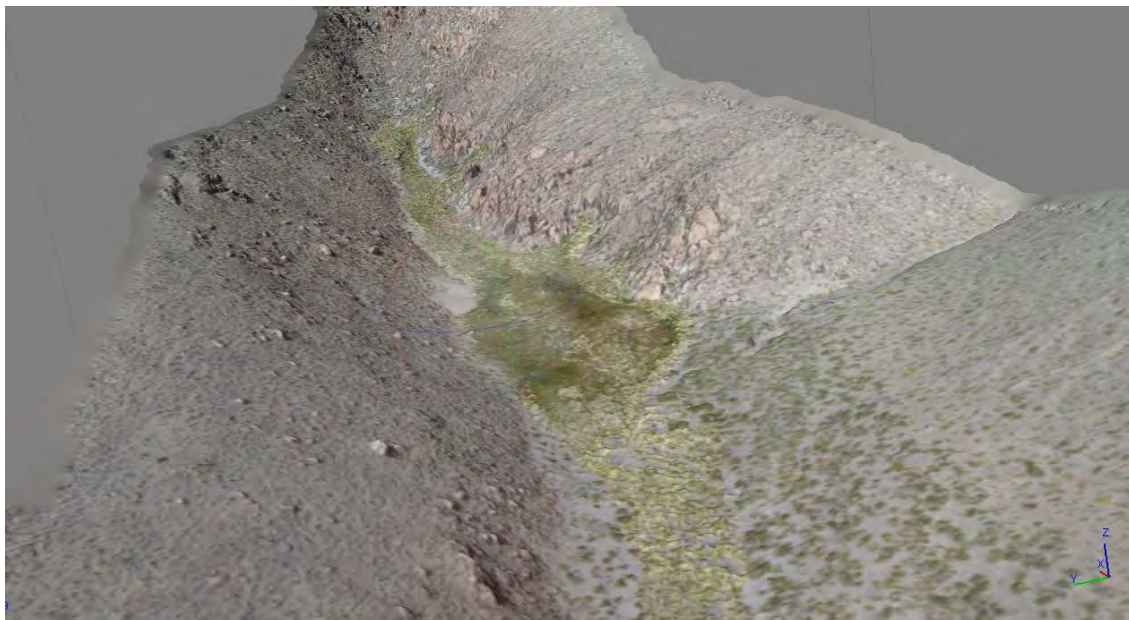


Figure 3-10. Three-dimensional surface model produced from image analysis, Quebrada Negra wetland.

4. METHODS

This section presents the methods used to investigate the Quebrada Negra wetland. First, a description of the Quebrada Negra Wetland meteorological station is provided (4.1). Then, the methods utilized to investigate the spatial and temporal distribution of the vegetation cover of the Quebrada Negra wetland are described. This methodology will also be applied to understand the temporal dynamics of the vegetation cover in both Cajones and Orientales (Bolivia) wetlands (4.2). Later, the methods used to investigate evapotranspiration processes in the wetland are presented (4.3). Next, the approach utilized to characterize the soils of the wetland is described (4.4). Finally, a description of the groundwater monitoring network is provided (4.5).

4.1 Quebrada Negra Wetland meteorological station

A meteorological station was installed in the Quebrada Negra wetland to monitor various environmental variables. Table 4-1 shows a list of components of the station, Figure 4-1 shows the deployment of the station and Figure 4-2 shows the heights above ground level of the different components of the station. The data provided by these components are being collected every 15 minutes. A Broadband Global Area Net (BGAN) module was added on 29 August and allows satellite transmission of the data

that can be accessed remotely through the internet. A data gap exists between 21 and 29 August that was due to a technical issue when installing the satellite transmission.

Instrument	Model	Manufacturer	Quantity
Weather-Resistant Enclosure, 16 x 18 inches	ENC16/18	Campbell Sci.	1
Datalogger	CR1000X	Campbell Sci.	1
16- or 32-Channel Relay Multiplexer	AM16/32B	Campbell Sci.	1
12V Power Supply with Charging Regulator and 7Ah Rechargeable Battery	PS200	Campbell Sci.	1
Propeller anemometer	05103	R.M. Young	1
Pressure transducer	U20L-04	Onset HOBO	1
Ambient temperature and relative humidity probe	CS215	Campbell Sci.	1
Tipping bucket rain gauge	TE525WS	Texas Electronics	1
Averaging soil thermocouple probe	TCAV	Campbell Sci.	1
Self-calibrating soil heat flux plate	HFP01SC	Hukseflux	2
Soil water content reflectometer	CS655	Campbell Sci.	1
4-Component net radiometer	CNR4	Kipp & Zonen	1
Broadband Global Area Net (BGAN)	-	-	1

Table 4-1. List of components of the Quebrada Negra Wetland meteorological station.

Additionally, MODIS satellite images were used to identify snowfall events. The MODIS snow algorithm output contains scientific data sets of snow cover, quality assurance, local attributes and global attributes (Hall et al., 2006). The temporal distribution of the snow cover in the Silala River basin was generated considering the same reported period as for the monitoring stations.



Figure 4-1. Deployment of the Quebrada Negra Wetland meteorological station.

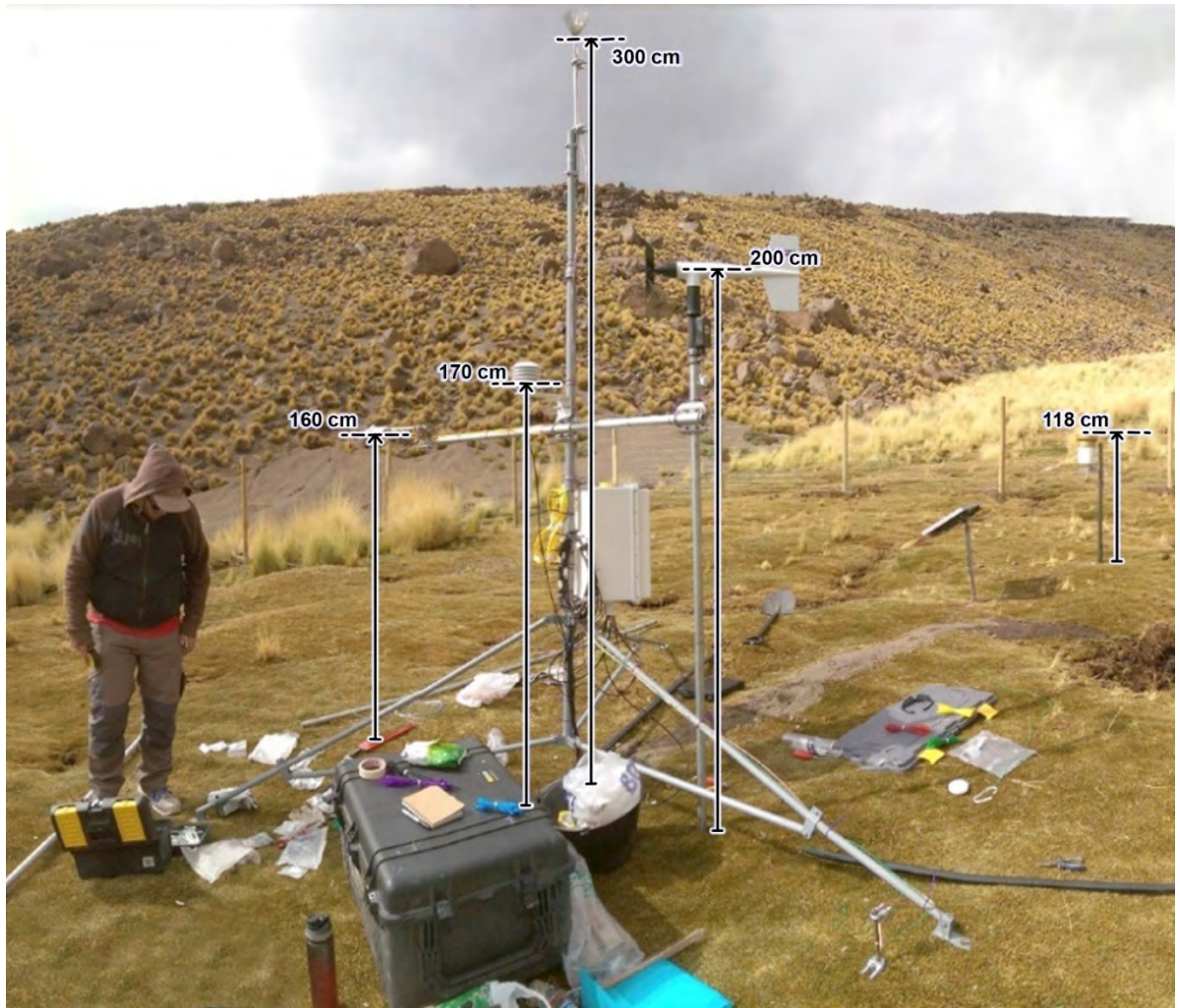


Figure 4-2. Heights above ground level of the different components of the Quebrada Negra Wetland meteorological station.

4.1.1 Anemometer

Measurements of wind speed are required at 2 metres height to obtain evaporation estimates using the FAO Penman-Monteith equation (Allen et al., 1998). The tallest element of the station must be the lightning rod, so the anemometer was installed on a cross-arm, secured to the ground and connected with a nu-rail to the cross-arm supporting the net radiometer to improve stability of the installation (Figure 4-1). The orientation of the sensor is such that north direction is recorded as zero degrees.

4.1.2 Net radiometer

The net radiometer was mounted on a cross-arm with the included nu-rail. The sensor is pointing towards the North. The elevation with respect to the ground is 160 centimetres

(Figure 4-2), in agreement with manufacturer recommendations (of at least 150 centimetres).

4.1.3 Tipping bucket rain gauge

A 2 metres length 1.25-inch steel pipe was inserted 1 metre into the ground to support the tipping bucket. The steel pipe was located as far from the central mast as the tipping bucket's cable length allowed, to minimize potential interference from other structures. The tipping bucket was installed so that the rim is at least 5 centimetres above the pipe. The height to the rim is 118 centimetres (Figure 4-2), which is within typical values reported by the World Meteorological Organization (WMO), which recommends installing the tipping bucket between 0.5 and 1.5 metres above ground level (WMO, 2014). The tipping bucket cannot be installed at a lower height as the installation of a snowfall adapter is required and the gauge must stand above any snowpack. The total height of the tipping bucket with snowfall adapter is ~90 centimetres. The distance to the closest obstruction is greater than twice the difference in height, in agreement with WMO recommendations (WMO, 2014).

The cables from the tipping bucket, solar panel and soil sensors were buried to prevent rodent damage (Figure 4-3).



Figure 4-3. Solar panel, tipping bucket and buried cables of the Quebrada Negra Wetland meteorological station.

4.1.4 Ambient temperature and relative humidity probe

The ambient temperature and relative humidity probe was installed inside the solar radiation shield at 170 centimetres above the ground (Figure 4-2). This height is within the range recommended by the WMO (WMO, 2014).

4.1.5 Soil sensors

The array of soil sensors consists of two self-calibrating soil heat flux plates (HFP01SC), an averaging soil thermocouple probe (TCAV) and a water content reflectometer (CS655). These sensors were deployed as depicted in Figure 4-4.

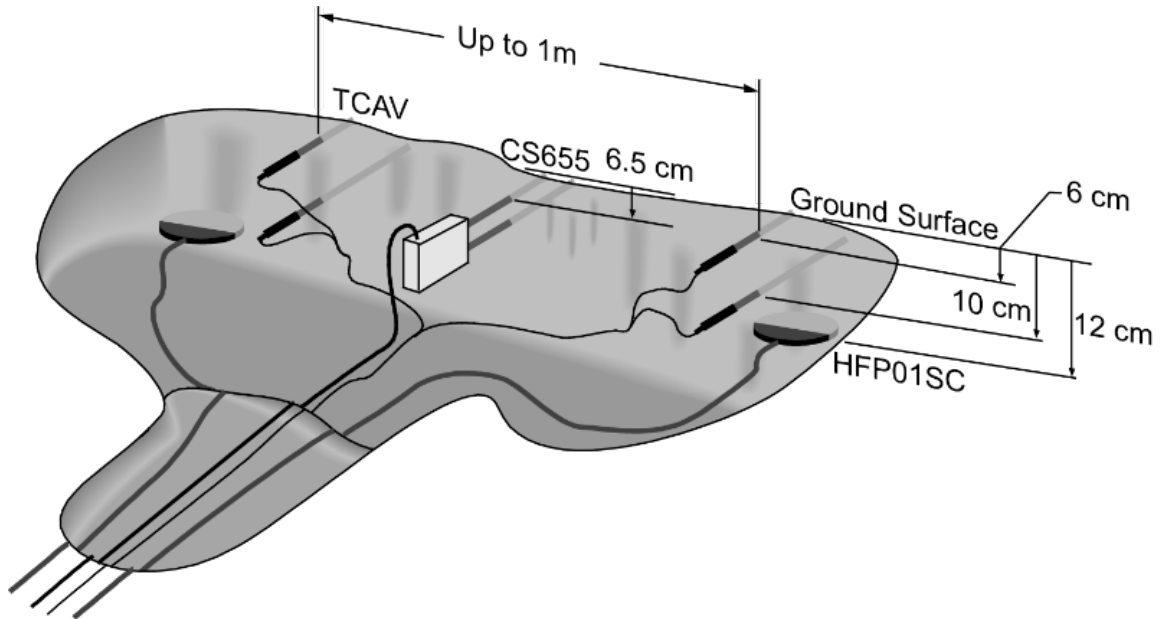


Figure 4-4. Soil sensors layout.

Figure 4-5 shows a photograph of the installation of the soil heat flux plate. If the 12 centimetres mark in the measuring tape is considered the ground surface, it can be seen that the soil heat flux plate is located at 12 centimetres depth (0 centimetre mark), as shown in Figure 4-4.



Figure 4-5. Soil heat flux plate installation.

During installation, the hole became flooded relatively quickly and soon the soil heat flux plates were completely submerged. Figure 4-6 shows the final conditions of the array of sensors installed, with the soil heat flux plates under water.

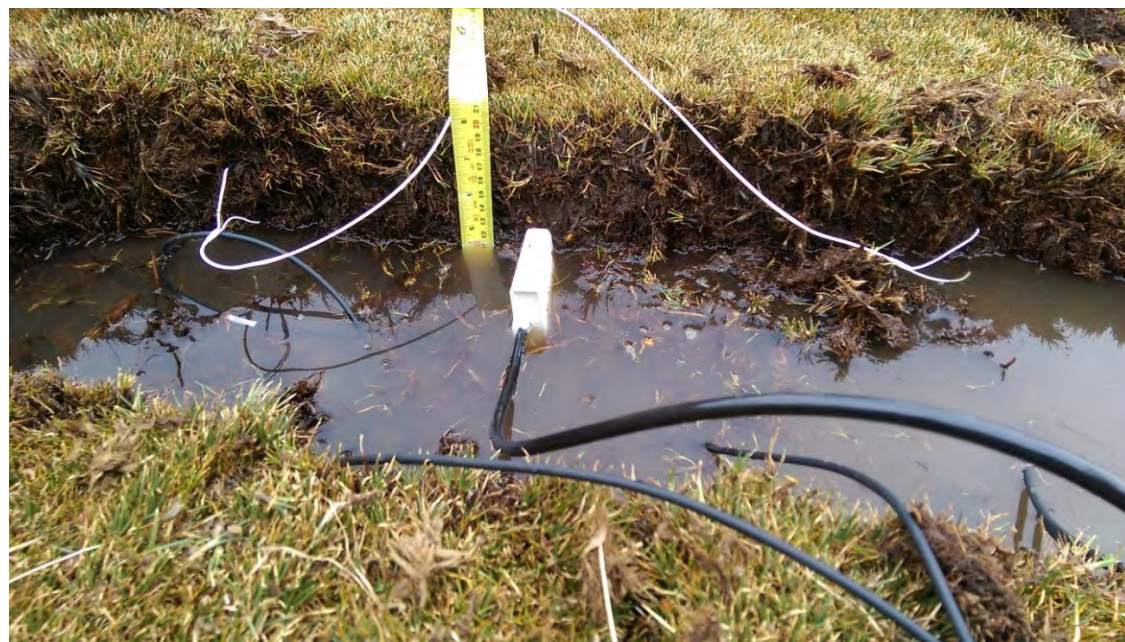


Figure 4-6. Soil sensors at the Quebrada Negra Wetland meteorological station.

4.2 Spatial and temporal distribution of vegetation cover

The Normalized Difference Vegetation Index (NDVI) is an indicator of vegetation vigor and it is calculated from satellite data using the red (R) and the near-infrared (NIR) bands in the electromagnetic spectrum (Groeneveld and Baugh, 2007):

$$\text{NDVI} = \frac{\text{NIR} - \text{R}}{\text{NIR} + \text{R}} \quad (1)$$

Since chlorophyll almost completely absorbs the red light and strongly reflects the NIR portion of the spectrum, the difference between both bands is a strong indicator of the health of vegetation (Groeneveld et al., 2007). The NDVI varies from -1.0 to 1.0, and according to Alcayaga, low, positive NDVI values (between 0.2 and 0.4) represent shrub and grassland (Alcayaga, 2017).

Two complimentary satellite products, Sentinel-2 (10 m resolution) and LANDSAT (30 m resolution), were used to compare the vegetation cover of the Quebrada Negra wetland (in Chile) with the Orientales and Cajones wetlands (in Bolivia). Sentinel-2 satellite images are obtained every 5 days and LANDSAT images every 15 days. Nevertheless, the values obtained from Sentinel-2 and LANDSAT products are not directly comparable because the latter are less accurate. However, LANDSAT presents a larger period over which imagery is offered and therefore allows for more years to be considered in the analysis.

4.2.1 Spatial distribution of vegetation cover

For the analysis of spatial distribution of vegetation cover of the Quebrada Negra (Chile), Cajones and Orientales (Bolivia) wetlands, monthly NDVI maps were calculated for July, August, September, October and November 2018, using the optical images provided by the Sentinel-2 mission (Table 4-2). Only images where no clouds in the studied wetlands occurred were used. To generate the monthly averaged NDVI maps, one NDVI map was generated for each sensed date, and these images were averaged in time for each month.

The aim of the Sentinel-2 mission, developed by the European Space Agency, is to monitor temporal variability in land surface conditions (due to its high revisit time), and the data can be used at the study area to monitor changes in vegetation. The sensors on Sentinel-2 satellites have 13 spectral bands; bands 4 and 8 are the R and NIR bands, respectively (Zhu et al., 2015).

Date	Name
03/07/2018	S2A_MSIL1C_20180703T143751_N0206_R096_T19KER_20180703T180946
08/07/2018	S2B_MSIL1C_20180708T143749_N0206_R096_T19KER_20180708T191932
18/07/2018	S2B_MSIL1C_20180718T143749_N0206_R096_T19KER_20180718T192157
17/08/2018	S2B_MSIL1C_20180817T143739_N0206_R096_T19KER_20180817T192123
22/08/2018	S2A_MSIL1C_20180822T143751_N0206_R096_T19KER_20180822T192224
27/08/2018	S2B_MSIL1C_20180827T143739_N0206_R096_T19KER_20180827T192139
01/09/2018	S2A_MSIL1C_20180901T143741_N0206_R096_T19KER_20180901T182920
06/09/2018	S2B_MSIL1C_20180906T143739_N0206_R096_T19KER_20180906T195021
16/09/2018	S2B_MSIL1C_20180916T143739_N0206_R096_T19KER_20180916T192127
21/09/2018	S2A_MSIL1C_20180921T143741_N0206_R096_T19KER_20180921T181736
26/09/2018	S2B_MSIL1C_20180926T143739_N0206_R096_T19KER_20180926T200955
01/10/2018	S2A_MSIL1C_20181001T143741_N0206_R096_T19KER_20181001T181115
11/10/2018	S2A_MSIL1C_20181011T143751_N0206_R096_T19KER_20181011T181532
21/10/2018	S2A_MSIL1C_20181021T143751_N0206_R096_T19KER_20181021T180732
26/10/2018	S2B_MSIL1C_20181026T143749_N0206_R096_T19KER_20181026T192118
31/10/2018	S2A_MSIL1C_20181031T143751_N0206_R096_T19KER_20181103T085637
05/11/2018	S2B_MSIL1C_20181105T143749_N0206_R096_T19KER_20181105T192245
10/11/2018	S2A_MSIL1C_20181110T143751_N0207_R096_T19KER_20181110T181533
15/11/2018	S2B_MSIL1C_20181115T143749_N0207_R096_T19KER_20181115T182029
20/11/2018	S2A_MSIL1C_20181120T143751_N0207_R096_T19KER_20181120T181100

Table 4-2. Sentinel-2 images used to calculate monthly NDVI map.

Before calculating the NDVI, the R and NIR bands were pre-processed and atmospherically corrected by dark object subtraction (DOS). The DOS is based on the assumption that within the image, there are some pixels in complete shadow and therefore, the reflectance sensed by the satellite is due only to atmospheric scattering (Chavez, 1996). This process was carried out using the Semi-Automatic Classification Plugin from QGIS plugin (Congedo, 2018).

After the R and NIR bands were atmospherically corrected, the NDVI was calculated for each Sentinel-2 image. The NDVI values of each pixel, for each month, were averaged and NDVI maps for July, August, September, October and November 2018 were obtained.

To visualize where the vegetation cover is located within the terrain in each wetland, the spatial distribution of vegetation estimated with the NDVI obtained from the Sentinel-2 images (averaged between July and November 2018) was combined with the topographic information from a digital elevation model (AW3DTM). The topographical information source was a Digital Elevation Model (DEM) with 5 m horizontal resolution, acquired from the Advanced Land Observing Satellite (ALOS) World 3D Digital Terrain Model (NTT DATA and RESTEC, 2014).

Additionally, it is important to mention that the comparison of a cross section of vegetation cover considers the period between June and November and hence the annual maximum extent of vegetation cover is not included. The maximum extents of vegetation cover occur between January and March. However, it is possible to show the variation in the dynamics of the extent of vegetation coverage of the Cajones and Orientales wetlands over the studied period, but for the Quebrada Negra wetland the variation of spatial extent was less than the resolution of the sensor for the studied period.

4.2.2 Temporal evolution of vegetation cover

The temporal evolution of the vegetation cover of the Quebrada Negra (Chile) and Cajones and Orientales (Bolivia) wetlands was analyzed using the historical repository of Landsat images (30 m resolution) for the period 1985-2017. To obtain this time series, the Google Earth Engine platform (Gorelick et al., 2017) and the computational tool developed by Sproles (Sproles et al., 2018) were used. The tool developed by Sproles (Sproles et al., 2018) allows obtaining the snow cover area through the NDSI values, and the script was modified for this study to derive the NDVI values (equation (1)).

To obtain the time series of vegetation cover over Cajones, Orientales and Quebrada Negra, we first filtered out the striped and distorted NDVI images every 8 days through visual inspection (314 valid images remaining were considered). Different Landsat

missions were considered: LANDSAT-5 between 1986-1999, LANDSAT-7 between 2000-2002 and between 2012-2013, LANDSAT-8 for 2014-2017.

4.3 Evapotranspiration estimation

Evapotranspiration (ET) is the combination of two separate processes that occur simultaneously, whereby water is lost on the one hand from the soil surface by evaporation and on the other hand from the crop (vegetation) by transpiration (i.e. due to evaporation within the plant leaf). Soil evaporation is mainly determined by the fraction of the solar radiation reaching the soil surface and the water availability. Transpiration is mainly determined by the meteorological conditions, plant cover and the water available to the plant root system (Allen et al., 1998).

4.3.1 Potential evapotranspiration

Potential evaporation (ET_o) is the ET rate for a reference surface, normally a hypothetical grass reference crop with specific characteristics (Allen et al., 1998). ET_o assumes that water is unlimited and is an idealized value that does not depend on crop type, crop development and management practices.

Many methods are available in the literature to determine ET_o (Allen et al., 1998; Summer and Jacobs, 2005; Yoder et al., 2005). The FAO Penman-Monteith method is recommended by the FAO for the calculation of ET_o (Allen et al., 1998). Also, Garcia et al. (Garcia et al., 2004) demonstrated that the FAO Penman-Monteith approach is suitable in the Bolivian Altiplano.

FAO Penman-Monteith equation

The FAO Penman-Monteith approach calculates ET_o (mm day^{-1}) using the following equation (Allen et al., 1998):

$$ET_o = \frac{0.408\Delta(R_n - G) + \gamma \frac{900}{T + 273} u_2 (e_s - e_a)}{\Delta + \gamma(1 + 0.34u_2)} \quad (2)$$

where R_n is the net radiation at the crop surface ($\text{MJ m}^{-2} \text{day}^{-1}$); G is the soil heat flux density ($\text{MJ m}^{-2} \text{day}^{-1}$); T is the mean daily air temperature measured at 2 m height ($^{\circ}\text{C}$); u_2 is the wind speed at 2 m height (m s^{-1}); e_s and e_a are the saturation and actual vapor pressure, respectively, and the term $(e_s - e_a)$ is called the vapor pressure deficit (VPD , kPa); Δ is the slope of the saturated vapor pressure-temperature curve ($\text{kPa } ^{\circ}\text{C}^{-1}$) and γ is the psychrometric constant ($\text{kPa } ^{\circ}\text{C}^{-1}$).

4.3.2 Spatial distribution of estimated actual evapotranspiration

Actual evapotranspiration (ET_a), and its spatial distribution, can be estimated by associating the NDVI with ET_o and precipitation measurements. Because the amount of

chlorophyll that a plant has is directly related to the rate of photosynthesis, and during photosynthesis the plant transpires water (Tucker and Sellers, 1986; Sellers et al., 1992), the NDVI can be used as an indicator of ET_a . Groeneveld et al. (2007) proposed a methodology suitable for arid and semi-arid areas where near surface groundwater supports vegetation, to produce a first-order estimate of annual ET_a as a function of NDVI, annual ET_o and annual precipitation:

$$ET_{a,NDVI} = (\text{Annual } ET_o - \text{Annual precipitation}) \cdot NDVI' + \text{Annual precipitation} \quad (3)$$

where $ET_{a,NDVI}$ is the estimated annual ET_a , and $NDVI'$ is the spatially averaged raw mid-summer NDVI (peak season NDVI) normalized by setting bare soil values ($NDVI_0$) at 0 and values of full vegetation cover ($NDVI_s$) at 1.0, as in equation (4).

$$NDVI' = \frac{NDVI - NDVI_0}{NDVI_s - NDVI_0} \quad (4)$$

To estimate the annual $ET_{a,NDVI}$, which requires mid-summer NDVI, Sentinel-2 satellite images from December 2017, January 2018 and February 2018 were used. Although mid-summer in the Altiplano is characterized by intense precipitation events, it was observed that in general the peak season NDVI in the studied area is also observed in the Austral summer. Because data from the Quebrada Negra wetland meteorological station were not available for an entire year, Quebrada Negra station (DGA) data were used to calculate annual precipitation (the DGA's Quebrada Negra station is ~800 m from the Quebrada Negra wetland station) and UC meteorological station data were used to estimate ET_o (1 June 2017 to 31 May 2018). It was not possible to estimate annual ET_o with Quebrada Negra station (DGA) records, because this station does not measure all the variables that are necessary to estimate potential evapotranspiration.

One NDVI map was generated for each satellite image (Table 4-3), as described in Section 4.2.1. Only images where there were no clouds in the studied wetlands were used. Note also that the images used correspond to the ones obtained during the summer, as required by the Groeneveld et al. method (Groeneveld et al., 2007), in which peak season NDVI is used. To analyze the sensitivity of this method to the selection of the mid-summer NDVI value, $ET_{a,NDVI}$ was calculated for each date using the spatially averaged $NDVI'$ for each NDVI map ($NDVI > 0.2$). The annual precipitation data were obtained from Quebrada Negra station (DGA) and the annual ET_o , calculated with the FAO Penman-Monteith method (Allen et al., 1998), were obtained from the UC meteorological station.

Date	Name
25/12/2017	S2A_MSIL1C_20171225T143751_N0206_R096_T19KER_20171225T180226
30/12/2017	S2B_MSIL1C_20171230T143739_N0206_R096_T19KER_20171230T192131
09/01/2018	S2B_MSIL1C_20180109T143749_N0206_R096_T19KER_20180109T180001
14/01/2018	S2A_MSIL1C_20180114T143741_N0206_R096_T19KER_20180114T180438
18/02/2018	S2B_MSIL1C_20180218T143749_N0206_R096_T19KER_20180218T211409
23/02/2018	2A_MSIL1C_20180223T143751_N0206_R096_T19KER_20180223T180301
28/02/2018	S2B_MSIL1C_20180228T143749_N0206_R096_T19KER_20180228T193153

Table 4-3. Satellite images used to estimate annual actual evapotranspiration.

Additionally, to observe the spatial distribution of $ET_{a,NDVI}$, equation (3) and (4) were applied for each pixel in the images used to obtain the $ET_{a,NDVI}$ map, as presented in equations (5) and (6):

$$ET_{a,NDVI,j} = (\text{Annual } ET_o - \text{Annual precipitation}) \cdot NDVI'(j) + \text{Annual precipitation} \quad (5)$$

$$NDVI'(j) = \frac{NDVI(j) - NDVI_0}{NDVI_s - NDVI_0} \quad (6)$$

where $ET_{a,NDVI,j}$ is the estimated annual ET_a in the pixel “j” of an NDVI image, and $NDVI'(j)$ is the raw mid-summer NDVI (peak season NDVI) of pixel “j”, normalized by setting bare soil values ($NDVI_0$) at 0 and values of full vegetation cover ($NDVI_s$) at 1.0, as in equation (4).

4.4 Soil characterization

4.4.1 Field campaign to determine peat depth, describe soil particle distribution and permeability

Three sites were chosen to carry out soil characterization within the Quebrada Negra wetland (P1, P2 and SA in Figure 4-7). The pit excavations and the soil sampling collection were performed at the Quebrada Negra wetland between 22 and 23 November 2018. The “P” locations correspond to the middle (P1) and downstream (P2) sections of the wetland, respectively. At each “P” location, a trial pit was excavated to extract soil samples for the soil characterization. The “SA” location corresponds to a site where a soil auger was used to determine the depth of the peat.

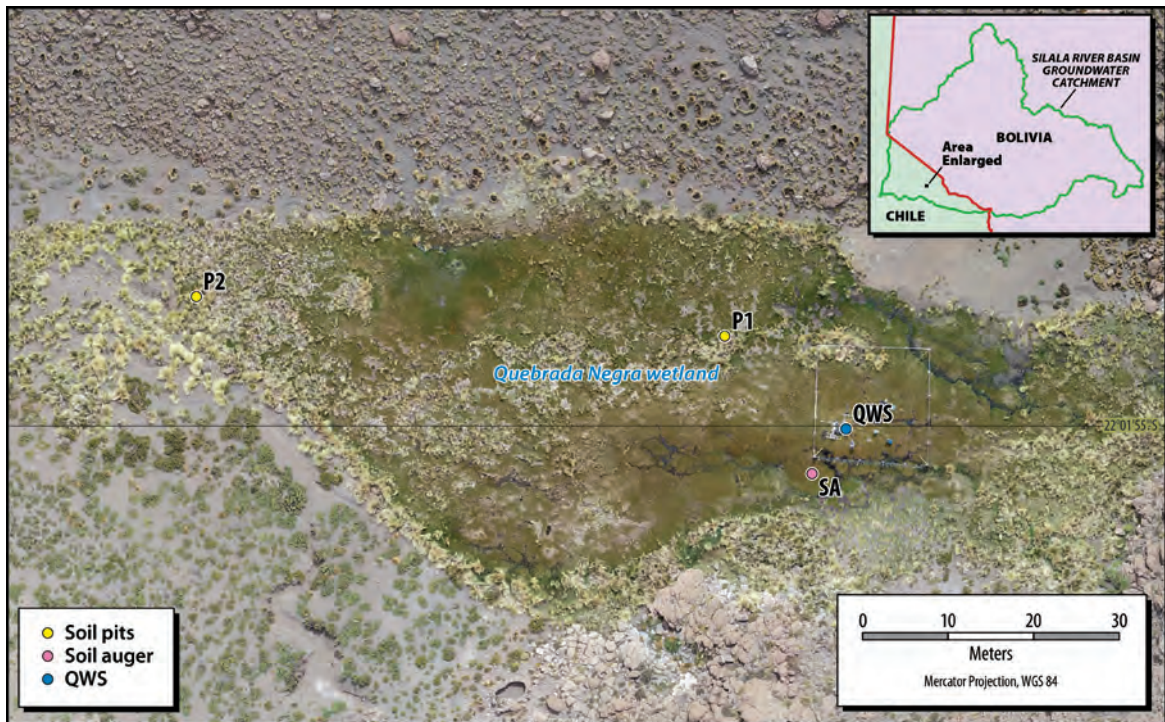


Figure 4-7. Pit locations (P1 and P2 in yellow), soil auger hole location (SA in pink) and Quebrada Negra wetland meteorological station (QWS in blue) at the Quebrada Negra wetland.

The pits excavated for this study (P1 and P2 in Figure 4-7) had a step at 0.5 m, and another at 1.5 m, to allow sample collection with Shelby tubes (see Section 4.4.1.3), and a deeper zone where water that emerged was accumulated and then removed. A schematic of the excavated trial pits at P1 and P2 is shown in Figure 4-8. This scheme includes the labeling system used for the Shelby tubes sample collection. Figure 4-9 shows the excavation work at the Quebrada Negra wetland. More photographs of the pits can be found in Appendix A.

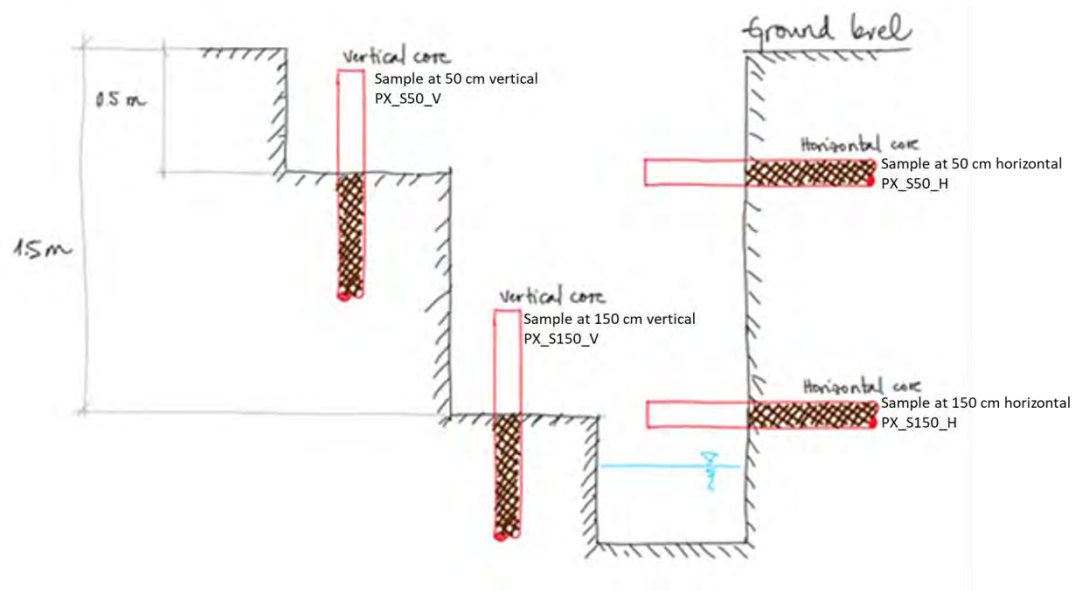


Figure 4-8. Trial pit design for soil characterization at the Quebrada Negra wetland. The labeling system used for the Shelby tubes sample is depicted. PX is for the trial pit at which the sample was collected, whether at pit P1 or P2. S50 and S150 refer to a sample taken at 50 (S50) or at 150 (S150) cm depth respectively. V and H identify Vertical and Horizontal samples respectively.



Figure 4-9. Excavation work of (a) P1 middle of the wetland and (b) P2 downstream, at the Quebrada Negra wetland.

4.4.1.1 Peat depth determination

Peat depth determination at the Quebrada Negra wetland was performed using a soil auger (similar to that presented in Figure 4-10). The location for the hole made with the soil auger to identify the peat depth was approximately 5 metres to the southwest of the Quebrada Negra meteorological station (see Figure 4-7).



Figure 4-10. Soil auger similar to that used at the Quebrada Negra wetland.

Soil samples at different depths were photographed and stored every 20 to 50 centimetres. Figure 4-11 shows peat samples taken between 30 and 190 centimetres depths at the Quebrada Negra wetland. As explained above, the 14 samples collected from the soil auger hole are labeled SA (Figure 4-7), where SA is soil auger and the remaining digits are the means of the depths at which the sample was taken. MX is the sample collection number used in the field campaign. Photographs of the other samples can be found in Appendix B.

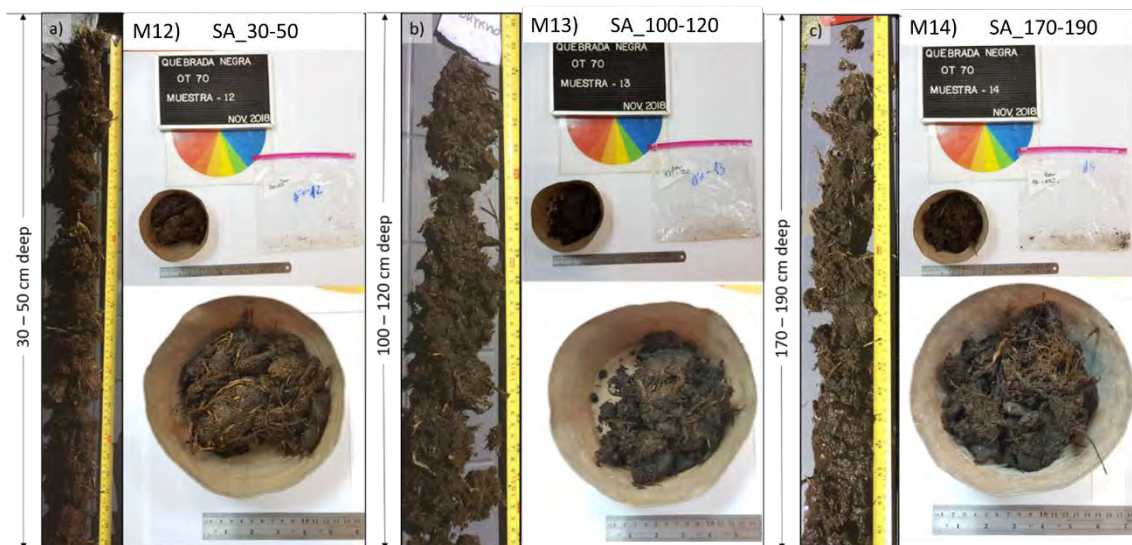


Figure 4-11. Soil samples between 30 and 190 cm deep at the Quebrada Negra wetland for peat characterization.

4.4.1.2 Soil particle distribution

Soil samples for soil particle distribution analysis were taken as follows: five at pit P1, six at pit P2 and 14 samples were extracted from the soil auger excavation. These samples were analyzed by Dictuc's Geotechnical and Soil Mechanics Laboratory using the methodology proposed by the American Society of Testing Materials in "Standard Test Method for Particle-Size Analysis of Soils D422" (ASTM, 2007). Sample preparation according to the D421 standard (ASTM, 2007) is carried out before the soil particle distribution analysis. This preparation consists of separating the sample using a No. 10 sieve by dry sieving and washing. The retained fraction in sieve No. 10 is then washed, dried and weighed.

The fraction that passes the No. 10 sieve is then separated into a series of fractions using 75 mm, 50 mm, 37.5 mm, 25 mm, 19 mm, 9.5 mm, 4.75 mm, 2.36 mm, 1.18 mm, 0.6 mm, 0.3 mm, 0.15 mm and 0.075 mm. After that, the resulting sample fractions are weighed on the balance to determine the mass of each.

Particle distribution analyses of the soil samples are presented in Figure 4-12 and Figure 4-13. The samples are labeled as PX_SX, after the pit where they were collected (PX) and a sample number (SX). MX is the sample collection number used in the field. The soil samples collected contained a large number of roots and organic matter, especially the samples that correspond to the upper few centimeters of soil (P1_S1 in Figure 4-12 and P2_S1 in Figure 4-13). This material had to be removed from the sample in the sample washing stage (before sieving). The 14 samples collected from the soil auger

hole are labeled SA_ (Figure 4-7), where SA is soil auger and the rest are the means of the depths at which the sample was taken. MX is the sample collection number for the laboratory.



Figure 4-12. Soil samples at different depths for soil particle distribution analysis in pit SPI.

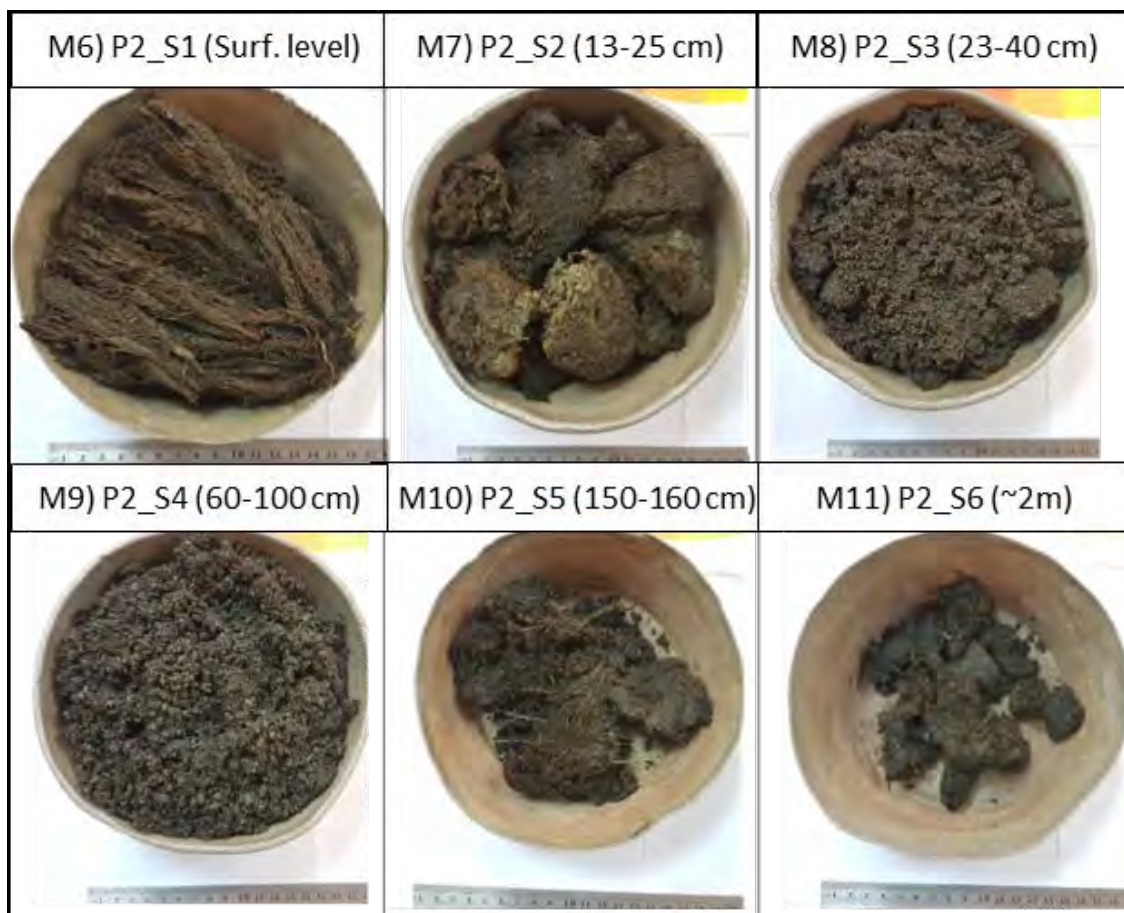


Figure 4-13. Soil samples at different depths for soil particle distribution analysis in pit SP2.

4.4.1.3 Shelby tubes for saturated hydraulic conductivity tests

Thin-walled tubes (Shelby tubes) were used to take undisturbed soil samples at 0.5 and 1.5 m depth at the two trial pits. The tube used for this study and corresponding dimensions are shown in Figure 4-14. At each of these depths, horizontal and vertical samples were taken to determine soil saturated hydraulic conductivity (K_s) in both directions (Figure 4-8). A total of eight samples were taken with the thin walled tubes, 4 at SP1 and 4 at SP2. The samples are labelled as shown in Figure 4-8. Later these samples were analyzed by the Geotechnical and Soil Mechanics department of Dictuc to undergo falling-head permeability tests to determine hydraulic conductivity.

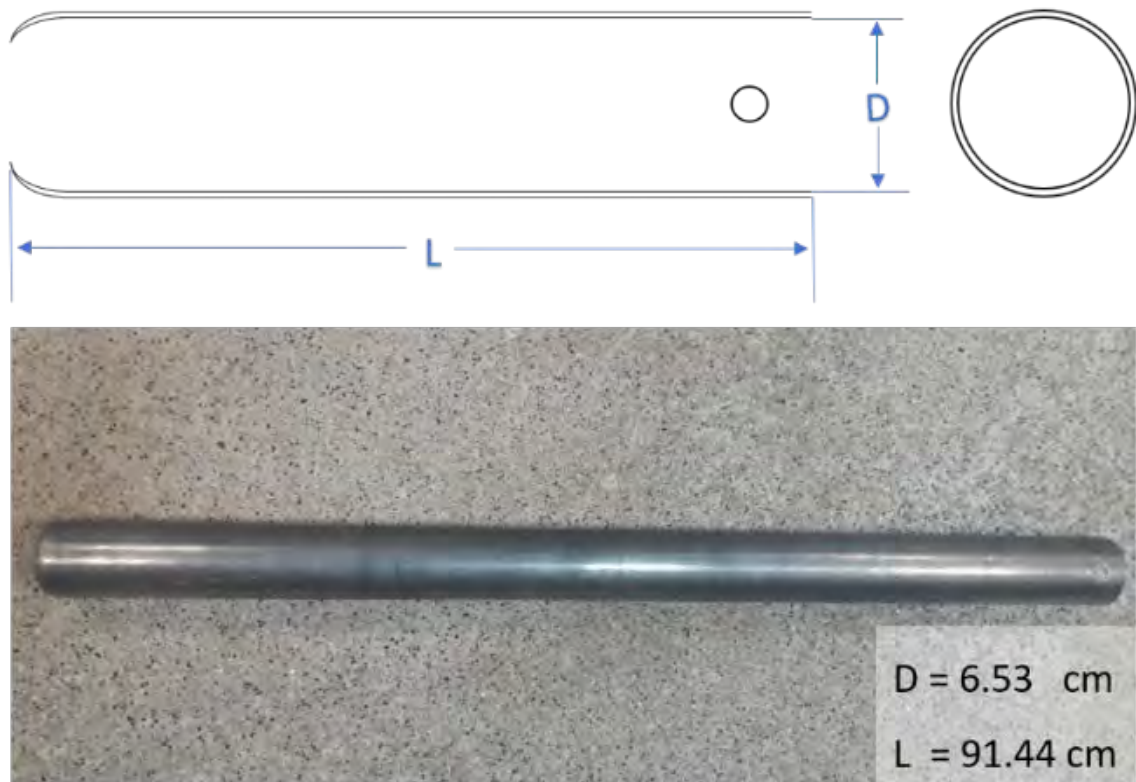


Figure 4-14. Photograph of one of the Shelby tubes used for collecting the soil samples at the Quebrada Negra wetland.

Undisturbed soil sampling was performed using the methodology proposed by the American Society of Testing Materials in “Standard Practice for Thin-Walled Tube Sampling of Fine-Grained Soils for Geotechnical Purposes D1587” (ASTM, 2015). The standard indicates the following procedure for soil sampling.

First, loose material has to be removed as carefully as possible. Then, the tube head is fitted concentrically and coaxially to ensure a uniform application of force to the tube when applying pressure. At the time of sampling, without rotation, the tube must be driven into the ground with a great and continuous push until reaching a point of rejection or until the tube head meets the ground. After introducing the tube into the ground, there should be a waiting period between 5 and 15 minutes before removing the tube, to generate soil adhesion inside the tube. Before taking the sample, the tube should be rotated once and then removed from the ground. Finally, the upper and lower part of the tube must be sealed and labeled, and then transported to the laboratory (ASTM, 2015).

The thin-walled tubes inserted for this study took between 10 seconds and 5 minutes to bury them approximately 50 cm in the pits' wall or in the steps of the pits.

In some cases, due to the amount of roots in the pit (e.g., see Figure 4-15), or due to the difficulty of placing the tube in the correct position, it took more time than that recommended as standard. Sometimes manual pressure was not enough to insert the tubes to the required depth (e.g. P1_S50_V, P2_S50_V, P2_S50_H, P2_S150_H). For those cases, the help of a sledge hammer was required to insert the tube to approximately 50 cm, the sample length required for laboratory analysis.

After inserting the thin walled tubes, they were left buried with the sample for 5 to 8 minutes for the soil to adhere to the tubes.

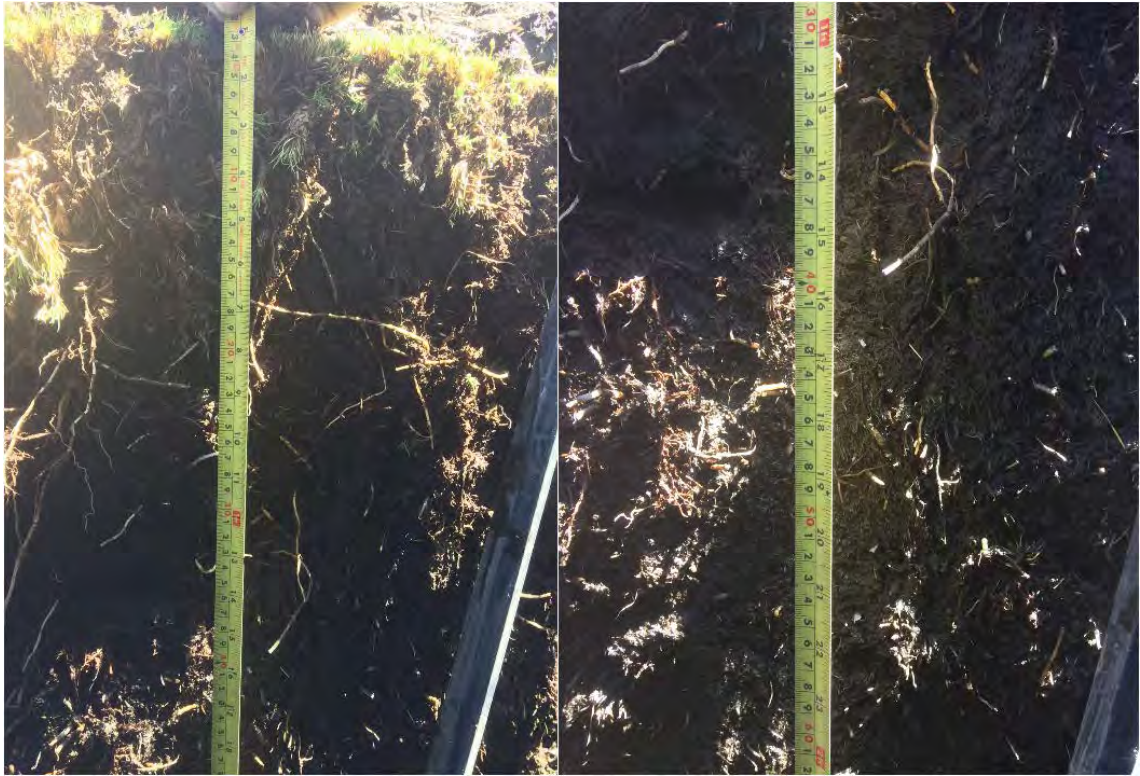


Figure 4-15. First 60 cm from the surface level at Pit P1 at the Quebrada Negra wetland.

The high groundwater level at the Quebrada Negra wetland makes the soil slurry-like at depth, making it difficult to remove the samples because of the low adhesion to the tube. At both pits the soil samples (or part of them) came out of the tube when they were being removed, in which case the sampling was repeated (sampling points P1_S50_V, P1_S50_H, P1_S150_V, P1_S150_H and P2_S150_V). In the case of the samples taken at 1.5 m vertically (P1_S150_V and P2_S150_V), it was decided to dig around the buried tube and then the tube was tilted to extract the sample intact.

In Figure 4-9 the level of water at the bottom of the pits is shown. The bottom of the pit had to be constantly drained, due to a continuously rising water level.

More details of the eight thin-walled tube soil sample collection carried out in this study are described in Appendix C.

4.4.1.4 Falling-head Permeability Test

To obtain values for the soil saturated hydraulic conductivity (K_s) of cohesive sediments with low conductivities, a falling-head permeameter should be used (Fetter, 1994). For this study, falling-head permeability tests were performed in the laboratory to obtain K_s . The falling-head permeability test consists of measuring the flow of water that passes

through a (relatively short) soil sample inside a permeameter (Figure 4-16). A set of standpipe tubes (or vertical falling-head tubes) are attached to the permeameter (see Figure 4-17). To fulfill the falling head permeability tests, the following materials are required:

- Permeameter cell (see Figure 4-16)
- Standpipe panel fitted with glass standpipe tubes of different diameters, each with a valve at its base and a connected tube (see Figure 4-17)
- Balance sensitive to 0.01 g.

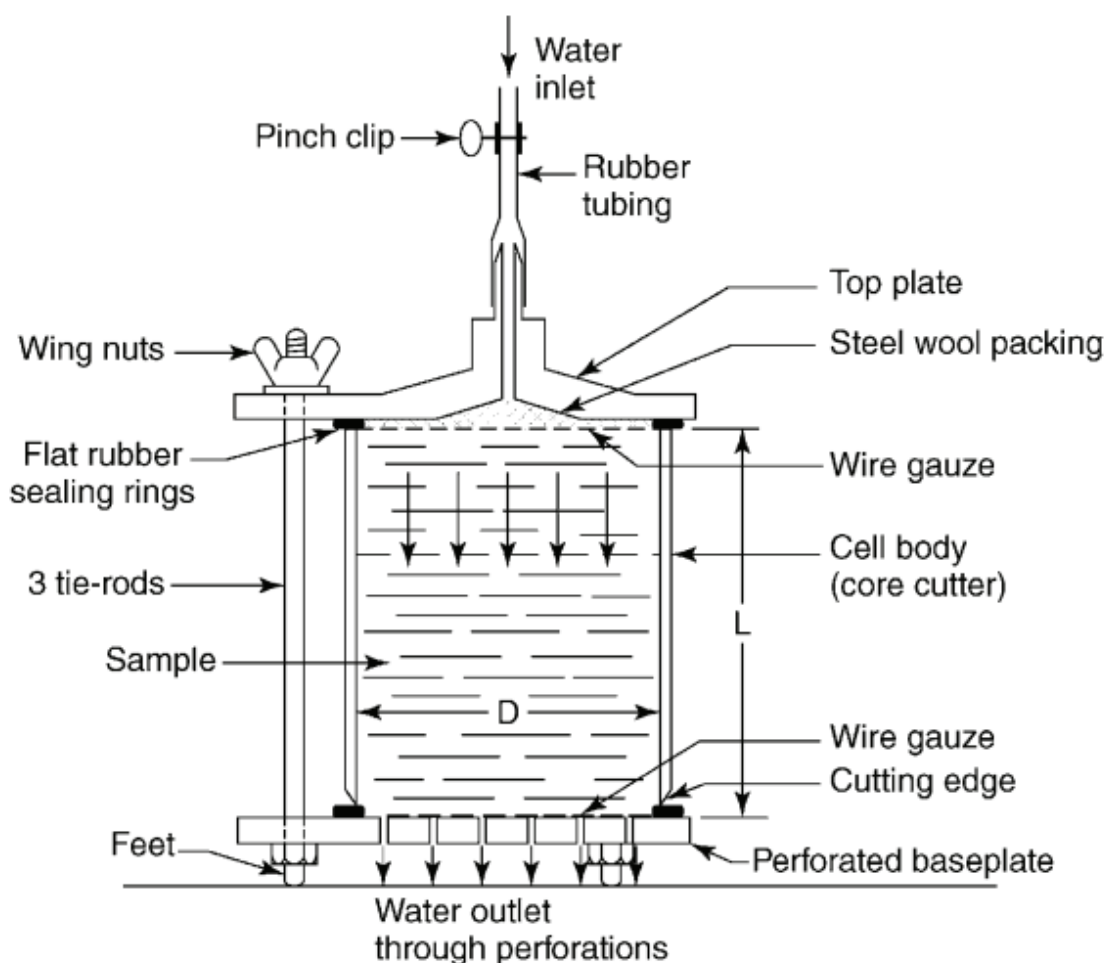


Figure 4-16. Permeameter cell for falling-head permeability tests (Head and Epps, 2011).

Furthermore, Figure 4-17 shows a general falling-head permeability test configuration together with the one used for this study.

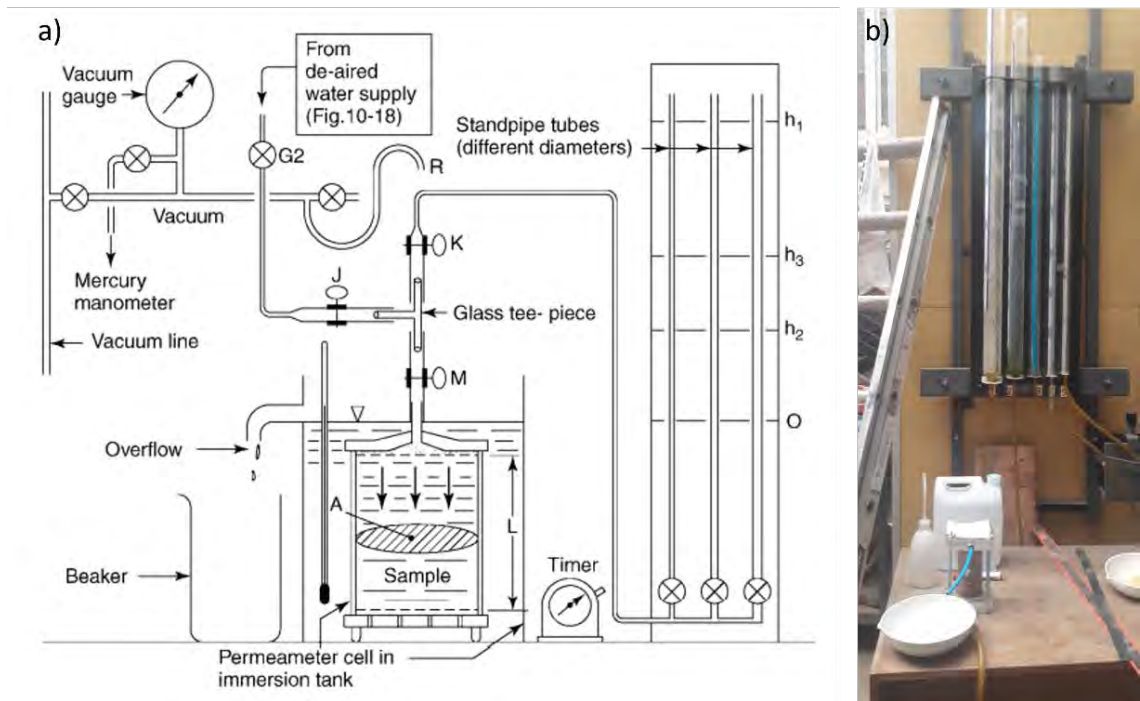


Figure 4-17. a) General falling-head permeability test configuration (Head and Epps, 2011); b) falling-head permeability test used for this study.

The initial water level of the standpipe tube must be measured at the beginning and the water level must be again measured after some time (generally, a few hours). The rate at which water will drain from the standpipe tube into the sample chamber is the change in head with time multiplied by the cross-sectional area of the standpipe tube (Fetter, 1994). This means that the diameter of the standpipe determines the duration of the test. The K_s of the sample can be obtained from Equation (7):

$$K_s = \frac{A_t L}{A_c t} \ln \left(\frac{h_0}{h_1} \right) \quad (7)$$

where K_s (m/s) is the soil saturated hydraulic conductivity; L is the sample length (m); A_c (m²) is the sample cross-section; A_t (m²) is the falling-tube cross-section; t (s) is the recorded time; h_0 (m) is the initial water level in the standpipe; and h_1 (m) is the final water level in the standpipe.

4.4.2 Field saturated hydraulic conductivity

Slug tests were performed to obtain the field saturated hydraulic conductivity in the radial direction (K_r) and the specific storage representative of field conditions. The slug test consists of measuring the recovery of head (water level) in a well after a near-instantaneous change in head (water level) in that well (Butler, 1997). This can be done, for example, by rapidly introducing a solid object or equivalent volume of water into the well (or removing the same), causing an abrupt increase (or decrease) in water level. Following this sudden change, the water level in the well returns to static conditions as water moves out of the well or into it (when the change was a decrease in water level) in response to the gradient imposed by the sudden change in head (Butler, 1997). These head changes through time, which are termed the response data, can be used to estimate the hydraulic conductivity of the formation through comparisons with theoretical models of test responses (Butler, 1997). Under certain conditions, the slug test can also be used to obtain an estimate of the specific storage (Butler, 1997).

In this case, the experiments were carried out by removing a defined volume of water, which is usually referred to as a slug-out, or withdrawal test. The recovery was measured at 5 second intervals using HOBO MX2001 Water Level Loggers.

To determine the hydraulic properties from the field data, the analytical model proposed by Cooper et al (1967). was used. The analytical solution to the mathematical model defined by Cooper et al. can be written as:

$$\frac{H(t)}{H_0} = f(\beta, \alpha) \quad (8)$$

where $\beta = K_r B t / r_c^2$ (dimensionless time parameter); $\alpha = (r_w^2 S_s B) / r_c^2$ (dimensionless storage parameter); K_r (m/s) is the radial component of the hydraulic conductivity; S_s (1/m) is the specific storage; B (m) is the formation thickness for fully-penetrating well, length of well screen otherwise; H (m) is the deviation of head in well from static conditions; H_0 (m) is the magnitude of initial displacement; r_w (m) is the effective radius of well screen; r_c (m) is the effective radius of well casing; and t (s) is the time;

The solution of equation (8), when plotted as normalized head vs. the logarithm of β , forms a series of type curves, with each type curve corresponding to a different value of α . The method to determine the hydraulic conductivity and specific storage then consists of plotting the recovery records in terms of the dimensionless time parameter (β) by adjusting the values of the hydraulic conductivity (K_r) to best fit one of the type curves corresponding to a specific value of α , which corresponds to a value for the specific storage (S_s). Figure 4-18 presents an example of field data fitted to the type curves.

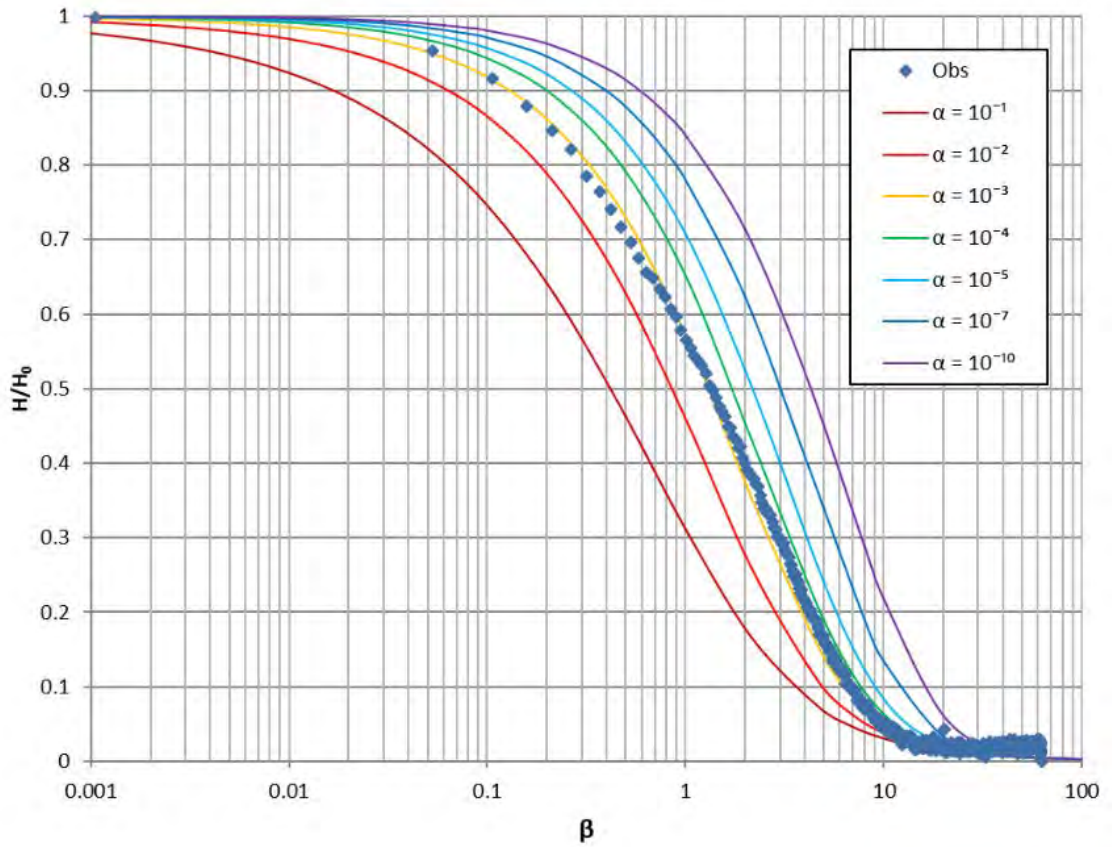


Figure 4-18. Example of slug test data adjusted to the Cooper et al. type curves (Cooper et al., 1967).

4.4.3 Thermal properties

Before backfilling the hole excavated for the soil sensors installation, thermal properties of the soil (thermal conductivity K , volumetric specific heat C and diffusivity D) were measured with a Thermal Properties Analyzer (KD2 Pro, Decagon), as shown in Figure 4-19. Measurements were taken at three different points of the uncovered portion of the vertical wall (Figure 4-19), of the underwater portion of the vertical wall and of the horizontal bottom of the hole, for a total of nine measurements.



Figure 4-19. Thermal properties of soil measured at the unsaturated vertical wall.

4.5 Groundwater level monitoring

4.5.1 Monitoring network

A network of monitoring points was designed to monitor groundwater levels in the Quebrada Negra at two different depths simultaneously. To achieve this, each monitoring point consists of a pair of piezometers as represented in the layout in Figure 4-20. The piezometers were marked with “D” indicating “deep” level and with “S” for “shallow” level.

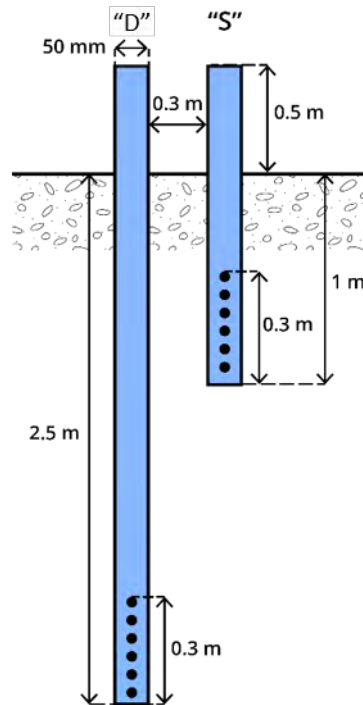


Figure 4-20. Pair of piezometers layout per monitoring point.

The piezometers were built using 50 mm diameter PVC tubes, with a 0.3 m screen consisting of 10 mm holes covered with geotextile fabric glued on the inside walls. The installation was performed by digging holes with an earth auger with a 60 mm bit as shown in Figure 4-21, then the PVC tubes were inserted, and the holes were backfilled with sand taken from nearby locations.



Figure 4-21. Use of earth auger at study site.

Initially, two locations were selected to test the piezometers and correspond to: (1) at the stream bank, and (2) inside the wetland (Figure 4-22). One shallow piezometer (1.5 m length) was installed at test site 1 (Figure 4-23) and a pair of piezometers was installed at test site 2 (Figure 4-24) as described in Figure 4-20. Table 4-4 shows measurements of water table depth respective to ground surface, one week after the installation of these piezometers.

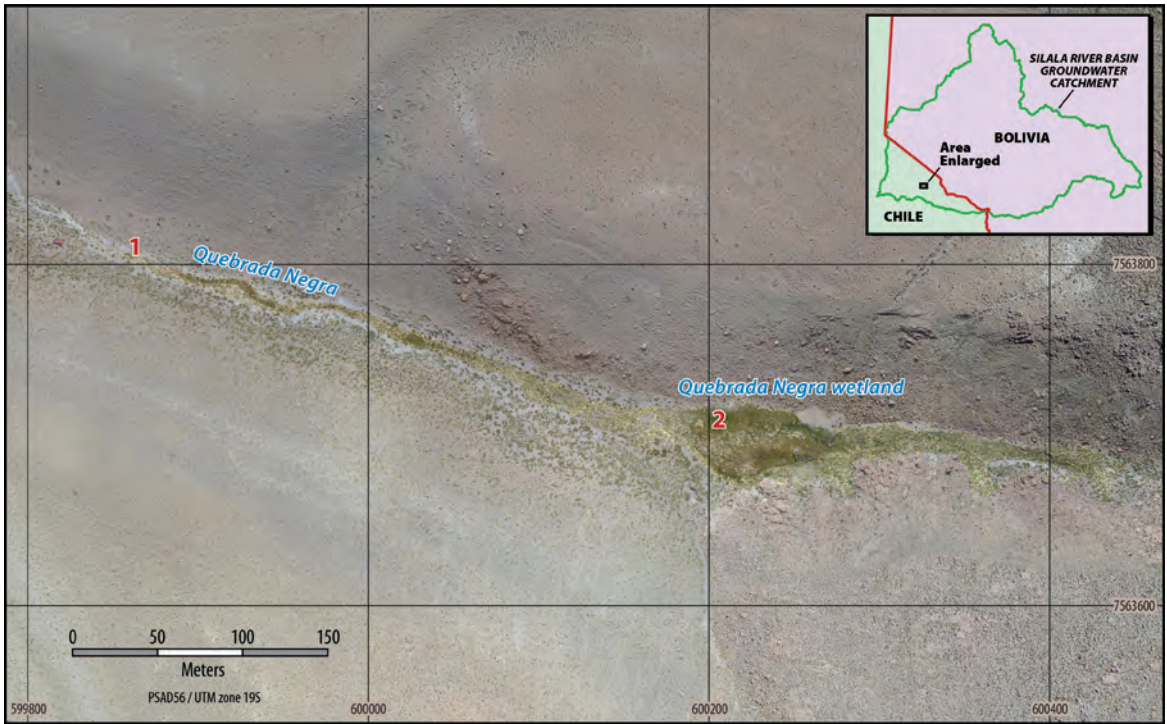


Figure 4-22. Location of test sites.

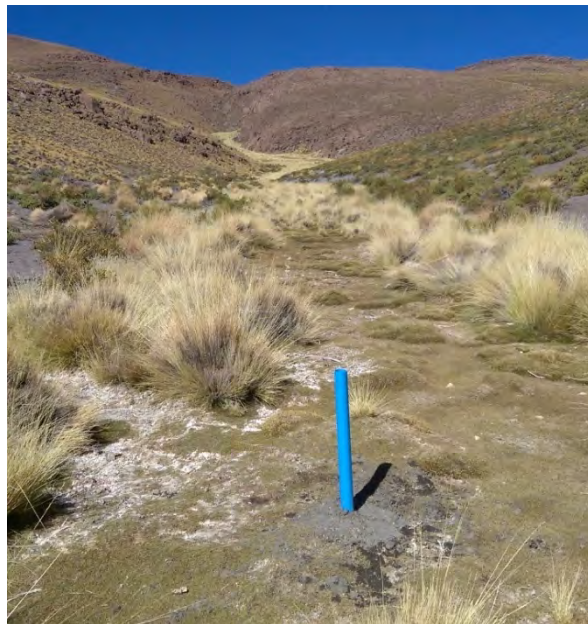


Figure 4-23. Shallow piezometer (1.5 m length) inserted 1 m at test site 1.



Figure 4-24. Pair of piezometers installed at test site 2.

Piezometer	1-shallow	2-shallow	2-deep
Depth to groundwater (cm)	49	12	23

Table 4-4. Depth of water table at test piezometers.

According to these preliminary results, useful measurements can be expected to be obtained with this piezometer design (Figure 4-20), even on the stream bank. Therefore, 82 monitoring points were constructed, distributed as shown in Figure 4-25 and Figure 4-26. The numbers indicate relative position or transect, increasing in the downstream direction. On the main grassland, where multiple monitoring points per transect were installed, the letter indicates its position relative to the northern or southern limits of the wetland, “A” being the northernmost monitoring point of the transect and “Z” the southernmost.

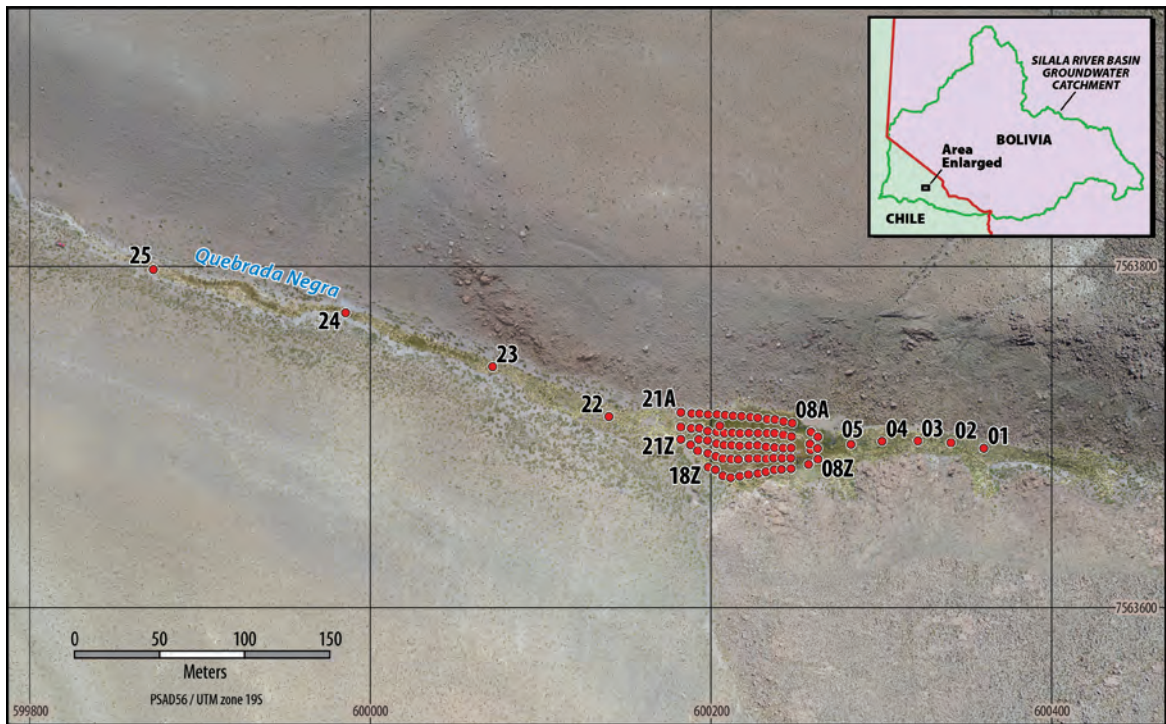


Figure 4-25. Layout of the monitoring wells in the Quebrada Negra ravine.

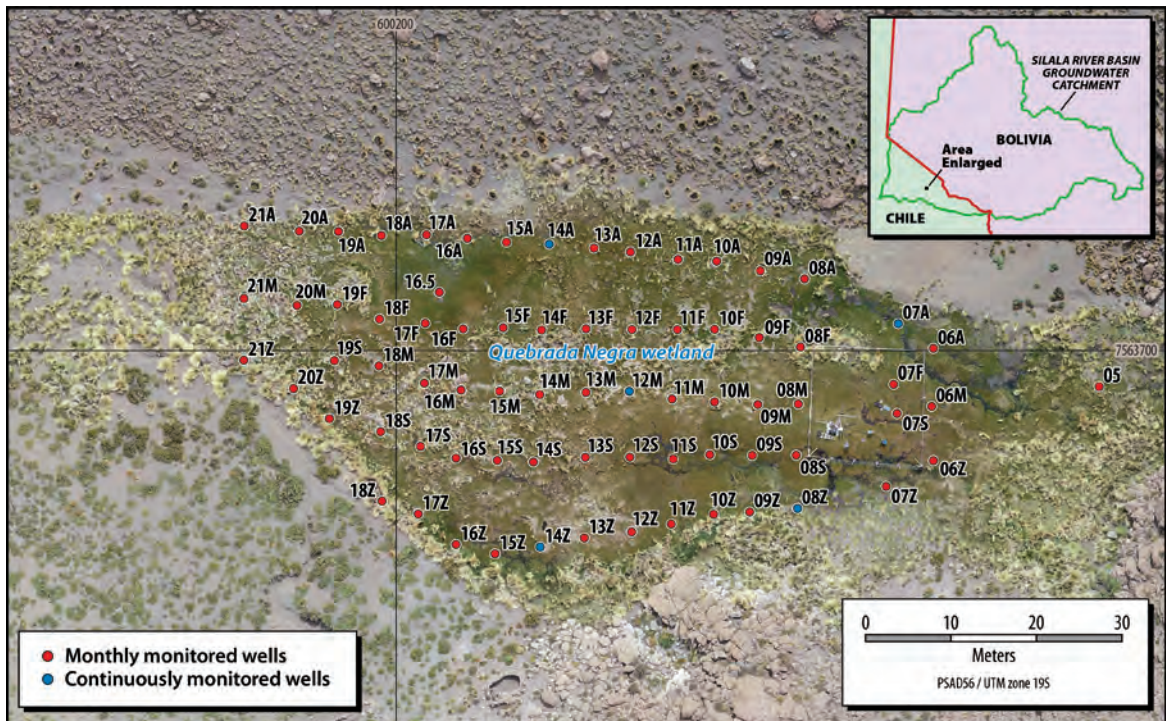


Figure 4-26. Layout of the monitoring wells in the Quebrada Negra wetland. Locations with sensors for continuous groundwater level monitoring are depicted in blue and locations where the groundwater level is monitored at a monthly time scale are shown in red.

The locations of the monitoring wells were measured using a multi-frequency GPS receiver (Carlson BRx5 GNSS receiver, Carlson Software Inc., Maysville, KY), but due to battery constraints, the positions of both piezometers could only be identified at the monitoring points between locations 21 to 25, for the rest only the position of the northernmost piezometer of the pair was recorded. Table 4-5 compiles the information of each monitoring point.

Point	X deep (PSAD56 19S)	Y deep (PSAD56 19S)	X shallow (PSAD56 19S)	Y shallow (PSAD56 19S)	Top Elevation deep (m.a.s.l.)	Top Elevation shallow (m.a.s.l.)	Distance Top-ground deep (m)	Distance Top-ground shallow (m)	Depth deep (m)	Depth shallow (m)
01			600360.183	7563693.641		4290.61	1.05	0.20	1.95	1.31
02			600340.906	7563696.889		4287.47	1.32	0.53	1.69	0.97
03			600321.426	7563698.013		4284.64	0.86	0.74	2.14	0.76
04			600300.385	7563697.771		4280.38	0.72	0.63	2.28	0.87
05	600282.143	7563695.873			4277.31		0.70	0.42	2.30	1.08
06A	600262.778	7563700.269			4274.53		0.51	0.49	2.49	1.01
06M	600262.583	7563693.566			4274.81		0.48	0.49	2.52	1.01
06Z	600262.78	7563687.209			4275.22		0.83	0.61	2.17	0.89
07A			600258.677	7563703.156		4273.91	0.88	0.61	2.12	0.89
07F	600258.128	7563696.144			4274.08		0.67	0.48	2.33	1.02
07S			600258.542	7563692.737		4274.91	0.62	0.49	2.39	1.01
07Z	600257.255	7563684.215			4274.65		0.99	0.62	2.01	0.89
08A	600247.716	7563708.4			4273.54		0.97	0.58	2.03	0.92
08F	600247.255	7563700.426			4273.27		0.70	0.55	2.30	0.95
08M			600246.984	7563693.836		4273.397	0.77	0.58	2.24	0.92
08S	600246.753	7563687.865			4273.76		0.75	0.45	2.25	1.05
08Z	600246.903	7563681.637			4273.90		0.86	0.62	2.14	0.88
09A	600242.554	7563709.332			4273.28		1.10	0.56	1.90	0.94
09F	600242.423	7563701.545			4272.81		0.68	0.57	2.32	0.93
09M	600242.263	7563693.782			4272.70		0.64	0.59	2.36	0.91
09S	600241.612	7563687.849			4272.96		0.83	0.57	2.17	0.93
09Z	600241.309	7563681.235			4273.11		0.81	0.47	2.19	1.03
10A	600237.456	7563710.454			4272.66		0.96	0.54	2.04	0.96
10F	600237.214	7563702.513			4272.51		0.84	0.65	2.16	0.85
10M			600237.213	7563694.099		4272.08	0.80	0.56	2.20	0.94
10S	600236.647	7563687.929			4272.48		0.78	0.46	2.22	1.04
10Z	600237.107	7563680.968			4272.56		0.71	0.61	2.29	0.89
11A	600232.933	7563710.657			4272.15		0.84	0.54	2.16	0.96
11F	600232.868	7563702.475			4271.95		0.69	0.58	2.31	0.92
11M	600232.237	7563694.431			4271.71		0.66	0.60	2.34	0.90
11S	600232.382	7563687.413			4271.61		0.61	0.63	2.39	0.87
11Z	600232.14	7563679.816			4271.83		0.73	0.53	2.27	0.97
12A	600227.373	7563711.535			4271.56		1.03	0.49	1.98	1.01
12F	600227.551	7563702.481			4271.01		0.70	0.63	2.30	0.87
12M	600227.248	7563695.334			4271.17		0.68	0.61	2.33	0.89
12S	600227.312	7563687.646			4270.92		0.58	0.51	2.43	0.99
12Z	600227.514	7563678.89			4271.92		0.77	0.58	2.23	0.92
13A	600223.124	7563711.995			4271.13		1.11	0.55	1.89	0.95
13F	600222.179	7563702.568			4270.31		0.64	0.48	2.36	1.02
13M	600222.178	7563695.211			4270.45		0.66	0.48	2.34	1.02
13S	600222.105	7563687.631			4270.12		0.55	0.50	2.45	1.00
13Z	600221.977	7563678.212			4270.09		0.85	0.53	2.15	0.97
14A	600217.892	7563712.441			4270.20		1.00	0.72	2.01	0.78
14F	600217.003	7563702.418			4269.75		0.62	0.50	2.38	1.00
14M	600216.787	7563694.948			4269.56		0.72	0.56	2.28	0.94
14S	600216.041	7563687.063			4269.04		0.66	0.60	2.34	0.90
14Z	600216.836	7563677.136			4269.65		0.89	0.56	2.11	0.95
15A	600212.883	7563712.677			4269.49		0.94	0.53	2.06	0.97
15F	600212.503	7563702.694			4269.15		0.68	0.52	2.32	0.98
15M	600212.085	7563695.346			4268.95		0.75	0.72	2.25	0.78
15S	600211.808	7563687.244			4268.73		0.66	0.61	2.34	0.89

Point	X deep (PSAD56 19S)	Y deep (PSAD56 19S)	X shallow (PSAD56 19S)	Y shallow (PSAD56 19S)	Top Elevation deep (m.a.s.l.)	Top Elevation shallow (m.a.s.l.)	Distance Top-ground deep (m)	Distance Top-ground shallow (m)	Depth deep (m)	Depth shallow (m)
15Z	600211.557	7563676.352			4268.60		0.53	0.53	2.47	0.97
16.5			600205.043	7563706.83		4267.80	0.67	0.46	2.33	1.04
16A	600208.303	7563713.129			4269.33		1.04	0.73	1.96	0.77
16F	600207.832	7563702.559			4268.05		0.97	0.65	2.03	0.85
16M	600207.582	7563695.472			4267.97		0.61	0.60	2.39	0.90
16S	600206.996	7563687.524			4267.93		0.69	0.63	2.31	0.87
16Z	600206.988	7563677.444			4268.52		1.49	0.61	1.51	0.89
17A	600203.536	7563713.539			4268.48		1.31	0.65	1.69	0.85
17F	600203.393	7563703.192			4267.69		0.68	0.41	2.32	1.09
17M	600203.299	7563696.284			4267.21		0.62	0.47	2.38	1.03
17S	600202.842	7563688.892			4267.23		0.80	0.53	2.20	0.97
17Z	600202.568	7563680.999			4267.58		0.92	0.59	2.08	0.91
18A	600198.278	7563713.45			4267.78		1.41	0.57	1.59	0.93
18F	600198.046	7563703.702			4267.09		0.51	0.63	2.49	0.87
18M	600197.967	7563698.223			4266.54		0.71	0.48	2.29	1.02
18S	600198.177	7563690.617			4266.67		0.74	0.58	2.26	0.92
18Z	600198.357	7563682.497			4267.11		0.99	0.51	2.01	0.99
19A	600193.244	7563713.938			4266.96		1.68	0.62	1.32	0.88
19F	600193.126	7563705.399			4266.24		0.68	0.53	2.32	0.97
19S	600192.779	7563698.847			4265.76		0.66	0.45	2.34	1.05
19Z	600192.192	7563692.131			4265.48		0.42	0.41	2.58	1.09
20A	600188.667	7563713.975			4266.02		1.36	0.55	1.64	0.95
20M	600188.411	7563705.304			4265.56		0.65	0.48	2.35	1.02
20Z	600187.99	7563695.638			4265.25		0.76	0.63	2.24	0.87
21A	600182.234	7563714.576	600182.381	7563714.185	4265.205	4263.92	1.85	0.57	1.15	0.93
21M	600182.192	7563706.095	600182.244	7563706.567	4264.42	4264.28	0.77	0.47	2.23	1.03
21Z	600182.181	7563698.901	600182.171	7563698.559	4264.86	4264.37	0.93	0.52	2.07	0.98
22	600139.982	7563712.238	600139.878	7563711.906	4259.87	4259.48	0.80	0.43	2.20	1.07
23	600071.769	7563741.156	600071.592	7563740.753	4251.97	4251.68	0.79	0.45	2.21	1.05
24	599985.429	7563772.838	599985.232	7563772.582	4243.91	4243.43	0.99	0.47	2.01	1.03
25	599872.601	7563798.155	599872.782	7563798.576	4237.15	4236.86	0.90	0.67	2.10	0.83

Table 4-5. Location, elevation and depth of groundwater level monitoring grid.

4.5.2 Ground water level measurements

Levels at each piezometer were measured manually with a water level dipper on a monthly schedule starting in August 2018. Additionally, an array of 10 Water Level Logger sensors (HOBO[®] MX2001, Onset Computer Corporation, Bourne, MA) were installed in pairs at 5 monitoring points distributed inside the main grassland. The location of these sensors is highlighted in blue in Figure 4-26. These sensors can measure simultaneously barometric pressure, water pressure and temperature to determine the water level, and were programmed to record all these variables at 15 minutes intervals.

5. RESULTS AND DISCUSSION

The results obtained from the various investigations performed in the Quebrada Negra wetland, including comparison with the Bolivian wetlands, are presented in this section.

5.1 Quebrada Negra Wetland meteorological station

The data measured by the Quebrada Negra Wetland meteorological station are temperature, precipitation, relative humidity, wind speed and direction, net radiation, soil moisture, soil temperature, and soil heat flux. These data are collected every 15 minutes.

The Quebrada Negra Wetland meteorological data collected from 14 June 2018 to 29 November 2018 are presented in the next section on a daily time-scale. These data are: air temperature and relative humidity, precipitation, wind speed and direction, net radiation (four components of radiation), soil moisture, soil temperature, and soil heat flux. Unfortunately, because of the work performed during the installation of the satellite transmission system, data between 21 and 29 August 2018 were lost.

5.1.1 Air temperature

Figure 5-1 shows the maximum, mean and minimum temperature time series at Quebrada Negra. The daily maximum temperatures vary between -3 and 17 °C, while the daily minima vary between -11 and 1 °C for the study period. The temperatures slowly rise as winter ends and summer approaches.

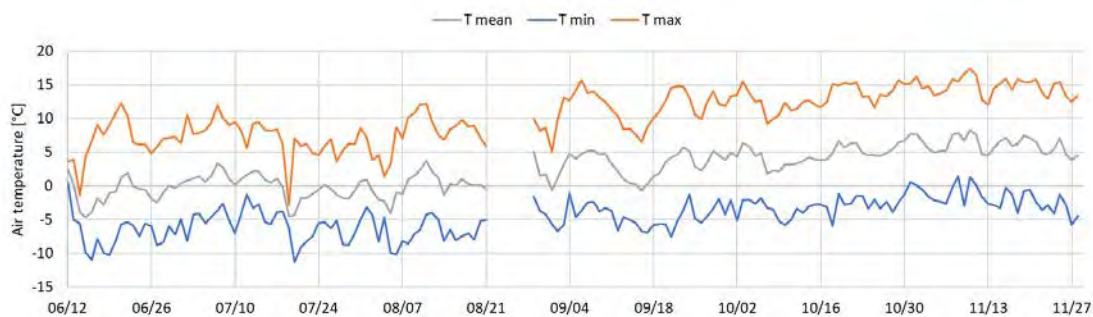


Figure 5-1. Temperature time series at the Quebrada Negra Wetland meteorological station.

5.1.2 Precipitation

Figure 5-2 shows daily precipitation at the Quebrada Negra wetland. Seven precipitation events were identified during the study period, with a maximum precipitation of 4.3 mm on 20 July 2018. Figure 5-3 shows the snow cover percentage in the Silala River basin between June and November 2018. As shown here, precipitation events detected by the meteorological station since June 2018 correspond to snowfall events. Figure 5-3 evidences a higher number of snowfall events than those registered by the Quebrada

Negra Wetland meteorological station. It should be noted that Figure 5-3 shows the snow cover of the whole basin, considering zones that have a much higher elevation than that of the Quebrada Negra wetland meteorological station. However, analysis of individual satellite images showed that there was abundant snow at the Quebrada Negra while the pluviometer remained reporting zero precipitation. This phenomenon probably occurs due to the inherent limitations of pluviometers designed to capture rainfall.



Figure 5-2. Precipitation time series at the Quebrada Negra Wetland meteorological station.

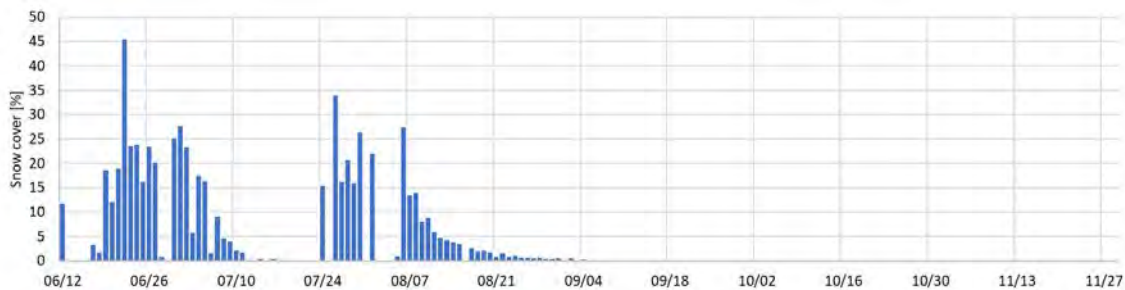


Figure 5-3. Snow cover percentage in the Silala River basin (obtained from MODIS images).

5.1.3 Relative Humidity

Figure 5-4 shows the maximum, mean and minimum daily relative humidity time series at Quebrada Negra. Figure 5-5 shows the relationship between the precipitation and relative humidity, which tends to increase before rainfall events.

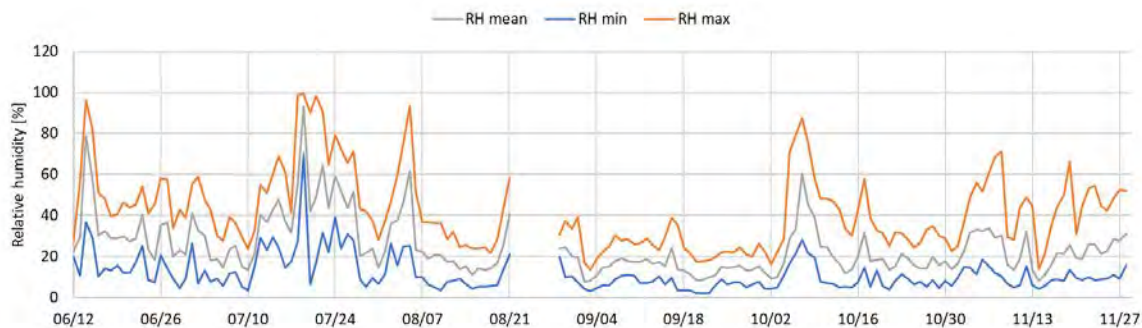


Figure 5-4. Daily maximum, mean and minimum relative humidity time series at the Quebrada Negra wetland meteorological station.

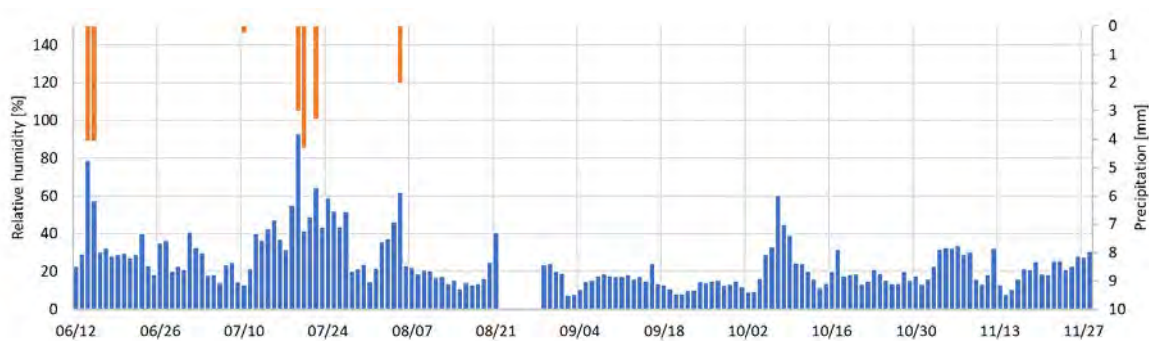


Figure 5-5. Daily mean relative humidity (lower, in blue) and precipitation (upper, in orange) time series at the Quebrada Negra wetland meteorological station.

5.1.4 Wind speed and Wind direction

Figure 5-6 shows the maximum, mean and minimum daily wind speed time series at the Quebrada Negra.

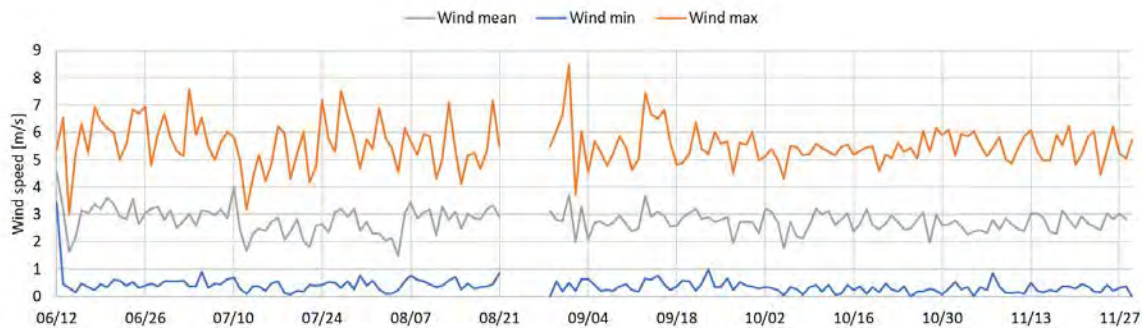


Figure 5-6. Daily mean, minimum and maximum wind speed time series at the Quebrada Negra wetland meteorological station.

Figure 5-7 shows the wind rose for daytime (between 8:00 and 21:00) and night-time (between 21:00 and 8:00) at Quebrada Negra. During daytime the predominant wind direction is from the west, while at night-time the strongest winds come from the east.

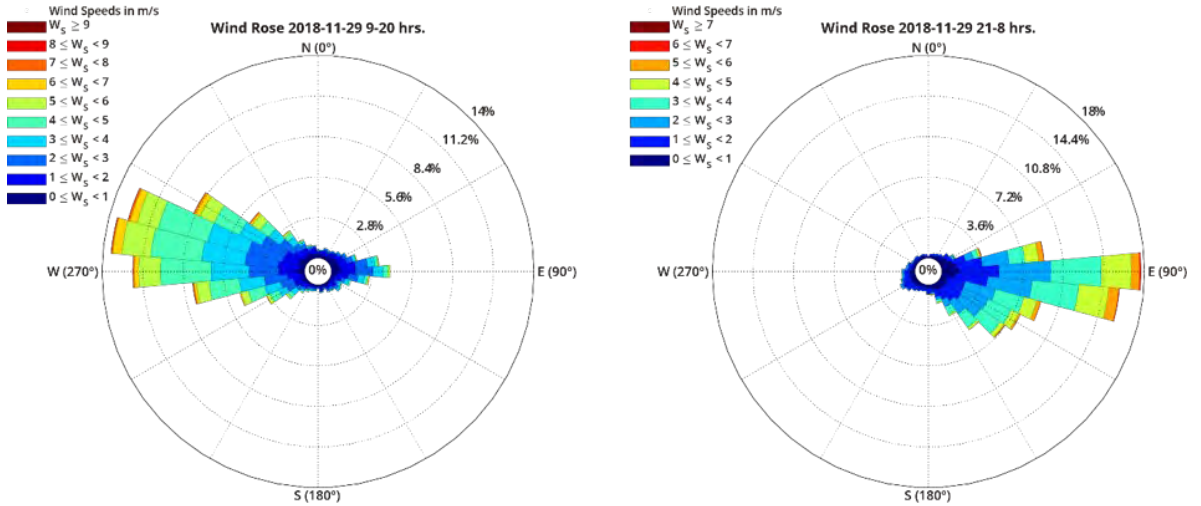


Figure 5-7. Wind rose at the Quebrada Negra wetland meteorological station. Left: daytime wind rose. Right: nighttime wind rose.

5.1.5 Net radiation

Figure 5-8 shows the mean daily net radiation and precipitation time series at the Quebrada Negra. Mean net radiation rises as winter ends and summer approaches. When comparing the net radiation with precipitation, it can be appreciated that mean daily net radiation decreases with rainfall events, resulting in negative values in some cases.

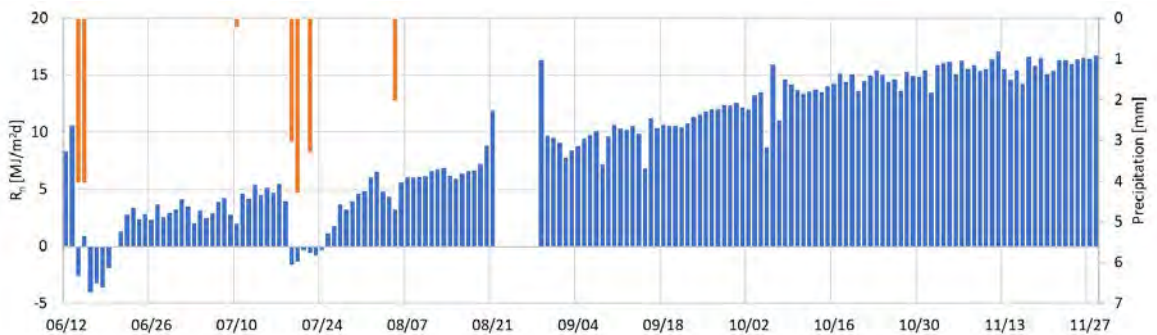


Figure 5-8. Mean daily net radiation (lower, in blue) and precipitation (upper, in orange) time series at the Quebrada Negra wetland meteorological station.

5.1.6 Soil heat flux

Figure 5-9 shows the daily average soil heat flux time series at the Quebrada Negra wetland. Fluxes directed downwards (towards the ground) are considered positive, while fluxes directed upwards (towards the atmosphere) are considered negative.

Soil heat flux rises as summer approaches. The negative values observed during winter could be attributed to the presence of snow on the surface and low temperatures in, and even freezing of, the ground (Figure 5-3 and Figure 5-9 below), as records became positive after soil temperature started to rise. More data at the Quebrada Negra wetland is needed to validate these measurements and to see if this behavior is consistent in time.

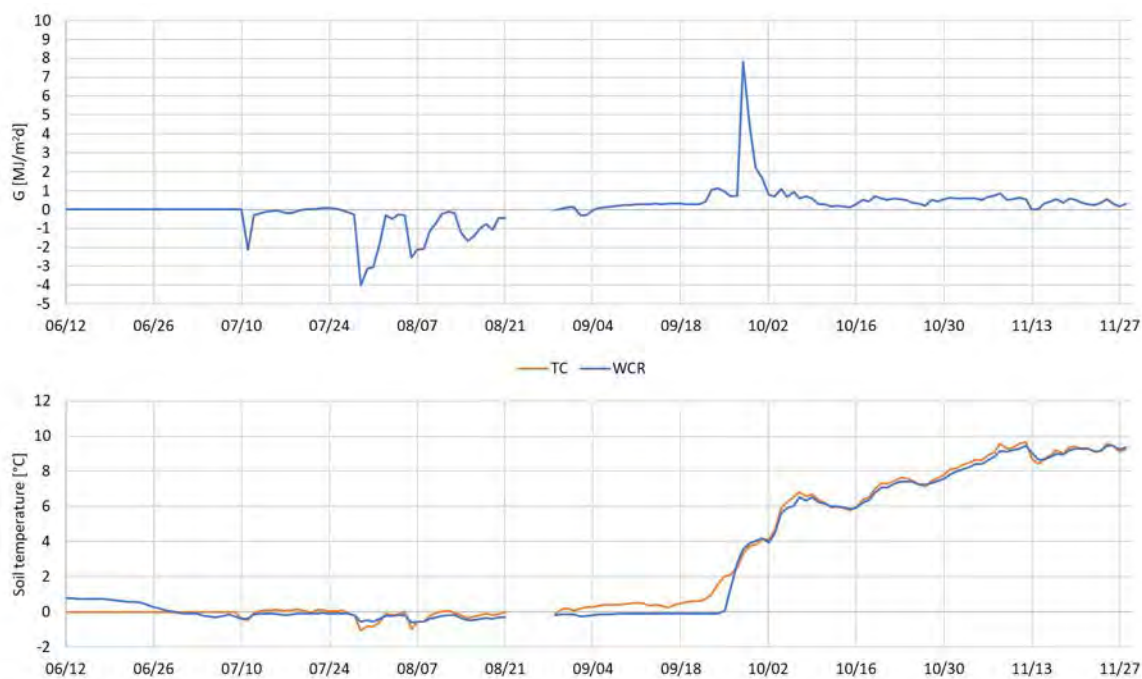


Figure 5-9. Soil heat flux (above) and soil temperature (below) time series at the Quebrada Negra Wetland meteorological station. TC: temperature measured with the soil thermocouple probe; WCR: temperature measured with the water content reflectometer.

5.2 Spatial and temporal distribution of vegetation cover

5.2.1 Spatial distribution of vegetation cover

The monthly average NDVI maps obtained using the Sentinel-2 images are presented in Figure 5-10 and the total area covered by vegetation is presented in Table 5-1. The NDVI is higher in the middle of all of the wetlands than at the edges, and we can see

from the Quebrada Negra that this corresponds to the area where dense vegetation can be observed, mostly composed of a green vegetation cover. Figure 5-11 shows a high-resolution Ortho mosaic taken with the UAV in the Quebrada Negra wetland. This image was used to validate the distribution of NDVI in the Quebrada Negra wetland, and as can be seen, NDVI is higher where more vegetation is observed in the Ortho mosaic.

Additionally, the mean NDVI in each wetland is presented in Table 5-2. As shown in Table 5-1, in general the total area covered by active vegetation increased with time over the observational period, except for the Quebrada Negra wetland, in which it is observed that the total area covered by active vegetation decreased in November, 2018, although the mean NDVI increased (Table 5-2).

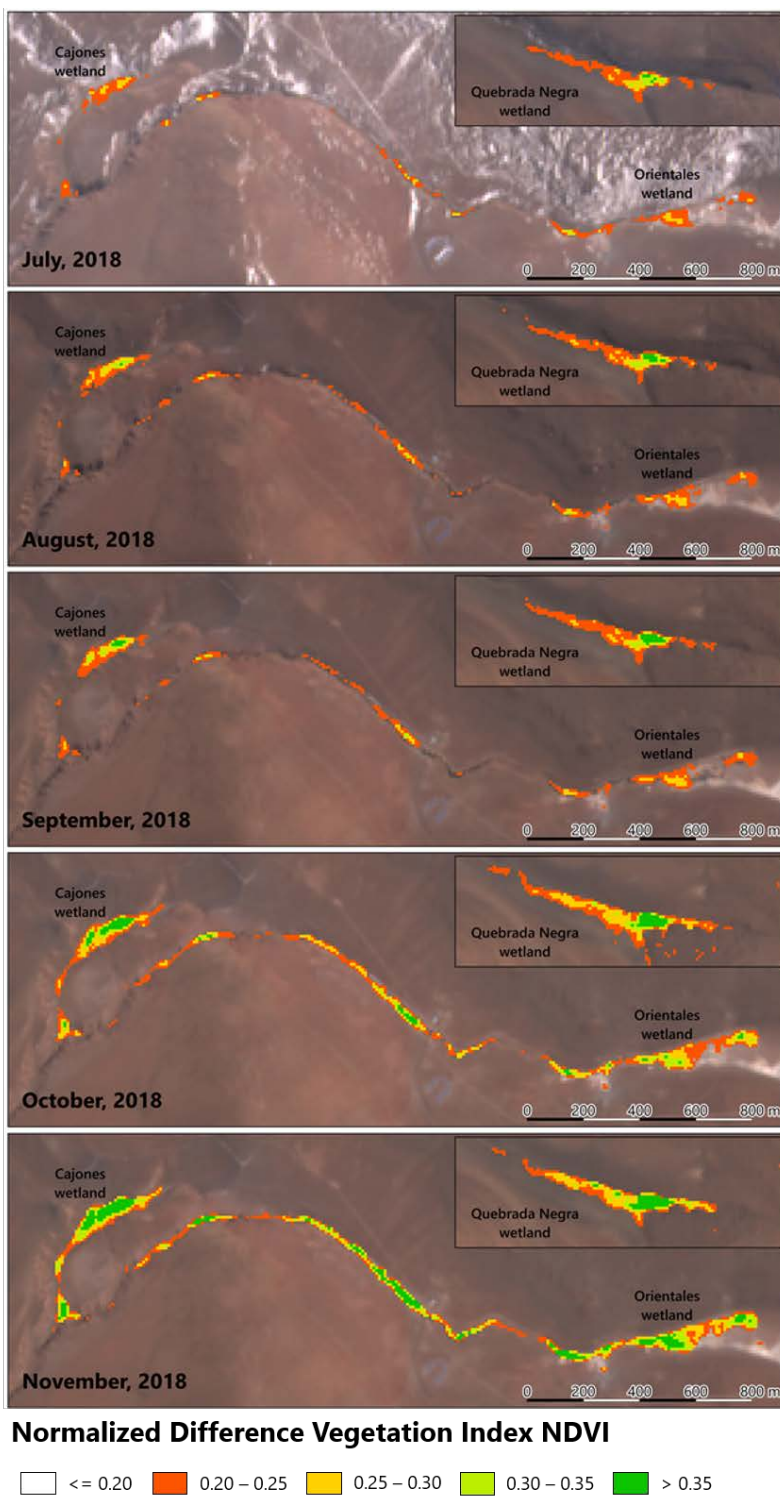


Figure 5-10. Quebrada Negra, Cajones and Orientales wetlands average NDVI distribution from July to November 2018.

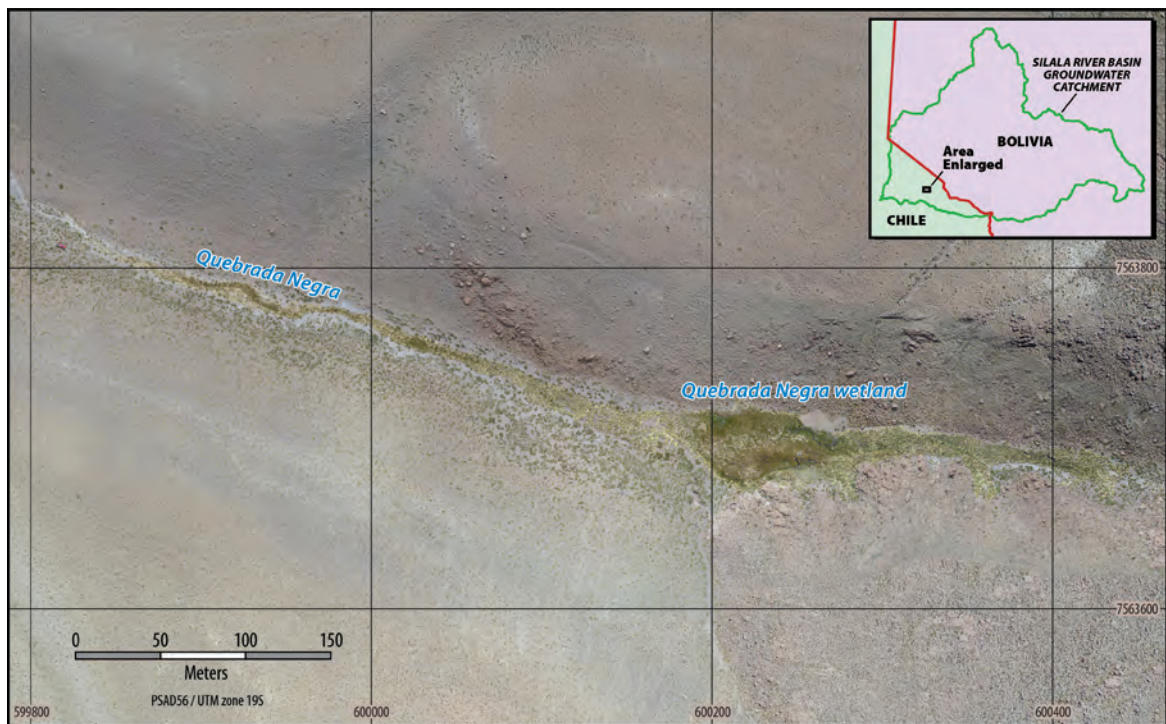


Figure 5-11. High-resolution ortho mosaic taken with the UAV.

	Area covered by active vegetation (ha)				
	July	August	September	October	November
Quebrada Negra wetland	2.13	2.31	2.58	4.12	3.43
Cajones wetland	0.81	1.12	1.31	2.20	2.41
Orientales wetland	2.23	2.70	2.86	6.09	7.50

Table 5-1. Area covered by active vegetation (NDVI > 0.2) in the Quebrada Negra, Cajones and Orientales wetlands, from July to November 2018.

	July	August	September	October	November
Quebrada Negra wetland	0.24	0.25	0.25	0.27	0.30
Cajones wetland	0.23	0.25	0.25	0.28	0.33
Orientales wetland	0.23	0.23	0.23	0.26	0.29

Table 5-2. Mean NDVI for the Quebrada Negra, Cajones and Orientales wetlands, from July to November 2018.

Figure 5-12, Figure 5-13 and Figure 5-14 show how the vegetation cover is located within the terrain of the Quebrada Negra, Cajones and Orientales wetlands, respectively.

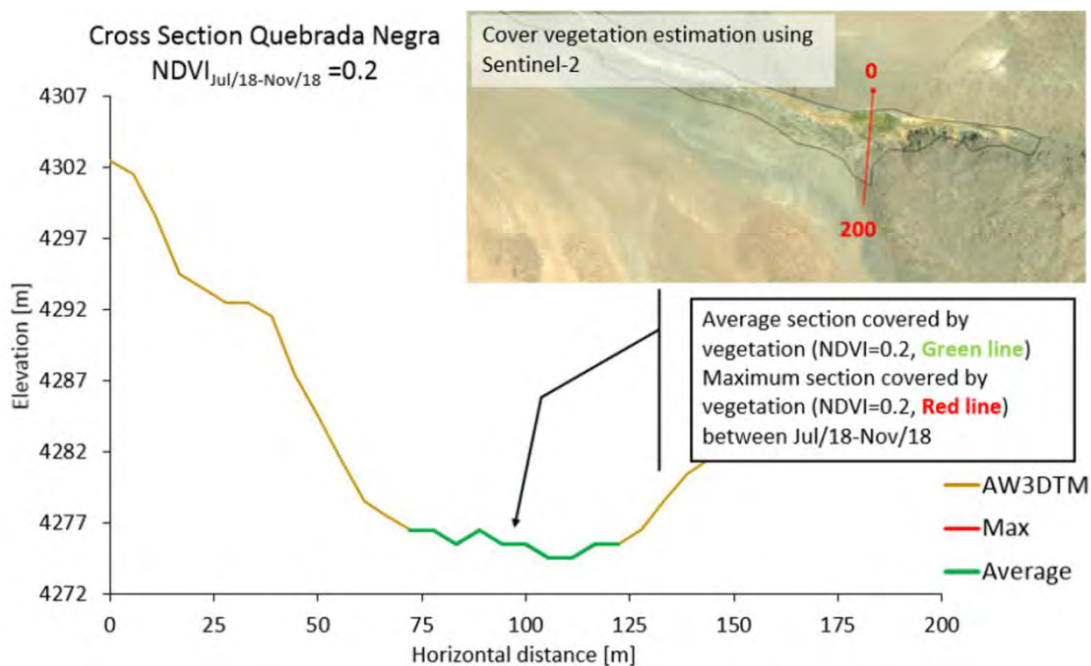


Figure 5-12. Cross section of vegetation cover ($NDVI > 0.2$) and topography of the Quebrada Negra wetland. The Average (Green Line) and Maximum (Red Line) cross section of vegetation cover have the same extent. For this reason, only the average green cover (green line) is visible.

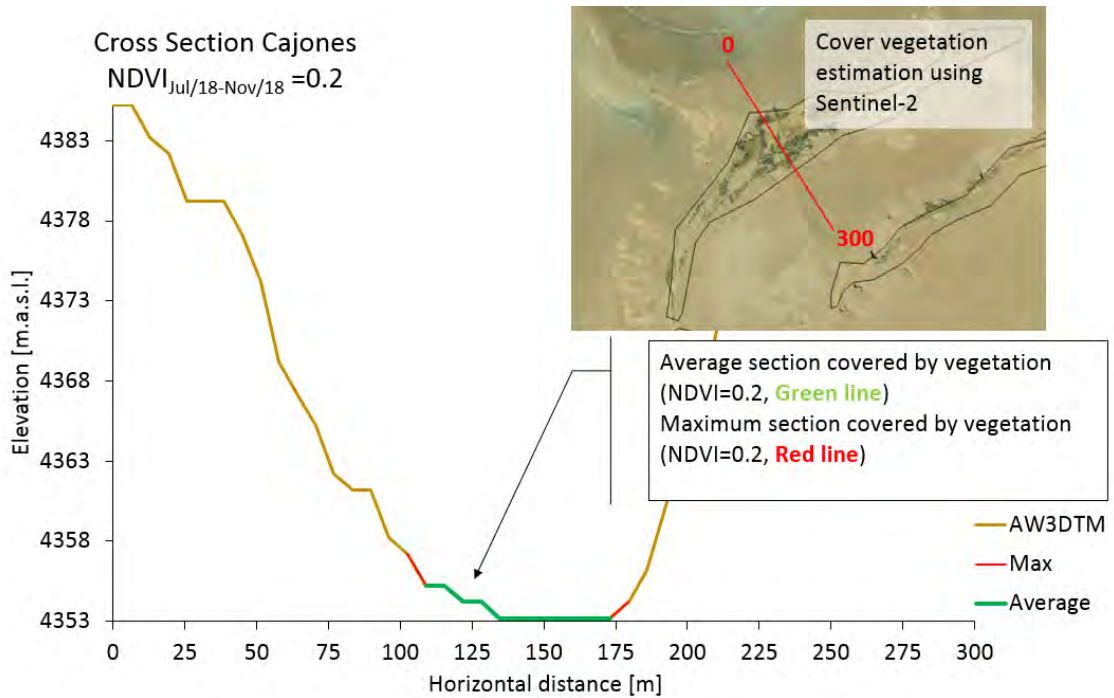


Figure 5-13. Cross section of vegetation cover (NDVI>0.2) and topography of the Cajones wetland.

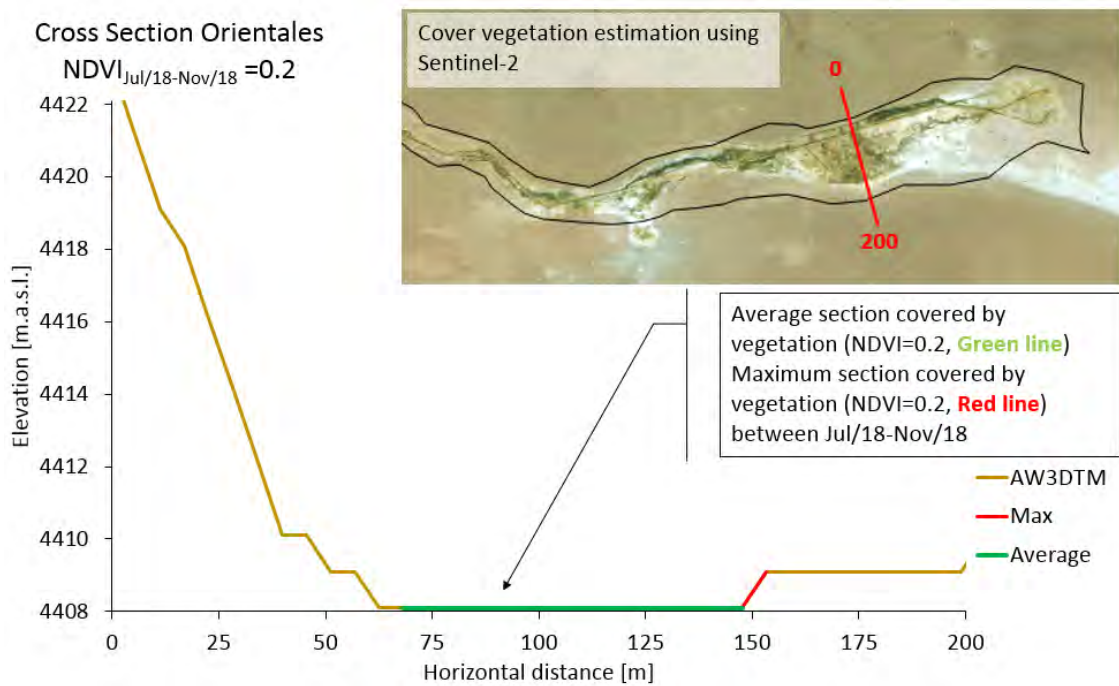


Figure 5-14. Cross section of vegetation cover (NDVI>0.2) and topography of the Orientales wetland.

It can be observed for each of the three wetlands that the distribution of active vegetation covers the flat area available and expands up the adjacent hillslopes where slopes are less than approximately 15%. However, the resolution of the digital elevation model prevents more accurate estimates of the relationship with slope.

In the case of the cross sections of Cajones and Orientales it is observed that between the months of July-2018 and November-2018 the maximum coverage extent is greater than the average extent (Figure 5-13 and Figure 5-14). In the case of the Quebrada Negra wetland cross-section (Figure 5-12), the maximum and mean extent do not vary significantly and cover the same transverse section, so although the NDVI value increases (showing greater photosynthetic activity), it does not increase in spatial extent at this location. However, an increase in vegetation cover in the Quebrada Negra wetland was observed for stream cross sections located downstream and upstream of the studied cross section, where the width of vegetation cover increased in the north-south direction. It should be noted that the range of variation is limited to the Sentinel raster resolution (10 m), so minor variations in this range are not captured.

5.2.2 Temporal evolution of vegetation cover

To determine a NDVI threshold value from the LANDSAT data we visually inspected the vegetation cover over the areas of interest (Figure 5-15) and validated the chosen value (0.2) by comparing the areas with high resolution drone pictures (Figure 5-16). The results for each zone are presented in Figures 5-17 to 5-19. Between 2012 and 2017 one can observe larger areas than in previous years, probably due to the better quality of information collected by the LANDSAT-8 satellite (higher spectral sensitivity). The increase for this period can be associated with the change in the technology of the acquisition of LANDSAT images. Roy et al. concluded for vegetated soil and vegetation surfaces ($0 \leq \text{NDVI} \leq 1$), the OLI NDVI (Landsat -8) is greater than the ETM+ NDVI (Landsat-7) (Roy et al., 2016).

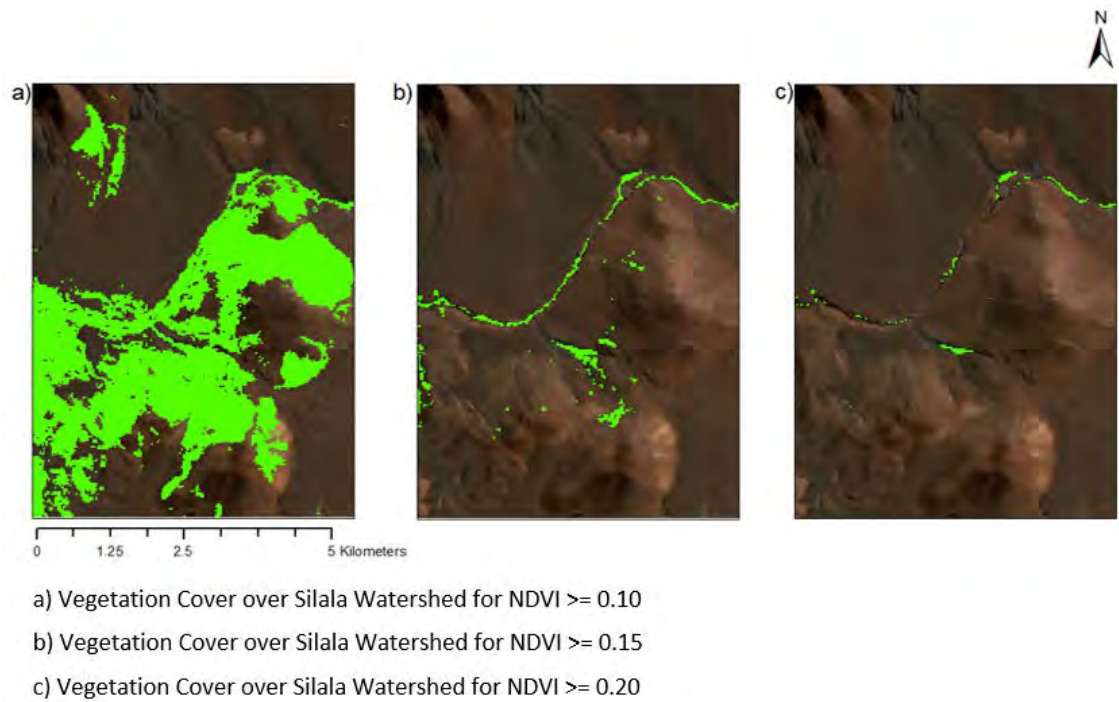


Figure 5-15. Vegetation cover over the Quebrada Negra, Orientales and Cajones wetlands for NDVI thresholds 0.1, 0.15 and 0.2.

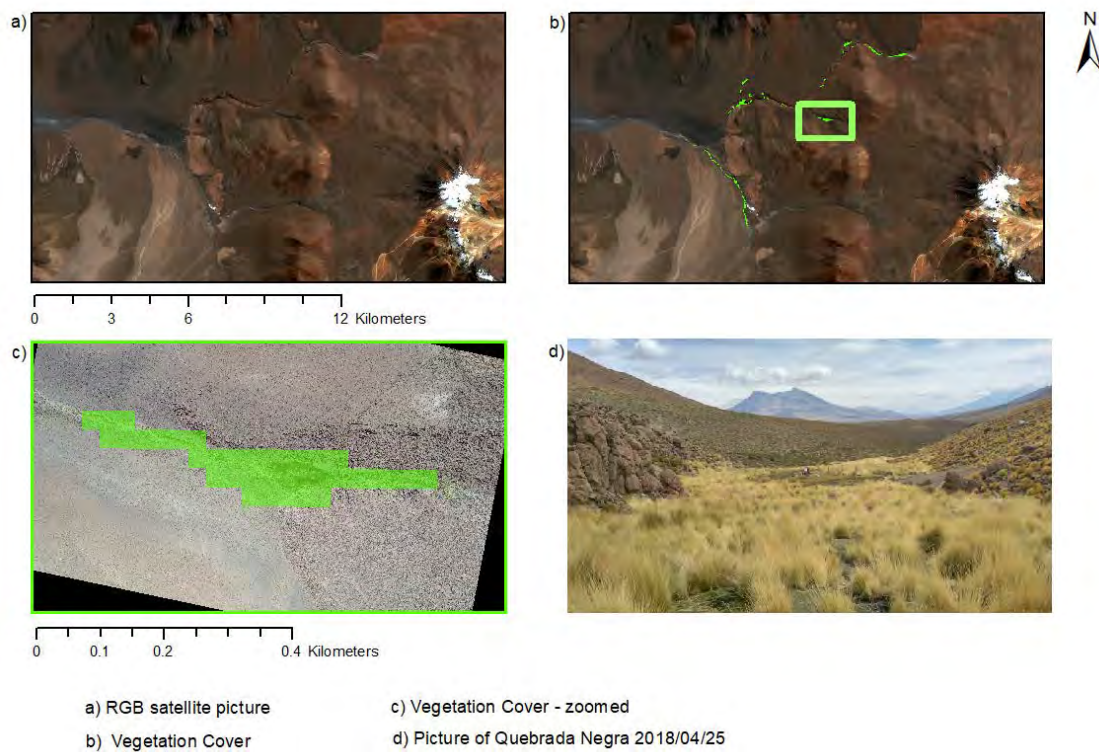


Figure 5-16. Validation of vegetation cover over the Quebrada Negra with an NVDI threshold value of 0.2.

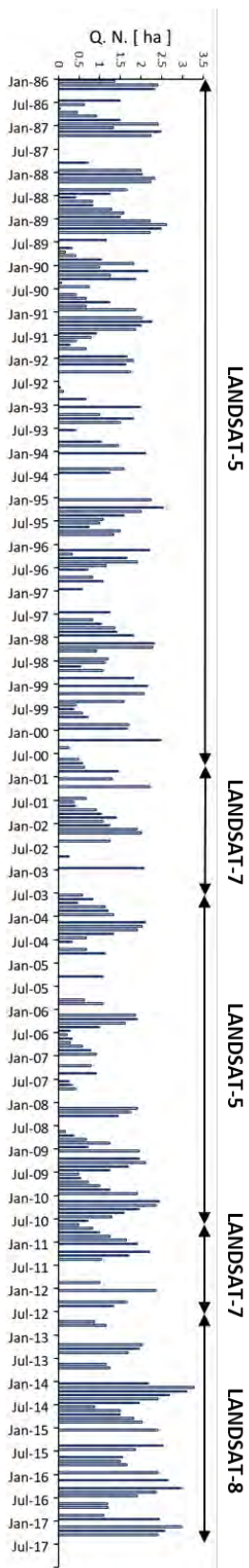


Figure 5-17. Time series of active vegetation cover ($NDVI \geq 0.2$) over the Quebrada Negra (Q.N.) wetland (1986-2017).

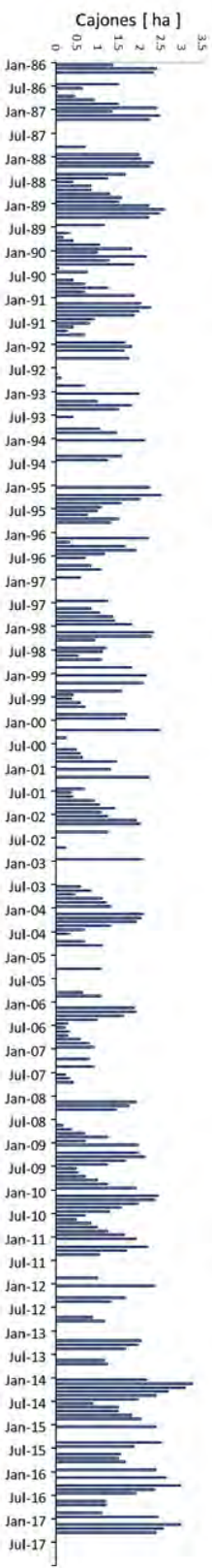


Figure 5-18. Time series of active vegetation cover ($NDVI \geq 0.2$) over the Cajones wetland (1986-2017).

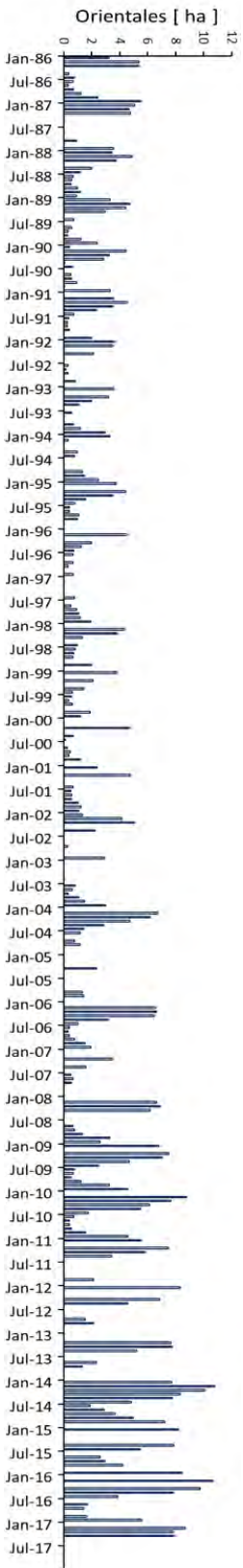


Figure 5-19. Time series of active vegetation cover ($NDVI \geq 0.2$) over the Orientales wetland (1986-2017).

Figure 5-20, Figure 5-21 and Figure 5-22 show box plots of the monthly active vegetation cover over the period between 1986 and 2017. Each box consists of a lower line representing the 25th percentile, and an upper line representing the 75th percentile; the centre line is the median, the whiskers represent the maximum and minimum values, while single dots are outliers. It can be observed that the vegetation cover peaks between April and May and that there is strong variability for all the sites, especially in the Cajones wetland, during the December-May period. Moreover, the average vegetation cover during the Austral summer (i.e., December, January and February) is 1.7, 1.9 and 4.5 ha, for Quebrada Negra, Cajones and Orientales, respectively, whereas during Austral winter (i.e., June, July and August) the values drop to 1.0, 0.8 and 1.1 ha. Table 5-1 shows that vegetation coverage increased from July to December as obtained from the Sentinel-2 images, which is consistent with the historical average variation curves (1986-2017) obtained by LANDSAT images. Nevertheless, the values obtained from Sentinel and LANDSAT products are not directly comparable, as the latter are less accurate. However, LANDSAT presents a larger period over which imagery is offered and therefore, allows for more years to be considered in the analysis of annual and seasonal variability.

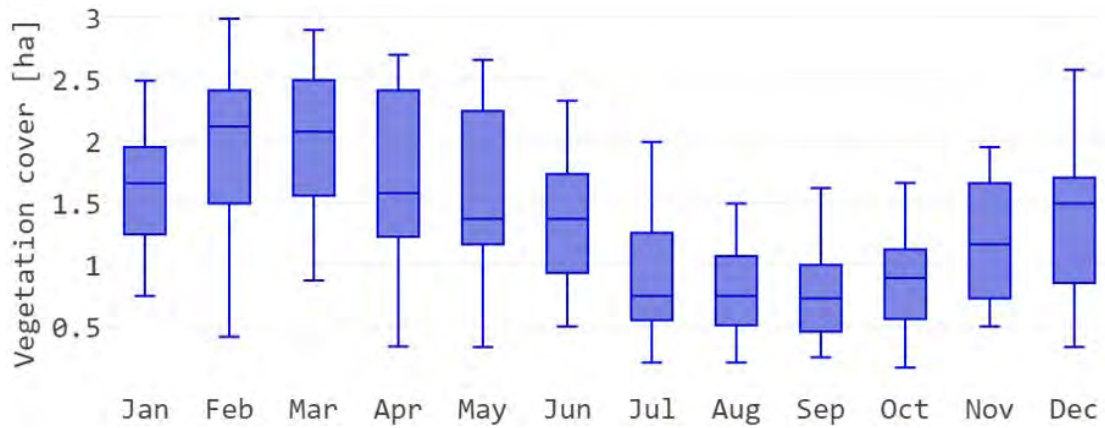


Figure 5-20. Monthly time series of active vegetation cover (NDVI >= 0.2) over the Quebrada Negra wetland (1986-2017).

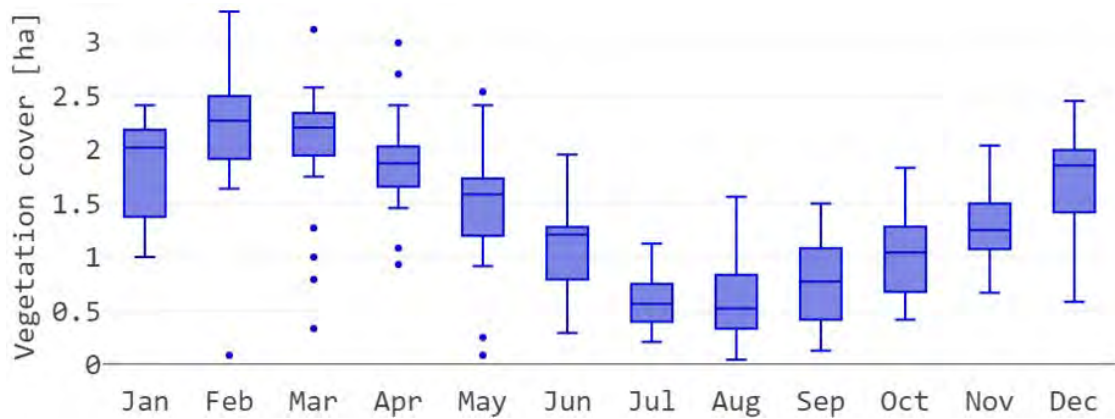


Figure 5-21. Monthly time series of active vegetation cover (NDVI >= 0.2) over the Cajones wetland (1986-2017).

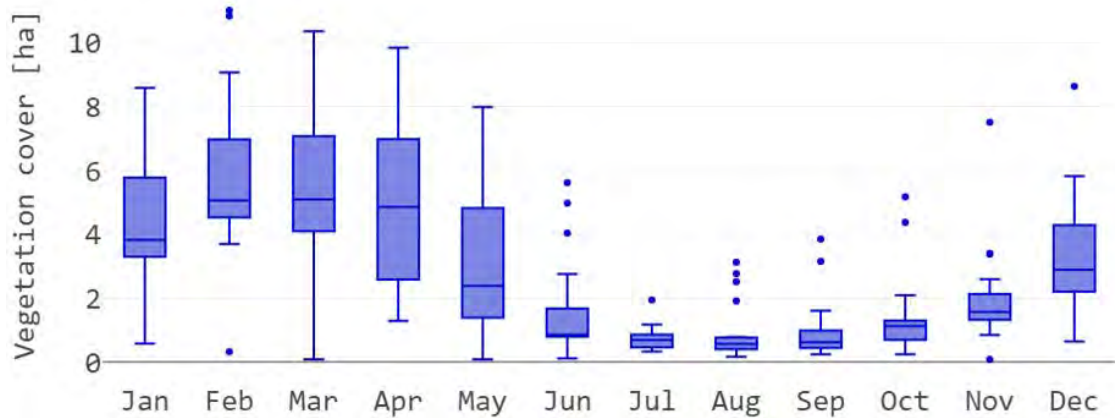


Figure 5-22. Monthly time series of active vegetation cover (NDVI >= 0.2) over the Orientales wetland (1986-2017).

5.3 Evapotranspiration estimates

5.3.1 Potential evapotranspiration

ET_o at the Quebrada Negra wetland was estimated with the FAO Penman-Monteith equation using the data from the Quebrada Negra Wetland meteorological station (Figure 5-23). The ET_o for the study period varies between ~0 and 5.7 mm/day (on 14 June and 10 November, respectively). The minimum value was observed on a rainy day, but the minimum value of days without rain events was 0.8 mm/day (24 July). As expected, ET_o increases as the summer approaches. Also, the FAO Penman-Monteith method results in a clear reduction of the ET_o when it rains.



Figure 5-23. Relationship between daily ET_o (lower data, in blue) and daily precipitation (upper data, in orange) at the Quebrada Negra Wetland meteorological station.

5.3.2 Spatial distribution of estimated actual evapotranspiration

After generating the NDVI maps, $ET_{a,NDVI}$ was calculated using equation (3). The annual ET_o from the UC meteorological station and the annual precipitation from the Quebrada Negra station (DGA) data were used to calculate $ET_{a,NDVI}$ at the Quebrada Negra, Cajones and Orientales wetlands. The annual ET_o at the UC meteorological station was 1284 mm and the annual precipitation at Quebrada Negra station (DGA) was 173 mm. In this analysis, it was decided to use data from UC meteorological station and Quebrada Negra station (DGA) because they have been collecting information for more than one year. Despite the fact that the Quebrada Negra wetland station measurements should represent better the conditions in the studied wetlands, the site does not have an entire year of data.

The $ET_{a,NDVI}$ results obtained for each satellite image are presented in Table 5-3. It was decided to estimate $ET_{a,NDVI}$ for each satellite image to analyze the sensitivity of the Groeneveld et al. (2007) method to the selection of the mid-summer NDVI (peak season NDVI) map. As shown in Table 5-3, since NDVI' does not vary significantly between

different satellite images, hence all NDVI' values should be appropriate to estimate annual $ET_{a,NDVI}$. Additionally, the mean $ET_{a,NDVI}$ values and its standard deviation for each wetland are presented in Table 5-3. Figure 5-24 shows the time-averaged $ET_{a,NDVI}$ map.

Taking into consideration the data presented in Table 5-3, when using the different satellite images to calculate mid-summer NDVI', the $ET_{a,NDVI}$ estimates for the Quebrada Negra wetland vary between 596 and 654 mm/year, whereas the Cajones $ET_{a,NDVI}$ varies between 670 and 729 mm/year. On the other hand, the Orientales wetland $ET_{a,NDVI}$ varies between 659 and 734 mm/year. Furthermore, the ET_a standard deviation for all three wetlands is of the order of ~ 20 mm/year, giving the estimated annual $ET_{a,NDVI}$ of 631 ± 21 mm/year for the Quebrada Negra wetland, 705 ± 17 mm/year for the Cajones wetland and 702 ± 23 mm/year for the Orientales wetland. It can be noted that Groeneveld et al. showed that their method has residual errors that decrease as measured ET_a increases (Groeneveld et al., 2007), with error values of the order of 3.5 – 16.9 % for $ET_{a,NDVI}$ estimates of the same magnitude as the ones obtained in this study.

In summary, the largest time-averaged evapotranspiration values are estimated for the Cajones wetland, while the lowest ones are observed in the Quebrada Negra wetland. Additionally, the mean equivalent water flow due to this evapotranspiration (i.e. considering the potential loss of river flow represented by this amount of evaporation) was estimated to be 0.6 L/s for the Cajones wetland, 2.3 L/s for the Orientales wetland (which has the largest area) and 0.7 L/s for the Quebrada Negra wetland.

Studied wetland	Satellite image date	Area covered by vegetation [ha]	Average NDVI raw [-]	NDVI' [-]	ET _{a,NDVI} [mm/year]
<i>Quebrada Negra wetland</i>	25-12-2017	4.48	0.31	0.38	596
	30-12-2017	3.10	0.32	0.43	647
	09-01-2018	2.64	0.32	0.43	654
	14-01-2018	3.68	0.30	0.43	653
	18-02-2018	3.51	0.32	0.40	620
	23-02-2018	3.01	0.31	0.42	638
	28-02-2018	3.76	0.31	0.39	609
Average		3.45	0.31	0.41	631
Standard deviation		0.56	0.01	0.02	21
<i>Cajones wetland</i>	25-12-2017	3.03	0.36	0.45	670
	30-12-2017	2.67	0.36	0.48	701
	09-01-2018	2.54	0.36	0.48	710
	14-01-2018	2.96	0.34	0.48	707
	18-02-2018	3.09	0.39	0.49	716
	23-02-2018	2.82	0.37	0.50	729
	28-02-2018	3.08	0.38	0.48	705
Average		2.88	0.37	0.48	705
Standard deviation		0.20	0.02	0.01	17
<i>Orientales wetland</i>	25-12-2017	10.34	0.35	0.44	659
	30-12-2017	9.06	0.35	0.47	691
	09-01-2018	8.72	0.34	0.47	692
	14-01-2018	10.05	0.34	0.48	703
	18-02-2018	11.14	0.39	0.50	724
	23-02-2018	10.30	0.38	0.51	734
	28-02-2018	11.09	0.39	0.48	710
Average		10.10	0.36	0.48	702
Standard deviation		0.86	0.02	0.02	23

Table 5-3. Average NDVI, NDVI' and ET_{a,NDVI} calculated from the seven Sentinel-2 products.

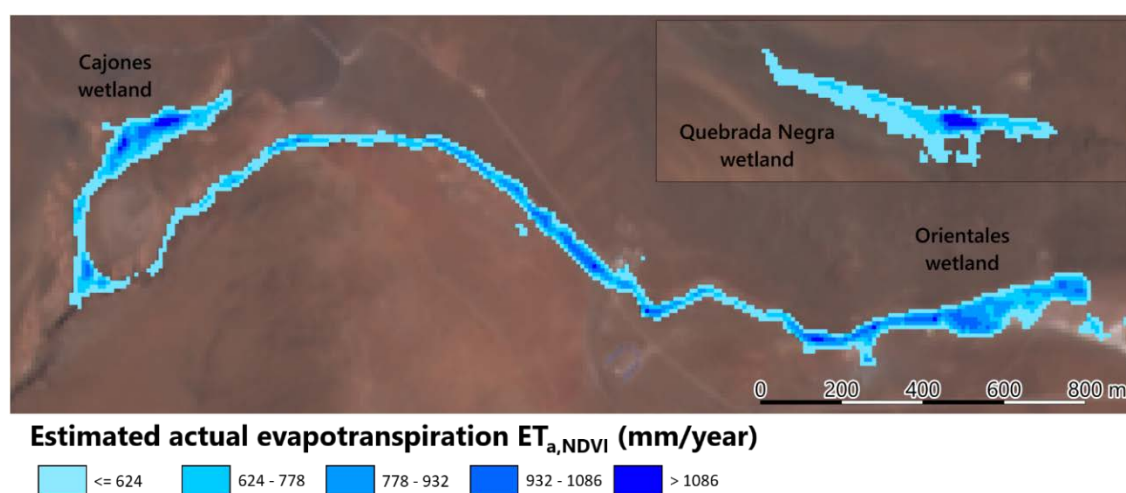


Figure 5-24. Annual ET_{a,NDVI} map estimated using the time-averaged data from the seven satellite images used.

5.4 Soil characterization

5.4.1 Peat depth determination

During the field work carried out in November 2018, a soil auger was used at the Quebrada Negra wetland, more specifically at the soil auger location shown in Figure 4-7. The soil auger was driven until it was impossible to continue, due to the presence of boulders, coarse gravel, consolidated rock or other hard material. A peat depth of 6.6 m was obtained, the depth at which rock was found.

5.4.2 Soil particle distribution

Soil particle distribution tests were performed on the five samples from P1, the six samples from P2 and the 14 samples extracted with the soil auger. The results from the P1 samples are presented in Table 5-4 and Figure 5-25, the results from P2 are presented in Table 5-5 and Figure 5-26, and the results from the 14 samples collected from the material extracted with the soil auger are presented in Table 5-6, Table 5-7, Table 5-8 and Figure 5-27. The soil particle size distribution was made following the Unified Soil Classification System (USCS), and coarse-grained soils were also classified for their particle size distribution curve. According to the USCS soil classification, well-graded sand (SW), silty sand (SM) and clayey sand (SC) were found. The USCS soil classification chart can be found in Appendix D. For some samples, especially those collected at depths of less than 2 m at the middle of the wetland, the test could not be performed due to the large proportion of organic material.

Sample number			M1*	M2*	M3*	M4*	M5
Sample name			P1_S1*	P1_S2*	P1_S3*	P1_S4*	P1_S5
Soil distribution	ASTM	(mm)					
Gravel %	(#4-3")	(4.75-75mm)	-	-	-	-	0 %
Sand %	(#200-#4)	(0.075-4.75mm)	-	-	-	-	30 %
Fines % (clay & silt)	(< #200)	(<0.075mm)	-	-	-	-	70 %
USCS soil classification			-	-	-	-	Fines**

*Soil particle distribution test couldn't be performed at the sample due to high organic material content (grass and roots).

**There is not enough information to determine whether there is more clay or silt in the sample.

Table 5-4. Soil particle size distribution from P1 samples.

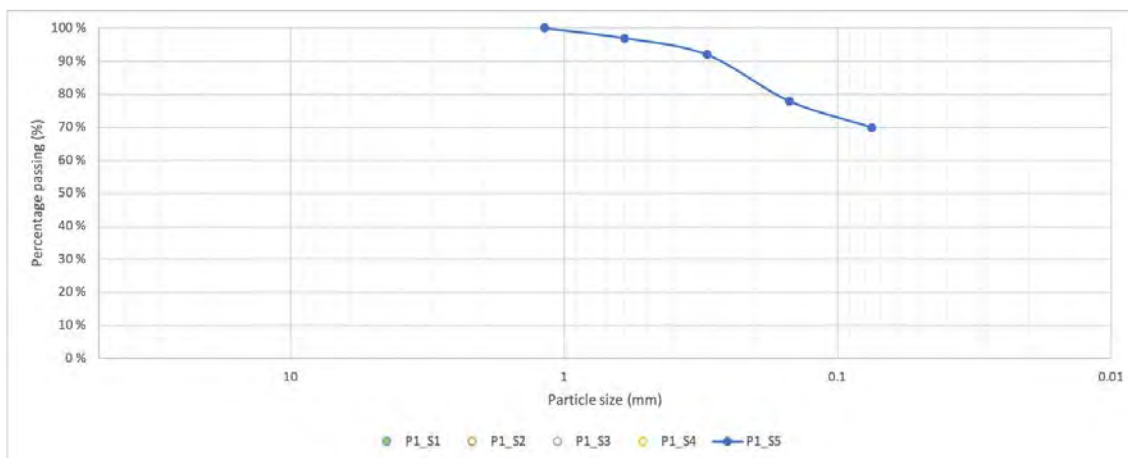


Figure 5-25. P1 sample particle size distribution curve.

Sample number		M6*	M10	M8	M7	M9	M11
Sample name		P2_S1*	P2_S2	P2_S3	P2_S4	P2_S5	P2_S6
Soil distribution	ASTM (mm)						
Gravel %	(#4-3") (4.75-75mm)	-	0 %	2 %	7 %	5 %	0 %
Sand %	(#200-#4) (0.075-4.75mm)	-	67 %	90 %	89 %	68 %	69 %
Fines % (clay & silt)	(< #200) (<0.075mm)	-	33 %	8 %	4 %	27 %	31 %
USCS soil classification		-	SW	SW-SM/SC**	SM/SC**	SW	SW

*Soil particle size distribution test could not be performed for the sample due to high organic material content (grass and roots).

**There is not enough information to determine whether there is more clay or silt in the sample.

Table 5-5. Soil particle size distribution from P2 samples.

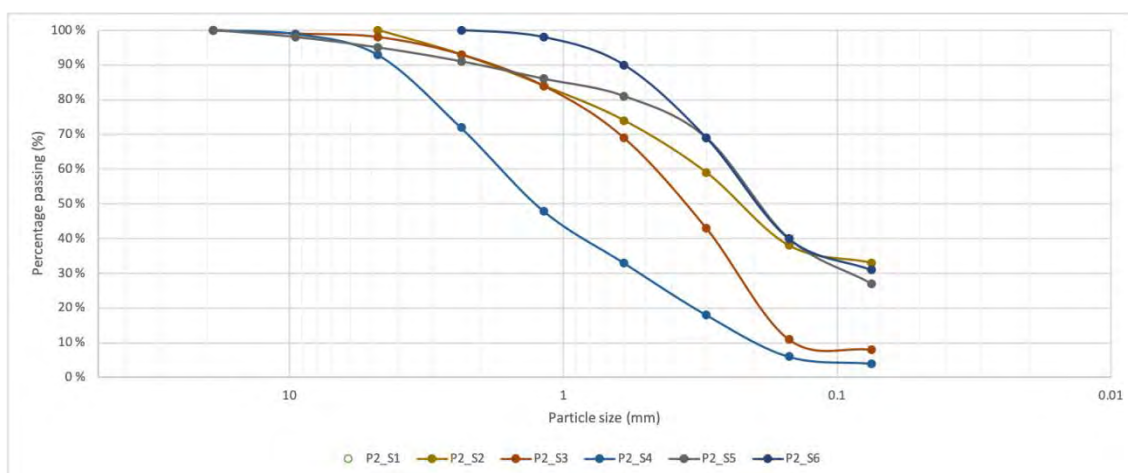


Figure 5-26. P2 samples soil particle size distribution curve.

Sample number			M12*	M13*	M14*	M15	M16
Sample name			SA_ 30-50	SA_ 100-120	SA_ 170-190	SA_ 204-234	SA_ 234-260
Soil distribution	ASTM	(mm)					
Gravel %	(#4-3")	(4.75-75mm)	-	-	-	0 %	0 %
Sand %	(#200-#4)	(0.075- 4.75mm)	-	-	-	75 %	77 %
Fines % (clay & silt)	(< #200)	(<0.075mm)	-	-	-	25 %	23 %
USCS soil classification			-	-	-	SW	SW

*Soil particle size distribution test could not be performed for the sample due to high organic material content (grass and roots)

Table 5-6. Soil particle size distribution from the soil auger hole samples (30-260 cm depth).

Sample number			M17	M18	M19	M20	M21
Sample name			SA_ 315- 325	SA_ 325-345	SA_ 345- 375	SA_ 375- 405	SA_ 405- 440
Soil distribution	ASTM	(mm)					
Gravel %	(#4-3")	(4.75-75mm)	0 %	6 %	0 %	0 %	1 %
Sand %	(#200- #4)	(0.075- 4.75mm)	84 %	84 %	82 %	61 %	85 %
Fines % (clay & silt)	(< #200)	(<0.075mm)	16 %	10 %	18 %	39 %	14 %
USCS soil classification			SW	SW- SM/ SC*	SW	SW	SW

Table 5-7. Soil particle size distribution from the soil auger hole samples (260- 440 cm depth).

Sample number			M22	M23	M24	M25
Sample name			SA_ 440-510	SA_ 510-565	SA_ 565-610	SA_ 610-660
Soil distribution	ASTM	(mm)				
Gravel %	(#4-3")	(4.75-75mm)	1 %	0 %	7 %	14 %
Sand %	(#200-#4)	(0.075-4.75mm)	86 %	91 %	83 %	69 %
Fines % (clay & silt)	(< #200)	(<0.075mm)	13 %	9 %	10 %	17 %
USCS soil classification			SP	SP- SM/SC*	SP- SM/SC*	SW

Table 5-8. Soil particle size distribution from the soil auger hole samples (440-660 cm depth).

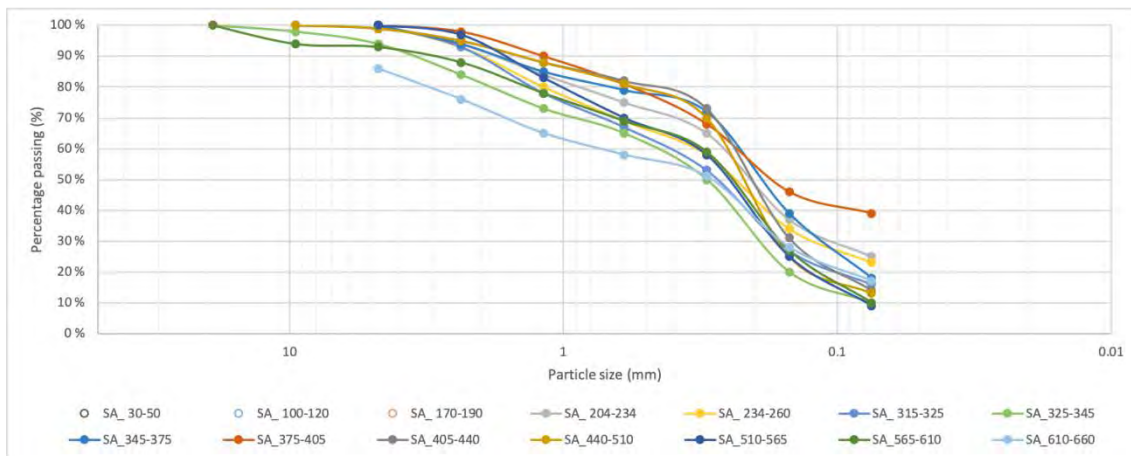


Figure 5-27. Soil auger hole samples particle size distribution curve.

Taking into consideration the particle size distribution curves (Figure 5-27), it is observed that the soil is getting coarser with depth.

High content of organic material was found for the P1 samples, located at the middle of the Quebrada Negra wetland. For this reason, particle distribution tests could not be performed for most of the samples taken at P1. The only P1 sample on which the test was applied was P1_S5, which was at approximately 2 m depth.

High content of organic material was found for the P2 samples, located at the downstream end of the Quebrada Negra wetland. Mostly sand particles were found, with varying percentages of fines. The only P2 sample on which the test could not be applied was P2_S1, which was near the surface.

The samples taken above 2 m depth at the soil auger hole showed mostly roots, sands and fine soils. At the samples collected at 2 m or deeper, a smaller amount of roots was found. A bigger percentage of gravels was found at 6 m depth. This is consistent with the results obtained from P1, which were taken near to the soil auger hole.

5.4.3 Falling-head Permeability Test results

The K_s results for falling-head permeability tests carried out to the thin walled tube soil samples from P1 and P2 pits are presented in Table 5-9 and Table 5-10. The values presented in the tables below are the mean from three tests performed at each sample.

Sample	K_s (m/s)	K_s (m/day)
P1_S50_V	9.717E-07	8.395E-02
P1_S50_H	1.662E-07	1.436E-02
P1_S150_V	1.723E-07	1.489E-02
P1_S150_H	1.280E-07	1.106E-02

Table 5-9. K_s results for pit P1 soil samples.

Sample	K_s (m/s)	K_s (m/day)
P2_S50_V	9.163E-08	7.917E-03
P2_S50_H	disturbed sample	disturbed sample
P2_S150_V	9.440E-07	8.156E-02
P2_S150_H	4.640E-08	4.009E-03

Table 5-10. K_s results for pit P2 soil samples.

The soil hydraulic conductivity results obtained from the Shelby tubes samples at pit P1 and P2 are in general low, with values that are typical of semi-pervious soils. The values obtained from P1 samples rank between 8.4×10^{-2} and 1.1×10^{-2} m/day. The values obtained from P2 samples rank between 7.9×10^{-3} and 8.2×10^{-2} m/day.

5.4.4 Field saturated hydraulic conductivity

The results of the estimation of the hydraulic conductivity are presented in Table 5-11. Experimental fits highlighted in red have substantial problems that compromise the validity of the estimates. Also, 40% of the valid results present specific storage values below 10^{-7} m⁻¹, which may suggest implausibly low values of porosity and compressibility, and according to Butler (Butler, 1997), it is recommended that other models such as Kansas Geological Survey (KGS) slug test model (Hyder et al., 1994) are used. This should be further explored, especially for future measurements. Figure 5-28 shows different examples of the fits. Both a) and b) show good fits but in the case of b) a considerable amount of recovery was not achieved. c) and d) present two different cases where the shape of the experimental data does not resemble the type curves, despite achieving an acceptable level of recovery. Repetition of the experiment should also be considered to produce more reliable and representative parameters.

Considering only the slug tests that did not show problems, starting upstream, a hydraulic conductivity that is characteristic of the lower end of semi-pervious soils (Table 5-12) was measured at wells 01 and 03, with values of the order of 10^{-2} and 10^{-1} m/day respectively. Continuing in the downstream direction, slug tests performed on wells 12, 13 and 14, located around the middle of the main grassland (Figure 4-26),

evidenced soils with, again, hydraulic conductivity values of the order of 10^{-2} to 10^{-1} m/day. Wells 17, 20 and 22 show that this situation appears to be maintained until the last portion (downstream) of the main grassland. Finally, the last well in the downstream direction (well 25) evidences a change in soil characteristics towards soils with higher hydraulic conductivity, with a value in the order of 10^0 m/day.

These results are consistent with the hydraulic conductivities obtained in the laboratory from the Shelby tubes samples taken at pit P1 and P2. The hydraulic conductivity obtained from the Shelby tubes samples at pit P1 is of the order of 10^{-2} m/day, while at well 12M, the nearest well where the slug test was performed, the measured hydraulic conductivity is 3.5×10^{-2} m/day. The values obtained from wells 13 and 14 are also of the same order of magnitude. The values obtained from P2 samples lie between 10^{-3} and 10^{-2} m/day. These are lower than the values obtained from the surrounding wells (17, 20 and 21), but they are still relatively similar.

As explained above, by looking only at the successful slug tests, it appears that the wetland has soils that fall under a semi-pervious classification, with a notable increase in hydraulic conductivity in the soils at the downstream tail of the wetland area. However, as is evidenced in Figure 5-29, the perturbation in the groundwater level arising from the slug test at well 8Z takes substantially more time to stabilize than the one arising from the slug test at well 12M. Therefore, one would expect a much lower hydraulic conductivity at soils near well 8Z than those near well 12M. Moreover, results obtained from the slug tests performed at 8Z, despite the limited validity of the test, support the observations from the continuous measurements of the well, as the hydraulic conductivity obtained is of 5.2×10^{-4} m/day. Assuming this to be correct, there would be evidence of a zone near well 8Z, in the first portion of the main grassland (upstream direction), exhibiting hydraulic conductivities two orders of magnitude lower than those measured at the rest of the wetland, with values that are characteristic of impervious soils. Furthermore, it is also interesting to point out that, according to UAV photogrammetry, such as that of Figure 4-26, and observation during field campaigns, superficial ponds and ephemeral surface discharge appear to be characteristic of the first portion of the main grassland. The spatial distribution of the slug test results is presented in Figure 5-30.

Location	K_r (m/s)	K_r (m/day)	S_s (1/m)	Observations
25-S	2.20E-05	1.90E+00	3.30E-03	
08Z-D	6.00E-09	5.18E-04	3.30E-03	Bad fit, 74% of recovery missing
07S-D	2.00E-08	1.73E-03	3.30E-04	Bad fit, 68% of recovery missing
05-D	5.50E-08	4.75E-03	3.30E-05	Bad fit, 39% of recovery missing
07A-D	1.50E-07	1.30E-02	3.30E-10	Bad fit, 36% of recovery missing
01-D	1.60E-07	1.38E-02	3.30E-07	
12Z-D	1.50E-06	1.30E-01	3.30E-07	
14A-D	7.00E-07	6.05E-02	3.30E-05	
12M-D	4.00E-07	3.46E-02	3.30E-07	
22-D	3.50E-07	3.02E-02	3.30E-05	
14M-D	2.80E-07	2.42E-02	3.30E-01	Double stage recovery
18A-S	2.80E-07	2.42E-02	3.30E-10	Erratic data and low initial displacement
13Z-D	3.30E-07	2.85E-02	3.30E-05	
17M-D	2.00E-07	1.73E-02	3.30E-05	
19Z-D	4.00E-08	3.46E-03	3.30E-10	Bad fit, 86% of recovery missing
06A-S	4.00E-07	3.46E-02	3.30E-10	Erratic data and low initial displacement
20M-D	4.70E-07	4.06E-02	3.30E-04	
03-D	1.50E-06	1.30E-01	3.30E-07	
04-D	-	-	-	Impossible fit, 96% of recovery missing
02-S	2.00E-07	1.73E-02	3.30E-07	Erratic data and low initial displacement

Table 5-11. Slug test results summary. Each location is represented using the following code: XXY-Z, where the XX number corresponds to the number of the piezometer (which indicates relative position in the wetland and increases in the downstream direction), the Y letter corresponds to the position of the piezometer relative to the northern or southern limits of the wetland (as shown in Figure 4-26), and the Z letter indicates deep (D) or shallow (S) level (as shown in Figure 4-20).

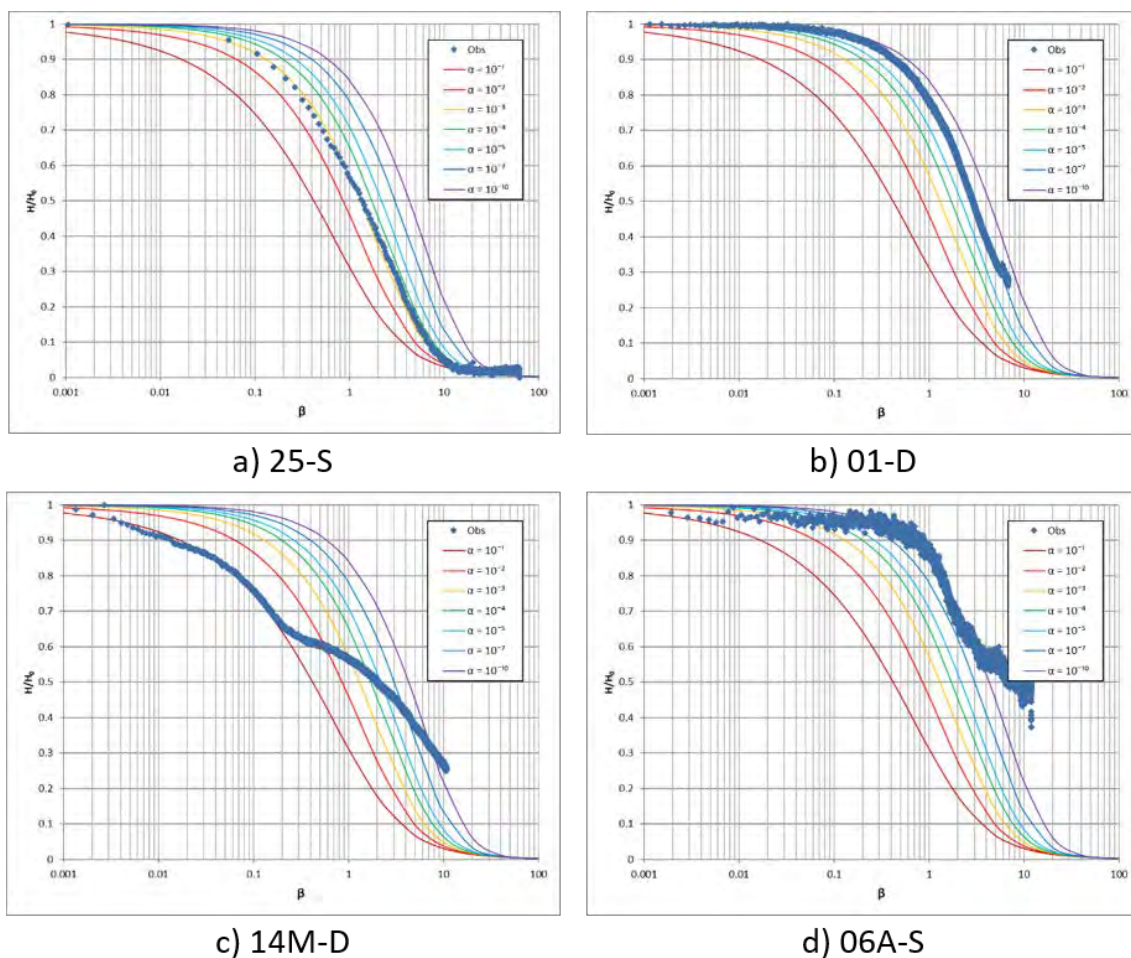


Figure 5-28. Examples of slug test fits.

Field saturated hydraulic conductivity values for the 14M-D and 06A-S wells (Figure 5-28 c) and d), respectively) were estimated using only the beginning of the slug test curves, before any abrupt change is observed. It was decided to use only a part of the data because the change in slope could be due to a change in the soil composition.

$\log_{10} K$ (m/s)	0	1	2	3	4	5	6	7	8	9	10	11	12	13
Permeability	Pervious				Semipervious				Impervious					

Table 5-12. Typical values of soil hydraulic conductivity. Modified from Bear (Bear, 1988).

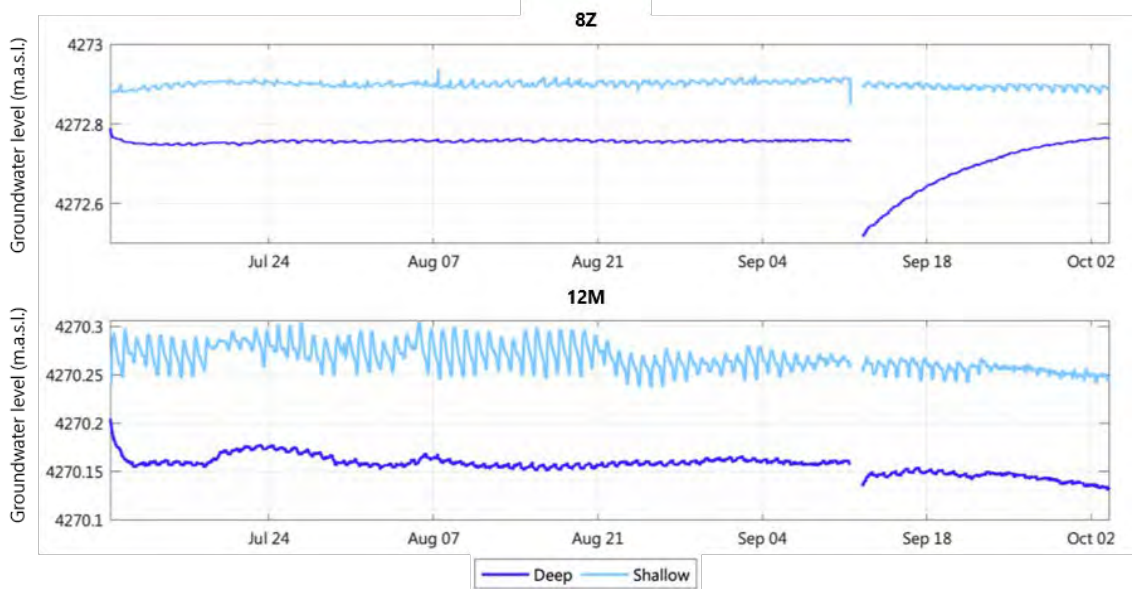


Figure 5-29. Groundwater level continuous measurements at wells 8Z and 12M. Discontinuities occurring during September in both plots correspond to the slug tests performed at both wells.

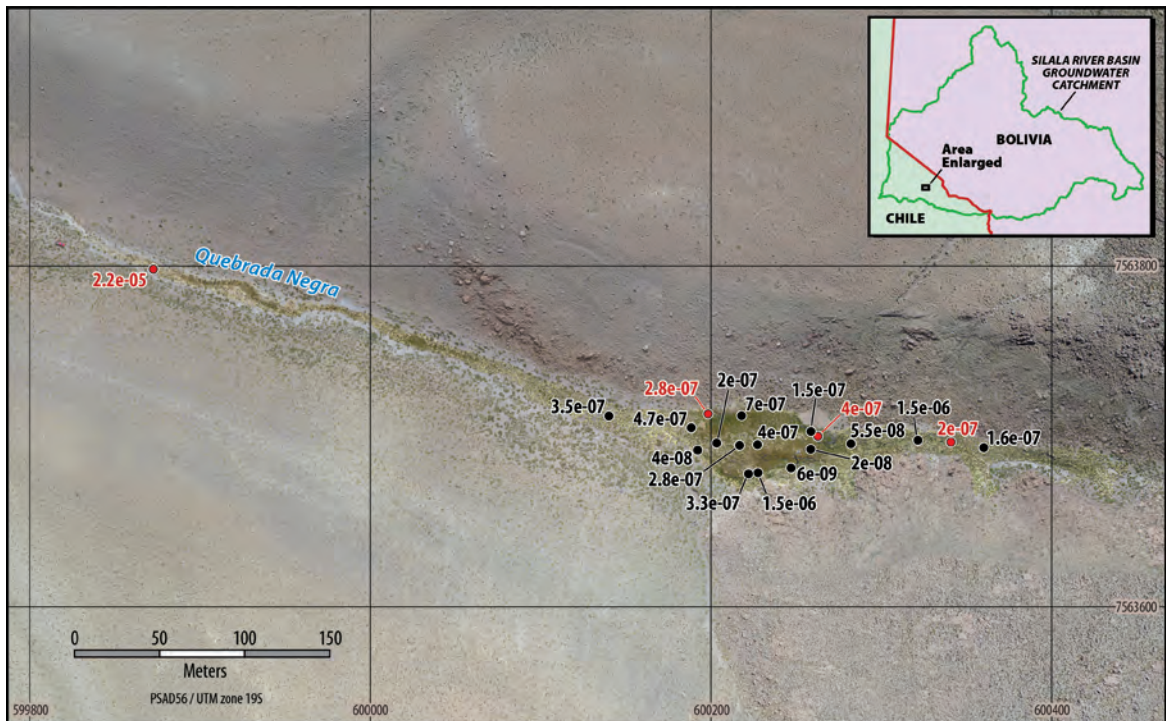


Figure 5-30. Spatial distribution of field saturated hydraulic conductivity. In red are presented the values measured in shallow piezometers and in black those measured in deep piezometers.

5.4.5 Thermal properties

Table 5-13 presents the results of the nine measurements performed at the site of the soil sensors installation. Even though the measurements were taken at sites with different water saturation conditions and orientation, the results are similar and do not suggest any kind of pattern.

	K W/(m·K)	C MJ/(m ³ ·K)	D mm ² /s
Uncovered wall	0.475	3.625	0.131
	0.510	4.381	0.116
	0.521	4.743	0.110
Underwater wall	0.521	4.743	0.110
	0.507	5.289	0.096
	0.511	5.188	0.099
Underwater bottom	0.603	5.494	0.110
	0.549	3.433	0.160
	0.550	3.431	0.160

Table 5-13. Measurements of thermal properties of the soil.

5.5 Groundwater level monitoring

5.5.1 Spatial interpolation

Figure 5-31 and Figure 5-32 show the main grassland area of the Quebrada Negra wetland, in which the surface water features and the different vegetation covers (Table 5-14) were visually identified from UAV photogrammetry captured during August 2018. The zones where an appearance of surface water is identified coincide with the presence of dense Tussock grasses. It seems likely that this surface water is fed by lateral spring sources (marked with a dashed yellow arrow), which are not evident from the photograph alone. These springs appear to emerge from the basal slopes of the ravine.

Cover type	Description
C1	Dense tussock grasses (<i>Calamagrostis cf. ampliflora</i>)
C2	<i>Oxychloe andina</i> bog cushion plants with <i>Patosia clandestina</i>
C3	<i>Oxychloe andina</i> with sparse and dried tussock <i>Calamagrostis</i> grasses
C4	Sparse Tussock grasses

Table 5-14. Different vegetation cover types identified from UAV photogrammetry captured during August 2018. The vegetation cover types were identified by C. Latorre (Personal Communication).

Figure 5-31 and Figure 5-32 also show examples of the contour maps of water level elevation constructed from the groundwater level measurements, and the direction of the vertical gradient at the individual monitoring locations. It is observed that there is a lateral gradient favoring flow in a direction from the Quebrada Negra towards the Silala River, i.e. from East to West.

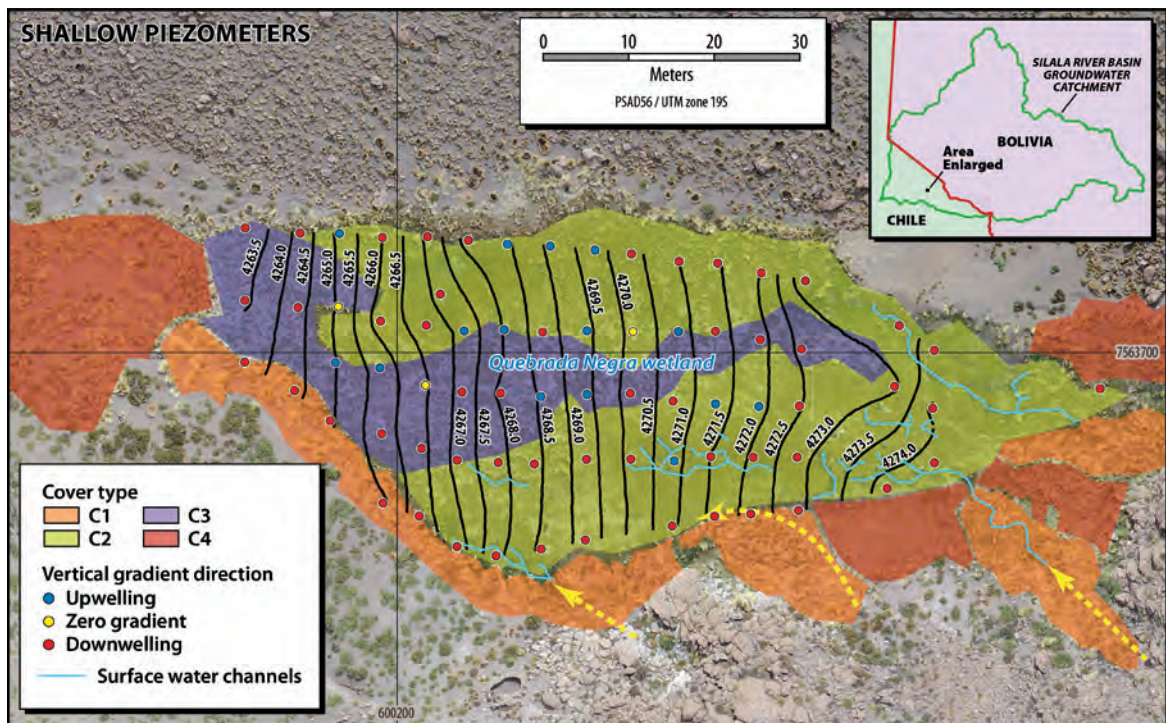


Figure 5-31. Contour lines of groundwater levels (m.a.s.l.), at shallow piezometers, measured during September 2018 at the main grassland of the Quebrada Negra wetland. Red circles represent points where positive gradient (downwelling) was observed, blue circles represent the points where negative gradient (upwelling) was observed and yellow circles represent points where zero-gradient was observed. Surface channels observed in the wetland are identified as light blue lines. Apparent surface water sources are marked with dashed yellow lines.

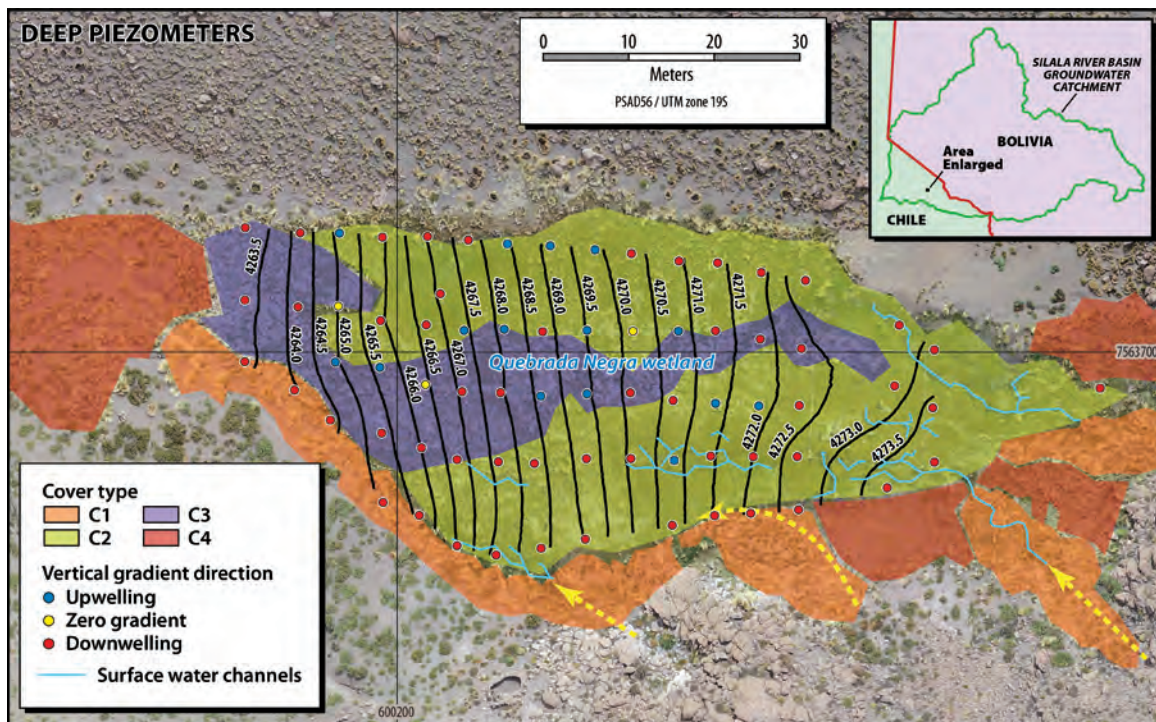


Figure 5-32. Contour lines of groundwater levels (m.a.s.l.), at deep piezometers, measured during September 2018 at the main grassland of the Quebrada Negra wetland. Red circles represent points where positive gradient (downwelling) was observed, blue circles represent the points where negative gradient (upwelling) was observed and yellow circles represent points where zero-gradient was observed. Surface channels observed in the wetland are identified as light blue lines. Apparent surface water sources are marked with dashed yellow lines.

Figure 5-33 shows the interpolated contours of the vertical hydraulic gradient, which was calculated from the difference in the levels of the shallow and deep piezometers at each location. Positive values mean that the shallow wells present higher levels than the deep ones, which implies downwelling conditions. Negative vertical hydraulic gradients represent the opposite, i.e., upwelling conditions. The spatially heterogeneous nature of the vertical gradients in the main wetland area can be seen more clearly when looking at the monitoring points in Figure 5-31 to Figure 5-33, where red shows the piezometer locations where downwelling was observed, blue the locations of upwelling and yellow the locations with zero gradient. It can be seen that: a) in the upslope (eastern) segment of the ravine leading into the main wetland, an area of upwelling occurs, which then leads to an area of downwelling; b) in the main areas of wetland vegetation in general the vertical gradient of groundwater levels is mostly dominated by zero or positive gradients (downwelling), but with localized areas of upwelling; and c) in the ravine below the main area of wetland, in general, upwelling conditions occur.

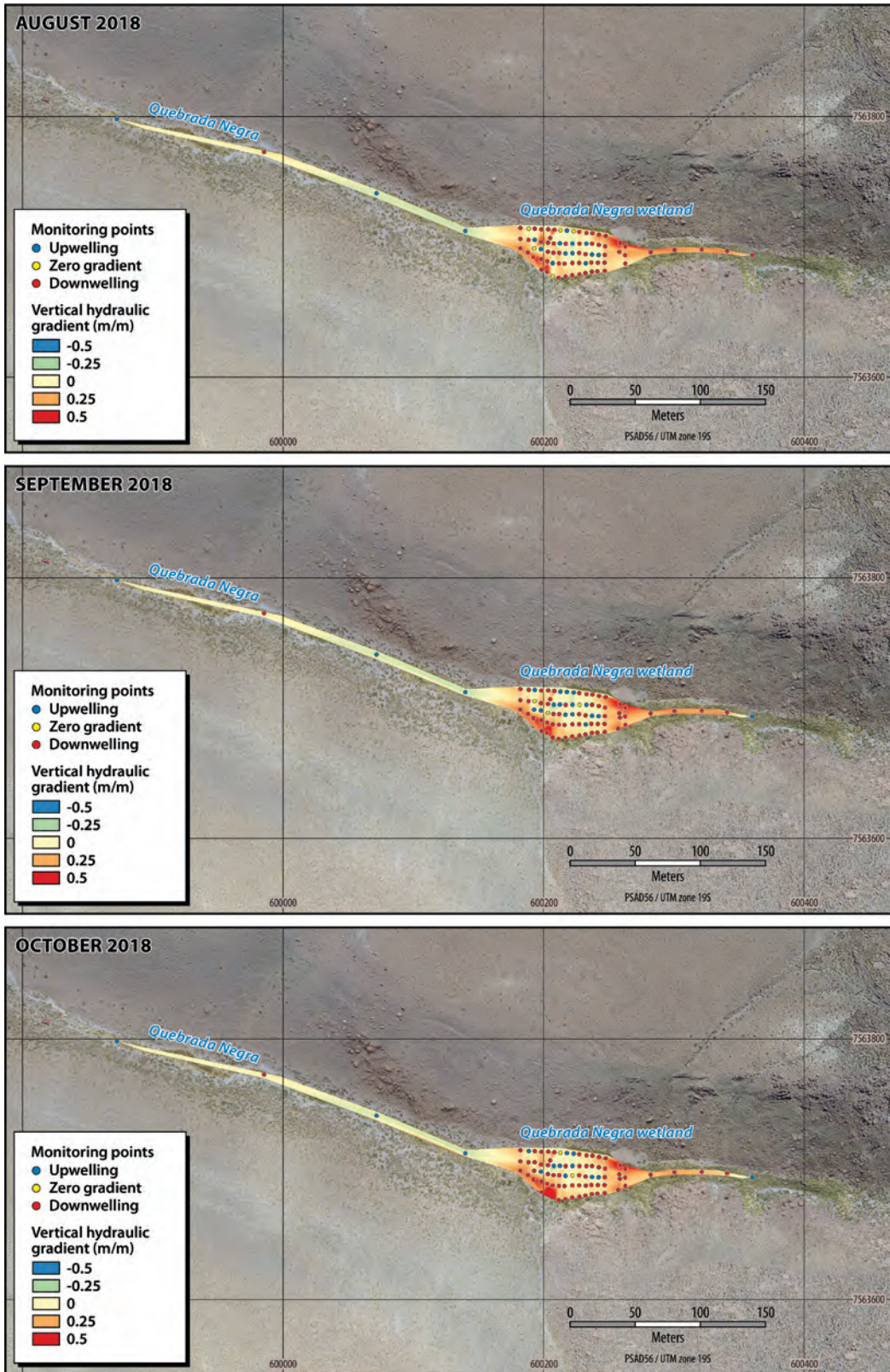


Figure 5-33. Vertical hydraulic gradient, calculated from well measurements. Positive hydraulic gradients correspond to downwelling conditions, whereas negative hydraulic gradients correspond to upwelling conditions.

5.5.2 Groundwater profiles

Five groundwater level profiles are used to show variability in the main wetland area in more detail, four of which are transverse to the principal wetland slope and one in the longitudinal direction. Figure 5-34 shows the location and distribution of the five profiles presented in Figure 5-35 and Figure 5-36.

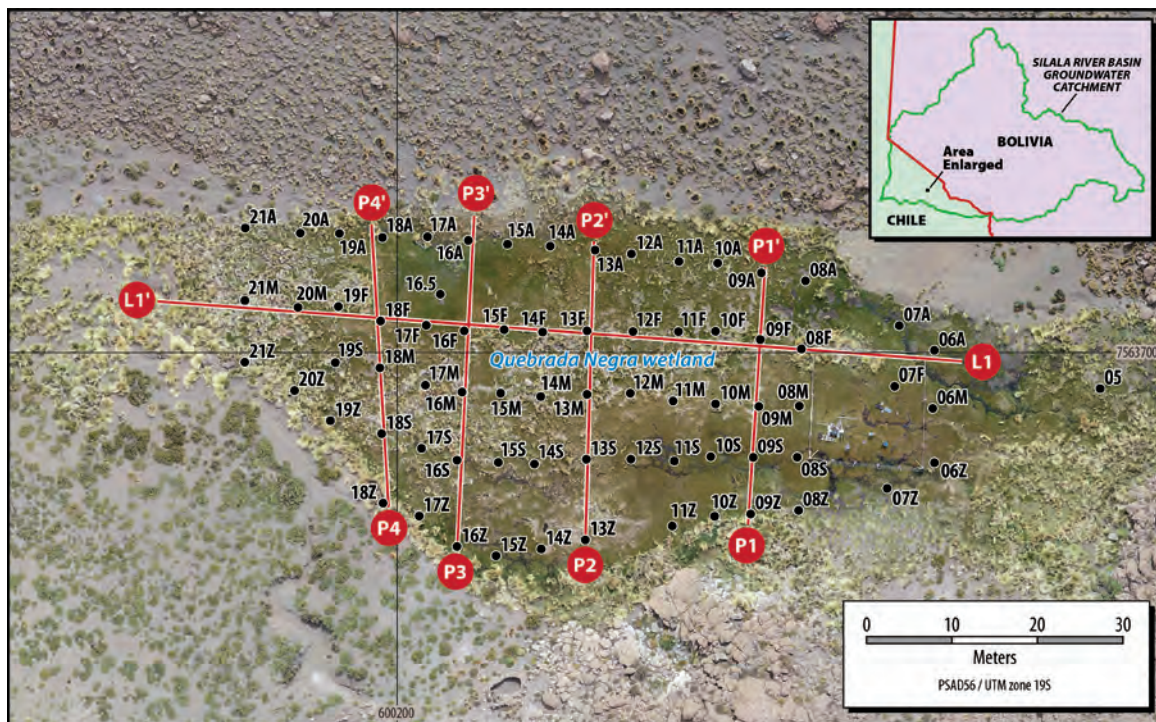


Figure 5-34. Map of transverse and longitudinal profiles.

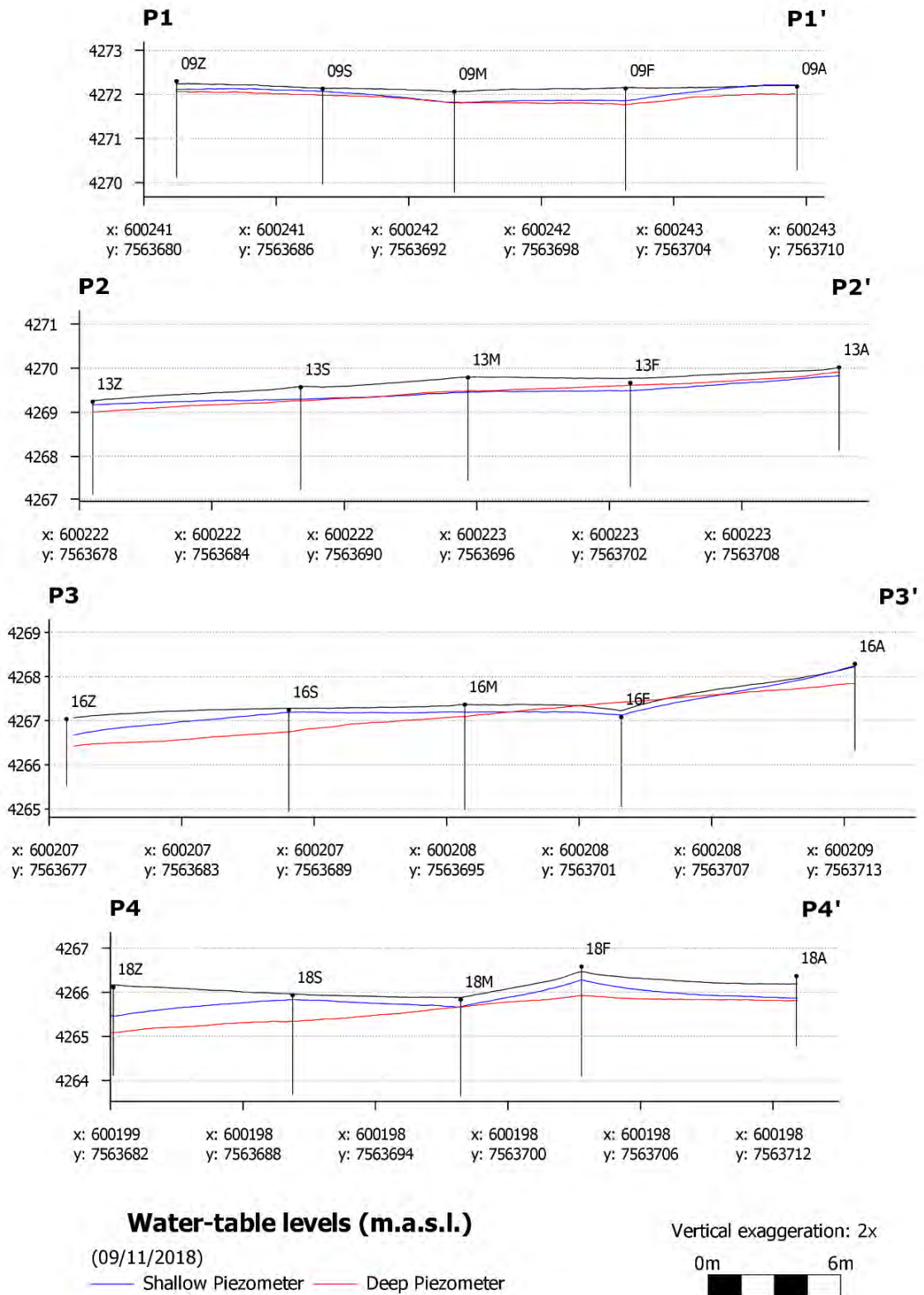


Figure 5-35. Groundwater level profiles from four transverse cross-sections, P1-P4.

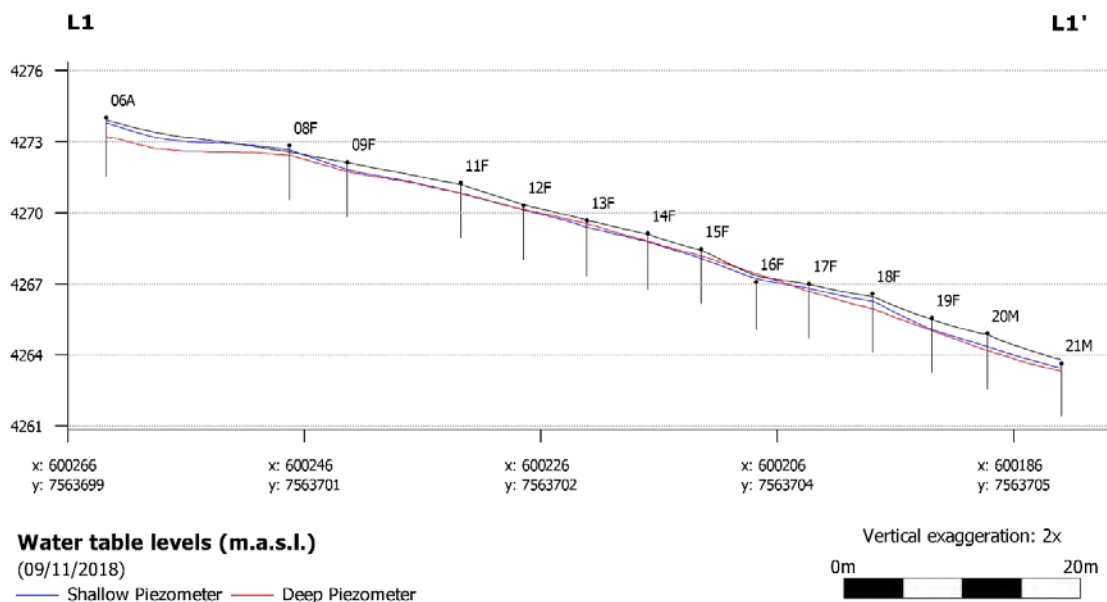


Figure 5-36. Groundwater level longitudinal profile L1.

Figure 5-35 and Figure 5-36 present the cross-sections of the topography and water-table levels measured at the deep and shallow piezometers in the main Quebrada Negra wetland, based on the manual measurements carried out on 11 September 2018. The position of each piezometer and the ground elevation were obtained by Real-time kinematic (RTK) positioning, with an error of 10-15 cm in the position and of 15-20 cm in the ground elevation. The interpolation was done using the Arcgis[®] software, using the Topo to Raster tool. In this case, the interpolation is used to estimate the water-table elevation and topography between known data points using a modified spline technique. The Topo to raster interpolation takes advantage of the types of input data commonly available and the known characteristics of elevation surfaces. This method uses an iterative finite difference interpolation technique. It is optimized to have the computational efficiency of local interpolation methods, such as inverse distance weighted (IDW) interpolation, without losing the surface continuity of global interpolation methods, such as Kriging and Spline (Hutchinson et al., 2011).

The cross-sections generally confirm the observations above, namely that the main wetland is characterized by zero gradients and downwelling, with localized upwelling as seen for locations 13F and 16F, for example.

5.5.3 Continuous monitoring records

Finally, Figure 5-37 presents the records of the continuous monitoring of groundwater level and shows that there are no major changes between June and September, although there is some variability at daily and longer time scales.

The step changes recorded in some wells (Figure 5-37) are related to the slug tests performed in those wells (Figure 4-26). Additionally, there are short periods (~2 days) with missing data because the sensors were used to perform slug tests in other wells. During these periods, the sensors were installed at different locations, and after the tests, they were replaced in their original locations. This accounts for the discrete changes. Sensors that present daily oscillations greater than the rest may have been out of the water, perhaps due to the presence of ice in the wells.

It can be seen for example that location 14A shows an upwelling gradient. As can be seen from Figure 4-26, this location lies at the northern edge of the wetland, at the base of the adjacent hillslope.

5.5.4 Discussion

The overall picture that emerges from the monitoring of groundwater levels and gradients in the Quebrada Negra wetland is one of complexity of groundwater flow paths and strong spatial heterogeneity. The wetland exists because it is fed by groundwater, and it is interesting to note that over much of the wetland, hydraulic gradients show conditions that promote downwelling, rather than upwelling. It can be seen that the springs that feed the wetland emerge at the edges of the wetland (in particular at the southern lateral boundary, as well as the upslope ravine), and that within the main wetland there are isolated locations where spring emergence occurs. Within the main wetland there are distinct channels and perennial flows, which then return subsurface, to flow as groundwater down the ravine towards the main Silala River.

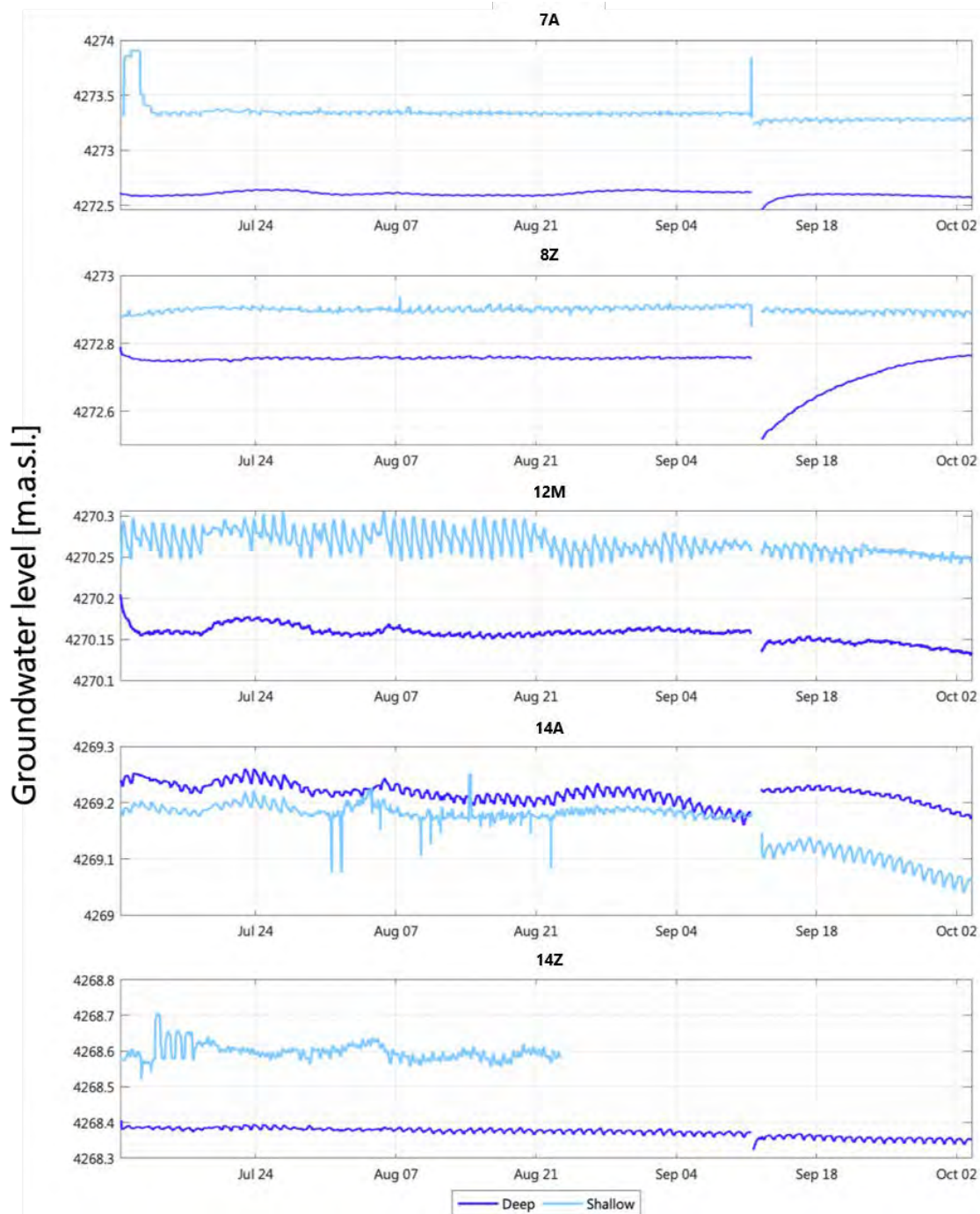


Figure 5-37. Continuous monitoring of groundwater levels at specific points.

6. CONCLUSIONS

In this study, the transition from winter to spring of the meteorological conditions, the vegetation cover and the groundwater levels of the Quebrada Negra wetland was captured and analyzed. Temperature records show that daily maximum temperatures vary between -3 and 17 °C, while the daily minima vary between -11 and 1 °C for the study period. The temperatures slowly rise as winter ends and summer approaches. Also, seven precipitation events were identified during the study period, which, according to satellite images, correspond to snowfall events. However, analysis of individual satellite images showed that there was abundant snow at Quebrada Negra while the pluviometer remained reporting zero precipitation. This phenomenon probably occurs due to the inherent limitations of pluviometers designed to capture rainfall. Additionally, negative values of soil heat flux were observed during winter, which could be attributed to the presence of snow on the surface and low temperatures in, and even freezing of, the ground.

The NDVI was used as an indicator of active vegetation coverage, where it was considered that $NDVI > 0.2$ corresponded to area covered by active vegetation. This threshold was determined by visual inspection of satellite images. The analysis of the satellite images used to investigate the spatial distribution of vegetation cover in the Quebrada Negra (Chile), Cajones and Orientales (Bolivia) wetlands showed that NDVI is higher in the middle of all the wetlands than at the edges. In general, the total area covered by vegetation increased with time over the observational period (July to November 2018), except for the Quebrada Negra wetland, in which the total area covered by vegetation decreased in November.

High-resolution NDVI images show, for each of the three wetlands, that the distribution of vegetation cover covers the flat area available and expands up the adjacent hillslopes where slopes are less than approximately 15%. In the case of the cross sections of Cajones and Orientales, it was observed that the maximum spatial coverage between the months of July-2018 and November-2018 is greater than the average extent. However, in the case of the Quebrada Negra wetland cross-section, the maximum and mean extent do not vary significantly and cover the same transverse section. However, an increase in vegetation cover in the Quebrada Negra wetland during the studied period was observed in river cross sections located downstream and upstream of the studied cross section, where the width of vegetation cover increased in the north-south direction. It should be noted that the range of variation is limited to the Sentinel raster resolution (10 m), so variations smaller than 10 m are not captured.

The temporal evolution of area covered by active vegetation ($NDVI > 0.2$) for each wetland was analyzed using low resolution but longer record length LANDSAT images. These showed that the peak vegetation cover occurs between April and May and that there is strong variability for all the sites, especially in the Cajones wetland, during the December-May period. The area covered by vegetation obtained with the Sentinel-2 images is consistent with the historical average variation curves (1986-2017) obtained by LANDSAT images. Nevertheless, the values obtained from Sentinel and LANDSAT products are not directly comparable because the latter are less accurate.

Potential evapotranspiration was estimated using the FAO Penman-Monteith method, and for the study period varies between ~ 0 and 5.72 mm/day on 14 June and 10 November respectively. As expected, ET_o increases as the summer approaches. Additionally, actual evapotranspiration was estimated at an annual time scale using the Groeneveld et al. (2007) method.

The highest annual $ET_{a,NDVI}$ values were observed in the Cajones wetland (705 mm/year), while the lowest ones were observed in the Quebrada Negra wetland (631 mm/year). The estimated $ET_{a,NDVI}$ in the Orientales wetland was estimated to be 702 mm/year. Additionally, the mean water flow due to evapotranspiration was estimated to be 0.7 L/s in the Quebrada Negra wetland, 0.6 L/s in the Cajones wetland and 2.3 L/s in the Orientales wetland. The highest water loss to the atmosphere observed in the Orientales wetland is due to its greater area of active vegetation, which is approximately three times the area of the Cajones and Quebrada Negra wetlands during summer.

The sensitivity of the Groeneveld et al. (2007) method to the selection of the mid-summer NDVI (peak season NDVI) was analyzed. Using seven satellite images as potential mid-summer NDVI map, the ET_a standard deviation for all three wetlands was of the order of ~ 20 mm/year. Additionally, Groeneveld et al. (2007) showed that their method has residual errors that decrease as measured ET_a increases, with error values on the order of 3.5 – 16.9 % for $ET_{a,NDVI}$ estimates of the same magnitude as the ones obtained in this study.

High content of organic material was found in the two pits excavated in the Quebrada Negra wetland. For this reason, particle distribution tests could not be performed for all the obtained samples. A very dense root system, sands and fine soils were found above a depth of two metres, compared to deeper samples. Also, it was observed that the soil gets coarser with depth.

The soil hydraulic conductivity results obtained from the falling head permeameter are in general low (between 4.0×10^{-3} and 8.4×10^{-2} m/day), with values that are typical of semi-pervious soils. In general, these results agree with the soil saturated hydraulic conductivity measured with the slug tests. Although there is a general agreement, some

slug tests results show hydraulic conductivity values that are characteristic of impermeable soils in the main grassland. Despite the fact that measured hydraulic conductivities show that the soil is semi-pervious to impervious, during the excavation of the pits, they needed to be constantly drained, because the water level kept rising as the excavation proceeded.

In the wetland as a whole, there are areas of upwelling at the upslope and downslope boundaries, and there is evidence of spring flow emergence from the adjacent (Northern and Southern) hillslopes. However, for the main grassland, the vertical hydraulic gradient is mostly close to zero and dominated by positive gradients (downwelling). Also, there is a groundwater gradient in a longitudinal direction down the Quebrada Negra ravine towards the Silala ravine. Therefore, the evidence suggests a subsurface flow that mainly follows the topography, with a small downwards component. Nevertheless, some locations with positive gradients (downwelling) coincide with the zones where small ponds and surface flows are observed and where the highest measured hydraulic conductivities were reported. Additionally, it was observed that the zones where an appearance of surface water is identified coincide with the presence of dense Tussock grasses.

The overall picture that emerges from observed groundwater levels in the Quebrada Negra wetland is one of complexity of groundwater flow paths and strong spatial heterogeneity. The wetland exists because it is fed by groundwater, but over much of the wetland, hydraulic gradients show conditions that promote downwelling, rather than upwelling. The springs that feed the wetland emerge at the edges of the wetland (in particular at the southern lateral boundary, as well as the upslope ravine), and within the main wetland there are isolated locations where spring emergence occurs. Within the main wetland there are distinct channels and perennial flows, which then return subsurface, to flow as groundwater down the ravine towards the main Silala River.

7. REFERENCES

- Alcayaga, H., 2017. *Characterization of the Drainage Patterns and River Network of the Silala River and Preliminary Assessment of Vegetation Dynamics Using Remote Sensing. (Chile's Memorial, Vol. 4, Annex I).*
- Allen, R.G., Pereira, L.S., Raes, D. and Smith, M., 1998. Crop Evapotranspiration-Guidelines for Computing Crop Water Requirements. *FAO Irrigation and Drainage, Paper 56.*
- ASTM, 2007. *Standard Test Method for Particle-Size Analysis of Soils D422-63.* ASTM International, West Conshohocken, Pennsylvania.
- ASTM, 2015. *Standard Practice for Thin-Walled Tube Sampling of Fine-Grained Soils for Geotechnical Purposes D1587M-15.* ASTM International, West Conshohocken, Pennsylvania.
- Bear, J., 1988. *Dynamics of Fluids in Porous Media. Dover Civil and Mechanical Engineering Series.* Dover, New York, pp. 800.
- Butler, J.J., 1997. *The design, performance, and analysis of slug tests.* Lewis Publishers, Boca Raton, Florida, pp. 262.
- Chavez, P., 1996. Image-Based Atmospheric Corrections - Revisited and Improved Photogrammetric Engineering and Remote Sensing. *American Society of Photogrammetry*, 62, 1025- 1036.
- Congedo, L., 2018. *Semi-Automatic Classification Plugin Documentation.* Technical Report. Release 6.0.1.1. Available at: <http://dx.doi.org/10.13140/RG.2.2.29474.02242/1>
- Cooper, H.H., Bredehoeft, J.D. and Papadopoulos, I.S., 1967. Response of a Finite-Diameter Well to an Instantaneous Charge of Water. *Water Resources Research*, 3(1), 263-269, doi:10.1029/WR003i001p00263.
- Fetter, C.W., 1994. *Applied Hydrogeology*, Third Edition, Macmillan College Publishing Company, United States.
- Garcia, M., Raes, D., Allen, R. and Herbas, C., 2004. Dynamics of reference evapotranspiration in the Bolivian Highlands (Altiplano). *Agricultural and Forest Meteorology*, 125(1), 67-82.
- Gorelick, N., Hancher, M., Dixon, M., Ilyushchenko, S., Thau, D. and Moore, R., 2017. Google Earth Engine: Planetary-scale geospatial analysis for everyone. *Remote Sensing Environment*, 202, 18-27.

Groeneveld, D.P. and Baugh, W.M., 2007. Correcting satellite data to detect vegetation signal for eco-hydrologic analyses. *Journal of Hydrology*, 344, 135-145 doi:10.1016/j.hydrol.2007.07.001.

Groeneveld, D.P., Baugh, W.M., Sanderson, J.S. and Cooper, D.J., 2007. Annual groundwater evapotranspiration mapped from single satellite scenes. *Journal of Hydrology*, 344, 146-156.

Hall, D.K., Riggs, G.A. and Salomonson, V.V., 2006. *MODIS/Terra Snow Cover 5-Min L2 Swath 500m. Version 5*. NASA National Snow and Ice Data Center Distributed Active Archive Center. Boulder, Colorado, USA.

Head, K. and Epps, R., 2011. *Manual of Soil Laboratory Testing. Volume II: Permeability, Shear Strength and Compressibility Tests*. Third Edition. Whittles Publishing. Scotland, UK.

Herrera, C. and Aravena, R., 2019(a). *Chemical and isotopic characterization of surface water and groundwater of the Silala River transboundary basin, Second Region, Chile. (Chile's Reply, Vol. 3, Annex XI)*.

Herrera, C. and Aravena, R., 2019(b). *Chemical characterization of surface water and groundwater of the Quebrada Negra, Second Region, Chile. (Chile's Reply, Vol. 3, Annex XII)*.

Hutchinson, M., Xu, T. and Stein, J., 2011. Recent Progress in the ANUDEM Elevation Gridding Procedure. In T. Hengel, I. Evans, J. Wilson, and M. Gould (Ed.). *Geomorphometry*, 2011, 19-22. Available at: <http://geomorphometry.org/HutchinsonXu2011>.

Hyder, Z., Butler Jr., J., McElwee, C. and Liu, W., 1994. Slug tests in partially penetrating wells. *Water Resources Research*, 30 (11), 2945-2957.

NTT DATA, and RESTEC, 2014. AW3D Standard DTM. Available at <http://aw3d.jp/en/>.

Roy, D., Kovalskyy, V., Zhang, H., Vermote, E., Yan, L., Kumar, S. and Egorov, A., 2016. Characterization of Landsat-7 to Landsat-8 reflective wavelength and normalized difference vegetation index continuity. *Remote Sensing Environment*, 185, 57-70.

Samtani, N.C. and Nowatzki, E.A., 2006. Soils and Foundations. Reference Manual – Volume I. *National Highway Institute, US Department of Transportation, Federal Highway Administration*. Publication No. FHWA NHI-06-088.

- Sellers, P.J., Berry, J.A., Collatz, G.J., Field, C.B. and Hall, F.G., 1992. Canopy reflectance, photosynthesis and transpiration. III A reanalysis using improved leaf models and new canopy integration scheme. *International Journal of Remote Sensing*, 42, 187-216.
- Sproles, E., Crumley, R., Nolin, A., Mar, E. and Lopez Moreno, J., 2018. SnowCloudHydro-A new framework for forecasting streamflow in snowy, data-scarce regions. *Remote Sensing*, 10(8), 1276, doi:10.3390/rs10081276.
- Summer, D.M. and Jacobs, J.M., 2005. Utility of Penman–Monteith, Priestley–Taylor, reference evapotranspiration, and pan evaporation methods to estimate pasture evapotranspiration. *Journal of Hydrology*, 308(1), 81-104.
- Tucker, C.J. and Sellers, P.J., 1986. Satellite remote sensing of primary production. *International Journal of Remote Sensing*, 7, 1395-1416.
- WMO, 2014. *Guide to Meteorological Instruments and Methods of Observation*. World Meteorological Organization, Geneva, Switzerland. Available at: https://library.wmo.int/index.php?lvl=notice_display&id=12407.
- Yoder, R.E., Odhiambo, L.O. and Wright, W.C., 2005. Evaluation of methods for estimating daily references crop evapotranspiration at a site in the humid southeast United States. *Applied Engineering in Agriculture*, 21, 197-202.
- Zhu, Z., Wang, S. and Woodcock, C. E., 2015. Improvement and expansion of the Fmask algorithm: cloud, cloud shadow, and snow detection for Landsats 4–7, 8, and Sentinel 2 images. *Remote Sensing Environment*, 159, 269-277.

APPENDIX A
PICTURES OF THE PITS

A-1 P1 middle of the stream





A-2 P2 downstream



APPENDIX B

SOIL SAMPLES FOR PEAT DEPTH DETERMINATION

Soil samples taken at the Quebrada Negra wetland for later particle distribution analysis in the laboratory are presented below. The first 30 to 190 cm deep are in the body of this report (see Figure 4-11).

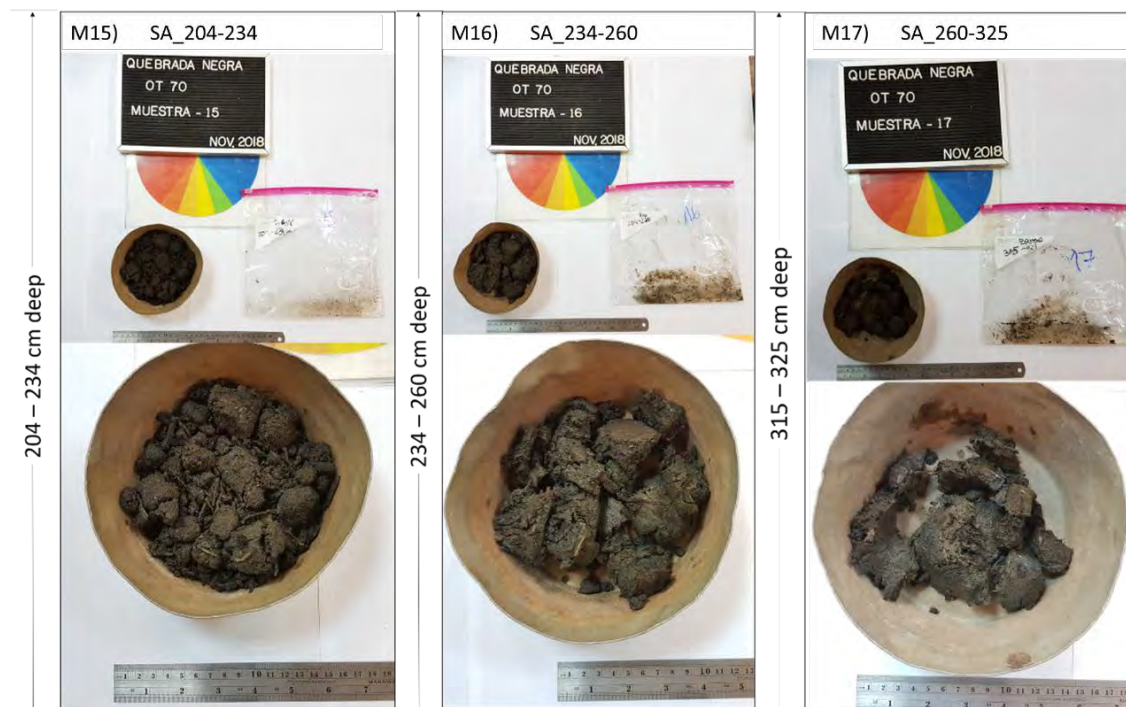


Figure B-1. Soil samples between 204 and 325 cm deep in the Quebrada Negra wetland for peat characterization.

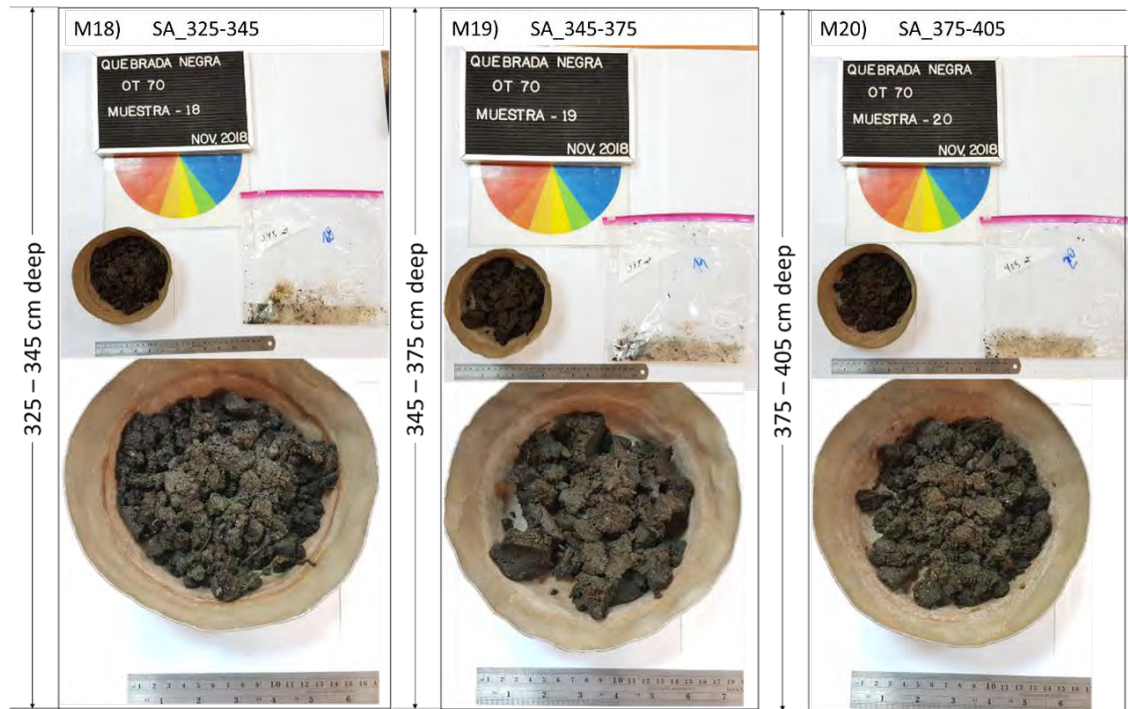


Figure B-2. Soil samples between 325 and 405 cm deep in the Quebrada Negra wetland for peat characterization.

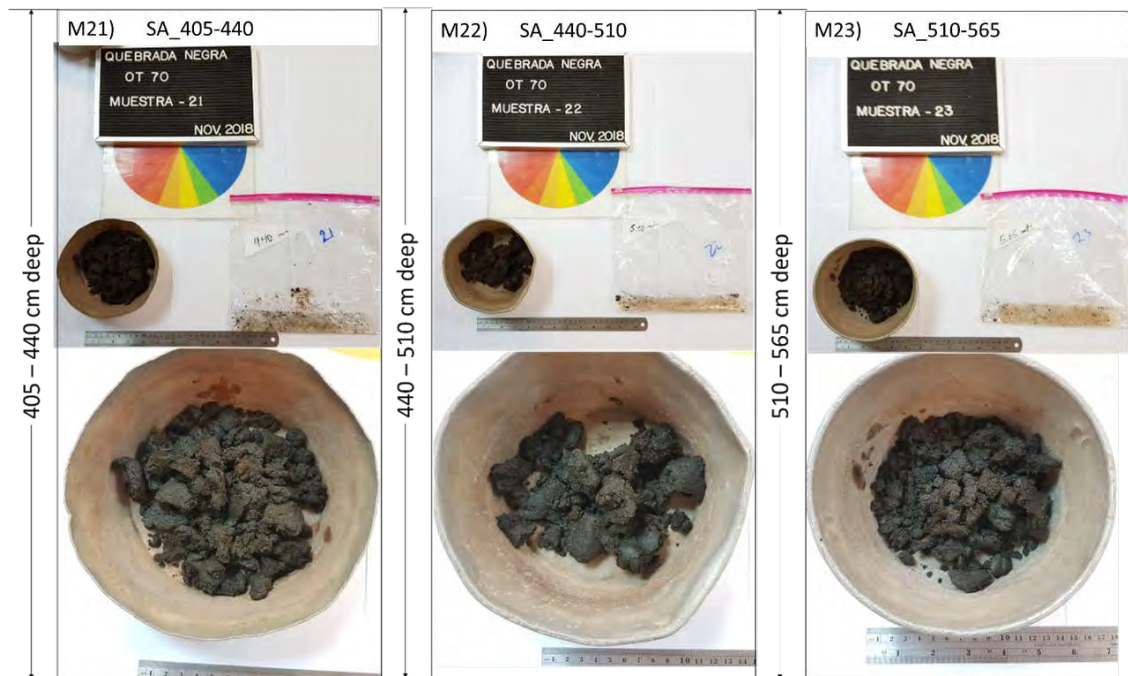


Figure B-3. Soil samples between 405 and 565 cm deep in the Quebrada Negra wetland for peat characterization.

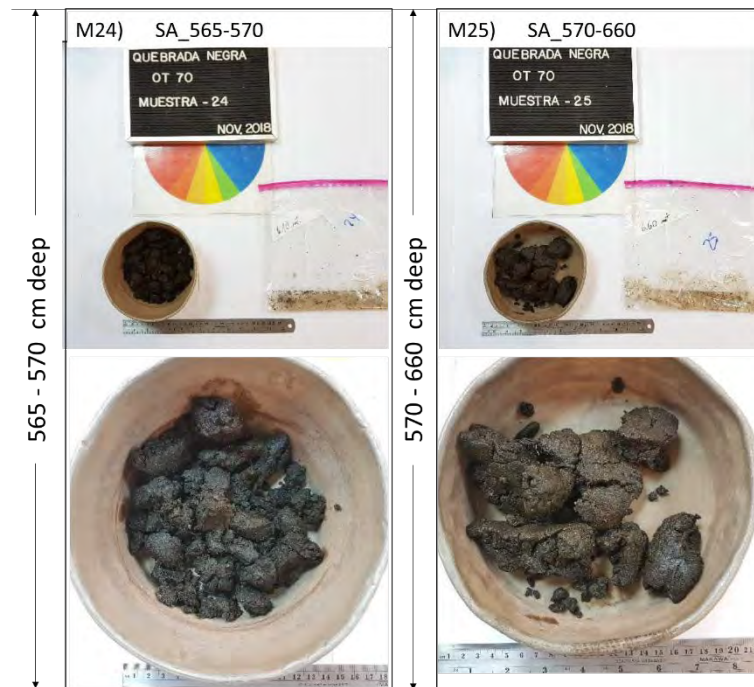


Figure B-4. Soil samples between 565 and 660 cm deep in the Quebrada Negra wetland for peat characterization.

Some pictures of the material extracted with the soil auger are shown below (from 0 to 260 centimetres depth).

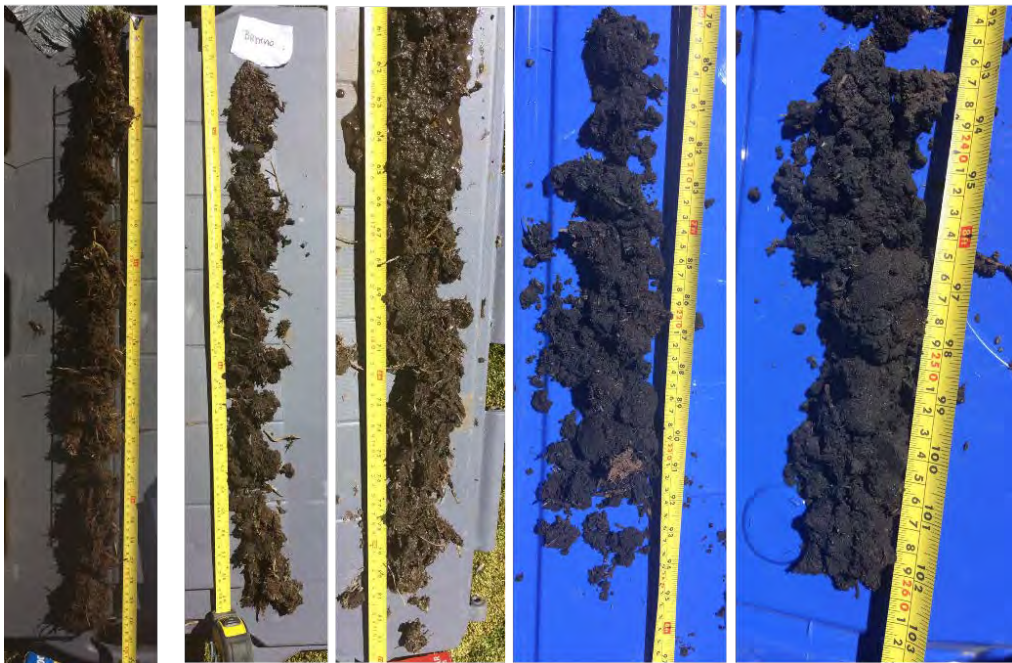


Figure B-5. Pictures of the material extracted with the soil auger (from 0 to 260 cm depth).

APPENDIX C

DESCRIPTION OF SOIL SAMPLES COLLECTION FOR K_s ANALYSIS AT PITS P1 AND P2

Tables C-1 and C-2 give more details about the performance of soil samples collection with the Shelby tubes at pit P1 and pit P2, respectively.

Sample	Date	Tube insertion (min:sec)	Waiting (min:sec)	period
P1_S50_V**	22/11/2018	1:00*	6:00	
P1_S50_H***	23/11/2018	0:30	6:00	
P1_S150_V**	23/11/2018	0:10	5:30	
P1_S150_H**	23/11/2018	1:52	5:10	

* *the use of a sledge hammer was required to insert the tube into the ground.*

** *sampling was repeated 2 times.*

*** *sampling was repeated 3 times.*

Table C-1. Undisturbed soil sampling in pit P1 at the Quebrada Negra wetland.

Sample	Date	Tube insertion (min:sec)	Waiting (min:sec)	period
P2_S50_V	22/11/2018	2:45*	5:36	
P2_S50_H	22/11/2018	4:12*	8:15	
P2_S150_V	22/11/2018	2:45*	5:15	
P2_S150_H***	22/11/2018	0:15	5:00	

* *the use of a sledge hammer was required to insert the tube into the ground.*

*** *sampling was repeated 3 times.*

Table C-2. Undisturbed soil sampling in pit P2 at the Quebrada Negra wetland.

APPENDIX D
USCS SOIL CLASSIFICATION CHART

Criteria for Assigning Group Symbols and Group Names Using Laboratory Tests ^a			Soil Classification	
COARSE-GRAINED SOILS (Sands and Gravels) - more than 50% retained on No. 200 (0.075 mm) sieve FINE-GRAINED (Silts and Clays) - 50% or more passes the No. 200 (0.075 mm) sieve			Group Symbol	Group Name ^b
GRAVELS More than 50% of coarse Fraction retained on No. 4 Sieve	CLEAN GRAVELS	$C_u \geq 4$ and $1 \leq C_c \leq 3^e$	GW	Well-graded gravel ^f
	< 5% fines	$C_u < 4$ and/or $1 > C_c > 3^e$	GP	Poorly-graded gravel ^f
	GRAVELS WITH FINES > 12% of fines ^e	Fines classify as ML or MH	GM	Silty gravel ^{f,g,h}
		Fines classify as CL or CH	GC	Clayey gravel ^{f,g,h}
SANDS 50% or more of coarse fraction passes No. 4 Sieve	CLEAN SANDS	$C_u \geq 6$ and $1 \leq C_c \leq 3^e$	SW	Well-graded Sand ^f
	< 5% fines ^d	$C_u < 6$ and/or $1 > C_c > 3^e$	SP	Poorly-graded sand ^f
	SANDS WITH FINES > 12% fines ^d	Fines classify as ML or MH	SM	Silty sand ^{g,h,i}
		Fines classify as CL or CH	SC	Clayey sand ^{g,h,i}
SILTS AND CLAYS Liquid limit less than 50	Inorganic	$PI > 7$ and plots on or above "A" line ^j	CL	Lean clay ^{k,l,m}
		$PI < 4$ or plots below "A" line ^j	ML	Silt ^{k,l,m}
	Organic	$\frac{\text{Liquid limit - overdried}}{\text{Liquid limit - not dried}} < 0.75$	OL	Organic clay ^{k,l,m,n} Organic silt ^{k,l,m,o}
SILTS AND CLAYS Liquid limit 50 or more	Inorganic	PI plots on or above "A" line	CH	Fat clay ^{k,l,m}
		PI plots below "A" line	MH	Elastic silt ^{k,l,m}
	Organic	$\frac{\text{Liquid limit - oven dried}}{\text{Liquid limit - not dried}} < 0.75$	OH	Organic clay ^{k,l,m,p} Organic silt ^{k,l,m,q}
Highly fibrous organic soils	Primary organic matter, dark in color, and organic odor		Pt	Peat

Table D-1. Soil classification chart (Samtani and Nowatzki, 2006).

NOTES:	
a	Based on the material passing the 3 in (75 mm) sieve.
b	If field sample contained cobbles and/or boulders, add “with cobbles and/or boulders” to group name.
c	Gravels with 5 to 12% fines require dual symbols: GW-GM, well-graded gravel with silt GW-GC, well-graded gravel with clay GP-GM, poorly graded gravel with silt GP-GC, poorly graded gravel with clay
d	Sands with 5 to 12% fines require dual symbols: SW-SM, well-graded sand with silt SW-SC, well-graded sand with clay SP-SM, poorly graded sand with silt SP-SC, poorly graded sand with clay
e	$C_u = \frac{D_{60}}{D_{10}} \quad C_c = \frac{(D_{30})^2}{(D_{10})(D_{60})}$ [C _u : Uniformity Coefficient; C _c : Coefficient of Curvature]
f	If soil contains ≥ 15% sand, add “with sand” to group name.
g	If fines classify as CL-ML, use dual symbol GC-GM, SC-SM.
h	If fines are organic, add “with organic fines” to group name.
i	If soil contains ≥ 15% gravel, add “with gravel” to group name.
j	If the liquid limit and plasticity index plot in hatched area on plasticity chart, soil is a CL-ML, silty clay.
k	If soil contains 15 to 29% plus No. 200 (0.075 mm), add “with sand” or “with gravel,” whichever is predominant.
l	If soil contains ≥ 30% plus No. 200 (0.075mm), predominantly sand, add “sandy” to group name.
m	If soil contains ≥ 30% plus No. 200 (0.075 mm), predominantly gravel, add “gravelly” to group name.
n	PI ≥ 4 and plots on or above “A” line.
o	PI < 4 or plots below “A” line.
p	PI plots on or above “A” line.
q	PI plots below “A” line.

Table D-1 (continued). Soil classification chart (Samtani and Nowatzki, 2006).

Annex XIV

SERNAGEOMIN (National Geology and Mining Service),
2019. *Geology of the Silala River Basin: An Updated
Interpretation*



**GEOLOGY OF THE SILALA RIVER BASIN: AN UPDATED
INTERPRETATION**

Edmundo Polanco (DSc)

Project Geologist of the Regional Geology Unit of the Department of Basic
Geology

January 2019

GLOSSARY

This glossary of geologic terms is based on the glossary in *Earth: An Introduction to Geologic Change*, by S. Judson and S.M. Richardson (Englewood Cliffs, NJ, Prentice Hall, 1995) and *The Encyclopedia of Volcanoes*, by H. Sigurdsson (editor) (Academic Press, USA, 2015). Where possible, definitions conform generally, and in some cases specifically, to definitions given in Robert L. Bates and Julia A. Jackson (editors), *Glossary of Geology*, 3rd ed., American Geological Institute, Alexandria, Virginia, 1987.

$^{39}\text{Ar}/^{40}\text{Ar}$ method: A different method that was invented to supersede K/Ar method, to be more accurate.

$^{40}\text{K}/^{40}\text{Ar}$ method: A method used for the dating of potassium-bearing rocks by using the ratio of radioactive ^{40}K to its daughter, ^{40}Ar .

Absolute time: Geologic time expressed in years before the present.

Amphibole: Any of a large group of minerals composed of a silicate joined to various metals, such as calcium, magnesium, iron, or sodium. Hornblende is a mineral of the amphibole group.

Andesite: A fine-grained volcanic rock of intermediate composition, consisting largely of plagioclase and one or more mafic minerals.

Aquifer: Geological formation capable of storing, transmitting and yielding exploitable quantities of water.

Autobreccia: Clastic aggregate generated as a by-product of lava flowage.

Autoclastic facies: Clastic facies generated by nonexplosive fragmentation accompanying lava effusion and flowage. Autobreccia and hyaloclastite are the two most common kinds of autoclastic facies.

Bedding: A collective term used to signify presence of beds, or layers, in sedimentary rocks and deposits.

Bedding plane: Surface separating layers of sedimentary rocks and deposits. Each bedding plane marks termination of one deposit and beginning of another of different character, such as a surface separating a sandstone bed from an overlying mudstone bed. Rock tends to break or separate readily along bedding planes.

Bedrock: Any solid rock exposed at the Earth's surface or overlain by unconsolidated material.

Breccia: A clastic rock in which the gravel-sized particles are angular in shape and make up an appreciable volume of the rock.

Biotite: Dark mica, $K(Mg,Fe)_3AlSi_3O_{10}(F,OH)_2$, a common silicate mineral. It is brown to black with shiny surfaces, and like all micas, it splits into very thin flakes along its one perfect cleavage.

Clastic: Refers to rock or sediments made up primarily of broken fragments of pre-existing rocks or minerals.

Crater: 1. A steep-walled, usually conical depression at the summit or on the flanks of a volcano, resulting from the explosive ejection of material from a vent. 2. A bowl-shaped depression with a raised, overturned rim produced by the impact of a meteorite or other energetic projectile.

Crystal: The multi-sided form of a mineral, bounded by planar growth surfaces, that is the outward expression of the ordered arrangement of atoms within it.

Dacite: An extrusive igneous rock type or magma of intermediate silica content falling between that of andesite and rhyolite; typically contains phenocrysts of potassium feldspar and plagioclase feldspar, and may contain quartz, biotite, and hornblende.

Debris flow: Fast-moving, turbulent mass movement with a high content of both water and rock debris. The more rapid debris flows rival the speed of rock slides.

Dome: An uplift or anticlinal structure, roughly circular in its outcrop exposure, in which beds dip gently away from the center in all directions.

Extrusive: Pertaining to igneous rocks or features formed from lava released on the Earth's surface.

Foot wall block: The body of rock that lies below an inclined fault plane.

Glassy: A texture of extrusive igneous rocks that develops as the result of rapid cooling, so that crystallization is inhibited.

Hanging wall block: The body of rock that lies above an inclined fault plane.

Igneous rock: A rock that has crystallized from a molten state.

Ignimbrite: Pyroclastic density current deposit composed of variable proportions of pumice, ash, and lithic clasts usually used for deposits formed during large explosive eruptions.

Lava: Molten rock that flows at the Earth's surface.

Lava dome: A steep-sided rounded extrusion of highly viscous lava squeezed out from a volcano and forming a dome-shaped or bulbous mass above and around the volcanic vent. The structure generally develops inside a volcanic crater.

Magma: Molten rock, containing dissolved gases and suspended solid particles. At the Earth's surface, magma is known as lava.

Mineral: A naturally occurring inorganic solid that has a well-defined chemical composition and in which atoms are arranged in an ordered fashion.

Normal fault: A geological fault where the hanging wall block has moved downwards relative to the foot wall block.

Pyroclastic: Pertaining to clastic material formed by volcanic explosion or aerial expulsion from a volcanic vent.

Pyroclastic flow: A dense, hot (sometimes incandescent) cloud of volcanic ash and gas produced in a Pelean eruption.

Reverse fault: A dip-slip fault on which the hanging wall block is offset upward relative to the foot wall block.

Rhyolite: A fine-grained silica-rich igneous rock, the extrusive equivalent of granite.

Rift (graben): A valley caused by extension of the Earth's crust. Its floor forms as a portion of the crust moves downward along normal faults.

Rock: An aggregate of one or more minerals in varying proportions.

Sedimentary rock: Rock formed from the accumulation of sediment, which may consist of fragments and mineral grains of varying sizes from pre-existing rocks, remains or products of animals and plants, the products of chemical action, or mixtures of these.

Silica: Silicon dioxide (SiO_2) as a pure crystalline substance makes up quartz and related forms such as flint and chalcedony. More generally, silica is the basic chemical constituent common to all silicate minerals and magmas.

Stratovolcano (composite volcano): A volcano that is composed of alternating layers of lava and pyroclastic material, along with abundant dikes and sills. Viscous, intermediate lava may flow from a central vent. Example: Mt. Fuji in Japan.

Terrace: A relatively flat surface along a valley, with a steep bank separating it either from the floodplain, or from a lower terrace.

Texture: The general appearance of a rock as shown by the size, shape, and arrangement of the materials composing it.

Tuff: A general term for all consolidated pyroclastic rock. Not to be confused with tufa.

Vesicle: A cavity in a lava, formed by the entrapment of a gas bubble during solidification of the lava.

Vesicular: A textural term applied to an igneous rock containing abundant vesicles, formed by the expansion of gases initially dissolved in the lava.

Volcanic ash: The dust-sized, sharp-edged, glassy particles resulting from an explosive volcanic eruption.

Volcanic breccia: Clastic aggregate composed predominantly of angular volcanic clasts.

Volcano: A vent in the surface of the Earth, from which lava, ash, and gases erupt, forming a structure that is roughly conical.

Welded tuff: A pyroclastic rock in which glassy clasts have been fused by the combination of the heat retained by the clasts, the weight of overlying material, and hot gases.

TABLE OF CONTENTS

1. INTRODUCTION.....	1
1.1. Context.....	1
1.2. Location of the study area.....	2
1.3. Regional geology.....	4
2. STRATIGRAPHY IN CHILE	5
3. INTERPRETATION AND MAPPING OF THE GEOLOGY OF THE ESTIMATED GROUNDWATER CATCHMENT IN BOLIVIA AND CHILE	9
4. EROSION AND DEPOSITION IN THE SILALA PALAEO-VALLEY	13
5. STRUCTURAL EVOLUTION.....	14
6. INACALIRI-APAGADO VOLCANIC CHAIN	18
7. SUMMARY AND CONCLUSIONS.....	19
8. REFERENCES	20
APPENDIX A	
APPENDIX B	
APPENDIX C	
APPENDIX D	

1. INTRODUCTION

1.1. Context

In 2017 Servicio Nacional de Geología y Minería (SERNAGEOMIN) remapped the Chilean area included in the topographic catchment of the Silala River (see Figure 1). This work was requested by the Dirección Nacional de Fronteras y Límites (DIFROL) of the Ministry of Foreign Affairs, Mrs. Ximena Fuentes, and involved the production of a report on the geological evolution of the Silala River basin (SERNAGEOMIN, 2017).

Over the period 2017 to 2018 a significant number of further geological investigations of the Silala topographic basin have been carried out, which have enabled a better understanding of the geology of the area. Additional information has been gained from re-examination of drill cuttings, new radiometric dates, re-interpretation of geophysical data, and further fieldwork, together with examination of several reports recently made available that were cited in support of the Bolivian Counter-Memorial (BCM) in the dispute before the International Court of Justice over the status and the use of the waters of the Silala (Chile v. Bolivia). These reports were unavailable before November 2018 and have enabled comparisons between information gained by Servicio Nacional de Geología y Minería (SERNAGEOMIN) in Bolivia and that gained by SERNAGEOMIN in Chile.

In the light of this evolution of knowledge, the DIFROL requested an updated report on the geology of the transboundary basin of the Silala River, including the review of the geology of an extended groundwater catchment area in Bolivia, which would be aimed at deepening the hydrogeological knowledge of this basin.

This report was elaborated under the supervision and instruction of Professors Denis Peach and Howard Wheeler.

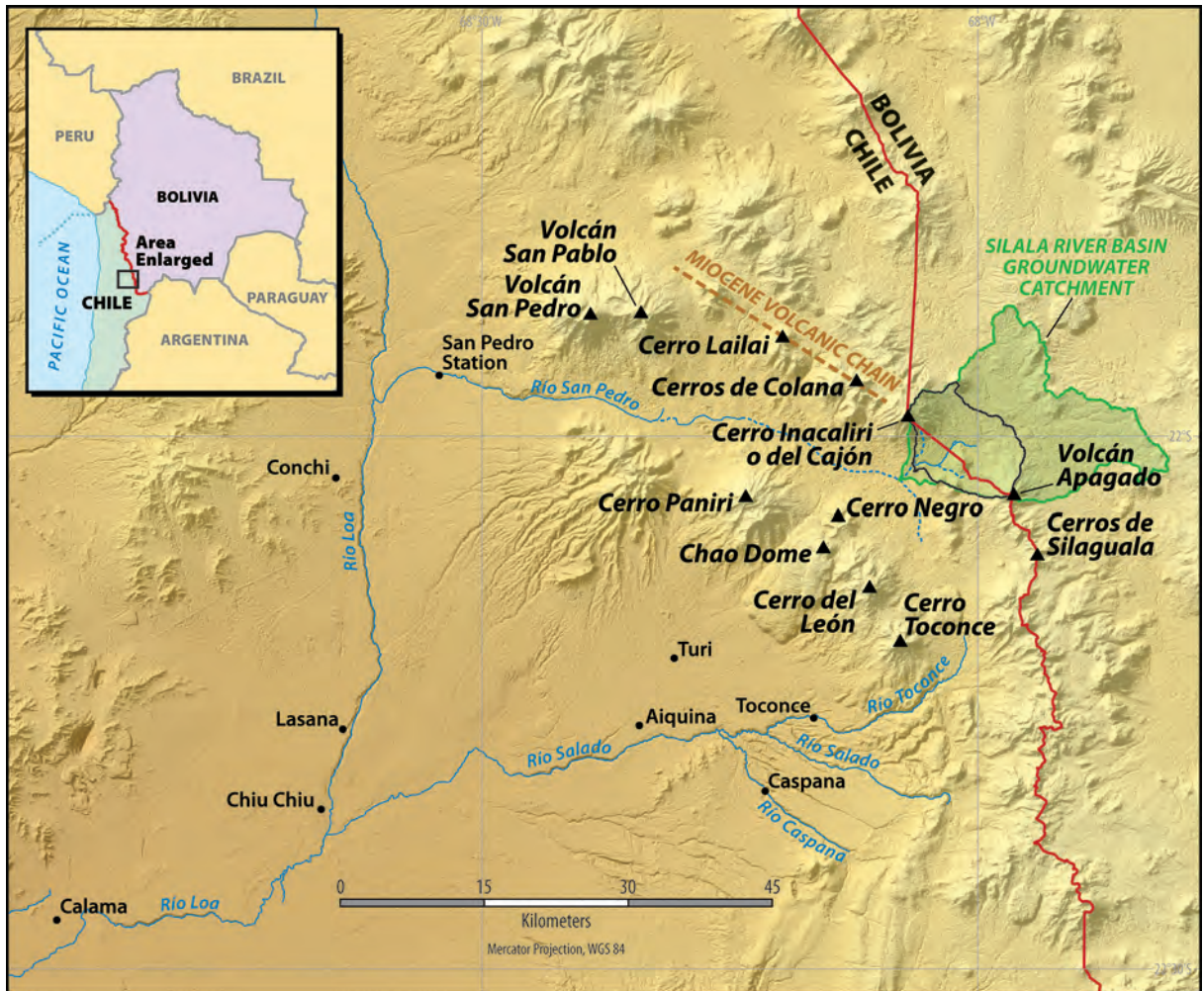


Figure 1. Location of study area, showing the Silala River basin (outlined in black) and the extended groundwater catchment (shown in green). The international border between Chile and Bolivia is shown in red.

1.2. Location of the study area

The Silala River basin is located in the volcanic arc of the high Andean Mountain Range in the Second Region of Chile (Antofagasta Region) and the Department of Potosí of Bolivia, approximately 100 km NE from the city of Calama (Figure 1). In particular, the Silala River basin crosses the border between Chile and Bolivia.

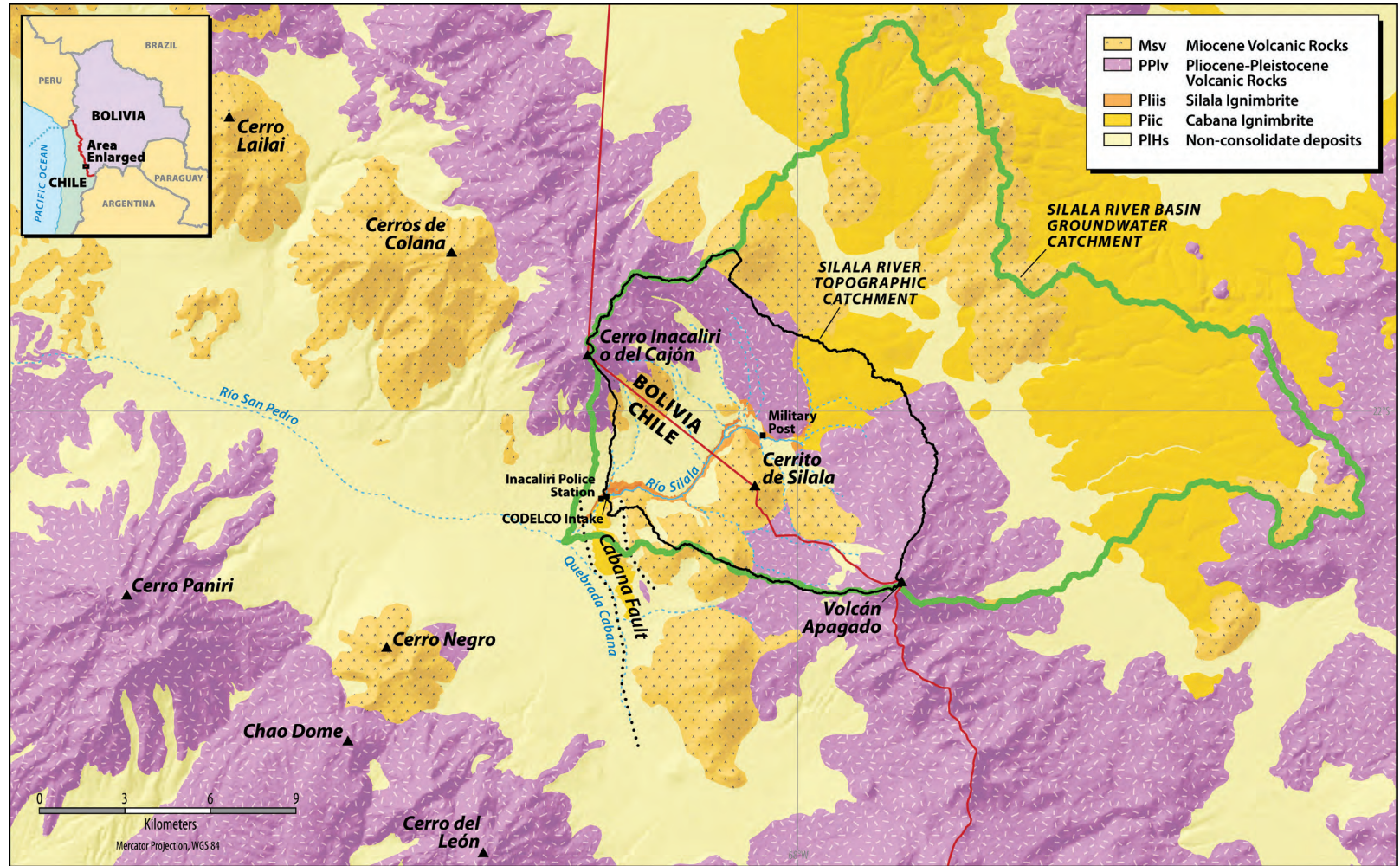


Figure 2. Synthesis of geology for the region in which the Silala River basin is located. Solid black line corresponds to the topographic catchment area of the Silala River and solid green line is the Silala River basin groundwater catchment.

1.3. Regional geology

The regional geology is shown in Figure 2. The oldest rocks that are exposed in the region are sequences of ignimbrites whose volume is considerable. These are chemically evolved rocks (dacites and rhyolites) that filled depressions and valleys in the existing relief. The radiometric ages found for these rocks indicate that at least two similar geological events took place in the region, their ages being 10.71 Ma (Lower Río San Pedro Ignimbrite: Ar/Ar in biotite; Salisbury et al., 2011) and 8.33 Ma (Sifón Ignimbrite: average Ar/Ar; Salisbury et al., 2011). These dated rocks represent part of a series of voluminous and extensive volcanic events that affected this part of the Highland region (Altiplano) (Salisbury et al., 2011). These ignimbrites form the oldest geological rocks in the Silala River basin area (labelled undifferentiated basement in Figure 4, SERNAGEOMIN, 2017). Ignimbrites are deposited from explosive volcanic eruptions. These volcanoes extrude a mix of volcanic gases, molten rock and ash in a highly fluid pyroclastic flow. They flow under gravity at speeds of at least 100 km/hour and are very destructive (Wilson and Houghton, 2000).

From 6.2 Ma (Polanco, 2012) several stratovolcanoes formed on the ignimbrite bedrock from underlying magma chambers. These have intermediate to more evolved compositions (andesites and dacites) that have been identified in the north of the basin, forming a volcanic chain spanning more than 30 km in a NW-SE direction (Cerro Lailai, Cerros de Colana and Cerro Inacaliri o del Cajón (henceforth Cerro Inacaliri): 5.4-5.8 Ma; K-Ar in total rock; Rivera et al., 2015), as well as in the South as an isolated volcano (Cerro Negro dated to 6.2 Ma; Polanco, 2012) (Figure 2). The volcanic products associated with these eruptive centers are mainly lava flows and domes and are referred to as Volcanic Sequences of the Upper Miocene/Pliocene.

Subsequently, at 4.12 Ma (U-Pb in zircon), the Cabana Ignimbrite was deposited in the Altiplano. This was a voluminous and highly evolved deposit and filled much of the pre-existing topography. Volcanic activity continued to develop several eruption centers located SW of the Quebrada Negra (see Figure 4), giving rise to the Volcanic Sequences of the Upper Pliocene (2.6 Ma) and the Inacaliri volcano (Cerro Inacaliri) (1.48 Ma), including Volcanic Sequences of the lower Pleistocene, and, in the south, an intense and episodic volcanism began along the volcanic chain called Paniri-Toconce, which is over 20 km long and also is aligned in a NW-SE (N130°E) direction (Polanco, 2012), the most recent activity of which corresponds to a lava flow from the Paniri Volcano (150 ka; Polanco, 2012) (Figure 2).

Lastly, the most recent volcanic activity in the area corresponds to pyroclastic fall deposits (630 ka; Blanco and Polanco, 2018) that resulted from an eruption of the Chao Dome (see Figure 2).

2. STRATIGRAPHY IN CHILE

The interpretation of the geology of the area of the Silala River made in SERNAGEOMIN 2017, with information then available, recognized four main volcanic lithological units. Further mapping, field observation and radiometric dating of dacitic lavas found outcropping in the Silala ravine downstream of the Quebrada Negra have led to the inclusion of a fifth lithological unit (Volcanic Sequences of the Upper Pliocene) in the stratigraphy of the Silala River basin in Chile. The radiometric age determinations that have been used to help construct the stratigraphy are listed in Table 1.

Sample	UTM N	UTME	Method	Material	Age (Ma)	Unit	Reference
RSP12t	7.563.439	596.708	Ar/Ar	biotite	630±310 ka**	Pyroclastic fall deposit	Blanco and Polanco, 2018
No inf.	No inf.	No inf.	K-Ar	biotite	1.48±0.02*	Volcanic sequences of the Lower Pleistocene	Almendras et al., 2002
AL-197	7.566.976	594.878	Ar/Ar	groundmass	1.612±0.018	Volcanic sequences of the Lower Pleistocene	Sellés and Gardeweg, 2017
RSP16d	7.563.146	595.801	Ar-Ar	plagioclase	1.61±0.08*	Silala Ignimbrite	Blanco and Polanco, 2018
No inf.	No inf.	No inf.	K-Ar	biotite	1.74±0.02*	Nlsg-Volcanic sequences of the Lower Pleistocene	SERGEOMIN, 2003
RSP13D	7.563.561	596.648	K-Ar	groundmass	2.6±0.4	Volcanic sequences of the Upper Pliocene	SERNAGEOMIN, 2017
No inf.	No inf.	No inf.	K-Ar	biotite	3.2±0.4*	Ntpg-Ignimbrites Silala (Bolivian)	SERGEOMIN, 2017
RSP14D	7.563.554	596.534	U-Pb	zircon	4.12±0.08	Cabana Ignimbrite	SERNAGEOMIN, 2017
No inf.	No inf.	No inf.	K-Ar	biotite	5.84±0.09*	MPv2-Volcanic sequences of the Upper Miocene	Almendras et al., 2002
No inf.	No inf.	No inf.	K-Ar	biotite	5.8±0.4*	MPv2-Volcanic sequences of the Upper Miocene	Almendras et al., 2002
No inf.	No inf.	No inf.	K-Ar	biotite	6.04±0.07*	Volcanic sequences of the Upper Miocene	SERGEOMIN, 2003
RSP50d	7.563.302	600.110	U-Pb	zircon	6.63±0.06*	Volcanic sequences of the Upper Miocene	Blanco and Polanco, 2018
No inf.	No inf.	No inf.	K-Ar	biotite	6.6±0.5*	Nis-3-Silala Ignimbrites (Bolivian)	SERGEOMIN, 2017
No inf.	No inf.	No inf.	K-Ar	biotite	7.8±0.3*	MPv1-Silala Ignimbrites (Bolivian)	Ríos et al., 1997

*Table 1. Compilation of the radiometric ages available of the Silala River area. * Ages from Ríos et al., (1997); Almendras et al., (2002); SERGEOMIN, (2003 and 2017). ** The age reports are in the Appendix B.*

The lithological units are presented in Figure 3 in order of the age of deposition, the youngest being at the top. The bedrock lithologies and stratigraphic relationships are also described below.

Volcanic Sequences from the Upper Miocene-Pliocene (MsPvd) ca 6.6 – 5.8 Ma

At this time a series of volcanic rocks including domes, lava domes, lava flows and autoclastic breccia were emplaced. Their composition is mostly dacitic (Sellés and Gardeweg, 2017). An available age date, located in Bolivian territory on the southeast side of the Cerro Inacaliri, was 5.84 ± 0.09 Ma (K-Ar in biotite; Almendras et al., 2002). This unit was correlated with the older part of the Inacaliri and Apagado volcanic structures, which have been dated at 5.8 Ma.

Cabana Ignimbrite (Pii) ca 4.12 Ma

The Cabana Ignimbrite is a medium to poorly welded tuff of white and white-pinky color with vesicular and dacitic pumice (biotite and amphibole) and subangular and angular lithics dominated by an ash matrix. It is at least 70 m thick in Chile. The first age for this unit was of <7.5 Ma (Layana and Aguilera, 2013). Before the 2017/18 investigations this was the oldest age determined in the area and for this reason the Cabana Ignimbrite was thought to lie below the Volcanic Sequences of the Upper Miocene-Pliocene. However a subsequent determination gave an age of 4.12 Ma, and so in the SERNAGEOMIN report of 2017 the Cabana Ignimbrite was thought to form a wedge in the Miocene-Pliocene Volcanic Sequence.

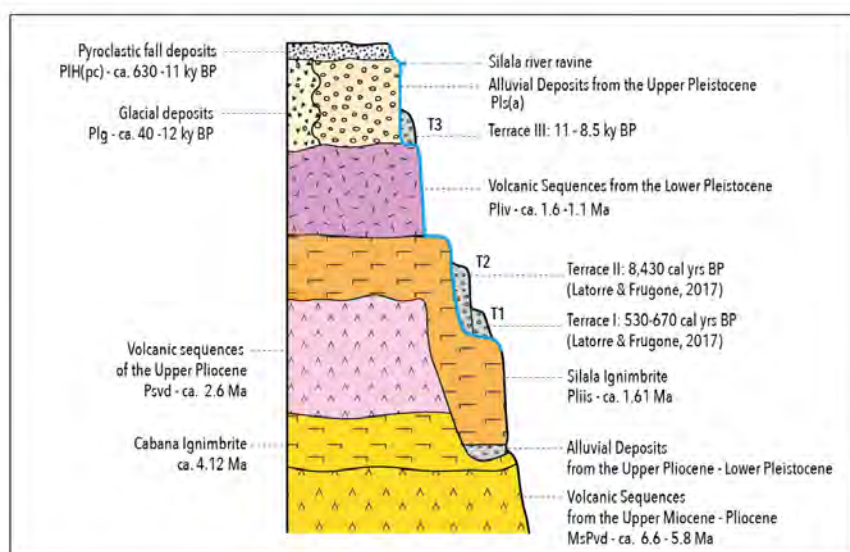


Figure 3. The updated integrated stratigraphic column of the Silala River area.

Volcanic Sequences of the Upper Pliocene (Psvd) ca 2.6 Ma

These lavas lie above the Cabana Ignimbrite and are dacitic (biotite and amphibole) of pale gray color and were dated at 2.6 Ma (SERNAGEOMIN, 2017). In SERNAGEOMIN (2017) they were thought contiguous with earlier Miocene lavas, but have since been observed directly underlying the Silala Ignimbrite (1.61 Ma in Blanco and Polanco, 2018) in both a borehole (see Annex A) and in outcrop.

Silala Ignimbrite (Pliis) ca 1.61 Ma

The Silala Ignimbrite is a more or less horizontal welded tuff of pink color and andesitic composition with distinct cooling units or flow levels that outcrops in the Silala River ravine in Chile. The age interval of this unit had been estimated in SERNAGEOMIN (2017) with reference to its stratigraphic relationships with the other deposits in the sequence. It provides the ignimbrite cover to the dacitic lava flow of 2.6 Ma (see above) and it is covered by an andesitic lava flow from the Inacaliri volcano dated at 1.48 Ma (Almendras et al., 2002) in Bolivia. Thus the Silala Ignimbrite unit was thought to lie in the age range 2.6-1.48 Ma. The new age date (see Table 1) of 1.61 Ma confirms its stratigraphic position.

Pyroclastic Fall Deposits (PIH(pc)) ca 630-11 ka

These deposits comprise well-stratified fine to medium-grained ash found in the central and southern parts of the Chilean study area. Recently an age of 630 ka has been determined for the Pyroclastic Fall Deposits. These pyroclastic deposits outcropping in the Silala basin are interpreted as being associated with an eruption of the Chao Dome.

In summary, the most important change to the stratigraphic interpretation in Chile is the inclusion of a fifth lithological unit (Volcanic Sequences of the Upper Pliocene), which is associated with volcanism with an age of 2.6 Ma, lying in between the Cabana Ignimbrite, which has an age of 4.2 Ma, and the Silala Ignimbrite, recently dated at 1.61 Ma and found overlying Upper Pliocene lavas, confirming its position in the stratigraphic column. The oldest rocks found in the basin in Chile are the Volcanic Sequences of the Upper Miocene with an age of 6.6-5.8 Ma.

3. INTERPRETATION AND MAPPING OF THE GEOLOGY OF THE ESTIMATED GROUNDWATER CATCHMENT IN BOLIVIA AND CHILE

It is important to understand the geology of the groundwater catchment in order to gain a good understanding of both the regional and local hydrogeology. By utilizing the geological maps of Ríos et al., (1997) and Almendras et al., (2002) by SERGEOMIN, including all the radiometric ages available (see Table 1), and satellite images from Google Earth, it has been possible to construct a geological map which includes this extended catchment in Bolivia as shown in Figure 4, which is very similar to the version of SERGEOMIN (2003). In developing the geological map presented in SERNAGEOMIN (2017) neither the reports of SERGEOMIN nor their geological maps were available to consult. They have been provided subsequent to the filing of the BCM and were obtained after reading the DHI (2018) report, which referred to these reports (SERGEOMIN, 2003 and 2017). Clearly, since access to Bolivia for field observation and further petrographic study and radiometric dating was not possible, the compilation map provided in Figure 4 has a greater uncertainty attached to it than would be the case if this work, including fieldwork, had been possible.

A new geological section (NE-SW Profile), also shown in Figure 4, has been constructed to visualize the geology with depth. The paucity of borehole information limits the three-dimensional accuracy of geological knowledge and understanding. Nevertheless, the compilation of Chilean and Bolivian data (radiometric dates; Table 1), field observations available in Bolivian reports, and the Chilean mapping observations would be expected to give the best understanding to date of the geology of the groundwater catchment of the Silala River.

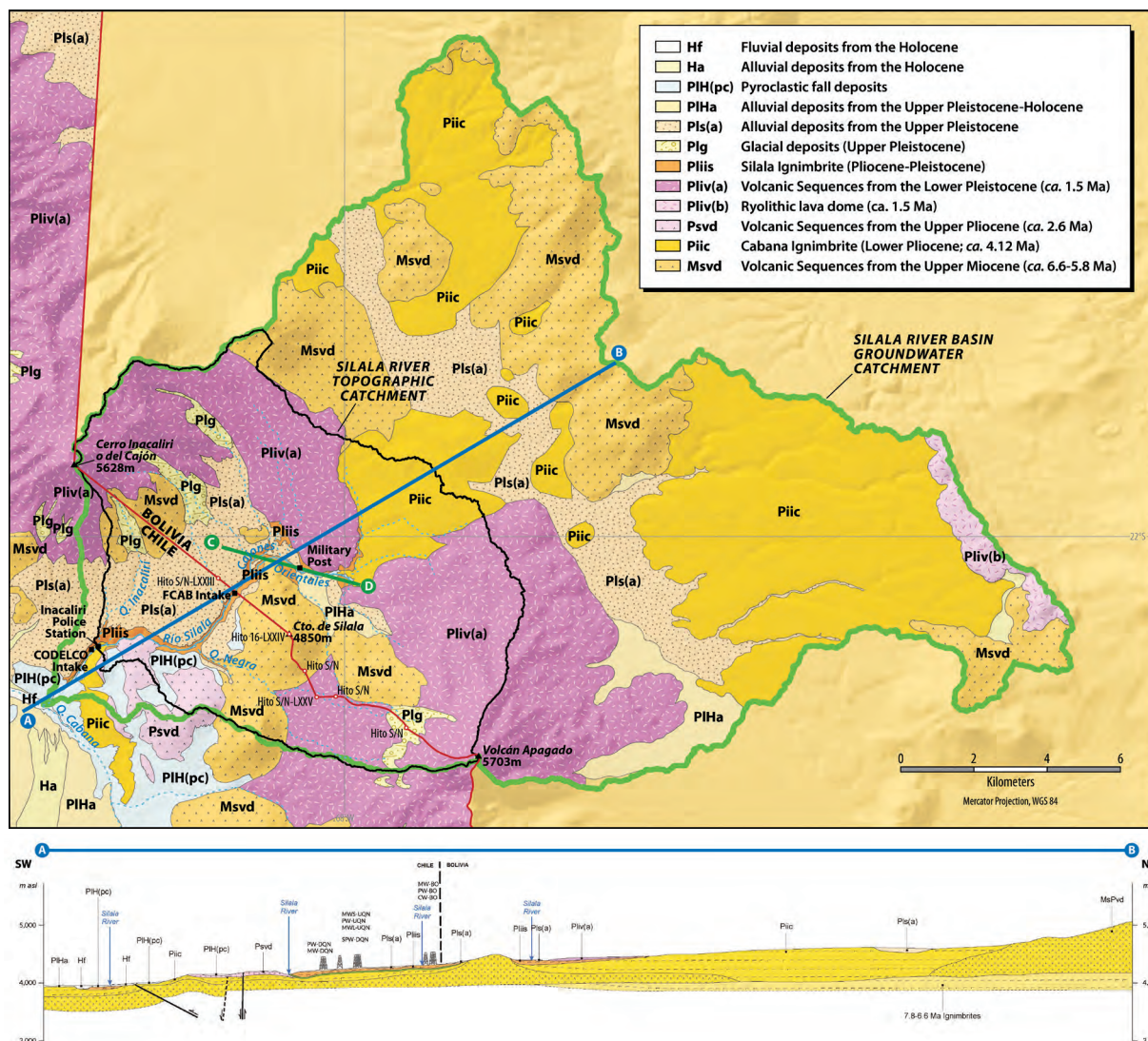


Figure 4. (a) Map showing a compilation and interpretation of the geology of the Silala River basin that includes the Bolivian territory and uses Bolivian maps and data (SERGEOMIN, 2003 and 2017). Blue line is the NE-SW profile (AB section) and green line is the NW-SE profile (CD section). (b) NE-SW profile (AB section)*. For the CD section see Figure 11.

The major bedrock unit in the Bolivian part of the groundwater catchment was previously interpreted by SERNAGEOMIN geologists as being the Cabana Ignimbrite, as found in Chile (Piic) (Figure 5). However, new descriptions and radiometric age dates available in the SERGEOMIN (2003 and 2017) reports have allowed the recognition of several levels of tuffaceous deposit of a variety of ages (7.8, 6.02 and 3.4 Ma, see Table 1). These deposits have variable thicknesses and have variable amounts of pumice lithics and ash, and different welding grades. They are lumped together on

* A fold-out version of this profile can be found in Peach and Wheatler (2019).

the map in Figure 4 under the name of Cabana Ignimbrite (Piic) but may include ignimbrites older than 4.12 Ma. Significantly, these reports identify three separate ignimbrite deposits associated with two debris flows. A single debris flow has been identified in Chile in a borehole close to the international border (see Appendix A) and in outcrop near the Inacaliri Police Station (see Figure 5) and lying between the Silala and Cabana Ignimbrites.

It would appear that the Silala basin was like a reservoir, which was successively filled by pyroclastic flows, now recognized and mapped as ignimbrites from differing sources and of differing ages, the oldest deposit being at least 7.8 Ma (Table 1).

Of these pyroclastic flows, from successive volcanic eruptions that filled or partially filled the Silala basin in Bolivian territory over several million years, at least two crossed the line of the Chile-Bolivia international border to the west. These flows surmounted the topographic high that formed the volcanic chain of Inacaliri and Apagado volcanoes (Figure 2), and can be seen in Chile (Figure 5). In both cases, the source of these two pyroclastic flows is interpreted as being in the east within Bolivian territory because their thicknesses tend to decrease to the west.



Figure 5. Two different pyroclastic deposits of ignimbrites exposed in Chilean territory, near the Inacaliri Police Station. Silala Ignimbrite (Pliis) above, Cabana Ignimbrite (Piic) below, separated by a thin debris flow (alluvial flow deposit) (see Figure 7).

The ages of the ignimbrites in Chile (4.12 and 1.61 Ma) are very well defined, as are their stratigraphic positions and physical relationships with other units. The upper

ignimbrite (in Chile called the Silala Ignimbrite) has an age of 1.61 Ma and overlies, in places, a dacitic lava flow of 2.6 Ma (Volcanic Sequences of the Upper Pliocene) (Figure 6), while the lower ignimbrite has an age of 4.12 Ma and is covered by the Volcanic sequences of the Upper Pliocene in places. From the Bolivian reports (SERGEOMIN, 2003 and 2017) it appears that in Bolivian territory there are three separate ignimbrites with associated debris flows. In Chile there are two ignimbrite flows that have been recognized, which are separated by a single debris flow (or alluvial flow). It would seem logical that the Chilean ignimbrite flows can be correlated with the upper two in Bolivia (Nis-2 and Nis-3; Nis is an abbreviation of Neogene Ignimbrites Silala). It is not possible that the upper ignimbrite, which has an age 1.61 Ma in Chile could also have an age of 7.8 Ma in Bolivia. So, this ignimbrite with this much older age must have been deposited earlier and in Chile perhaps might be found at depth beneath both Silala and Cabana Ignimbrites. Here there is a major difference in geological interpretation between that discussed in SERGEOMIN (2003 and 2017) and in this report.



Figure 6. Silala Ignimbrite (Pliis) (1.61 Ma) covers the dacitic lava flow of 2.6 Ma (Volcanic Sequences of the Upper Pliocene, Psvd).

In summary the interpretation of the solid geology of the Silala area in this report, which is based on the most complete information to date, is that there are at least three ignimbrite deposits to be found in the Silala extended groundwater catchment, only two of which outcrop in Chile with an interbedded debris flow and in places separated by Pliocene dacitic lavas. The radiometric dating and field observations for this provide very good confirmation.

4. EROSION AND DEPOSITION IN THE SILALA PALAEO-VALLEY

In two localities along the Silala River in Chile it is possible to recognize the upper and lower ignimbrites (Silala and Cabana, respectively) with a debris flow deposit (or alluvial flow deposit) lying between them. One of the locations is near the Inacaliri Police Station (Figure 7), where the debris flow thickness is 20 cm, while close to the international border between Chile and Bolivia, in the borehole CW-BO (Arcadis, 2017; SERNAGEOMIN, 2017, see Appendix A), the debris flow deposit (an alluvial deposit) was found to have a thickness of 13 metres. The distance between both localities is about 4.5 km and the difference in altitude about 300 metres, indicating a significant change in a small distance. The thinning toward the lower end of the Silala ravine and the associated fining of the sedimentary grain size suggests flow from what is now Bolivian territory down the proto Silala River valley towards the southwest (SERNAGEOMIN, 2017).



Figure 7. Outcrop showing the upper and lower ignimbrites (Silala and Cabana ignimbrite, respectively) with a thin fluvial deposit between them, exposed in Chilean territory near the Inacaliri Police Station.

Over the time between the deposition of the two ignimbrites in Chilean territory (upper and lower ignimbrites), a period of approximately 2.5 Million years, there is no geological record (volcanic or sedimentary) in the Chilean part of the basin, except for the small debris flow. This gap in deposition suggests that a dynamic environment with intense processes of minor deposition (fluvial deposits and debris flows) and high erosion occurred along the Silala palaeo-valley. This suggests that a fluvial system, of higher energy than at present, functioned in this area at that time.

5. STRUCTURAL EVOLUTION

In Chilean territory to the south west of the Silala extended catchment, it is possible to recognize an alignment of volcanic centres in a NW-SE direction (Paniri-Toconce volcanic chain: 1.6 Ma to 150 ka, see Figure 2). This direction is coincident with the graben system in the area (the Apacheta dome (1.43 Ma to 50 ka) to the NW of the Silala basin). Both lineaments are consistent with extension in the NE-SW direction. Although this structural configuration gave rise to the volcanism mentioned above, it is likely to have provided the plane of weakness for much earlier volcanism because the NW-SE Miocene volcanic chain (6.8-5.4 Ma) can also be seen along a similar line (see Figures 1 and 2).

There is an alignment of volcanic centres, including Cerrito Silala (Figures 2 and 4), in a N-S direction, which has an age of 6.6-6.0 Ma and represents a local crustal extension in the W-E direction. This extension is likely to have provided a plane of weakness that favored the later structural configuration.

Along the Silala River a vertical normal fault has been mapped in Chile (Figure 8), trending N-S, which affects the front of the dacitic lava flow of 2.6 Ma (Table 1) (Volcanic Sequences of the Upper Pliocene) but does not affect the overlying ignimbrite (Chilean-named Silala Ignimbrite). This structural configuration (Figure 8) occurred as a response to the compression in a W-E direction such that the N-S inverse fault (Cabana Fault) lifted and rotated the NE block with respect to SW (Figure 8). This tectonic event occurred between 2.6 to 1.6 Ma.

Finally, an important morphological feature along the ravine of the Silala River is that the level of the Chilean-named Silala Ignimbrite found on both sides of the ravine is practically the same, as can be seen in the terraces (see Figure 9).

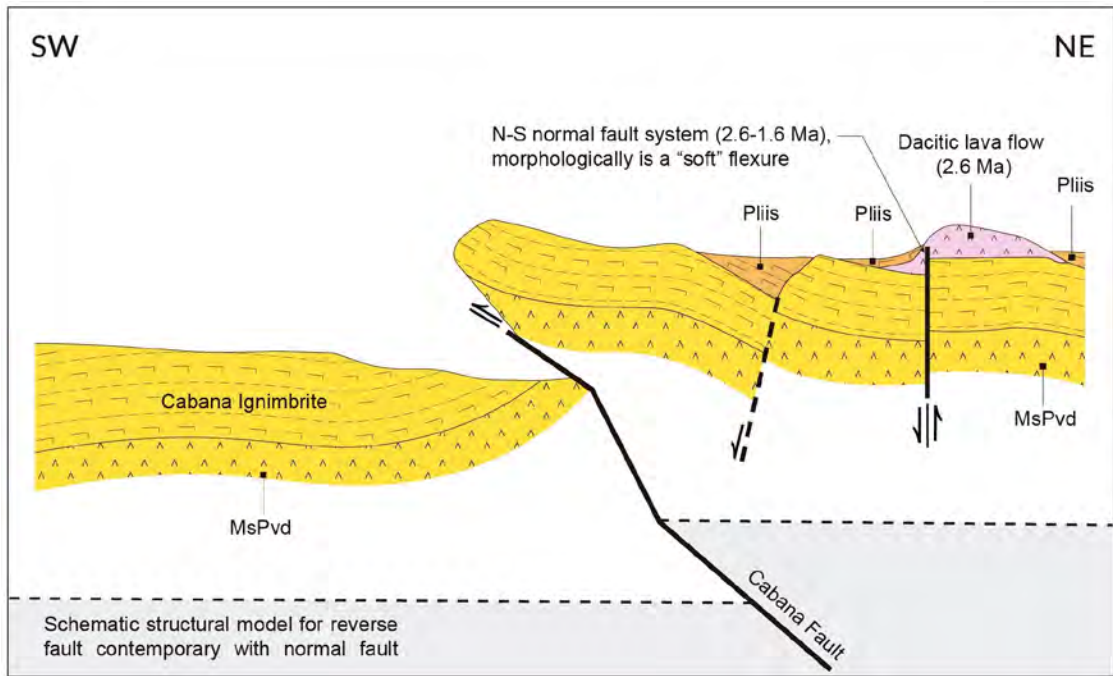


Figure 8. Schematic structural profile in the SW sector of the Silala River.



Figure 9. Photography of an excellent example of no slip (relative movement) on both sides of the ravine of the Silala River.

The modelling (DHI, 2018) that was carried out in support of the BCM has employed very high hydraulic conductivities along a fault which is mapped (SERGEOMIN, 2017) as running from the Orientales wetland to the Cajones wetland and bending around to follow the line of the Silala River to cross the international border into Chile (see Figure 10).

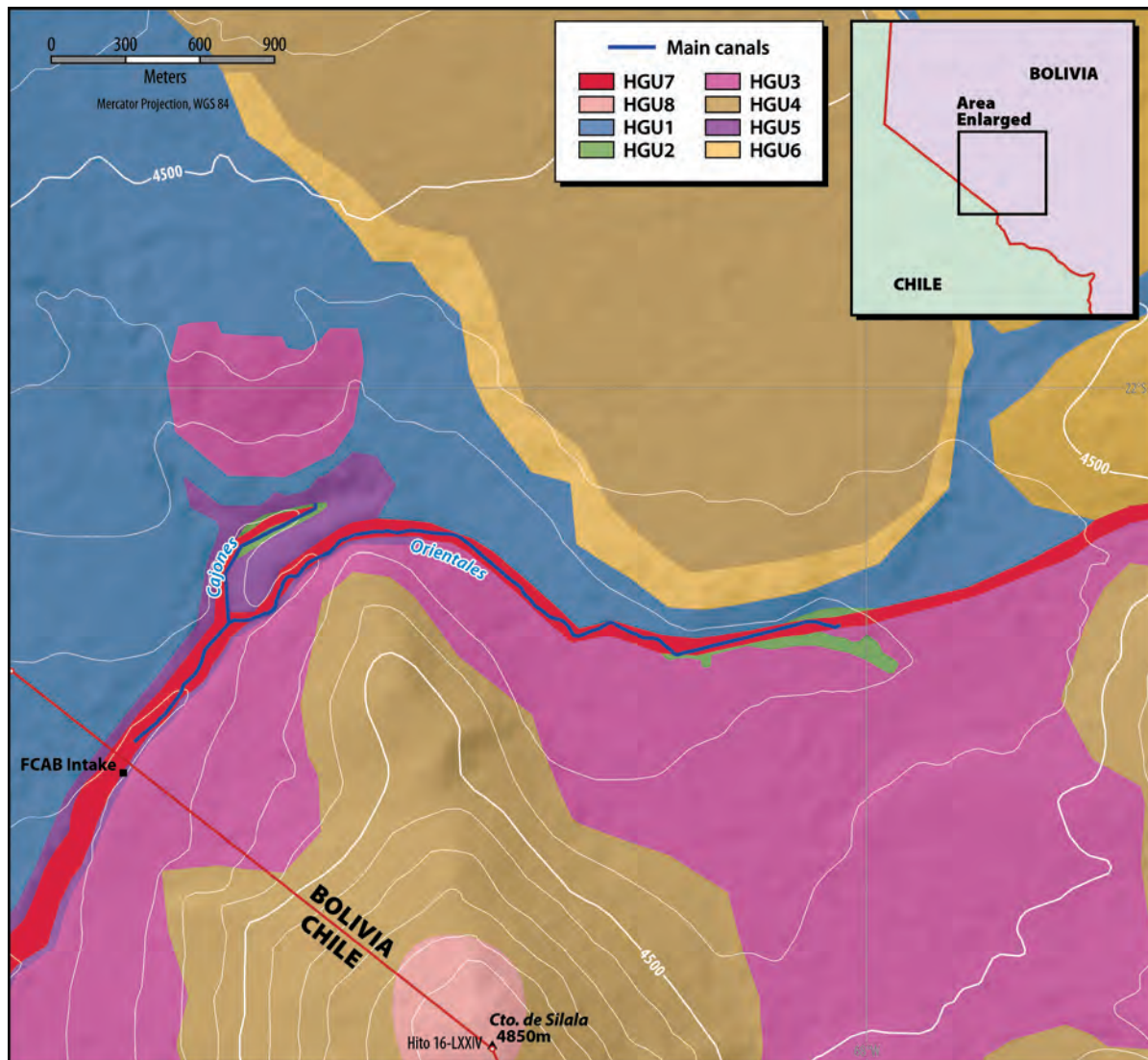


Figure 10. Amended map from DHI (2018) (BCM, Vol. 4, p.76, Figure 29) showing in red (HGU 7) the postulated fault system.

No evidence, including displacements, fault gouge deposits or rock shattering has been found in Chile to support the presence of such a fault (see Figure 9). No evidence of displacement is provided by SERGEOMIN in their 2003 or 2017 reports, although they do provide evidence of fractures and their directions. This fault has been assumed to be

vertical by DHI (2018) yet such a fault system showing such outcrop sinuosity could only occur in the manner assumed by DHI (2018) if it had a very low angle. There appears no evidence for this.

A NW-SE profile through the Cajones ravine and Orientales areas (Figure 11) shows the distribution of the Chilean-named Silala Ignimbrite, the debris flow and the Chilean-named Cabana Ignimbrite as well as the line of the alignment of at least three centres of Volcanic Sequence of Upper Miocene (Cerrito Silala to Cerro Silaguala) (see Figure 2).

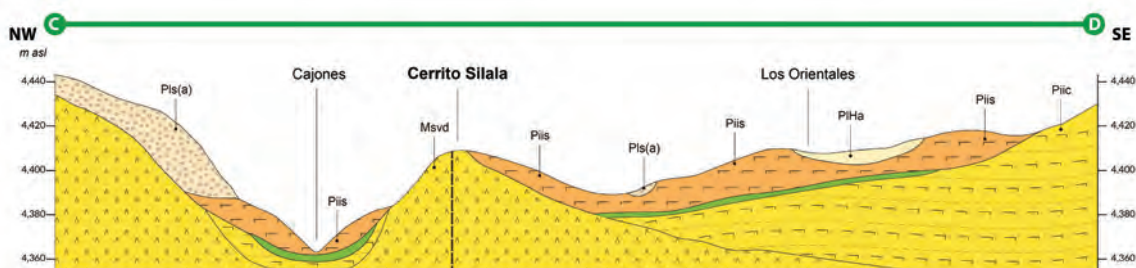


Figure 11. NW-SE profile showing the Cajones and Orientales areas (CD green line in Figure 4). The vertical black dashed line represents the axis of alignment of at least three volcanic centres of Volcanic Sequences of Upper Miocene (Msvd). The Debris flow (solid green color) that is showing to the SE of Cerrito Silala is interpreted. The legend for the abbreviations can be found in Figure 4.

A simple explanation for the locations of the springs in Cajones and Orientales is that they might be related to the intersection of the N-S alignment with projection of regional NW-SE structure in Chilean territory (Miocene chain, graben, Pliocene-Pleistocene volcanism).

6. INACALIRI-APAGADO VOLCANIC CHAIN

The activity of the Inacaliri-Apagado volcanic chain was episodic but over a long period. The high topography of these mountains formed a natural barrier that limited the transport of the various pyroclastic flows that originated from the east in different periods as demonstrated by at least three different ages as found for the ignimbrite lithologies in Bolivian territory. One of the main differences in the geological interpretation from that of the DHI (2018) report is the position of ignimbrite recognized along the Silala River. The contact relationships as discussed in sections 2, 3 and 4 and the ages obtained (Table 1) are consistent with the schematic section shown in Figure 12.

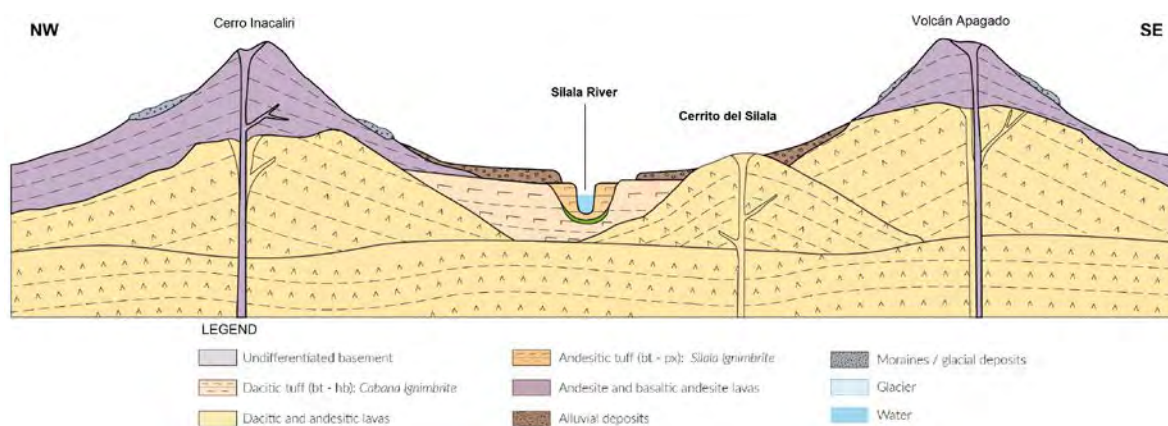


Figure 12. Schematic profile of Inacaliri-Apagado volcanic chain at the border of Chile and Bolivia, including Cerrito Silala. The solid green color corresponds to the debris flow deposit (or alluvial deposit).

7. SUMMARY AND CONCLUSIONS

A variety of further investigations have been carried out to improve the knowledge of the geology of the groundwater catchment area of the Silala River. These have included new radiometric dates for rock deposits found in Chile, new field observations in Chile, re-interpretation of drill cuttings from boreholes drilled in Chile, and examination of Bolivian reports and map data. From this work a revised map of the groundwater basin, a revised stratigraphy for the area and a three-dimensional conceptual understanding of the geology of the Silala groundwater catchment have been developed.

The major conclusions are that the Ignimbrite succession is comprised of at least three deposits that are associated or interbedded with debris flow deposits. These rocks were deposited over a period from 7.8 Ma to 1.61 Ma but included long periods between the deposition of the ignimbrites during which high energy fluvial erosional processes took place. It is proposed that the pyroclastic flows that formed the ignimbrites were restricted in their south-westward flow into what is now Chile by the Inacaliri-Apagado volcanic chain and this topographic high held back much of the pyroclastic flow until it overtopped this ridge.

New radiometric dates have shown that two separate sequences of dacitic volcanism outcrop and in places the younger deposits (Pliocene dacitic lavas) are found between the Cabana and Silala Ignimbrites in Chile.

There appears no evidence in Chile for the major fault system invoked by DHI (2018) and used in their integrated model, and the sinuosity of this system appears highly implausible.

8. REFERENCES

- ARCADIS, 2017. *Detailed hydrogeological study of the Silala River. (Chile's Memorial, Vol. 4, Annex II).*
- Almendras, A.O., Balderrama Z.B., Menacho L.M. and Quezada C.G., 2002. Mapa Geológico Hoja Volcán Ollagüe, escala 1:250.000. *Mapas Temáticos de Recursos Minerales de Bolivia.* SERGEOMIN, Bolivia.
- Blanco, N., and Polanco E., 2018. *Geology of the Silala River Basin, Northern Chile.* Servicio Nacional de Geología y Minería (SERNAGEOMIN). **(Appendix C).**
- Danish Hydraulic Institute (DHI), 2018. *Study of the Flows in the Silala Wetlands and Springs System. (Bolivia's Counter-Memorial, Vol. 4, Annex 17).*
- Latorre, C. and Frugone, M., 2017. *Holocene sedimentary history of the Río Silala (Antofagasta Region, Chile). (Chile's Memorial, Vol. 5, Annex IV).*
- Layana, S. and Aguilera, F., 2013. *Stratigraphy of three new ignimbrites from Altiplano Puna Volcanic Complex, northern Chile.* In Actas GEOSUR 2013, 171-172, Viña del Mar, Chile.
- Polanco, E., 2012. *Geología a escala 1:50.000 del área de la Cadena Volcánica Paniri-Toconce, Provincia del Loa, Región de Antofagasta. (Chile's Memorial, Vol. 5, Annex VIII, Appendix D).*
- Ríos, H., Baldellón, E., Mobarec, R. and Aparicio, H., 1997. Mapa Geológico Hojas Volcán Inacaliri y Cerro Zapalero, escala 1:250.000. *Mapas Temáticos de Recursos Minerales de Bolivia,* SGM Serie II-MTB-15B. SERGEOMIN.
- Rivera, G., Morata, D. and Ramírez, C., 2015. *Evolución Vulcanológica y Tectónica del Área del Cordón Volcánico Cerro del Azufre – Cerro de Inacaliri y su Relación con el Sistema Geotérmico de Pampa Apacheta, II Región de Antofagasta, Chile,* XIV Congreso Geológico de Chile, La Serena.
- Salisbury, M.J., Jicha, B., de Silva, S., Singer, B., Jiménez, N. and Ort, M., 2011. $^{44}\text{Ar}/^{39}\text{Ar}$ chronostratigraphy of Altiplano-Puna volcanic complex ignimbrites reveals the development of a major magmatic province. *Geological Society of America Bulletin,* 123, 821–840.
- Sellés, D. and Gardeweg, M., 2017. *Geología del área Ascotán-Cerro Inacaliri, Región de Antofagasta.* Servicio Nacional de Geología y Minería, Carta Geológica de Chile, Serie Geología Básica 190, 1 mapa, escala 1:100.000. Santiago. **(Chile's Memorial, Vol. 6, Appendix G)**
- SERGEOMIN, 2003. *Estudio de cuencas hidrográficas, Cuenca manantiales del Silala, Cuenca 20.* Proyecto de Integración Regional, Departamento de Geología y Recursos

Minerales, Servicio Nacional de Geología y Minería (SERGEOMIN), Bolivia. (**Chile's Reply, Vol. 2, Annex 94**).

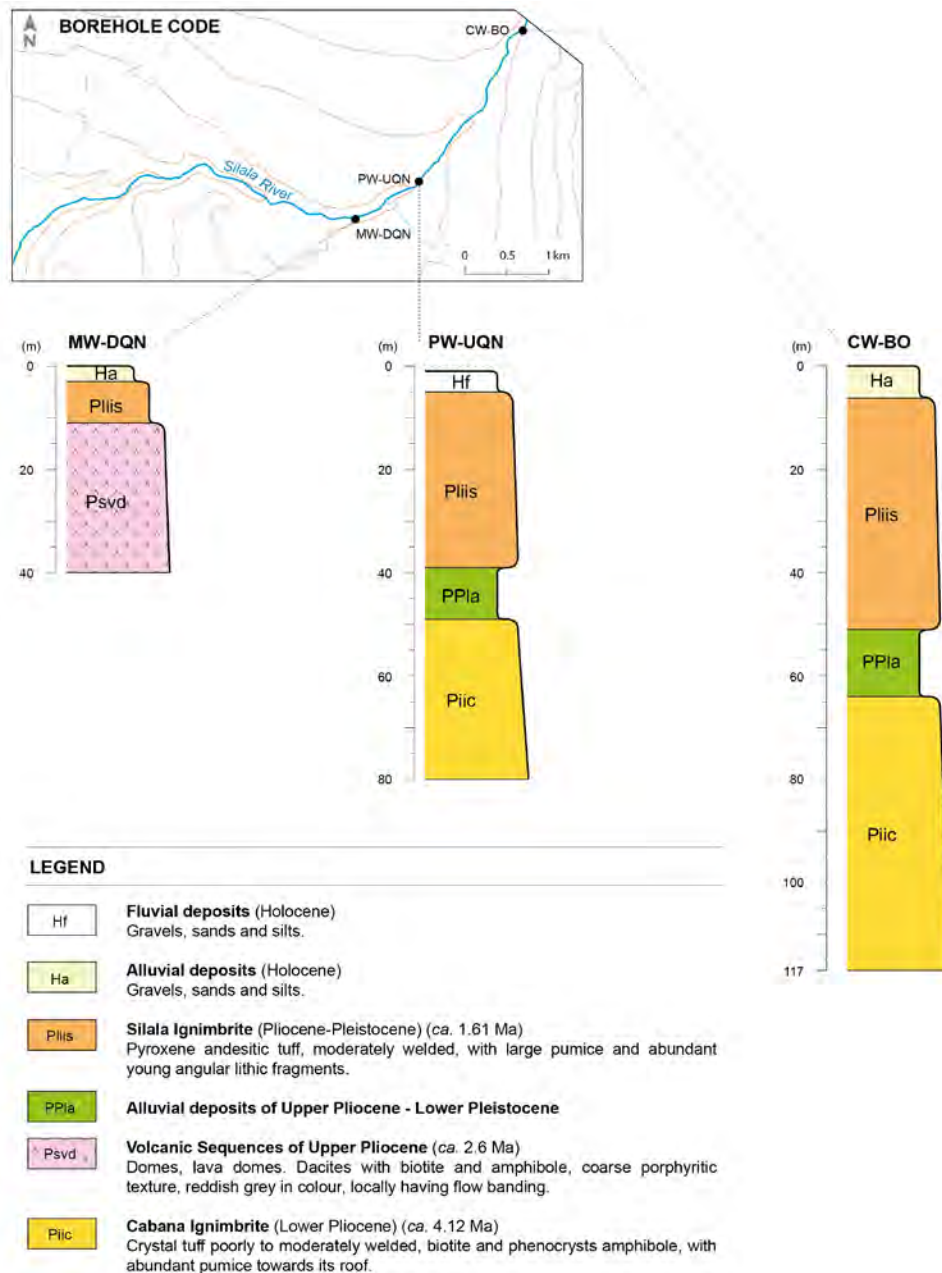
SERGEOMIN, 2017. *Proyecto Mapeo Geológico-Estructural del área circundante al manantial del Silala, Departamento de Potosí*. Convenio Interinstitucional, Servicio Geológico Minero (SERGEOMIN)-DIREMAR. La Paz, Bolivia. (**Appendix D**).

SERNAGEOMIN, 2017. *Geology of the Silala River Basin*. (**Chile's Memorial, Vol. 5, Annex VIII**).

Wilson, C. and Houghton, B., 2000. Pyroclast Transport and Deposition. In: Sigurson, H., Houghton, B., Mc Nutt, S., Rymel, H., Stix, J. (eds.), *Encyclopedia of Volcanoes*, San Diego CA, Academic Press, pp. 545-554.

APPENDIX A

STRATIGRAPHIC COLUMN OF BOREHOLES MW-DQN, PW-UQN AND CW-BO



APPENDIX B
AR/AR AND U-PB AGE REPORTS OF RADIOMETRIC DATING



Servicio Nacional de Geología y Minería
Subdirección Nacional de Geología
Departamento de Laboratorios

Sr. Edmundo Polanco

SDNG

UNIDAD DE GEOLOGIA ISOTOPICA
INFORME $^{40}\text{Ar}/^{39}\text{Ar}$ N° 019/2017 ARGUS VI

Departamento de Laboratorios Servicio Nacional de Geología y Minería
Til Til 1993, Ñuñoa - Santiago - FONO: (56-2) 2385292 FAX: (56-2) 2385332 - www.sernageomin.cl
E-mail: jefe_lab@sernageomin.cl – Casilla: 10465 y 1347, correo 21- SANTIAGO – CHILE



**National Geology and Mining Service
National Sub-directorate of Geology
Department of Laboratories**

Mr. Edmundo Polanco

SDNG

**ISOTOPIC GEOLOGY UNIT
 $^{40}\text{Ar}/^{39}\text{Ar}$ REPORT N° 019/2017 ARGUS VI**

Department of Laboratories Servicio Nacional de Geología y Minería

Til Til 1993, Nunoa - Santiago - PHONE: (56-2) 2385292 FAX: (56-2) 2385332 - www.sernageomin.cl

E-mail: jefe_lab@sernageomin.cl – Postal Box 10465 and 1347, Post 21- SANTIAGO – CHILE



En el presente informe se encuentran contenidos los resultados y análisis realizados a las muestras que se detallan en la precedente tabla resumen:

Muestra	Nº Análisis	Material	Edad Integrada $\pm 2\sigma$	Edad Plateau $\pm 2\sigma$	Edad Isoc. Inversa $\pm 2\sigma$
RSP-12d	13983-01	Biotita	830 \pm 350 ka	630 \pm 310 ka	2000 \pm 1700 ka

Departamento de Laboratorios. Servicio Nacional de Geología y Minería
 Ttl Ttl 1993, Nuhua - Santiago - FONO: (56-2) 2385292 FAX: (56-2) 2385332 - www.sernageomin.cl
 E-mail: Jefe_lab@sernageomin.cl - Casilla: 10465 y 1347, correo 21- SANTIAGO - CHILE

GEOCRONOLOGIA ARGUS VI



This report contains the results and analyses conducted on the samples that are detailed in the preceding summary table:

Sample	Nº Analysis	Material	Integrated Age $\pm 2\sigma$	Plateau Age $\pm 2\sigma$	Inverse Isochron Age $\pm 2\sigma$
RSP-12d	13983-01	Biotite	830 \pm 350 ka	630 \pm 310 ka	2000 \pm 1700 ka

Department of Laboratories Servicio Nacional de Geología y Minería

Til Til 1993, Nunoa - Santiago - PHONE: (56-2) 2385292 FAX: (56-2) 2385332 - www.sernageomin.cl

E-mail: jefe_lab@sernageomin.cl - Postal Box 10465 and 1347, Post 21 - SANTIAGO - CHILE

ARGUS VI GEOCHRONOLOGY



Muestra : **RSP-12d**
Material : Biotita
Nº interno : 13983-01

Análisis de Step Heating

Edad integrada: 830 ± 350 ka

Edad Plateau: **630 ± 310 ka**

Pasos en el Plateau: 5/8 (85,2% de ³⁹Ar)

MSWD Plateau: 0.69

Análisis de Isócrona Inversa

Edad Isócrona: 2000 ± 1700 ka

Pasos: 5/8 (63 % de los pasos)

Intercepto 40/36: 292.4 ± 3.9

MSWD Isócrona: 0.074

Comentarios:

Todas las edades son concordantes. No se aprecia la presencia de argón heredado. Se recomienda usar la edad obtenida con el plateau.

GEOCRONOLOGIA ARGUS VI

Departamento de Laboratorios Servicio Nacional de Geología y Minería
 T11 T11 1993, Nunoa - Santiago - FONO: (56-2) 2385292 FAX: (56-2) 2385332 - www.sernageomin.cl
 E-mail: jefe_lab@sernageomin.cl - Casilla: 10465 y 1347, correo 21 - SANTIAGO - CHILE



Sample : **RSP-12d**
Material : Biotite
Internal Nº : 13983-01

Step Heating Analysis

Integrated Age: 830 ± 350 ka
Plateau Age: **630 ± 310 ka**
 Steps at the Plateau: 5/8 (85,2% of ³⁹Ar)
 Plateau MSWD: 0,69

Inverse Isochron Analysis

Isochron Age: 2000 ± 1700 ka
 Steps: 5/8 (63 % of the steps)
 40/36 Intercept: 292 ± 3.9
 Isochron MSWD: 0.074

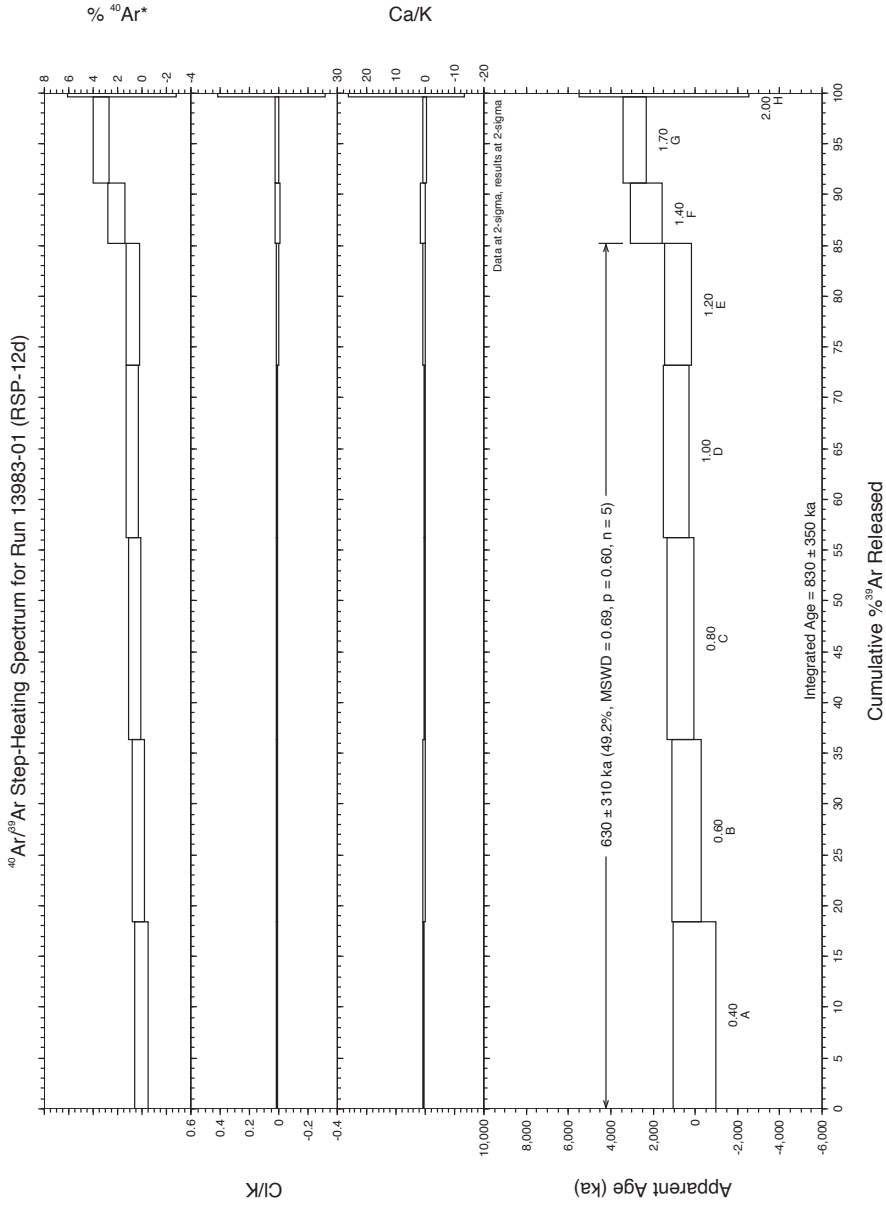
Comments:

All ages are concordant. The presence of inherited argon has not been observed. It is recommended to use the age obtained with the plateau.

Department of Laboratories Servicio Nacional de Geología y Minería

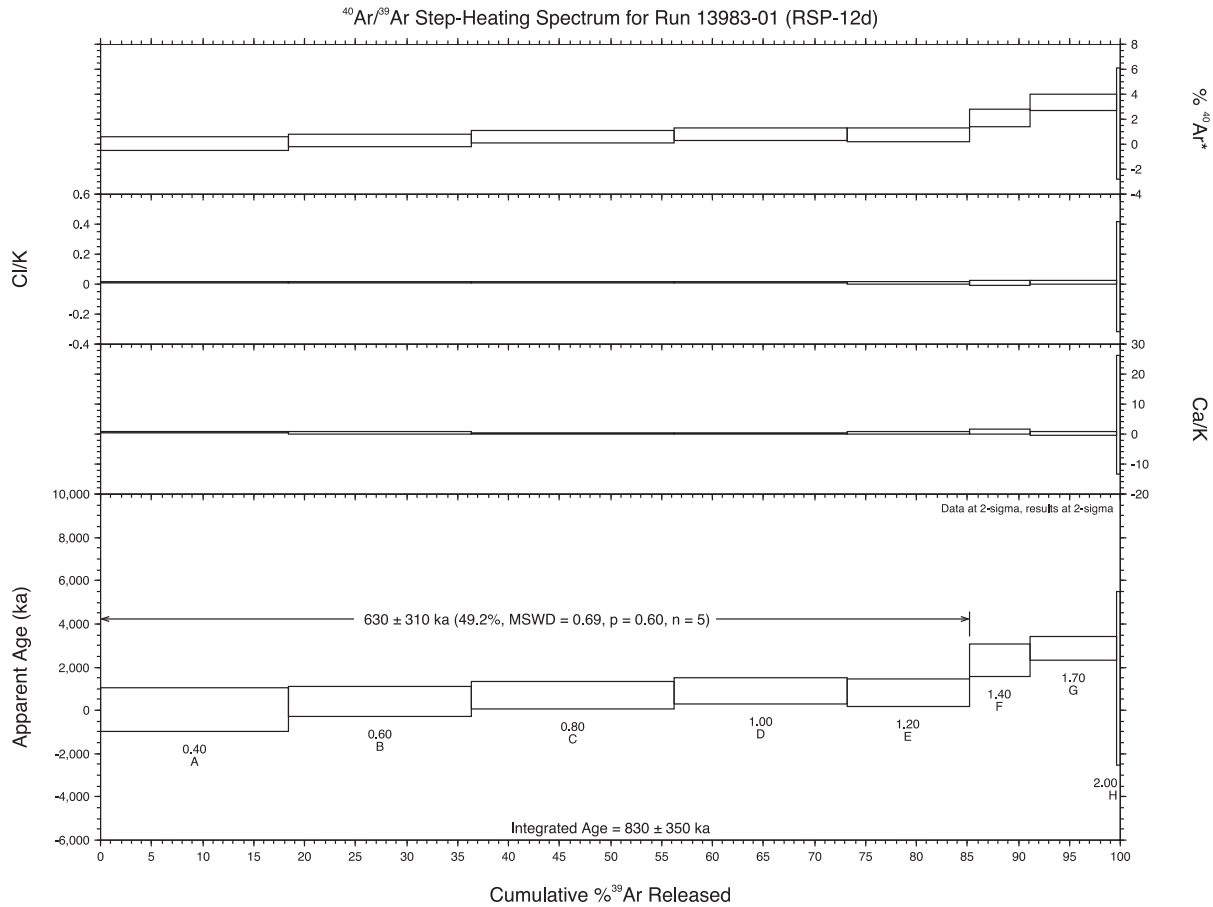
Til Til 1993, Nuñoa - Santiago - PHONE: (56-2) 2385292 FAX: (56-2) 2385332 - www.sernageomin.cl
 E-mail: lefe_lab@sernageomin.cl - Postal Box: 10465 and 1347, Post 21- SANTIAGO - CHILE

ARGUS VI GEO



GEOCRONOLOGIA ARGUS VI

Departamento de Laboratorios Servicio Nacional de Geología y Minería
 Ttl Tll 1993, Nuhooa - FONDO: (56-2) 2385292 FAX: (56-2) 2385332 - www.sernageomin.cl
 E-mail: jefe_lab@sernageomin.cl - Casilla: 10465 y 1347, correo 21- SANTIAGO - CHILE



Department of Laboratories Servicio Nacional de Geología y Minería

Til Til 1993, Nuñoa - Santiago - PHONE: (56-2) 2385292 FAX: (56-2) 2385332 - www.sernageomin.cl

E-mail: jefe_lab@sernageomin.cl - Postal Box 10465 and 1347, Post 21- SANTIAGO - CHILE

ARGUS VI GEOCHRONOLOGY



40Ar/39Ar Step-Heating Data for Run 13983-01; RSP-12d

Sample: RSP-12d		J: 0.0013809 ± 0.0000003										D: 0.99969 ± 0.00003			Heating: 76 s Total						
Material: Biotita															36 s Rise						
Hole: 4/21																					
N	Power (W)	⁴⁰ Ar (moles)	⁴⁰ Ar (fA)	³⁹ Ar (fA)	± 0 ₄₀ (fA)	³⁹ Ar (fA)	± 0 ₃₉ (fA)	³⁸ Ar (fA)	± 0 ₃₈ (fA)	³⁷ Ar (fA)	± 0 ₃₇ (fA)	³⁶ Ar (fA)	± 0 ₃₆ (fA)	% ⁴⁰ Ar* ³⁹ Ar/ ³⁹ Ar _h	± 0	Age (ka)	± 0 (ka)	Ca/K	± 0	Cl/K	± 0
A	0.4	7.19E-14	1915.24	0.13	24.75	0.03	1.61	0.02	0.08	0.03	6.482	0.017	0.02	0.0	0.2	32	506	0.43	0.14	0.010	0.003
B	0.6	5.16E-14	1373.70	0.11	24.01	0.03	1.24	0.02	0.04	0.03	4.637	0.012	0.27	0.15	0.14	379	357	0.21	0.14	0.010	0.003
C	0.8	4.90E-14	1305.05	0.11	26.67	0.03	1.23	0.02	0.01	0.03	4.393	0.012	0.54	0.27	0.13	661	323	0.05	0.13	0.009	0.002
D	1.0	3.92E-14	1044.76	0.10	22.68	0.03	1.02	0.02	0.02	0.03	3.509	0.009	0.76	0.35	0.12	872	309	0.10	0.15	0.010	0.003
E	1.2	2.74E-14	730.88	0.08	16.05	0.03	0.69	0.02	0.01	0.03	2.456	0.007	0.69	0.31	0.13	784	324	0.1	0.2	0.006	0.004
F	1.4	1.33E-14	355.60	0.06	8.01	0.03	0.33	0.02	0.03	0.03	1.179	0.004	2.07	0.92	0.15	2285	375	0.5	0.4	0.002	0.008
G	1.7	1.48E-14	395.61	0.06	11.42	0.03	0.42	0.02	0.00	0.03	1.294	0.004	3.31	1.15	0.11	2852	276	0.0	0.3	0.009	0.006
H	2.0	4.91E-16	13.08	0.05	0.36	0.03	0.02	0.02	0.02	0.03	0.0439	0.0008	1.61	0.6	0.8	1457	2005	6	10	0.05	0.18
Plateau Age (steps A-E):		630 155																			
Standard: FC		Interpolation										Age: 28.201 Ma			D: 0.99900 ± 0.00003		Heating: 77 s Total				
Hole: 4/21																	37 s Rise				
N	Power (W)	⁴⁰ Ar (moles)	⁴⁰ Ar (fA)	± 0 ₄₀ (fA)	³⁹ Ar (fA)	± 0 ₃₉ (fA)	³⁸ Ar (fA)	± 0 ₃₈ (fA)	³⁷ Ar (fA)	± 0 ₃₇ (fA)	³⁶ Ar (fA)	± 0 ₃₆ (fA)	% ⁴⁰ Ar* ³⁹ Ar/ ³⁹ Ar _h	± 0	Age (Ma)	± 0 (Ma)	Ca/K	± 0	Cl/K	± 0	
I	3.4	4.71E-14	1255.68	0.13	109.90	0.05	1.44	0.02	0.01	0.03	0.0158	0.0007	99.63	11.366	0.006	28.201	0.014	0.01	0.03	0.0024	0.0006

Departamento de Laboratorios Servicio Nacional de Geología y Minería
 T11 1993, Nuhoa - Santiago - FON0: (56-2) 2385292 FAX: (56-2) 2385332 - www.sernageomin.cl
 E-mail: lefe_lab@sernageomin.cl - Casilla: 10465 y 1347, correo 21- SANTIAGO - CHILE

GEOCRONOLOGIA ARGUS VI

40Ar/39Ar Step-Heating Data for Run 13983-01; RSP-12d

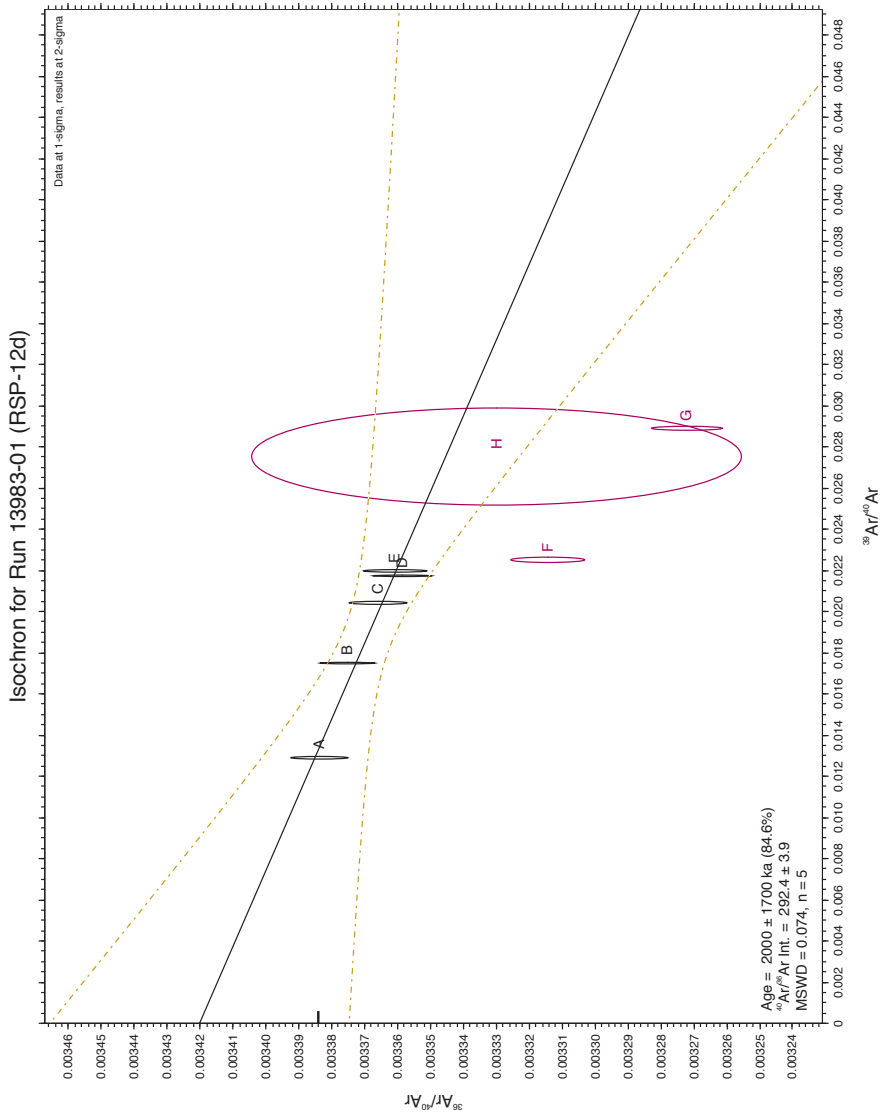
Sample: RSP-12d		J: 0.0013809 ± 0.0000003										D: 0.99969 ± 0.00003			Heating: 76 s Total						
Material: Biotite		36 s Rise																			
Hole: 4/21																					
N	Power (W)	⁴⁰ Ar (moles)	⁴⁰ Ar (fA)	± σ_{40} (fA)	³⁹ Ar (fA)	± σ_{39} (fA)	³⁸ Ar (fA)	± σ_{38} (fA)	³⁷ Ar (fA)	± σ_{37} (fA)	³⁶ Ar (fA)	± σ_{36} (fA)	% ⁴⁰ Ar* / ³⁹ Ar _t	± σ	Age (ka)	± σ (ka)	Ca/K	± σ	Cl/K	± σ	
A	0.4	7.19E-14	1915.24	0.13	24.75	0.03	1.61	0.02	0.08	0.03	6.482	0.017	0.02	0.0	0.2	32	506	0.43	0.14	0.010	0.003
B	0.6	5.16E-14	1373.70	0.11	24.01	0.03	1.24	0.02	0.04	0.03	4.637	0.012	0.27	0.15	0.14	379	357	0.21	0.14	0.010	0.003
C	0.8	4.90E-14	1305.05	0.11	26.67	0.03	1.23	0.02	0.01	0.03	4.393	0.012	0.54	0.27	0.13	661	323	0.05	0.13	0.009	0.002
D	1.0	3.92E-14	1044.76	0.10	22.68	0.03	1.02	0.02	0.02	0.03	3.509	0.009	0.76	0.35	0.12	872	309	0.10	0.15	0.010	0.003
E	1.2	2.74E-14	730.88	0.08	16.05	0.03	0.69	0.02	0.01	0.03	2.456	0.007	0.69	0.31	0.13	784	324	0.1	0.2	0.006	0.004
F	1.4	1.33E-14	355.60	0.06	8.01	0.03	0.33	0.02	0.03	0.03	1.179	0.004	2.07	0.92	0.15	2285	375	0.5	0.4	0.002	0.008
G	1.7	1.48E-14	395.61	0.06	11.42	0.03	0.42	0.02	0.00	0.03	1.294	0.004	3.31	1.15	0.11	2852	276	0.0	0.3	0.009	0.006
H	2.0	4.91E-16	13.08	0.05	0.36	0.03	0.02	0.02	0.02	0.03	0.0439	0.0008	1.61	0.6	0.8	1457	2005	6	10	0.05	0.18
Plateau Age (steps A-E):		630 155																			
Standard: FC		Interpolation										Age: 28.201 Ma			D: 0.99900 ± 0.00003		Heating: 77 s Total				
Hole: 4/21		37 s Rise																			
N	Power (W)	⁴⁰ Ar (moles)	⁴⁰ Ar (fA)	± σ_{40} (fA)	³⁹ Ar (fA)	± σ_{39} (fA)	³⁸ Ar (fA)	± σ_{38} (fA)	³⁷ Ar (fA)	± σ_{37} (fA)	³⁶ Ar (fA)	± σ_{36} (fA)	% ⁴⁰ Ar* / ³⁹ Ar _t	± σ	Age (Ma)	± σ (Ma)	Ca/K	± σ	Cl/K	± σ	
I	3.4	4.71E-14	1255.68	0.13	109.90	0.05	1.44	0.02	0.01	0.03	0.0158	0.0007	99.63	11.366	0.006	28.201	0.014	0.01	0.03	0.0024	0.0006

Department of Laboratories Servicio Nacional de Geología y Minería

Til Til 1993, Nuñoa - Santiago - PHONE: (56-2) 2385292 FAX: (56-2) 2385332 - www.sernageomin.cl

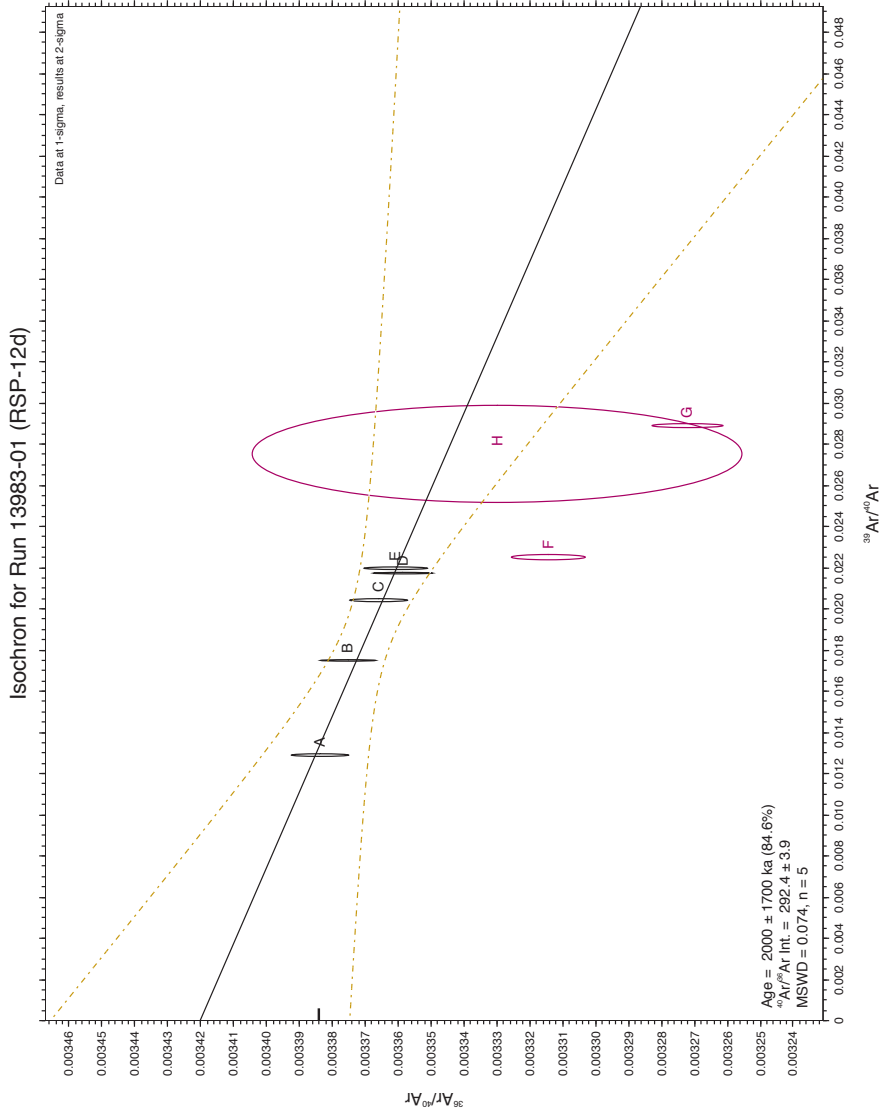
E-mail: lefe_lab@sernageomin.cl - Postal Box 10465 and 1347, Post 21 - SANTIAGO - CHILE

ARGUS VI GEOTHERMOMETRY



GEOCRONOLOGIA ARGUS VI

Departamento de Laboratorios Servicio Nacional de Geología y Minería
 Til Til 1993, Nunoa - Santiago - FON0: (56-2) 2385292 FAX: (56-2) 2385332 - www.sernageomin.cl
 E-mail: jefe_lab@sernageomin.cl - Casilla: 10465 y 1347, correo 21- SANTIAGO - CHILE



Department of Laboratories Servicio Nacional de Geología y Minería
 Ttl Tll 1993, Nuñoa - Santiago - PHONE: (56-2) 2385292 FAX: (56-2) 2385332 - www.sernageomin.cl
 E-mail: lefe_lab@sernageomin.cl - Postal Box 104665 and 1347, Post 21 - SANTIAGO - CHILE

ARGUS VI GEOCHRONOLOGY

Isochron Data for 13983-01A to 13983-01H

Run ID	Status	$^{40}\text{Ar}^{*}/^{39}\text{Ar}$	(36/40) isoch	% \pm	(39/40) isoch	% \pm	Correl 36/39	Group
13983-01A	OK	0.01279	0.003384	0.30	0.01294	0.13	0.007	1
13983-01B	OK	0.15209	0.003375	0.30	0.01751	0.14	0.007	1
13983-01C	OK	0.26512	0.003366	0.30	0.02047	0.12	0.008	1
13983-01D	OK	0.35005	0.003358	0.30	0.02174	0.14	0.007	1
13983-01E	OK	0.31455	0.003361	0.30	0.02199	0.21	0.005	1
13983-01F	User omitted	0.91742	0.003314	0.30	0.02255	0.40	0.004	1
13983-01G	User omitted	1.14540	0.003272	0.30	0.02891	0.27	0.005	1
13983-01H	User omitted	0.58467	0.003330	2.20	0.02754	8.48	0.007	1

Sample	ID	Age [ka]	M.S.E.	(40/36) tr	M.S.E.	MSWD	Prob	n
RSP-12d	13983-01	2000	1700	292.4	3.9	0.074	9.74E-01	5

Isochron Data for 13983-01A to 13983-01H

Run ID	Status	⁴⁰ Ar* ³⁹ /Ar	(36/40) isoch	%±	(39/40) isoch	%±	Correl 36/39	Group
13983-01A	OK	0.01279	0.003384	0.30	0.01294	0.13	0.007	1
13983-01B	OK	0.15209	0.003375	0.30	0.01751	0.14	0.007	1
13983-01C	OK	0.26512	0.003366	0.30	0.02047	0.12	0.008	1
13983-01D	OK	0.35005	0.003358	0.30	0.02174	0.14	0.007	1
13983-01E	OK	0.31455	0.003361	0.30	0.02199	0.21	0.005	1
13983-01F	User omitted	0.91742	0.003314	0.30	0.02255	0.40	0.004	1
13983-01G	User omitted	1.14540	0.003272	0.30	0.02891	0.27	0.005	1
13983-01H	User omitted	0.58467	0.003330	2.20	0.02754	8.48	0.007	1

Sample	ID	Age [ka]	M.S.E.	(40/36) tr	M.S.E.	MSWD	Prob	n
RSP-12d	13983-01	2000	1700	292.4	3.9	0.074	9.74E-01	5

Department of Laboratories Servicio Nacional de Geología y Minería

Til Til 1993, Nunoa - Santiago - PHONE: (56-2) 2385292 FAX: (56-2) 2385332 - www.sernageomin.cl

E-mail: lefe_lab@sernageomin.cl - Postal Box 10465 and 1347, Post 21 - SANTIAGO - CHILE

ARGUS VI GEOCHRONOLOGY



A continuación se detallan las particularidades de los análisis realizados a las muestras contenidas en el informe:

Equipamiento principal:

Espectrómetro Argus VI (multicolector, CDD en ^{36}Ar); Thermo Scientific
Láser de CO_2 (10,6 μ); Photon Machines.

Condiciones de medición:

Cada dos o tres pasos se realizó una medición del background, el cuál fue descontado directamente en las mediciones subsiguientes.

La irradiación de neutrones fue realizada en el reactor nuclear de la CCHEN por un periodo de 23 hrs, existiendo un escudo de cadmio para las muestras.

Criterios de análisis:

Para determinar J de cada lugar de irradiación, se realizó un regresión polinomial de 21 standards presentes en el disco de irradiación.

La definición de un plateau se determina por: ≥ 3 pasos de fusión consecutivos; $\geq 50\%$ de ^{39}Ar liberado en el análisis; Error overlap a 2σ .

Un MSWD < 3 se considera aceptable

Departamento de Laboratorios - Servicio Nacional de Geología y Minería
Til Til 1993, Ñuñoa - FONO: (56-2) 2385292 FAX: (56-2) 2385332 - www.sernageomin.cl
E-mail: jefe_lab@sernageomin.cl - Casilla: 10465 y 1347, correo 21- SANTIAGO - CHILE

GEOCRONOLOGIA ARGUS VI



The details of the analyses conducted to the samples contained in the report are given below:

Main Equipment:

Argus VI Spectrometer (multicollector, CDD in ^{36}Ar); Thermo Scientific CO₂ Laser (10,6 μ); Photon Machines.

Measurement Conditions:

Every two or three steps, the background was measured, which was discounted directly in the subsequent measurement.

The neutron irradiation was carried out at the CCHEN nuclear reactor during a 23-hour period: there was a cadmium shield for the samples.

Analysis Criteria:

To determine J of each irradiation site, a polynomial regression was done of 21 standards present in the radiation disk.

The definition of a plateau is determined by: ≥ 3 consecutive fusion steps; $\geq 50\%$ of ^{39}Ar released in the analysis; Error overlap at 2σ .

A MSWD < 3 is considered to be acceptable.

Department of Laboratories Servicio Nacional de Geología y Minería

Til Til 1993, Nuñoa - Santiago - PHONE: (56-2) 2385292 FAX: (56-2) 2385332 - www.sernageomin.cl

E-mail: jefe_lab@sernageomin.cl - Postal Box: 10465 and 1347, Post 21- SANTIAGO - CHILE

ARGUS VI GEOCHRONOLOGY



Presentación de los datos:

La información presentada en el informe, se ajusta a las normas de información de datos para geocronología de $^{40}\text{Ar}/^{39}\text{Ar}$, publicadas en "Data reporting norms for $^{40}\text{Ar}/^{39}\text{Ar}$ geochronology", *Quaternary Geochronology* 4 (2009) 346-352.

Parámetros utilizados:

	Source	Decay constants	Source
Atmospheric argon ratios			
$(^{40}\text{Ar}/^{36}\text{Ar})_{\lambda}$	Steiger and Jäger (1977)	$^{40}\text{K } \lambda_e$ (5.81 ± 0.17)E-11 y ⁻¹	Steiger and Jäger (1977)
$(^{40}\text{Ar}/^{38}\text{Ar})_{\lambda}$	Nier (1950)	$^{40}\text{K } \lambda_{40}$ (4.96 ± 0.09)E-10 y ⁻¹	Steiger and Jäger (1977)
Interfering isotope production ratios			
$(^{40}\text{Ar}/^{39}\text{Ar})_{\text{K}}$	Source	^{39}Ar (7.05 ± 0.08)E-06 d ⁻¹	Stoemmer et al. (1965)
$(^{38}\text{Ar}/^{39}\text{Ar})_{\text{K}}$	In house	^{37}Ar (19.83 ± 0.06)E-03 d ⁻¹	Renne and Norman (2001)
$(^{39}\text{Ar}/^{37}\text{Ar})_{\text{Ca}}$	Renne et al. (2005)	$^{36}\text{Cl } \lambda_{40}$ (6.31 ± 0.04)E-09 d ⁻¹	Endt (1998)
$(^{38}\text{Ar}/^{37}\text{Ar})_{\text{Ca}}$	In house		
$(^{38}\text{Ar}/^{37}\text{Ar})_{\text{Ca}}$	Renne et al. (2005)		
$(^{36}\text{Ar}/^{37}\text{Ar})_{\text{Ca}}$	In house		
$(^{36}\text{Ar}/^{38}\text{Ar})_{\text{Ca}}$	Renne et al. (2008)		


 Marco Suárez
 Jefe Geología Isotópica (S)


 Adán Ramírez
 Analista

Departamento de Laboratorios Servicio Nacional de Geología y Minería
 Til Til 1993, Ñuñoa - Santiago - FONDO: (56-2) 2385292 FAX: (56-2) 2385332 - www.sernageomin.cl
 E-mail: jefe_lab@sernameomin.cl - Casilla: 10465 y 1347, correo 21- SANTIAGO - CHILE

Informe 019; Argus 2017
 Edmundo Polanco
 SDNG



Data Presentation:

The information presented in the report conforms to the data reporting rules for $^{40}\text{Ar}/^{39}\text{Ar}$ geochronology, published in "Data reporting norms for $^{40}\text{Ar}/^{39}\text{Ar}$ geochronology", *Quaternary Geochronology* 4 (2009) 346-352.

Parameters used:

	Source	Decay constants	Source
Atmospheric argon ratios			
$(^{40}\text{Ar}/^{36}\text{Ar})_A$	Steiger and Jäger (1977)	$^{40}\text{K} \lambda_{\text{ec}}$ $(5.81 \pm 0.17)\text{E}-11 \text{ y}^{-1}$	Steiger and Jäger (1977)
$(^{40}\text{Ar}/^{38}\text{Ar})_A$	Nier (1950)	$^{40}\text{K} \lambda_{\text{p}}$ $(4.96 \pm 0.09)\text{E}-10 \text{ y}^{-1}$	Steiger and Jäger (1977)
		^{39}Ar $(7.05 \pm 0.08)\text{E}-06 \text{ d}^{-1}$	Stoerner et al. (1965)
Interfering isotope production ratios		^{37}Ar $(19.83 \pm 0.06)\text{E}-03 \text{ d}^{-1}$	Renne and Norman (2001)
$(^{40}\text{Ar}/^{39}\text{Ar})_K$	Source	$^{36}\text{Cl} \lambda_{\text{p}}$ $(6.31 \pm 0.04)\text{E}-09 \text{ d}^{-1}$	Endt (1998)
$(^{38}\text{Ar}/^{39}\text{Ar})_K$	In house		
$(^{39}\text{Ar}/^{37}\text{Ar})_{\text{Ca}}$	Renne et al. (2005)		
$(^{38}\text{Ar}/^{37}\text{Ar})_{\text{Ca}}$	In house		
$(^{36}\text{Ar}/^{37}\text{Ar})_{\text{Ca}}$	Renne et al. (2005)		
$(^{36}\text{Ar}/^{37}\text{Ar})_{\text{Ca}}$	In house		
$(^{36}\text{Ar}/^{38}\text{Ar})_{\text{Cl}}$	Renne et al. (2008)		



Marco Suárez
Head of Isotopic Geology (Dep.)



Adán Ramírez
Analyst

Department of Laboratories Servicio Nacional de Geología y Minería

Til Til 1993, Nunoa - Santiago - PHONE: (56-2) 2385292 FAX: (56-2) 2385332 - www.sernageomin.cl

E-mail: jefe_lab@sernageomin.cl - Postal Box 10465 y 1347, Post 21 - SANTIAGO - CHILE

019 Report; Argus 2017

Edmundo Polanco

SDNG



Servicio Nacional de Geología y Minería
Subdirección Nacional de Geología
Departamento de Laboratorios

Sr. Edmundo Polanco

Depto. Geología Regional

UNIDAD DE GEOLOGIA ISOTOPICA
INFORME $^{40}\text{Ar}/^{39}\text{Ar}$ N° 023/2017 ARGUS VI

Departamento de Laboratorios - Servicio Nacional de Geología y Minería
Til Til 1993, Ñuñoa - Santiago - FONO: (56-2) 2385292 FAX: (56-2) 2385332 - www.sernageomin.cl
E-mail: jefe_lab@sernageomin.cl – Casilla: 10465 y 1347, correo 21- SANTIAGO – CHILE



**National Geology and Mining Service
National Sub-directorate of Geology
Department of Laboratories**

Mr. Edmundo Polanco

Regional Department of Geology

**ISOTOPIC GEOLOGY UNIT
⁴⁰Ar/³⁹Ar REPORT N° 023/2017 ARGUS VI**

Department of Laboratories Servicio Nacional de Geología y Minería

Til Til 1993, Ñuñoa - Santiago - PHONE: (56-2) 2385292 FAX: (56-2) 2385332 - www.sernageomin.cl

E-mail: jefe_lab@sernageomin.cl – Postal Box 10465 and 1347, Post 21- SANTIAGO – CHILE



En el presente informe se encuentran contenidos los resultados y análisis realizados a las muestras que se detallan en la precedente tabla resumen:

Muestra	Nº Análisis	Material	Edad Integrada $\pm 2\sigma$	Edad Plateau $\pm 2\sigma$	Edad Isoc. Inversa $\pm 2\sigma$
RSP-16d	14031-01	Plagioclasa	1.56 \pm 0.08 Ma	1.61 \pm 0.08 Ma	1.6 \pm 0.2 Ma

Departamento de Laboratorios Servicio Nacional de Geología y Minería
 Til Til 1993, Nuñoa - Santiago - FONO: (56-2) 2385292 FAX: (56-2) 2385332 - www.sernageomin.cl
 E-mail: jefe_lab@sernageomin.cl - Casilla: 10465 y 1347, correo 21- SANTIAGO - CHILE

GEOCRONOLOGIA ARGUS VI



This report contains the results and analyses conducted on the samples that are detailed in the preceding summary table:

Sample	Nº Analysis	Material	Integrated Age $\pm 2\sigma$	Plateau Age $\pm 2\sigma$	Inverse Isochron Age $\pm 2\sigma$
RSP-16d	14031-01	Plagioclase	1.56 \pm 0.08 Ma	1.61 \pm 0.08 Ma	1.61 \pm 0.02 Ma

Department of Laboratories Servicio Nacional de Geología y Minería

Til Til 1993, Nunoa - Santiago - PHONE: (56-2) 2385292 FAX: (56-2) 2385332 - www.sernageomin.cl
 E-mail: jefe_lab@sernageomin.cl - Postal Box 10465 and 1347, Post 21- SANTIAGO - CHILE

ARGUS VI GEOCRONOLOGY



Muestra : **RSP-16d**
Material : Plagioclasa
Nº interno : 14031-01

Análisis de Step Heating

Edad integrada: 1.56 ± 0.08 Ma
Edad Plateau: 1.61 ± 0.08 Ma
Pasos en el Plateau: 4/8 (71.8% de ^{39}Ar)
MSWD Plateau: 0.99

Análisis de Isócrona Inversa

Edad Isócrona: 1.6 ± 0.2 Ma
Pasos: 4/8 (50 % de los pasos)
Intercepto 40/36: 295 ± 4
MSWD Isócrona: 1.4

Comentarios:

Todas las edades son concordantes. No se aprecia la presencia de argón heredado. Se recomienda usar la edad obtenida con el plateau.



Sample : **RSP-16d**
Material : Plagioclase
Internal Nº : 14031-01

Step Heating Analysis

Integrated Age: 1.56 ± 0.08 Ma
Plateau Age: 1.61 ± 0.08 Ma
 Steps at the Plateau: 4/8 (71.8% de ^{39}AR)
 Plateau MSWD: 0,99

Inverse Isochron Analysis

Isochron Age: 1.6 ± 0.2 Ma
 Steps: 4/8 (50% steps)
 40/36 Intercept: 295 ± 4
 Isochron MSWD: 1.4

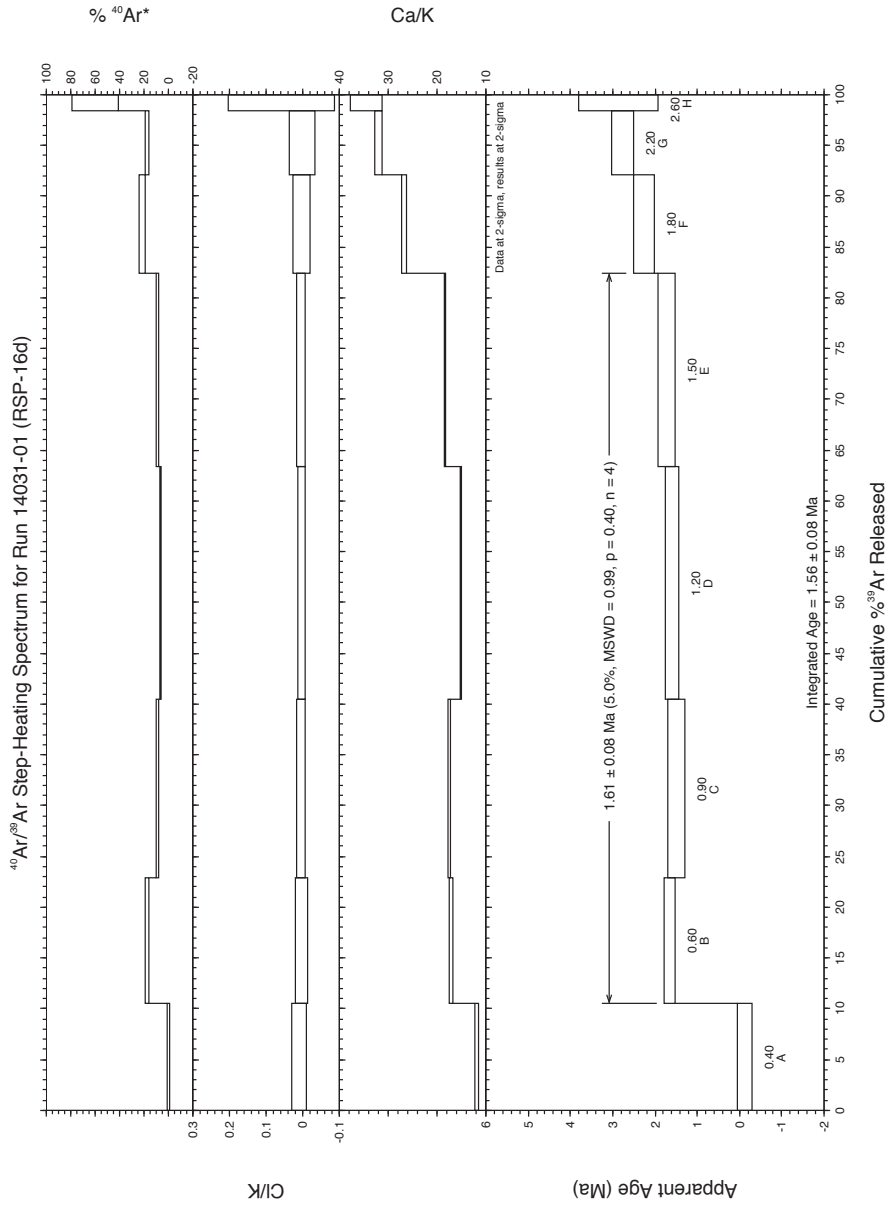
Comments:

All ages are concordant. The presence of inherited argon has not been observed. It is recommended to use the age obtained with the plateau.

Department of Laboratories Servicio Nacional de Geología y Minería

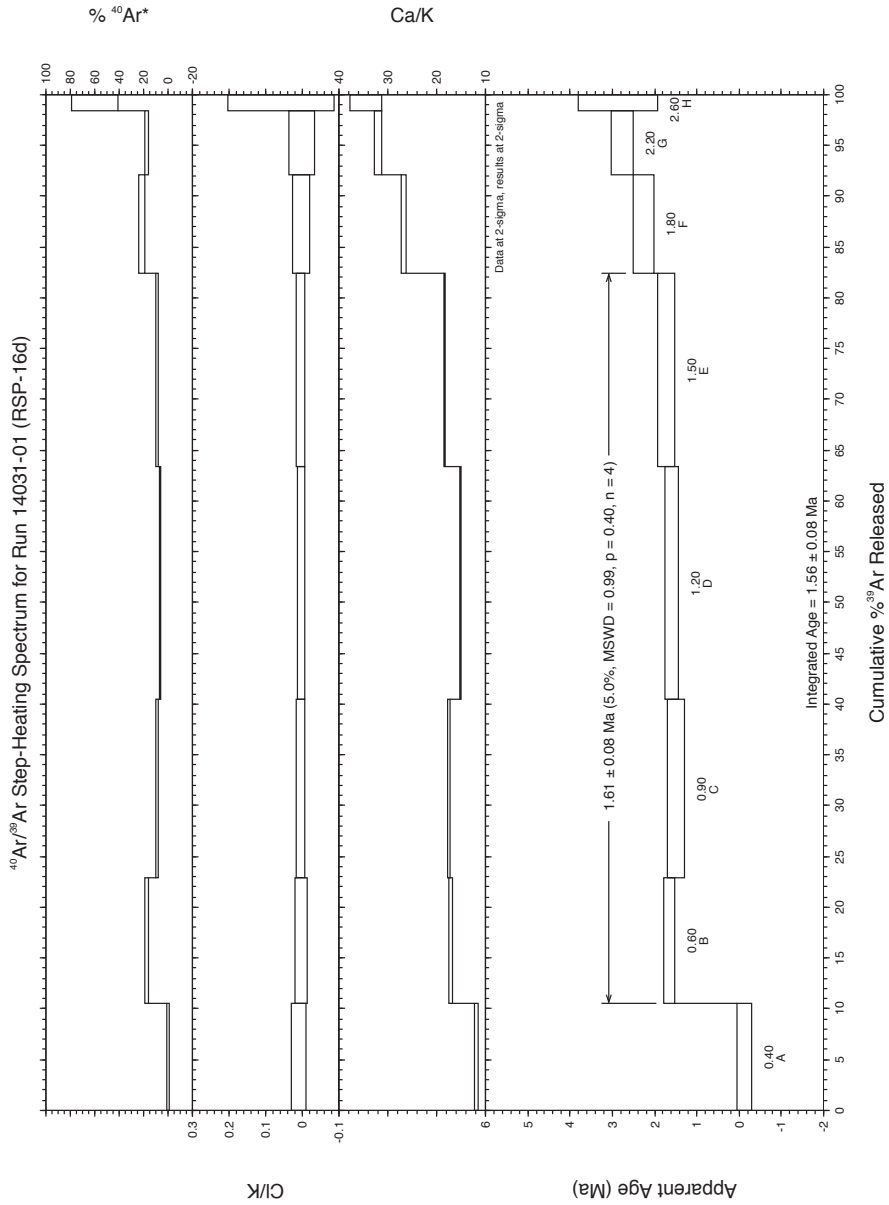
Tll Tll 1993, Nuñoa - Santiago - PHONE: (56-2) 2385292 FAX: (56-2) 2385332 - www.sernageomin.cl
 E-mail: jefe_lab@sernageomin.cl - Postal Box: 10465 and 1347, Post 21- SANTIAGO - CHILE

ARGUS VI GEOTHERMOLOGY



GEOCRONOLOGIA ARGUS VI

Departamento de Laboratorios Servicio Nacional de Geología y Minería
 Til Til 1993, Nuhoa - Santiago - FONDO: (56-2) 2385292 FAX: (56-2) 2385332 - www.sernageomin.cl
 E-mail: jefe_lab@sernageomin.cl - Casilla: 10465 y 1347, correo 21- SANTIAGO - CHILE



Department of Laboratories Servicio Nacional de Geología y Minería
 Ttl Tll 1993, Nunoa - Santiago - PHONE: (56-2) 2385292 FAX: (56-2) 2385332 - www.sernageomin.cl
 E-mail: Jefe_lab@sernageomin.cl - Postal Box 10465 and 1347, Post 21- SANTIAGO - CHILE

ARGUS VI GEODATUM

40Ar/39Ar Step-Heating Data for Run 14031-01; RSP-16d

Sample: RSP-16d		J: 0.0013369 ± 0.0000002										D: 1.00010 ± 0.00003			Heating: 76 s Total							
Material: Plagioclasa												36 s Rise										
Hole: 16/21																						
N	Power (W)	⁴⁰ Ar (moles)	⁴⁰ Ar (fA)	± σ ₄₀ (fA)	³⁹ Ar (fA)	± σ ₃₉ (fA)	³⁸ Ar (fA)	± σ ₃₈ (fA)	³⁷ Ar (fA)	± σ ₃₇ (fA)	³⁶ Ar (fA)	± σ ₃₆ (fA)	% ⁴⁰ Ar* ³⁹ Ar/Ar ₀	± σ	Cu/K	± σ	Age (Ma)	± σ (Ma)	Cu/K	± σ		
A	0.4	1.68E-15	44.76	0.05	6.59	0.03	0.13	0.02	1.97	0.03	0.1658	0.0008	-0.85	0.04	11.79	0.17	-0.14	0.09	11.79	0.17	0.007	0.010
B	0.6	1.14E-15	30.38	0.05	7.64	0.03	0.12	0.02	3.27	0.03	0.1070	0.0007	16.99	0.03	16.95	0.15	1.64	0.07	16.95	0.15	0.002	0.009
C	0.9	2.94E-15	78.27	0.05	10.92	0.02	0.19	0.02	4.81	0.03	0.2742	0.0015	8.51	0.04	17.45	0.10	1.48	0.10	17.45	0.10	0.002	0.006
D	1.2	6.08E-15	162.02	0.05	14.21	0.03	0.28	0.02	5.42	0.03	0.5529	0.0016	5.71	0.03	15.09	0.08	1.58	0.08	15.09	0.08	0.001	0.004
E	1.5	3.55E-15	94.58	0.05	11.81	0.03	0.22	0.02	5.43	0.03	0.3280	0.0016	8.79	0.04	18.24	0.10	1.71	0.10	18.24	0.10	0.004	0.006
F	1.8	1.01E-15	26.87	0.05	6.03	0.03	0.09	0.02	3.99	0.03	0.0989	0.0010	20.82	0.05	26.7	0.2	2.26	0.12	26.7	0.2	0.001	0.011
G	2.2	1.00E-15	26.66	0.05	3.93	0.03	0.06	0.02	3.11	0.03	0.0962	0.0007	16.63	0.06	31.9	0.4	2.75	0.13	31.9	0.4	0.001	0.017
H	2.6	6.81E-17	1.82	0.05	0.92	0.03	0.03	0.02	0.79	0.02	0.0078	0.0005	59.42	0.19	34.4	1.6	2.9	0.5	34.4	1.6	0.06	0.07
Plateau Age (steps B-E):		1.61 0.04																				
Standard: FC		Interpolation										Age: 28.201 Ma			D: 1.00027 ± 0.00003			Heating: 77 s Total				
Hole: 16/21															37 s Rise							
N	Power (W)	⁴⁰ Ar (moles)	⁴⁰ Ar (fA)	± σ ₄₀ (fA)	³⁹ Ar (fA)	± σ ₃₉ (fA)	³⁸ Ar (fA)	± σ ₃₈ (fA)	³⁷ Ar (fA)	± σ ₃₇ (fA)	³⁶ Ar (fA)	± σ ₃₆ (fA)	% ⁴⁰ Ar* ³⁹ Ar/Ar ₀	± σ	Cu/K	± σ	Age (Ma)	± σ (Ma)	Cu/K	± σ		
I	3.4	5.40E-14	1438.32	0.13	121.44	0.04	1.56	0.02	0.07	0.03	0.0243	0.0008	99.51	0.005	0.019	0.008	28.201	0.012	0.019	0.008	0.0018	0.0006

Departamento de Laboratorios Servicio Nacional de Geología y Minería
 T11 T11 1993, Nuhoa - Santiago - FON0: (56-2) 2385292 FAX: (56-2) 2385332 - www.sernageomin.cl
 E-mail: lefe_lab@sernageomin.cl - Casilla: 10465 y 1347, correo 21- SANTIAGO - CHILE

GEOCRONOLOGIA ARGUS VI

40Ar/39Ar Step-Heating Data for Run 14031-01; RSP-16d

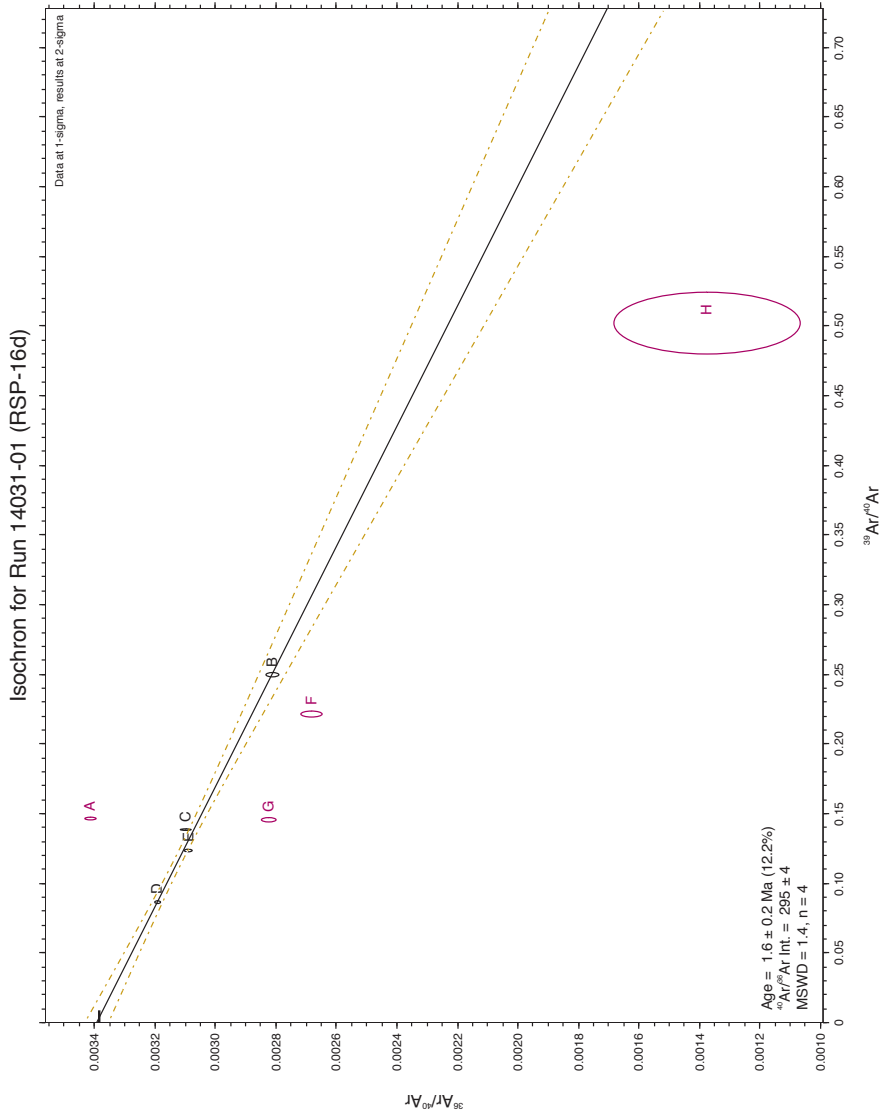
Sample: RSP-16d		J: 0.0013369 ± 0.0000002		D: 1.00010 ± 0.00003		Heating: 76 s Total		36 s Rise													
Material: Plagioclase																					
Hole: 16/21																					
N	Power (W)	⁴⁰ Ar (moles)	⁴⁰ Ar (fA)	± σ ₄₀ (fA)	³⁹ Ar (fA)	± σ ₃₉ (fA)	³⁸ Ar (fA)	± σ ₃₈ (fA)	³⁷ Ar (fA)	± σ ₃₇ (fA)	³⁶ Ar (fA)	± σ ₃₆ (fA)	% ⁴⁰ Ar*	⁴⁰ Ar*/Ar _t	± σ	Age (Ma)	± σ (Ma)	Cu/K	± σ	Cl/K	± σ
A	0.4	1.68E-15	44.76	0.05	6.59	0.03	0.13	0.02	1.97	0.03	0.1658	0.0008	-0.85	-0.06	0.04	-0.14	0.09	11.79	0.17	0.007	0.010
B	0.6	1.14E-15	30.38	0.05	7.64	0.03	0.12	0.02	3.27	0.03	0.1070	0.0007	16.99	0.68	0.03	1.64	0.07	16.95	0.15	0.002	0.009
C	0.9	2.94E-15	78.27	0.05	10.92	0.02	0.19	0.02	4.81	0.03	0.2742	0.0015	8.51	0.61	0.04	1.48	0.10	17.45	0.10	0.002	0.006
D	1.2	6.08E-15	162.02	0.05	14.21	0.03	0.28	0.02	5.42	0.03	0.5529	0.0016	5.71	0.65	0.03	1.58	0.08	15.09	0.08	0.001	0.004
E	1.5	3.55E-15	94.58	0.05	11.81	0.03	0.22	0.02	5.43	0.03	0.3280	0.0016	8.79	0.71	0.04	1.71	0.10	18.24	0.10	0.004	0.006
F	1.8	1.01E-15	26.87	0.05	6.03	0.03	0.09	0.02	3.99	0.03	0.0989	0.0010	20.82	0.94	0.05	2.26	0.12	26.7	0.2	0.001	0.011
G	2.2	1.00E-15	26.66	0.05	3.93	0.03	0.06	0.02	3.11	0.03	0.0962	0.0007	16.63	1.14	0.06	2.75	0.13	31.9	0.4	0.001	0.017
H	2.6	6.81E-17	1.82	0.05	0.92	0.03	0.03	0.02	0.79	0.02	0.0078	0.0005	59.42	1.18	0.19	2.9	0.5	34.4	1.6	0.06	0.07
Plateau Age (steps B-E):		1.61 0.04																			
Standard: FC		Interpolation		Age: 28.201 Ma		D: 1.00027 ± 0.00003		Heating: 77 s Total		37 s Rise											
N	Power (W)	⁴⁰ Ar (moles)	⁴⁰ Ar (fA)	± σ ₄₀ (fA)	³⁹ Ar (fA)	± σ ₃₉ (fA)	³⁸ Ar (fA)	± σ ₃₈ (fA)	³⁷ Ar (fA)	± σ ₃₇ (fA)	³⁶ Ar (fA)	± σ ₃₆ (fA)	% ⁴⁰ Ar*	⁴⁰ Ar*/Ar _t	± σ	Age (Ma)	± σ (Ma)	Cu/K	± σ	Cl/K	± σ
I	3.4	5.40E-14	1438.32	0.13	121.44	0.04	1.56	0.02	0.07	0.03	0.0243	0.0008	99.51	11.772	0.005	28.201	0.012	0.019	0.008	0.0018	0.0006

Department of Laboratories Servicio Nacional de Geología y Minería

Til Til 1993, Nunoa - Santiago - PHONE: (56-2) 2385292 FAX: (56-2) 2385332 - www.sernageomin.cl

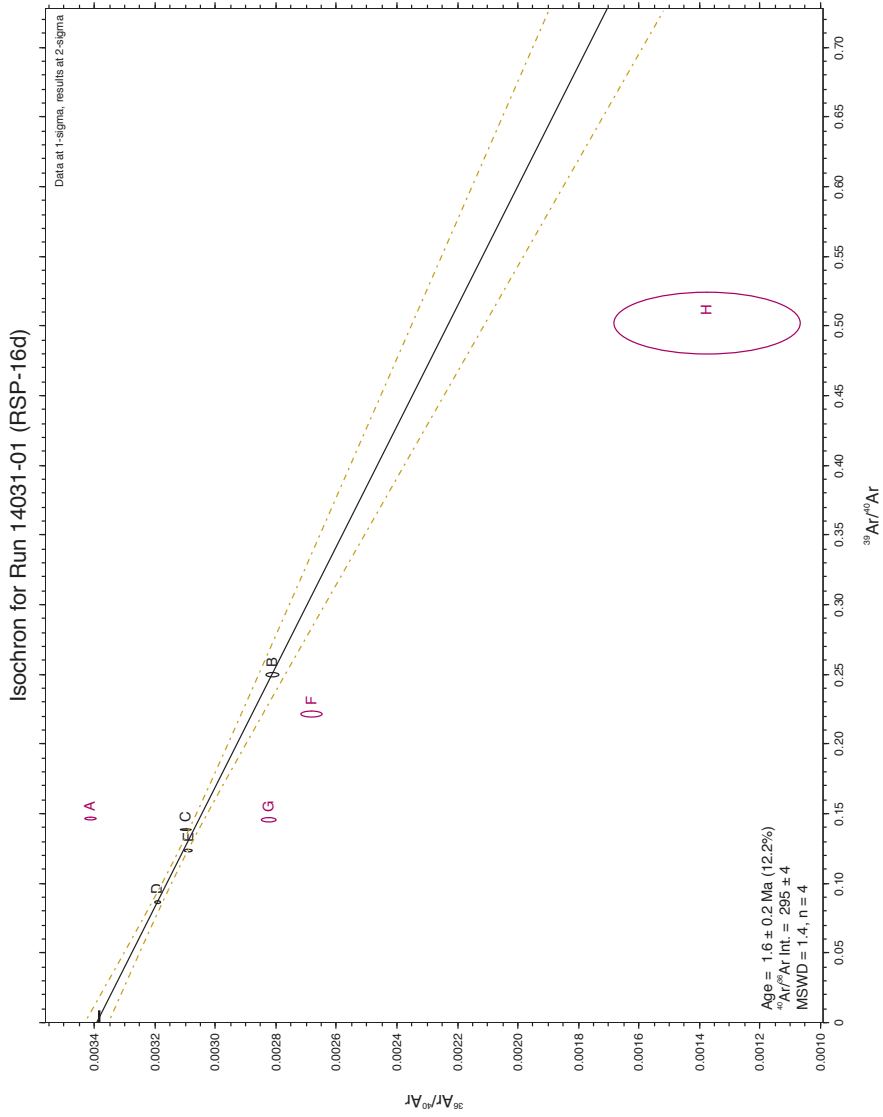
E-mail: jefe_lab@sernageomin.cl - Postal Box 10465 and 1347, Post 21 - SANTIAGO - CHILE

ARGUS VI GEOSCIENCE



Departamento de Laboratorios Servicio Nacional de Geología y Minería
 Til Til 1993, Nuñoa - Santiago - FONO: (56-2) 2385292 FAX: (56-2) 2385332 - www.sernageomin.cl
 E-mail: jefe_lab@sernageomin.cl - Casilla: 10465 y 1347, correo 21- SANTIAGO - CHILE

GEOCRONOLOGIA ARGUS VI



Department of Laboratories Servicio Nacional de Geología y Minería
 TIL TIL 1993, Nunoa - Santiago - PHONE: (56-2) 2385292 FAX: (56-2) 2385332 - www.sernageomin.cl
 E-mail: lefe_lab@sernageomin.cl - Postal Box 10465 and 1347, Post 21- SANTIAGO - CHILE

ARGUS VI GEOCRONOLOGY

Isochron Data for 14031-01A to 14031-01H

Run ID	Status	⁴⁰ Ar/ ³⁹ Ar	(36/40) isoch	%±	(39/40) isoch	%±	Correl 36/39	Group
14031-01A	User omitted	-0.05763	0.003413	0.60	0.14673	0.50	0.048	1
14031-01B	OK	0.67894	0.002809	0.80	0.25023	0.43	0.075	1
14031-01C	OK	0.61351	0.003096	0.60	0.13877	0.25	0.026	1
14031-01D	OK	0.65435	0.003191	0.30	0.08728	0.23	0.018	1
14031-01E	OK	0.70843	0.003087	0.50	0.12414	0.27	0.022	1
14031-01F	User omitted	0.93619	0.002680	1.40	0.22235	0.58	0.043	1
14031-01G	User omitted	1.13930	0.002821	0.90	0.14597	0.83	0.044	1
14031-01H	User omitted	1.18224	0.001373	22.50	0.50260	4.32	0.071	1

Sample	ID	Age [Ma]	M.S.E.	(40/36) tr	M.S.E.	MSWD	Prob	n
RSP-16d	14031-01	1.6	0.2	295	4	1.4	2.47E-01	4

Isochron Data for 14031-01A to 14031-01H

Run ID	Status	⁴⁰ Ar ^{*/39} Ar	(36/40) isoch	%±	(39/40) isoch	%±	Correl 36/39	Group
14031-01A	User omitted	-0.05763	0.003413	0.60	0.14673	0.50	0.048	1
14031-01B	OK	0.67894	0.002809	0.80	0.25023	0.43	0.075	1
14031-01C	OK	0.61351	0.003096	0.60	0.13877	0.25	0.026	1
14031-01D	OK	0.65435	0.003191	0.30	0.08728	0.23	0.018	1
14031-01E	OK	0.70843	0.003087	0.50	0.12414	0.27	0.022	1
14031-01F	User omitted	0.93619	0.002680	1.40	0.22235	0.58	0.043	1
14031-01G	User omitted	1.13930	0.002821	0.90	0.14597	0.83	0.044	1
14031-01H	User omitted	1.18224	0.001373	22.50	0.50260	4.32	0.071	1

Sample	ID	Age [Ma]	M.S.E.	(40/36) tr	M.S.E.	MSWD	Prob	n
RSP-16d	14031-01	1.6	0.2	295	4	1.4	2.47E-01	4

Department of Laboratories Servicio Nacional de Geología y Minería

Til Til 1993, Nunoa - Santiago - PHONE: (56-2) 2385292 FAX: (56-2) 2385332 - www.servnageomin.cl

E-mail: lefe_lab@servnageomin.cl - Postal Box 10465 and 1347, Post 21 - SANTIAGO - CHILE

ARGUS VI GEOCHRONOLOGY



A continuación se detallan las particularidades de los análisis realizados a las muestras contenidas en el informe:

Equipamiento principal:

Espectrómetro Argus VI (multicolector, CDD en ^{36}Ar); Thermo Scientific
Láser de CO_2 (10,6 μ); Photon Machines.

Condiciones de medición:

Cada dos o tres pasos se realizó una medición del background, el cuál fue descontado directamente en las mediciones subsiguientes.

La irradiación de neutrones fue realizada en el reactor nuclear de la CCHEN por un periodo de 23 hrs, existiendo un escudo de cadmio para las muestras.

Criterios de análisis:

Para determinar J de cada lugar de irradiación, se realizó un regresión polinomial de 21 standards presentes en el disco de irradiación.

La definición de un plateau se determina por: ≥ 3 pasos de fusión consecutivos; $\geq 50\%$ de ^{39}Ar liberado en el análisis; Error overlap a 2σ .

Un MSWD < 3 se considera aceptable

Departamento de Laboratorios - Servicio Nacional de Geología y Minería
Til Til 1993, Ñuñoa - FONO: (56-2) 2385292 FAX: (56-2) 2385332 - www.sernageomin.cl
E-mail: jefe_lab@sernageomin.cl - Casilla: 10465 y 1347, correo 21- SANTIAGO — CHILE

GEOCRONOLOGIA ARGUS VI



The details of the analyses conducted to the samples contained in the report are given below:

Main Equipment:

Argus VI Spectrometer (multicollector, CDD in ^{36}Ar); Thermo Scientific CO_2 Laser (10,6 μ); Photon Machines.

Measurement Conditions:

Every two or three steps, the background was measured, which was discounted directly in the subsequent measurement.

The neutron irradiation was carried out at the CCHEN nuclear reactor during a 23-hour period: there was a cadmium shield for the samples.

Analysis Criteria:

To determine J of each irradiation site, a polynomial regression was done of 21 standards present in the radiation disk.

The definition of a plateau is determined by: ≥ 3 consecutive fusion steps; $\geq 50\%$ of ^{39}Ar released in the analysis; Error overlap at 2σ .

A MSWD < 3 is considered to be acceptable.

Department of Laboratories Servicio Nacional de Geología y Minería
 Ttl Ttl 1993, Ñuñoa - PHONE: (56-2) 2385292 FAX: (56-2) 2385332 - www.sernageomin.cl
 E-mail: lefe_lab@sernageomin.cl - Postal Box: 10465 and 1347, Post 21- SANTIAGO - CHILE

ARGUS VI GEOCHRONOLOGY



Presentación de los datos:

La información presentada en el informe, se ajusta a las normas de información de datos para geocronología de $^{40}\text{Ar}/^{39}\text{Ar}$, publicadas en "Data reporting norms for $^{40}\text{Ar}/^{39}\text{Ar}$ geochronology", *Quaternary Geochronology* 4 (2009) 346-352.

Parámetros utilizados:

	Source	Decay constants	Source
Atmospheric argon ratios			
$(^{40}\text{Ar}/^{36}\text{Ar})_{\lambda}$	Steiger and Jäger (1977)	$^{40}\text{K } \lambda_e$ (5.81 ± 0.17)E-11 y ⁻¹	Steiger and Jäger (1977)
$(^{40}\text{Ar}/^{38}\text{Ar})_{\lambda}$	Nier (1950)	$^{40}\text{K } \lambda_{40}$ (4.96 ± 0.09)E-10 y ⁻¹	Steiger and Jäger (1977)
		^{39}Ar (7.05 ± 0.08)E-06 d ⁻¹	Stoemmer et al. (1965)
Interfering isotope production ratios	Source	^{37}Ar (19.83 ± 0.06)E-03 d ⁻¹	Renne and Norman (2001)
$(^{40}\text{Ar}/^{39}\text{Ar})_{\text{K}}$	In house	$^{36}\text{Cl } \lambda_{40}$ (6.31 ± 0.04)E-09 d ⁻¹	Endt (1998)
$(^{38}\text{Ar}/^{39}\text{Ar})_{\text{K}}$	Renne et al. (2005)		
$(^{39}\text{Ar}/^{37}\text{Ar})_{\text{Ca}}$	In house		
$(^{38}\text{Ar}/^{37}\text{Ar})_{\text{Ca}}$	Renne et al. (2005)		
$(^{36}\text{Ar}/^{37}\text{Ar})_{\text{Ca}}$	In house		
$(^{36}\text{Ar}/^{38}\text{Ar})_{\text{Ca}}$	Renne et al. (2008)		


 Marco Suárez
 Jefe Geología Isotópica (S)


 Adán Ramírez
 Analista

Departamento de Laboratorios Servicio Nacional de Geología y Minería
 Til Til 1993, Ñuñoa - Santiago - FONDO: (56-2) 2385292 FAX: (56-2) 2385332 - www.sernageomin.cl
 E-mail: jefe_lab@sernameomin.cl - Casilla: 10465 y 1347, correo 21- SANTIAGO - CHILE

Informe 023; Argus 2017
 Edmundo Polanco
 Depto. Geología Regional



Data Presentation:

The information presented in the report conforms to the data reporting rules for $^{40}\text{Ar}/^{39}\text{Ar}$ geochronology, published in "Data reporting norms for $^{40}\text{Ar}/^{39}\text{Ar}$ geochronology", *Quaternary Geochronology* 4 (2009) 346-352.

Parameters used:

Atmospheric argon ratios	Source	Decay constants	Source
$(^{40}\text{Ar}/^{36}\text{Ar})_{\text{A}}$ 295.5 ± 0.5	Steiger and Jäger (1977)	$^{40}\text{K } \lambda_{\text{e}}$ $(5.81 \pm 0.17)\text{E-11 } \text{y}^{-1}$	Steiger and Jäger (1977)
$(^{40}\text{Ar}/^{38}\text{Ar})_{\text{A}}$ 1575 ± 2	Nier (1950)	$^{40}\text{K } \lambda_{\text{p}}$ $(4.96 \pm 0.09)\text{E-10 } \text{y}^{-1}$	Steiger and Jäger (1977)
Interfering isotope production ratios	Source	^{39}Ar $(7.05 \pm 0.08)\text{E-06 } \text{d}^{-1}$	Stoerner et al. (1965)
$(^{40}\text{Ar}/^{39}\text{Ar})_{\text{K}}$ 0.0017 ± 0.0002	In house	^{37}Ar $(19.83 \pm 0.06)\text{E-03 } \text{d}^{-1}$	Renne and Norman (2001)
$(^{38}\text{Ar}/^{39}\text{Ar})_{\text{K}}$ 0.01220 ± 0.00003	Renne et al. (2005)	$^{36}\text{Cl } \lambda_{\text{p}}$ $(6.31 \pm 0.04)\text{E-09 } \text{d}^{-1}$	Endt (1998)
$(^{39}\text{Ar}/^{37}\text{Ar})_{\text{Ca}}$ 0.00077 ± 0.00003	In house		
$(^{38}\text{Ar}/^{37}\text{Ar})_{\text{Ca}}$ 0.0000196 ± 0.0000008	Renne et al. (2005)		
$(^{36}\text{Ar}/^{37}\text{Ar})_{\text{Ca}}$ 0.0003308 ± 0.0000012	In house		
$(^{36}\text{Ar}/^{38}\text{Ar})_{\text{Cl}}$ 262.8 ± 1.7	Renne et al. (2008)		



Marco Suárez
Head of Isotope Geology (Dep.)



Adán Ramírez
Analyst

Department of Laboratories Servicio Nacional de Geología y Minería
 TIL TIL 1993, Nunoa - Santiago - PHONE: (56-2) 2385292 FAX: (56-2) 2385332 - www.sernageomin.cl
 E-mail: lefe_lab@sernageomin.cl - Postal Box 10465 y 1347, Post 21- SANTIAGO - CHILE

023 Report; Argus 2017
 Edmundo Polanco
 Dept. Regional Geology



Servicio Nacional
de Geología y
Minería

**Unidad de Geología Isotópica
Laboratorio U-Pb**

INFORME : UPb-011-18
SOLICITANTE : Edmundo Polanco
AFILIACIÓN : Departamento de Geología General
SERNAGEOMIN
PROYECTO : --
CORRELATIVO INTERNO : C170725
FECHA INFORME : 25-04-2018

MUESTRAS : **RSP-50d**

Marco Suárez
Jefe Unidad Geología Isotópica (S)

Felipe Llona
Análisis LA-ICP-MS





Servicio Nacional
de Geología y
Minería

**Isotopic Geology Unit
U-Pb Laboratory**

REPORT : UPb-011-18
APPLICANT : Edmundo Polanco
AFFILIATION : Department of General Geology
SERNAGEOMIN
PROJECT : --
IN-HOUSE CORRELATIVE : C170725
DATE OF REPORT : 25-04-2018

SAMPLES : **RSP-50d**

Marco Suárez
Head of Isotopic Geology Unit (Dep.)

Felipe Llona
LA-ICP-MS Analysis





Servicio Nacional
de Geología y
Minería

Muestra RSP-50d

Número de puntos analizados : 30 puntos, 3 puntos excluidos de los resultados.
Edades $^{206}\text{Pb}/^{238}\text{U}$ corregidas por plomo común.

Edad:

Número de puntos utilizados en edad: 27

Edad propuesta para 15 valores coherentes (algoritmo Zircon age extractor / Isoplot):

6.63 ± 0.06 Ma





**Servicio Nacional
de Geología y
Minería**

RSP-50d Sample

Number of points analysed : 30 points, 3 points excluded from results
²⁰⁶Pb/²³⁸U ages corrected with common lead

Age:

Number of points used in dating : 27

Age proposed for 15 coherent values (Zircon age extractor algorithm / Isoplot):

6.63 ± 0.06 Ma



Muestra: RSP-50		RAZONES									
N° spot	Observ.	U [ppm] ^a	Pb [ppm] ^a	Th [ppm] ^a	$2\sigma^d$ $^{207}\text{Pb}/^{235}\text{U}^b$	$2\sigma^d$ $^{206}\text{Pb}/^{238}\text{U}^b$	$2\sigma^d$	rho ^c	$^{207}\text{Pb}/^{206}\text{Pb}^b$	$2\sigma^d$	
RSP-50_1		992	14	929	0,00883	0,00032	0,001002	0,000024	0,30393	0,0647	0,0018
RSP-50_2		387	13	301	0,02662	0,00120	0,000035	0,000035	0,57587	0,154	0,0045
RSP-50_4		658	7	390	0,01086	0,00057	0,001071	0,000026	0,48118	0,077	0,0043
RSP-50_5		1147	15	226	0,01740	0,00170	0,001243	0,000030	0,47776	0,102	0,0095
RSP-50_6		276	4	168	0,01581	0,00089	0,001104	0,000027	0,12066	0,1069	0,0059
RSP-50_7		577	9	414	0,01428	0,00066	0,001076	0,000027	0,59602	0,0982	0,0036
RSP-50_8		556	8	344	0,01298	0,00075	0,001249	0,000031	0,13534	0,078	0,0043
RSP-50_9		572	11	467	0,01554	0,00110	0,001113	0,000027	0,5937	0,1023	0,0064
RSP-50_11		1020	7	412	0,00913	0,00030	0,001113	0,000026	0,5092	0,0612	0,0014
RSP-50_12		936	11	548	0,01063	0,00058	0,001046	0,000024	0,55198	0,0755	0,0034
RSP-50_13		569	7	387	0,01067	0,00045	0,001101	0,000026	0,0079291	0,0706	0,0028
RSP-50_14		494	7	391	0,01197	0,00073	0,001085	0,000029	0,4785	0,0824	0,0042
RSP-50_15		748	9	554	0,01033	0,00038	0,001134	0,000026	0,14535	0,0665	0,0021
RSP-50_16		1254	37	2706	0,00852	0,00030	0,001045	0,000027	0,49509	0,0615	0,0016
RSP-50_17		485	8	245	0,01690	0,00095	0,001215	0,000030	0,31944	0,103	0,0051
RSP-50_18		876	10	639	0,00986	0,00095	0,001052	0,000025	0,14693	0,0688	0,0069
RSP-50_19		624	5	265	0,00984	0,00043	0,001053	0,000025	0,36526	0,0691	0,0024
RSP-50_20		567	7	351	0,01285	0,00100	0,001069	0,000025	0,54615	0,0875	0,0064
RSP-50_21		699	8	532	0,01047	0,00039	0,001077	0,000025	0,13359	0,0712	0,0021
RSP-50_23		438	13	445	0,02279	0,00130	0,001223	0,000029	0,54897	0,1349	0,0072
RSP-50_24		837	21	708	0,01834	0,00120	0,001177	0,000030	0,7032	0,1138	0,0065
RSP-50_25		826	13	648	0,01243	0,00170	0,001109	0,000028	0,16291	0,082	0,011
RSP-50_26		1687	21	1361	0,00853	0,00042	0,001007	0,000024	0,21051	0,0625	0,0027
RSP-50_27		531	5	212	0,01228	0,00050	0,001308	0,000030	0,09453	0,069	0,0024
RSP-50_28		610	7	399	0,01083	0,00043	0,001120	0,000026	0,16694	0,0718	0,0025
RSP-50_29		430	7	258	0,01637	0,00130	0,001122	0,000029	0,63274	0,1077	0,0073
RSP-50_30		369	5	293	0,01284	0,00063	0,001089	0,000028	0,22473	0,0866	0,0038
RSP-50_3	(1)	352	40	443	0,04709	0,00170	0,001209	0,000032	0,67874	0,106	0,01
RSP-50_10	(1)	450	51	109	0,06444	0,00860	0,007341	0,001000	0,99474	0,0669	0,002
RSP-50_22	(1)	447	40	262	0,02041	0,00310	0,001165	0,000042	0,97132	0,121	0,01

(1) Valores no considerados en los cálculos debido a patrón incorrecto en curvas de razones isotópicas (inhomogeneidad en el contenido isotópico)

^a Concentraciones de U, Pb y Th son calculadas en relación al círculo de referencia GJ-1 (Jackson et al. 2004 Chem. Geol. 211 47-69)

^b Corregido por background, por fraccionamiento y normalizado al círculo de referencia GJ-1

^c Rho es la correlación del error definido como el cociente de los errores propagados de las razones $^{206}\text{Pb}/^{238}\text{U}$ y $^{207}\text{Pb}/^{235}\text{U}$

^d Dos veces el valor de la propagación de los errores estándar.

^e Williams, I.S., 1998. U–Th–Pb geochronology by ion microprobe. In: McKibben, M.A., Shanks, III W.C., Ridley, W.I. (Eds.), Applications of Microanalytical Techniques to Understanding Mineralizing Processes. Reviews in Economic Geology 7(1):1–35.

Sample: RSP-50

N° spot	Observ.	U [ppm] ^a	Pb [ppm] ^a	Th [ppm] ^a	RATIOS						
					$^{207}\text{Pb}/^{235}\text{U}^b$	$2\sigma^d$	$^{206}\text{Pb}/^{238}\text{U}^b$	$2\sigma^d$	rho ^c	$^{207}\text{Pb}/^{206}\text{Pb}^b$	$2\sigma^d$
RSP-50_1		992	14	929	0.00883	0.00032	0.001002	0.000024	0.30393	0.0647	0.0018
RSP-50_2		387	13	301	0.02662	0.00120	0.000175	0.000035	0.57587	0.154	0.0045
RSP-50_4		658	7	390	0.01086	0.00057	0.001071	0.000026	0.48118	0.077	0.0043
RSP-50_5		1147	15	226	0.01740	0.00170	0.001243	0.000030	0.4776	0.102	0.0095
RSP-50_6		276	4	168	0.01581	0.00089	0.001104	0.000027	0.12066	0.1069	0.0059
RSP-50_7		577	9	414	0.01428	0.00066	0.001076	0.000027	0.59602	0.0982	0.0036
RSP-50_8		556	8	344	0.01298	0.00075	0.001249	0.000031	0.13534	0.078	0.0043
RSP-50_9		572	11	467	0.01554	0.00110	0.001113	0.000027	0.5937	0.1023	0.0064
RSP-50_11		1020	7	412	0.00913	0.00030	0.001113	0.000026	0.5092	0.0612	0.0014
RSP-50_12		936	11	548	0.01063	0.00058	0.001046	0.000024	0.55198	0.0755	0.0034
RSP-50_13		569	7	387	0.01067	0.00045	0.001101	0.000026	0.0079291	0.0706	0.0028
RSP-50_14		494	7	391	0.01197	0.00073	0.001085	0.000029	0.4785	0.0824	0.0042
RSP-50_15		748	9	554	0.01033	0.00038	0.001134	0.000026	0.14535	0.0665	0.0021
RSP-50_16		1254	37	2706	0.00852	0.00030	0.001045	0.000027	0.49509	0.0615	0.0016
RSP-50_17		485	8	245	0.01690	0.00095	0.001215	0.000030	0.31944	0.103	0.0051
RSP-50_18		876	10	639	0.00986	0.00095	0.001052	0.000025	0.14693	0.0688	0.0069
RSP-50_19		624	5	265	0.00984	0.00043	0.001053	0.000025	0.36526	0.0691	0.0024
RSP-50_20		567	7	351	0.01285	0.00100	0.001069	0.000025	0.54615	0.0875	0.0064
RSP-50_21		699	8	532	0.01047	0.00039	0.001077	0.000025	0.13359	0.0712	0.0021
RSP-50_23		438	13	445	0.02279	0.00130	0.001223	0.000029	0.54897	0.1349	0.0072
RSP-50_24		837	21	708	0.01834	0.00120	0.001177	0.000030	0.7032	0.1138	0.0065
RSP-50_25		826	13	648	0.01243	0.00170	0.001109	0.000028	0.16291	0.082	0.011
RSP-50_26		1687	21	1361	0.00853	0.00042	0.001007	0.000024	0.21051	0.0625	0.0027
RSP-50_27		531	5	212	0.01228	0.00050	0.001308	0.000030	0.09453	0.069	0.0024
RSP-50_28		610	7	399	0.01083	0.00043	0.001120	0.000026	0.16694	0.0718	0.0025
RSP-50_29		430	7	258	0.01637	0.00130	0.001122	0.000029	0.63274	0.1077	0.0073
RSP-50_30		369	5	293	0.01284	0.00063	0.001089	0.000028	0.22473	0.0866	0.0038
RSP-50_3	(1)	352	30	443	0.01709	0.00170	0.001203	0.000032	0.67874	0.106	0.001
RSP-50_10	(1)	450	51	409	0.06444	0.00860	0.007341	0.001000	0.99474	0.0669	0.002
RSP-50_22	(1)	447	30	262	0.02041	0.00310	0.003165	0.000042	0.97132	0.121	0.001

(1) Values not considered in the calculations due to incorrect pattern in isotopic ratios (inhomogeneity in the isotopic content).

^a Concentrations of U, Pb, and Th are calculated in connection with the reference zircon GJ-1 (Jackson et al., 2004 Chem. Geol., 211, 47-69)

^b Corrected by background, by fractionation, and standardized to the reference zircon GJ-1

^c $^{207}\text{Pb}/^{235}\text{U}$ is calculated using $(^{207}\text{Pb}/^{206}\text{Pb}) / (^{238}\text{U}/^{206}\text{Pb}) \cdot 1/137.88$.

^d Rho is the correlation of the error defined as the quotient of errors propagation of the ratios $^{206}\text{Pb}/^{238}\text{U}$ y $^{207}\text{Pb}/^{235}\text{U}$.

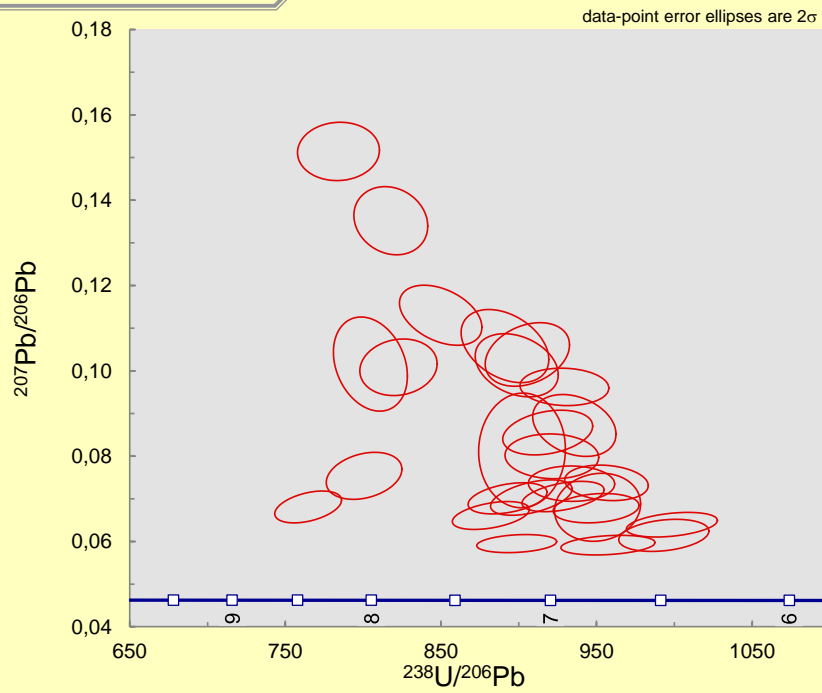
^e Twice the value of the standard error propagation.

^f Williams, I. S., 1998. U–Th–Pb geochronology by ion microprobe. In: McKibben, M.A., Shanks, III W. C., Ridley, W.I. (Eds.), Applications of Microanalytical Techniques to Understanding Mineralizing Processes. Reviews in Economic Geology 7(1):1–35.

EADADES [Ma]				Edad corregida por Pb común (e)			
$^{207}\text{Pb}/^{235}\text{U}$	2σ	$^{206}\text{Pb}/^{238}\text{U}$	2σ	$^{207}\text{Pb}/^{206}\text{Pb}$	2σ	$^{206}\text{Pb}/^{238}\text{U}$	2σ
8,9	0,3	6,5	0,2	753	58	6,3	0,2
26,7	1,1	8,2	0,2	2387	50	7,1	0,2
11,0	0,6	6,9	0,2	1110	100	6,6	0,2
17,5	1,7	8,0	0,2	1490	190	7,4	0,2
15,9	0,9	7,1	0,2	1724	98	6,6	0,2
14,4	0,7	6,9	0,2	1588	72	6,5	0,2
13,1	0,8	8,0	0,2	1140	110	7,7	0,2
15,7	1,1	7,2	0,2	1620	120	6,7	0,2
9,2	0,3	7,2	0,2	637	49	7,0	0,2
10,7	0,6	6,7	0,2	1044	90	6,5	0,2
10,8	0,5	7,1	0,2	933	78	6,9	0,2
12,1	0,7	7,0	0,2	1238	97	6,7	0,2
10,4	0,4	7,3	0,2	831	68	7,1	0,2
8,6	0,3	6,7	0,2	646	56	6,6	0,2
17,0	1,0	7,8	0,2	1649	93	7,3	0,2
10,0	1,0	6,8	0,2	761	87	6,6	0,2
9,9	0,4	6,8	0,2	905	67	6,6	0,2
13,0	1,0	6,9	0,2	1320	130	6,5	0,2
10,6	0,4	6,9	0,2	967	63	6,7	0,2
22,9	1,3	7,9	0,2	2149	95	7,0	0,2
18,4	1,2	7,6	0,2	1830	110	6,9	0,2
12,5	1,7	7,1	0,2	1110	240	6,8	0,2
8,6	0,4	6,5	0,2	658	86	6,4	0,2
12,4	0,5	8,4	0,2	908	73	8,2	0,2
10,9	0,4	7,2	0,2	970	75	7,0	0,2
16,5	1,3	7,2	0,2	1700	130	6,7	0,2
12,9	0,6	7,0	0,2	1335	80	6,7	0,2
17,2	1,7	7,7	0,2	1690	180		
63,4	8,3	47,2	6,6	829	63		
20,5	3,0	7,5	0,3	1890	130		

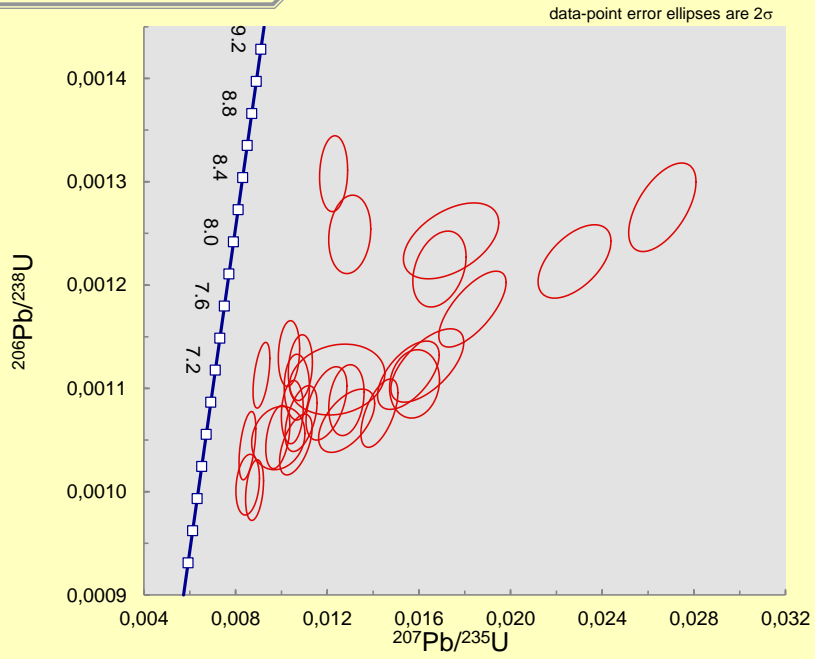
AGES [Ma]		Age corrected by common Pb(e)		$^{207}\text{Pb}/^{206}\text{Pb}$ corr
$^{207}\text{Pb}/^{235}\text{U}$	2σ	$^{206}\text{Pb}/^{238}\text{U}$	2σ	
8,9	0,3	6,5	0,2	0,83603
26,7	1,1	8,2	0,2	0,83614
11,0	0,6	6,9	0,2	0,83606
17,5	1,7	8,0	0,2	0,83613
15,9	0,9	7,1	0,2	0,83607
14,4	0,7	6,9	0,2	0,83606
13,1	0,8	8,0	0,2	0,83613
15,7	1,1	7,2	0,2	0,83608
9,2	0,3	7,2	0,2	0,83608
10,7	0,6	6,7	0,2	0,83605
10,8	0,5	7,1	0,2	0,83607
12,1	0,7	7,0	0,2	0,83607
10,4	0,4	7,3	0,2	0,83609
8,6	0,3	6,7	0,2	0,83605
17,0	1,0	7,8	0,2	0,83612
10,0	1,0	6,8	0,2	0,83605
9,9	0,4	6,8	0,2	0,83605
13,0	1,0	6,9	0,2	0,83606
10,6	0,4	6,9	0,2	0,83606
22,9	1,3	7,9	0,2	0,83612
18,4	1,2	7,6	0,2	0,83610
12,5	1,7	7,1	0,2	0,83608
8,6	0,4	6,5	0,2	0,83603
12,4	0,5	8,4	0,2	0,83616
10,9	0,4	7,2	0,2	0,83608
16,5	1,3	7,2	0,2	0,83608
12,9	0,6	7,0	0,2	0,83607
17,2	1,7	7,7	0,2	
62,4	8,3	47,2	6,6	
20,5	3,0	7,5	0,3	
		1690	180	
		829	63	
		1890	130	

Razones no corregidas por plomo común

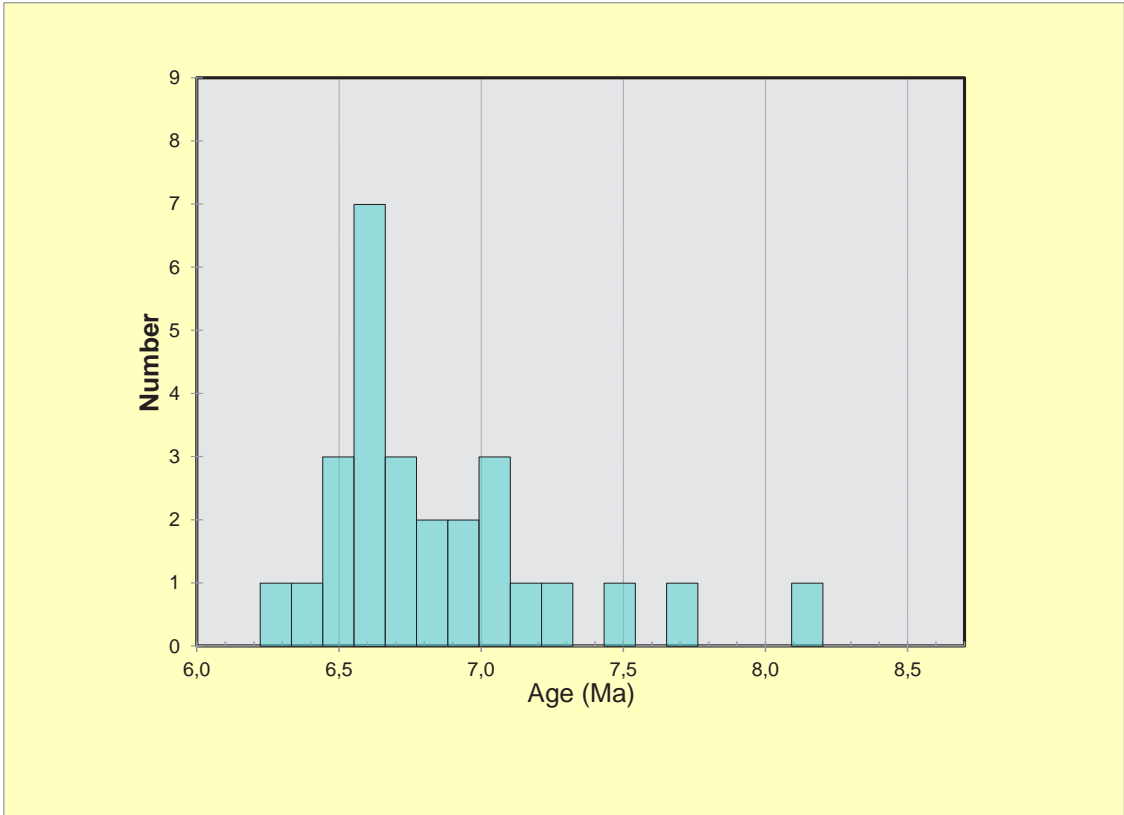


Ratios not corrected by common lead

Razones no corregidas por plomo común

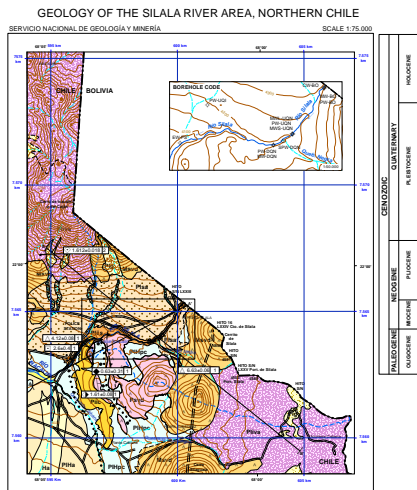


Ratios not corrected by common lead

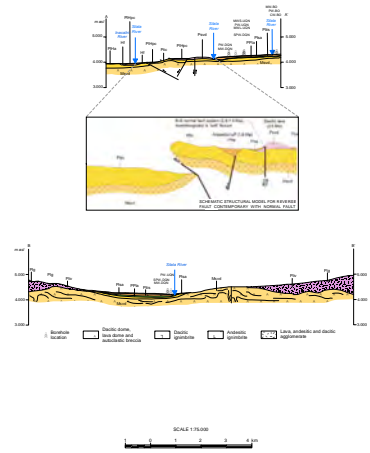


APPENDIX C

GEOLOGY OF THE SILALA RIVER BASIN, NORTHERN CHILE



SCHEMATIC GEOLOGIC SECTIONS

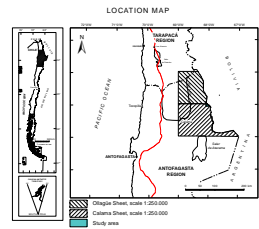


LEGEND

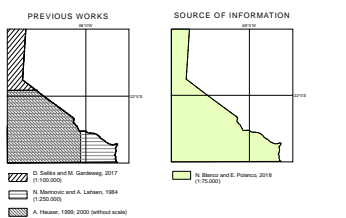
- | | |
|--|--|
| | F1 Fluvial deposits (Pliocene) |
| | F2 Alluvial deposits (Pliocene) |
| | F3a Alluvial deposits of the Upper Pleistocene-Holocene |
| | F3b Pyroclastic fall deposits (Pliocene-Holocene) |
| | F4 Alluvial deposits of the Upper Pleistocene |
| | F5 Glacial deposits (Upper Pleistocene) |
| | F6 Volcanic Sequences of the Lower Pleistocene (ca. 1.61-1.46 Ma) |
| | F7 Volcanic Sequences of the Upper Pleistocene (ca. 0.6-0.54 Ma) |
| | F8 Alluvial deposits of the Upper Pleistocene - Lower Pleistocene |
| | F9 Volcanic Sequences of the Upper Pleistocene (ca. 2.6 Ma) |
| | F10 Volcanic Sequences of the Upper Pleistocene (ca. 4.0-4.2 Ma) |
| | F11 Volcanic Sequences of the Upper Pleistocene (ca. 4.0-5.4 Ma) |
| | F12 Volcanic Sequences of the Upper Pleistocene (ca. 4.0-5.4 Ma) |

SYMBOLY

- | | | | | | |
|--|-----------------------|--|-----------------------|--|--|
| | Fault | | Inferred fault | | Erosion escarpment |
| | Control network fault | | Control network fault | | Alignment of volcanic sources |
| | Control network fault | | Control network fault | | Hydrographic basin limit |
| | Control network fault | | Control network fault | | Hydrographic basin limit |
| | Control network fault | | Control network fault | | Control lines |
| | Control network fault | | Control network fault | | Altitude (meters asl) |
| | Control network fault | | Control network fault | | Flow direction |
| | Control network fault | | Control network fault | | RADIOMETRIC DATING (Ma ± 2σ) |
| | Control network fault | | Control network fault | | K/Ar groundmass |
| | Control network fault | | Control network fault | | ⁴⁰ Ar/ ³⁹ Ar gas release |
| | Control network fault | | Control network fault | | ¹⁴⁷ Sm/ ¹⁴³ Sm ratio |
| | Control network fault | | Control network fault | | U/Pb Zircon |
| | Control network fault | | Control network fault | | Dating location |
| | Control network fault | | Control network fault | | RADIOMETRIC DATING SOURCE |
| | Control network fault | | Control network fault | | This work |
| | Control network fault | | Control network fault | | Saizis and Gertseeg (2017) |
| | Control network fault | | Control network fault | | |



LOCATION MAP AND CALAMA PARTIAL SHEETS



SERVICIO NACIONAL DE GEOLOGÍA Y MINERÍA - CHILE

**GEOLOGY OF THE SILALA AREA
NORTHERN CHILE**

Nicolas Blanco
Eduardo Polanco

Scale 1:75,000

REGISTERED REPORT R-1270
192AP

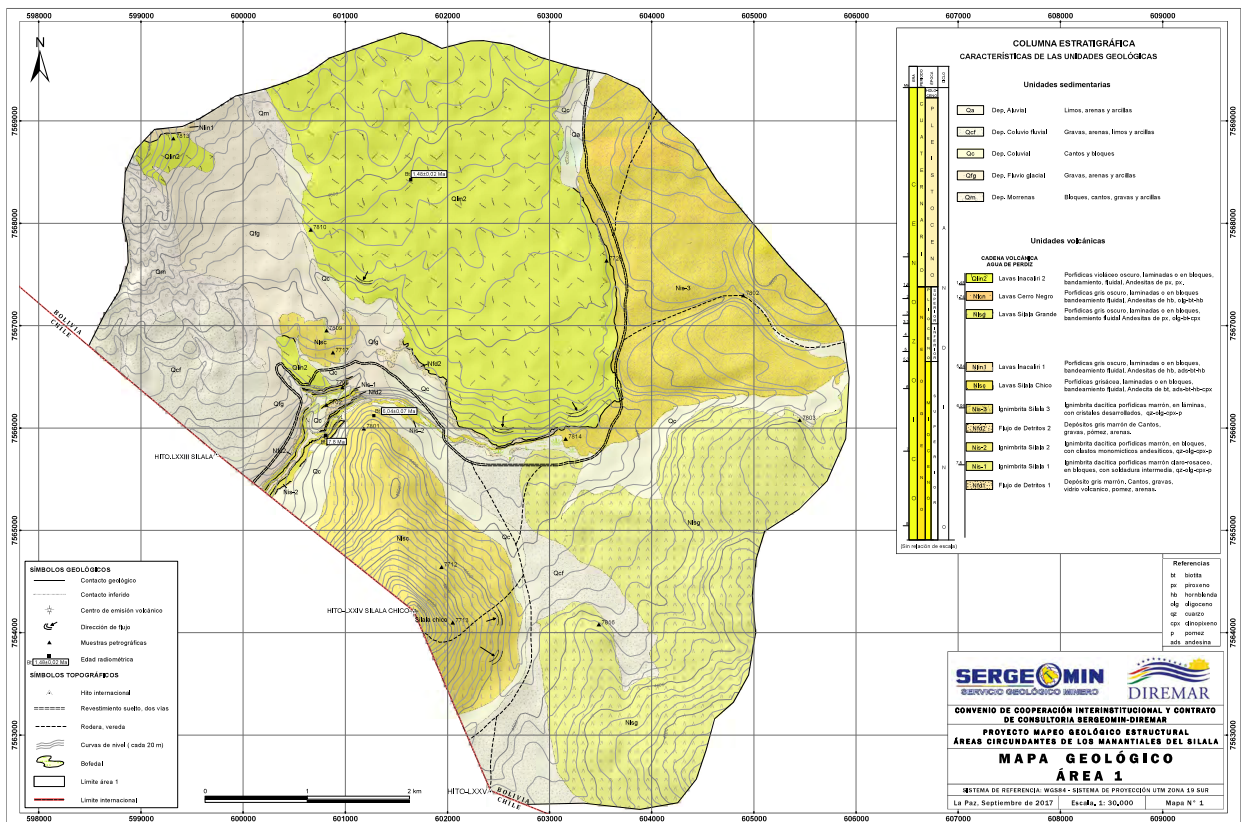
SUBDIRECCION NACIONAL DE GEOLOGÍA

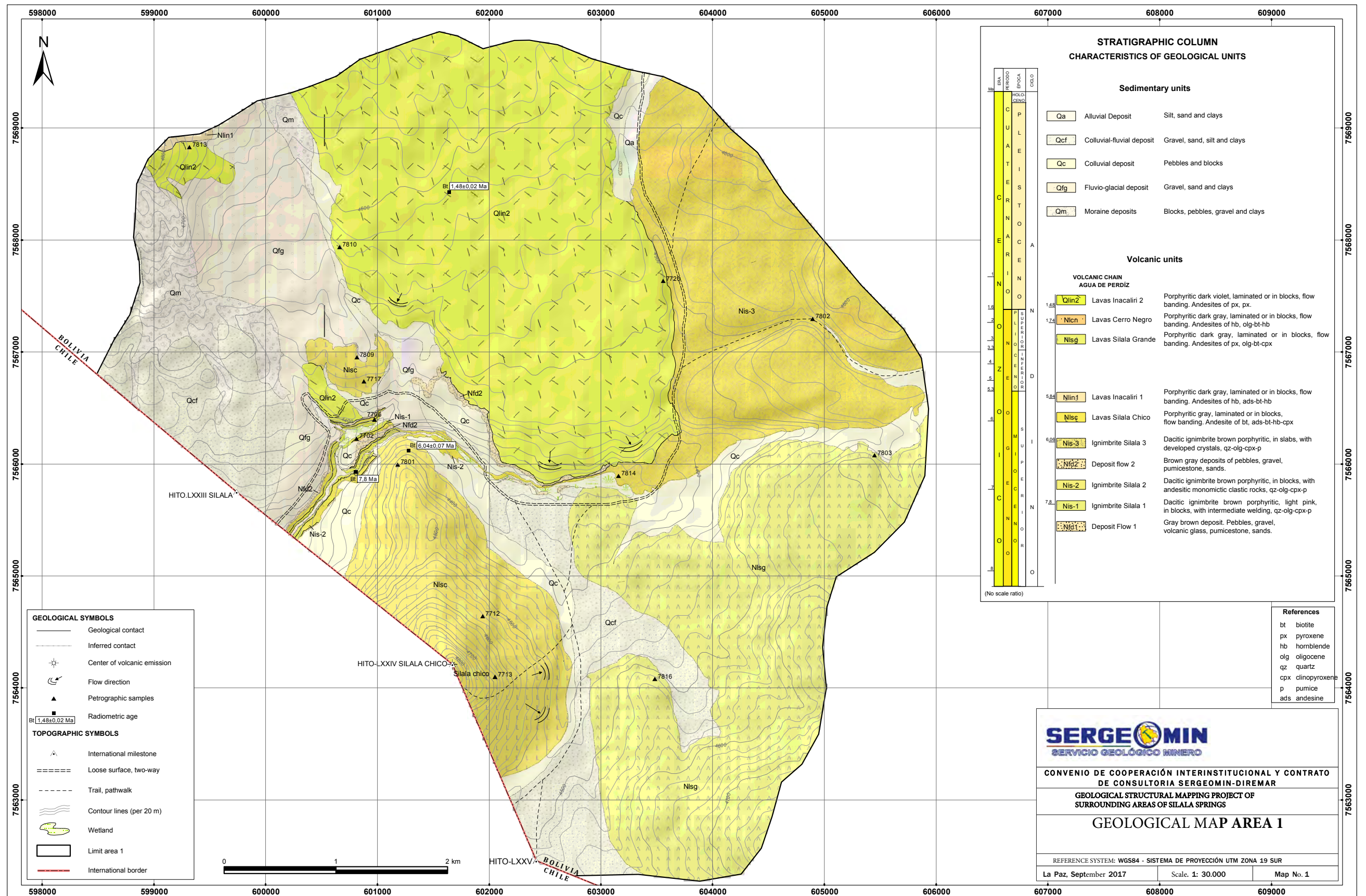
2018

Larger size map in pocket on the back cover of this volume.

APPENDIX D

PROYECTO MAPEO GEOLÓGICO-ESTRUCTURAL DEL ÁREA CIRCUNDANTE AL MANANTIAL DEL SILALA, DEPARTAMENTO DE POTOSÍ





STRATIGRAPHIC COLUMN
CHARACTERISTICS OF GEOLOGICAL UNITS

ERA	PERIODO	EPOCA	CICLO	UNIDAD	DESCRIPCION				
CUATERNARIO	HOLOCENO	CENOCENO	Pleistoceno	Qa	Alluvial Deposit Silt, sand and clays				
				Qcf	Colluvial-fluvial deposit Gravel, sand, silt and clays				
				Qc	Colluvial deposit Pebbles and blocks				
				Qfg	Fluvio-glacial deposit Gravel, sand and clays				
				Qm	Moraine deposits Blocks, pebbles, gravel and clays				
				CUATERNARIO	HOLOCENO	CENOCENO	Pleistoceno	Nlin2	Lavas Inacaliri 2 Porphyritic dark violet, laminated or in blocks, flow banding. Andesites of px, px.
								Nlcn	Lavas Cerro Negro Porphyritic dark gray, laminated or in blocks, flow banding. Andesites of hb, olg-bt-hb
								Nlsg	Lavas Silala Grande Porphyritic dark gray, laminated or in blocks, flow banding. Andesites of px, olg-bt-cpx
								Nlin1	Lavas Inacaliri 1 Porphyritic dark gray, laminated or in blocks, flow banding. Andesites of hb, ads-bt-hb
								Nlsc	Lavas Silala Chico Porphyritic gray, laminated or in blocks, flow banding. Andesite of bt, ads-bt-hb-cpx
Nis-3	Igimbrite Silala 3 Dacitic ignimbrite brown porphyritic, in slabs, with developed crystals, qz-olg-cpx-p								
Nfd2	Deposit flow 2 Brown gray deposits of pebbles, gravel, pumicestone, sands.								
Nis-2	Igimbrite Silala 2 Dacitic ignimbrite brown porphyritic, in blocks, with andesitic monomictic clastic rocks, qz-olg-cpx-p								
Nis-1	Igimbrite Silala 1 Dacitic ignimbrite brown porphyritic, light pink, in blocks, with intermediate welding, qz-olg-cpx-p								
Nfd1	Deposit Flow 1 Gray brown deposit. Pebbles, gravel, volcanic glass, pumicestone, sands.								

(No scale ratio)

GEOLOGICAL SYMBOLS

- Geological contact
- Inferred contact
- Center of volcanic emission
- Flow direction
- Petrographic samples
- Radiometric age

TOPOGRAPHIC SYMBOLS

- International milestone
- Loose surface, two-way
- Trail, pathwalk
- Contour lines (per 20 m)
- Wetland
- Limit area 1
- International border

References

- bt biotite
- px pyroxene
- hb hornblende
- olg oligocene
- qz quartz
- cpx clinopyroxene
- p pumice
- ads andesine

SERGEOMIN
SERVICIO GEOLÓGICO MINERO

CONVENIO DE COOPERACIÓN INTERINSTITUCIONAL Y CONTRATO DE CONSULTORIA SERGEOMIN-DIREMAR

GEOLOGICAL STRUCTURAL MAPPING PROJECT OF SURROUNDING AREAS OF SILALA SPRINGS

GEOLOGICAL MAP AREA 1

REFERENCE SYSTEM: WGS84 - SISTEMA DE PROYECCIÓN UTM ZONA 19 SUR

La Paz, September 2017 Scale: 1: 30.000 Map No. 1

Data CD

CD-ROM containing supporting data to
Annexes XI – XIV

Appendix C to Annex XIV

Blanco, N. and Polanco, E., 2018. *Geology of
the Silala River Basin, Northern Chile*